The fatigue behaviour of unidirectional mono-fibre and hybrid kevlar/xas/914 composites

Fernando, Gerard Franklyn

Award date:
1989

Awarding institution:
University of Bath

THE FATIGUE BEHAVIOUR OF UNIDIRECTIONAL MONO-FIBRE AND HYBRID KEVLAR / XAS / 914 COMPOSITES.

submitted by

Gerard Franklyn Fernando

for the degree of Ph. D
of the University of Bath.

G.F. Fernando

December 1989.

ProQuest LLC
789 East Eisenhower Parkway
P.O. Box 1346
Ann Arbor, MI 48106-1346

Dedicated to my loving mother and father

ABSTRACT

The static and fatigue properties of a 16 ply unidirectional XAS/914 and Kevlar/914 mono-fibre composite were evaluated and compared with the response of their unidirectional inter-ply hybrids. The hybrid compositions investigated consisted of 16 ply unidirectional 25%, 37.5% and 50% Kevlar/XAS composites. Both tension/tension and tension/compression fatigue tests were carried out. The diffusion of moisture into the neat resin, mono-fibre and hybrid composites was also investigated. A detailed investigation into the observed macroscopic and microscopic failure modes was also carried out.

The rule of mixtures was found to adequately describe the tensile modulus of the unidirectional hybrid composites. The rule of mixtures over estimated the tensile strength of the hybrid composites. The fatigue behaviour of the mono-fibre Kevlar and XAS composites were best described by a two-stage and one stage fatigue curve respectively. In general, the fatigue behaviour of the 25% and 37.5% Kevlar hybrids were akin to the fatigue behaviour of the XAS mono-fibre composite. The fatigue response of the 50% hybrid was similar to that observed for the mono-fibre Kevlar composite.

The fatigue performance of the hybrid composite was found to be marginally superior to the mono-fibre composites on a simple rule of mixtures basis. The Dual Mode Sorption model was found to accurately describe the moisture diffusion processes in the neat resin. A 10°C lowering of the glass transition temperature was observed per % of absorbed moisture. The effect of absorbed moisture in the Kevlar and hybrid composites were found to be detrimental when subjected to tension/compression fatigue loading.

ACKNOWLEDGEMENTS

My sincere thanks and appreciation to members of staff, secretaries and colleagues at the School of Materials Science for all the help, encouragement and facilities extended to me during the course of this research programme.

In particular, I would like to thank my supervisors Harry Reiter, Professor Bryan Harris and Tom Adam for their encouragement, guidance, patience and support throughout and beyond the period of the research programme. I also wish to acknowledge the assistance given by the technicians: Peter Wakeford, Peter Taylor, Peter Dicken, Brian Gosling, Simon Bowman and Chris Arnold. The assistance given by Kou Tsai, Bruno Charriere, Chris Jones, Janice Hayward, Dick Dickson, Simon Phillips, and Robin Jones is duly acknowledged. I also wish to thank members of the Electron Optics Department in the School of Materials Science, in particular Hugh Perrott and Kate Powell for their help on the SEM. My thanks are also due to Peter Reynolds, Barry Ford and Mrs. Cox for light relief and entertainment.

Thanks are extended to Drs. Paul Curtis and Graham Dorey of the Royal Aircraft Establishment, Charles Evans of Westlands Helicopters and Drs. David Packham and Martin Ansell of the School of Materials Science for their helpful advice and discussions. The work was sponsored by the Procurement Executive of the Ministry of Defence Under Agreement 2112/052 XR/MAT. The electron optics facilities were funded by the Science and Engineering Research Council.

Last but not least I wish to thank my dear wife for her encouragement, moral support and tolerance over the prolonged writing period of this thesis.

CONTENTS

CHAPTER 3

CHAPTER 4

CHAPTER 5

CHAPTER 6

CHAPTER 7

CHAPTER 8

CHAPTER 9

APPENDIX 1

1.1 INTRODUCTION

Fibre reinforced composites are a class of materials which are among the fastest growing advanced materials. The international market for advanced composites was valued at £1.1 billion in 1986 and is forecast to increase at a rate of 11% annually to reach £2.9 billion by 1996[1]. The aircraft and aerospace industries are the largest end-users of advanced composites. These industries account for about 63% of the worldwide market for advanced composites and the remainder is used by other industries including the automobile and recreational industries. In geographic terms, the United States is the largest user of advanced composites[1].

Table 1.1 outlines a range of properties of some of the major engineering materials. Unidirectional carbon fibre reinforced epoxy composites (cfrp) and aramid reinforced epoxy composites (afrp) exhibit specific tensile strengths that are approximately four to six times greater than that of steel or aluminium. The specific modulus is approximately three to five times that of steel or aluminium. Therefore, in applications where weight is at a premium, the utilisation of fibre reinforced composites can result in significant weight saving[2-3]. Modern military aircraft contain between 10-30% advanced fibre composites but commercial aircraft contain only about 10% advanced fibre composites as a percentage of airframe weight[3]. A 1 Kg weight reduction on a DC-10 aircraft was estimated to save over 2900 litres of fuel per year[4]. Reductions in aircraft weight can result in increased range, speed and/or payload. However, it is worth

noting that a weight reduction as a result of the use of fibre reinforced composites instead of other engineering materials does not always translate into cost savings[7]. Other factors such raw materials and manufacturing costs, damage tolerance, quality control, tooling etc. also need to be considered[7]. Specific examples where composite materials are utilized in the aerospace, marine, automotive and recreational industries are discussed in greater detail, for example, in reference number 3.

Fibres	Specific gravity	Young's modulus (GPa)	Str. (GPa)	Strain to failure (%)	Sp. Str. (GPa)	Sp. Mod (GPa)	Dia. (um)	CTE $*10^{-6}$ $^oC^{-1}$	MST ^oC
E Glass	2.6	72	3.5	3	1.18	27.6	5-25	5	350
S Glass	2.48	85	4.8	5.3	1.94	24.3	5-15	2.9	300
Boron	2.6	440	2.8	1.0	1.08	191	140	4.85	700
HM Carbon	1.96	517	1.86	0.38	0.95	164	8.4	5	600
HS Carbon	1.8	295	5.6	1.8	3.11	164	5.5	5.5	500
Kevlar 49	1.44	135	4.0	2.87	2.78	94	12	-2.0	180
Aluminium	3.95	379	2.1	0.4	0.46	96	20	7.6	10^3
Nicalon SiC	2.8	193	1.5	0.75	0.53	69	12	3.5	$>10^3$
SiO_2	2.5	72	5.9	1.8	2.7	32	3	4	$>10^3$
Steel	7.9	200	2.75	2.5	0.35	25	200	8.5	1200

Table 1.1 Comparison of typical values of the properties of some engineering materials-Compiled from reference numbers 3, 31 and 57. (Sp.Str=Specific Strength; Sp. Mod.=Specific Modulus; Dia. = Fibre Diameter; CTE=Coefficient of Thermal Expansion; MST= Maximum Service Temperature).

In addition to the excellent specific properties of fibre reinforced composite materials, there are also other factors which make them attractive compared with other engineering materials[3].

For example, properties such as the electronic transparency of glass fibre reinforced composites (gfrp), their high specific properties and their ability to form complex shapes have led to their extensive use in airborne warning and control radar systems.

The dimensional stability offered by carbon fibre reinforced composites lends them to use in precision instruments and machines. Fibre reinforced composites (frc) can be tailored to give a broad range of thermal expansion design requirements. The low coefficient of thermal expansion of cfrp and its high specific properties has led to its extensive use in space and missile applications. These include space platforms, shells, pressure vessels and tanks[3].

The fatigue endurance limit for cfrp and aramid fibre reinforced plastics (afrp) can approach 60% of the ultimate tensile strength under tensile loading. However, under reverse loading conditions this superiority is not always maintained. Understanding and characterizing the response of fibre reinforced composites to cyclic loading is of paramount importance as most mobile structures can experience numerous load cycles in their lifetime. Depending on the magnitude of these cyclic loads, micro and/or macro damage can take place leading to a loss in structural performance and ultimately to failure.

One of the major advantages of composite materials is that they can be tailored to meet specific design requirements. This is achieved by orienting the fibres in the direction of expected load and/or by introducing a second fibre type (hybridising). A hybrid composite is a material where two or more different types of fibres are present in a common matrix.

Hybridisation facilitates the engineering of fibre reinforced composites to yield the desired properties which can not be realized by the the utilisation of mono-filament composites. For example, the blending of brittle fibres like carbon with Kevlar or glass fibres has been shown to give significant improvements in the impact properties. Furthermore, the catastrophic failure modes usually associated with brittle fibre composites can be modified by hybridisation with higher elongation fibres to yield a progressive failure mode. The required thermal expansion coefficient, flexural and tensile stiffness can also be tailored to comply with a broad range of design requirements. From an economic viewpoint, hybridisation can result in cost savings in the sense that expensive fibres, like carbon, can be "diluted" with relatively cheaper fibres like glass without compromising too much on the desired properties. A detailed review of the classification and commercial exploitation of hybrid composites was discussed by Summerscales and Short[5,6].

A considerable amount of work has been reported in the literature on hybrids with regards to their impact, tensile and flexural properties[237]. However, there is very little available information relating to the fatigue response of

hybrid composites, especially under tension/compression cycling and elevated temperature cycling. Furthermore, there is only limited information regarding environmental effects on the performance and long term durability of hybrid composites.

1.2 OBJECTIVES

The objectives and aims of this programme were as follows:

(I) Investigate the Fatigue Response of Kevlar/Carbon/914 Mono-Fibre and Hybrid Composites.

(II) Characterize the Failure Modes and Failure Processes of these Composite Materials Under the Imposed Loading Conditions.

(III) Determine If A Hybrid Effect Exists Under Fatigue Loading For The Inter-Ply Kevlar/XAS Hybrid Composites.

(IV) Characterize the Moisture Diffusion Behaviour of these Composites and the Neat Resin.

(V) Define Quality Control Procedures for the Prepregs.

2 CONSTITUENT MATERIALS - LITERATURE REVIEW

2.1 FIBRES

The processing routes and micro-structures of the fibres and matrix used in this programme are of interest, as they may explain and help in the understanding of the various failure modes exhibited under different loading conditions. Furthermore, the fibre and resin composition and micro-structures may also assist in the understanding of the sensitivity of these materials to environmental conditioning.

The fibres used in this programme were XAS, HMS and Kevlar fibres. The XAS/HMS combination was used in the short fibre intra-ply hybrids and the XAS/Kevlar continuous fibres were used in the inter-ply hybrids. The matrix in all the cases was Fiberdux 914.

2.1.1 Carbon Fibres

The element Carbon, atomic number 6, has two allotropes, namely, graphite and diamond. Graphite has a hexagonal structure in which there is strong bonding in the hexagonal-layer planes. However, only weak Van der Walls forces exist in between the planes and hence mechanical properties in this plane are weak. Diamond on the other hand possesses a cubic structure, and does not exhibit a low shear modulus.

Carbon fibres can be made from a variety of precursors, eg. rayon, cellulose, pitch, polyacrylonitrite (PAN) etc. PAN precursors have become the most important source for carbon

fibres[99]. The monomer in the production of PAN is made almost exclusively by propylene ammoxidation.

$$CH_3CH{=}CH_2 + NH_3 + 1.5\,O_2 \text{ ------> } CH_2\,CH{=}CN + 3H_2O$$

Acrylonitrile polymerises rapidly in the absence of inhibitors. Since the monomer is insoluble in the polymer, it precipitates out of solution. PAN fibres are made by a wet spinning process in which, first, a solution of the polymer and an appropriate solvent are spun in a coagulation bath. The fibres are then washed, stretched and dried. In practice PAN is copolymerised with other monomers such as methyl acrylate or vinyl acetate to aid processing because of the high polarity of the nitrile groups which are capable of forming strong intermolecular bonds[97]. A general description of the transformation of acrylonitrile to carbon fibres is illustrated in Figure 2.1 and is based on a discussion presented by Rose[8]. A detailed discussion on the conversion of PAN based precursors to carbon fibres was presented by Jain and Abhiraman[22]. With reference to Figure 2.1, Polyacrylonitrile (I) is stable up to about 180^{o}C, above this temperature it resorts to a thermodynamically more stable form which results in distortion and shrinkage. Therefore, to maintain molecular orientation it is necessary to subject the fibres to accurately controlled tension. The polyimine (II) is stable up to 345^{o}C, above this temperature the oxidation of the polyimine yields a cyclised ladder polymer (III). Subsequent crosslinking of the polyimine is generally termed carbonisation. This is a crosslinking reaction between the cyclised ladder polymer and is carried out between 700-1000^{o}C, leading to the formation of a layered polymer which is well oriented but with poor crystal

arrangements. It is during this stage that the high mechanical properties of carbon fibres are developed. The development of these properties is said to be directly related to the formation and orientation of turbostratic graphite-like fibrils within each individual fibre. These are arranged with their basal planes oriented along the axis of the filament, the degree of axial orientation of these layers determines the modulus of the fibres. The strength of the the fibre is determined by the axial and radial textures as well as by the distribution of flaws. The final stage in this process is graphitisation, where the carbonised product is heated to temperatures between 1000-3000^{o}C. This is said to improve the crystalline structure and orientation of the graphite crystallites within each individual fibre.

[I] PAN

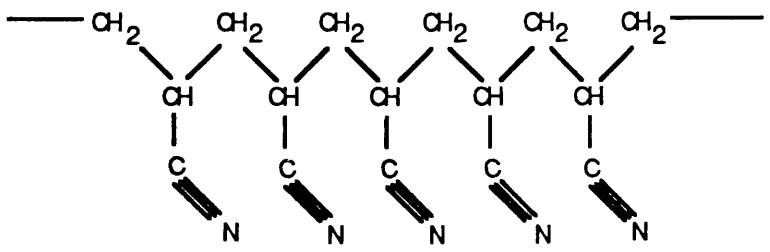

Oriented polymer stable upto 180 °C

II Zipper reaction 180 - 250 °C

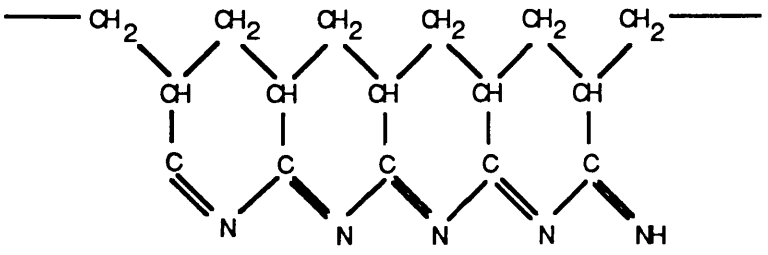

Oriented ladder polymer, stable up to 345 °C

III Oxidation of II to 350 °C

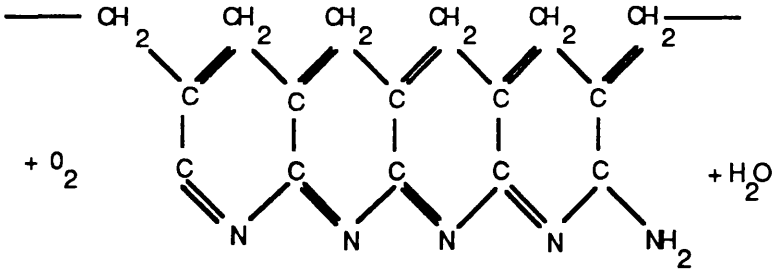

Cyclised ladder polymer which will no longer fuse

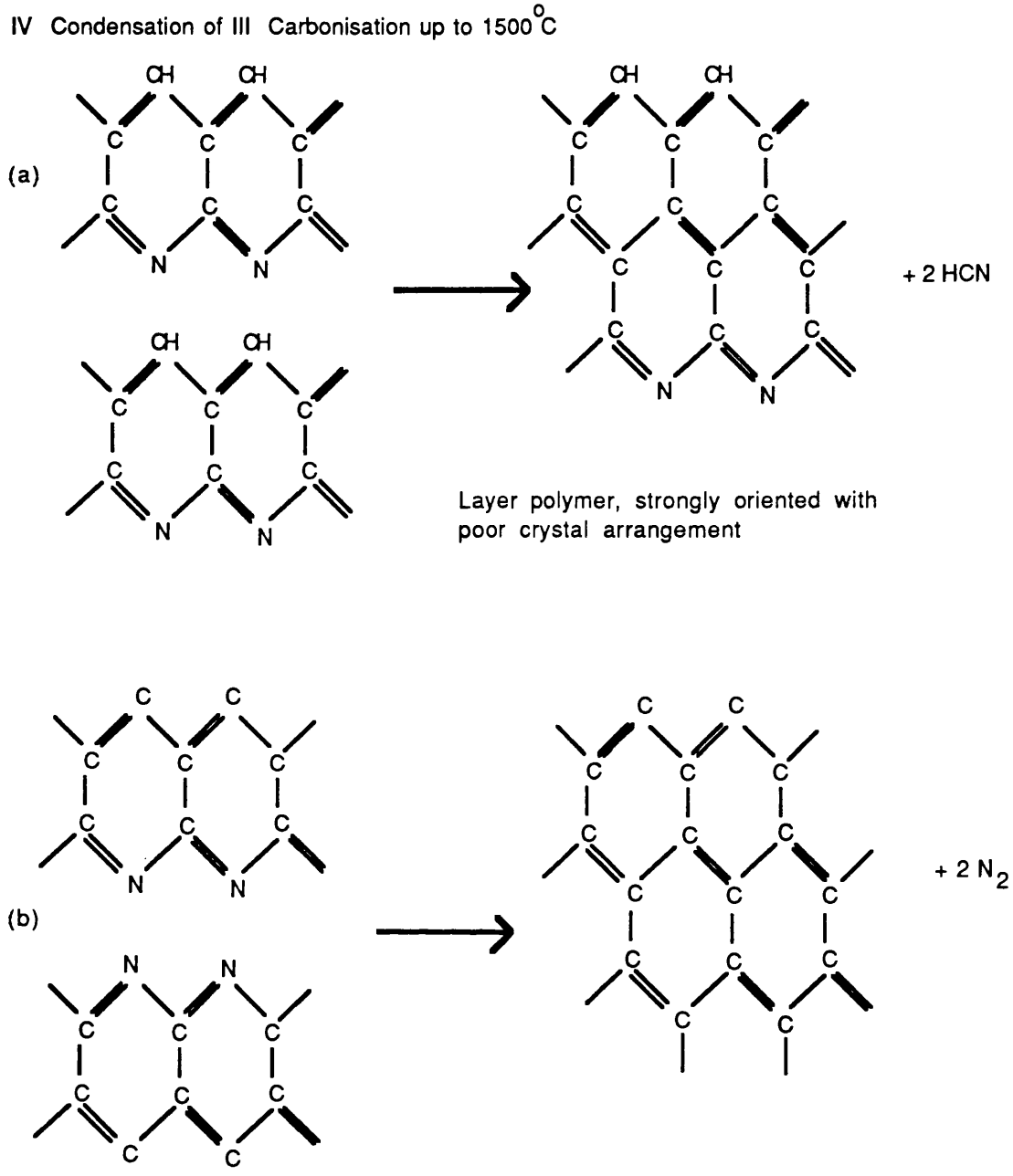

Figure 2.1 Illustration of a possible conversion route of PAN to carbon fibres. Reproduced from reference number 8.

2.1.2 Micro-Structures of Carbon Fibres

The following discussion is based on the excellent reviews presented by Jain and Abhiraman[22] and Donnet and Bansal[170] on the physical and morphological aspects of carbon fibre production from PAN based precursors. Their literature reviews identified five major structural models for carbon fibres.

(1) Circumferential-Radial Model

Kibbs[170] identified three different types of PAN carbon fibre structures for fibres made under different processing conditions. These structures were found to differ in the orientation of the graphitic crystallites within the transverse plane; three main structures were identified, see Figure 2.2(a). Barnet and Norr[253] proposed a three dimensional structural model for high modulus PAN fibres. They based their conclusions from scanning electron microscopy of oxygen plasma-etched fibres. The artifacts produced by this process were interpreted as originating from a highly crystalline sheath surrounding a radial structure of crystalline webs separated by large voids, see Figure 2.2(b).

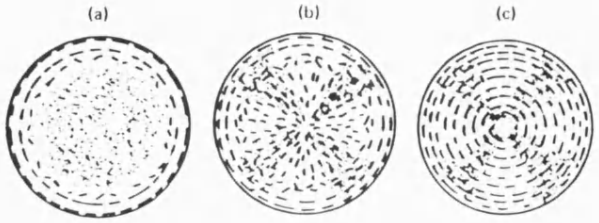

Figure 2.2(a) Kibbs - Schematic representation of carbon fibre structure. (a) Isotropic centre and circumferentially oriented outer skin. (b) The outer layer crystallites exhibit a radial preferred orientation and the central zone has a radial preferred orientation. (c) One type of preferred orientation, ie. circumferential. Reproduced from reference number 170.

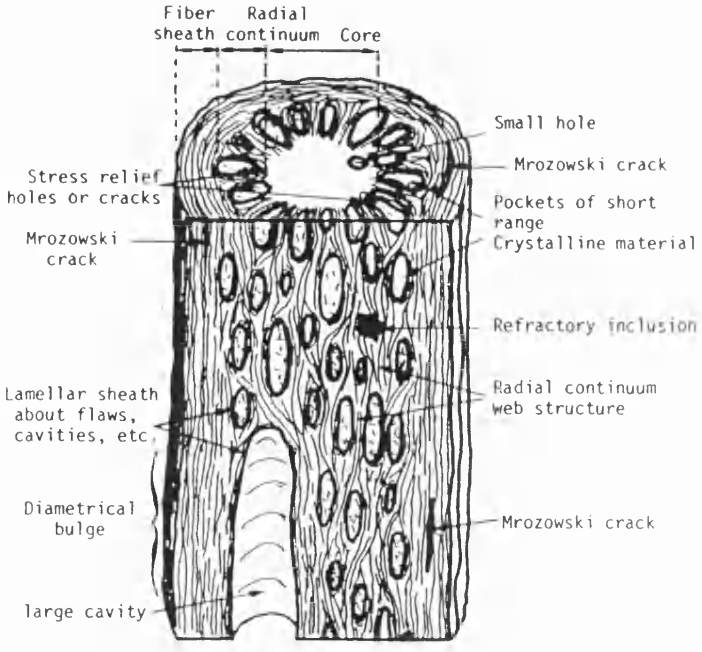

Figure 2.2(b) Skin-core type of structural model of carbon fibres proposed by Barnet and Norr Copied from - Proc. Int. Conf. Carbon Fibres Their Applications, Plastics Institute, p 32, 1974.

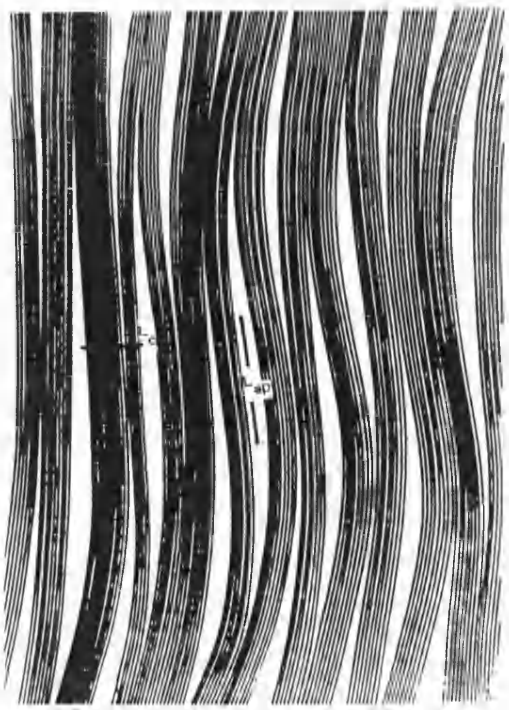

Figure 2.3(a) Ribbon model carbon fibres proposed by Perret and Ruland, J. Appl.Crystvol.3, p 525, 1970.

(2) Microfibrillar Model

Perret and Ruland[254] proposed a ribbon-type structure where the ribbons were described as slowly undulating with straight sections of 6-13 nm. These ribbons were also said to exhibit extensive parallel stacking and pass smoothly from one plane to another. They proposed that needle-like voids are created because of the mismatch in the contours of the microfibrils. These voids were said to be approximately 20-30nm long and 1-2nm in cross-section. A schematic representation of the model proposed by Perret and Ruland is illustrated in Figure 2.3(a). Johnson and Tyson proposed that the idealized structure of PAN-based fibres to consist of arrays of misoriented turbostratic graphitic crystallites stacked approximately end to end in a columnar arrangement forming tilt and twist boundaries between them. The average width of the crystallites was reported to be 6.5nm and the mean width of the voids was estimated to be less than 1nm. A schematic illustration of the model proposed by Johnson and Tyson is presented in Figure 2.3(b).

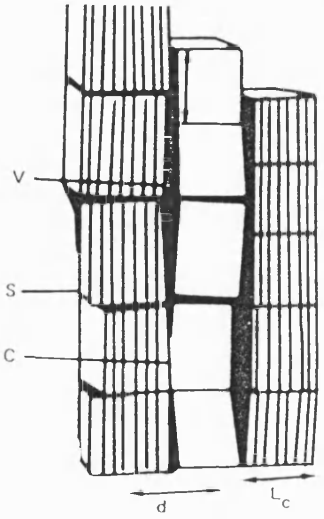

Figure 2.3(b) Johnson and Tyson Schematic illustration of carbon fibre structure with columnar arrangement of misoriented turbostratic crystallites. Copied from ref. no. 170.

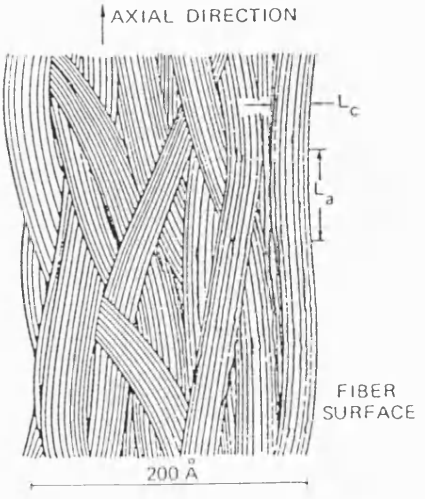

Figure 2.3(c) Diefendorf and Tokarsky- Undulating ribbon structure of carbon fibre (Basket Weave) Polym. Eng. Sci.vol.15, p 150, 1975.

A model similar to that of Perret and Ruland was proposed by Diefendorf and Tokarsky[255], where the structural units of the model were microfibrils made up of 10 to 30 basal planes in the form of ribbons, see Figure 2.3(c). The ribbons were said to have almost zero amplitude and to be parallel to the fibre axis. They suggested that the structure could better be described as a wrinkled sheet. For carbon fibres with a modulus of about $3X10^5$ Nmm^{-2} the ribbons were said to to be typically 13 layer planes thick and 4nm wide. However this was said to increase to 30 layers and 9nm wide for carbon fibres having modulus values of about $7X10^5$ Nmm^{-2}. The microfibril undulation was greater than the wavelength for high strength fibres; however, the amplitude of the undulation decreased as the modulus increased. Oberlin proposed a model for the longitudinal and transverse structure of HMS and HTS PAN-based fibres where the two types of fibres were said to differ only in their radius of curvature of the sheets of aromatic layers. The HMS fibres were reported as having aromatic layers with a large radius of curvature, which decreased from the periphery to the centre of the fibre. The HTS fibres were said to possess a smaller but uniform radius of curvature.

(3) Lamellar Model

Oberlin's[170] lamellar structure for PAN-based carbon fibres is illustrated in Figure 2.3(d).

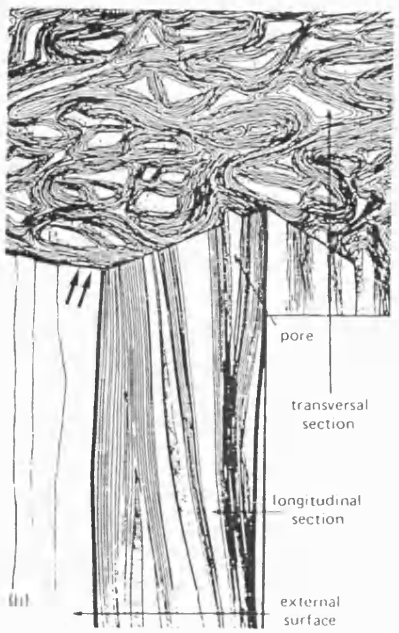

Figure 2.3(d) Oberlin's proposed model. Copied from reference number 170.

(4) Skin-Core Model

Various researchers[170] have postulated that the structure of PAN-based carbon fibres consist of an outer zone surrounded by a darker inner zone. The thickness of the outer zone was found to be a function of the heat treatment time in air during the pre-oxidation stage of the carbon fibre preparation.

(5) Three-Dimensional Models

A three dimensional model was proposed by Bennett and Johnson[256], where the axial orientation was higher at the surface than at the core. The layer planes were shown to inter-link in a highly complex manner, giving rise to a range of crystallite sizes enclosing an intricate void system, see Figure 2.3(e). Diefendorf and Tokarsky[255] proposed a 3-D model by combining the axial and radial structures for PAN-based fibres, see Figure 2.3(f).

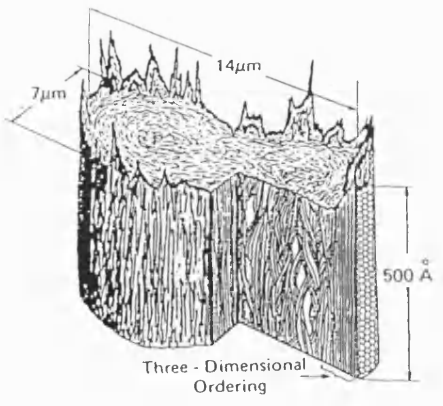

Figure 2.3(e) 3-D model for carbon fibres proposed by Diefendorf and Tokarsky. Poly. Eng. Sci. 15, p150, (1975)

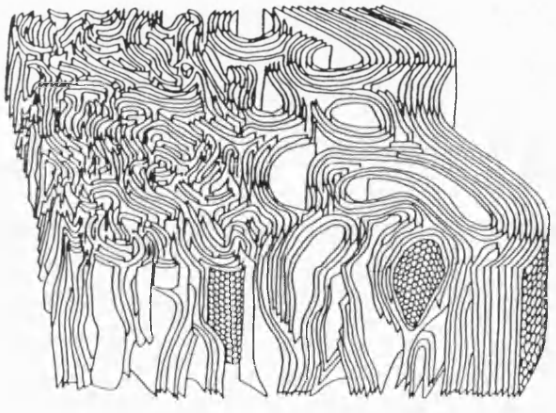

Figure 2.3(f) 3D model by Bennett and Johnson, Proc. 5th London Carbon and Graphite Conf. Vol.1, p 377, (1978).

2.1.3 Kevlar™ Fibres

Kevlar™ is the trade name of a class of aramid fibres manufactured by Dupont. It is made from the polycondensation product of para-phenylene diamine and trephthaloyl chloride at low temperatures to yield poly(p-phenylene terephthalamide)[9] (PPTA), see Figure 2.4.

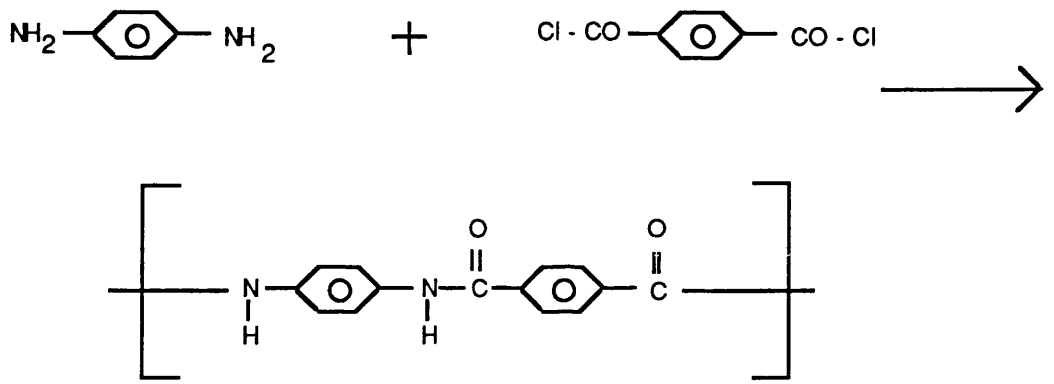

Figure 2.4 Chemical structure of Kevlar [95].

The PPTA fibres are extruded at about 80°C in the form of liquid-crystalline PPTA-H_2SO_4 dopes (~20 Wt.% PPTA) from spinnerets at 0.1-6m/s[93-94,173]. The spinneret face is separated from a 1°C water bath by an air gap of ~ 5mm. The resulting yarn is washed with water, neutralized with NaOH, and subsequently washed with water to remove the Na_2SO_4. The yarns are then dried on rollers at about 65°C under tension and then subjected to further drawing of approximately 0.5% at 550°C. The fibre properties are sensitive to solvent additives, spinning conditions and post-spinning heat treatments[14].

There are two types of Kevlar fibres which have been

extensively used, namely, Kevlar 49 and Kevlar 29. Kevlar 49 has a higher modulus and is used extensively in high performance composites. Kevlar 29 has a comparable strength to Kevlar 49 and is used in areas where toughness, or ballistic stopping ability is required. A recent addition to this family is Kevlar 149, which is an ultra-high modulus fibre [3].

2.1.4 Microstructure of Kevlar Fibres

Like carbon fibres, the structure of Kevlar has been the subject of many investigations. The repeat unit for Kevlar fibres is illustrated in Figure 2.4. Para-oriented aramid fibres (substitutions in the 1 and 4 positions in the benzene ring) can aggregate to form ordered domains in parallel arrays[95]. The presence of the benzene ring inhibits folding of the fibres, and this results in rod like structures. The rigid linear polymer chains are highly oriented in the fibre direction. This in turn gives the fibre its high modulus. In the transverse direction, the polymer chains are only bonded by relatively weaker hydrogen bonds and hence the transverse properties are significantly weaker. A number of theories have been put forward for the micro-structure of Kevlar fibres, a summary of these proposed structures are discussed below.

M. G. Dobbs et al[10-13], in a series of papers, proposed a structure for Kevlar as possessing radially oriented but axially pleated sheets. Each sheet was said to be composed of an array of extended molecular chains stablised laterally by hydrogen bonds, see Figure 2.5. Each component of the pleat was said to be about 500nm long and separated by short

transitional bands. Dobb et al[13] used a staining technique to determine the presence of microvoids. Their technique involved first treating the fibres with gaseous hydrogen sulphide, followed by a silver nitrate solution. The presence of the deposited silver sulphide in the fibre section was taken to be an indicator of microvoids. They presented micrographic evidence, which indicated the possible presence of rod-shaped microvoids with their long axis almost parallel to the fibre axis. These microvoids were typically, 25nm long and 5.6nm wide. They also found silver sulphide aggregates, 16um long and 0.8um wide near the centre on the fibres. Hagege et al[96] confirmed the radially arranged pleated structure of Kevlar and also found voids in the pleated sheet lamelle. Their staining studies revealed the possibility of a skin-core type structure for Kevlar.

Morgan et al[14,15] carried out an extensive investigation into the production, structure and deformation modes of PPTA fibres and they proposed a "chain-end model" for PPTA fibres, see Figure 2.6(a). In this model the chain ends are randomly distributed in the fibre exterior but progressively become more clustered in the interior. This results in a fibre outer layer "skin" with continuous structural integrity in the fibre direction and a core which consists of periodic transverse weak planes that occur about every 200 nm. The model assumes that the outer layer of the fibre is less crystalline than the core.

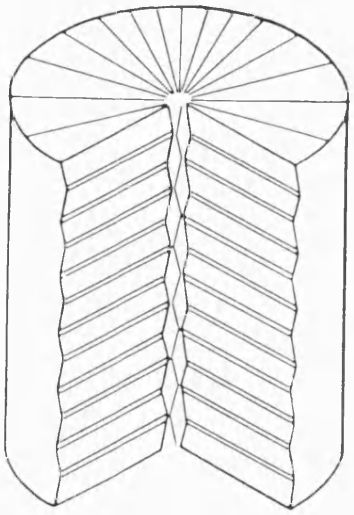

Figure 2.5 Schematic diagram of Kevlar 49 fibres showing the radial arranged pleated sheets, proposed by Dobb et al [10-13].

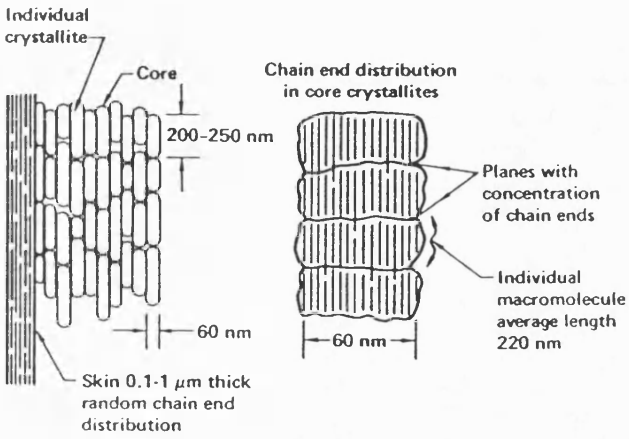

Figure 2.6(a) Chain-end distribution in PPTA fibres, proposed by Morgan et al [14].

Morgan et al[14] utilized the chain-end model to account for the deformation and failure processes of Kevlar fibres, see Figure 2.6(b). The preferred crack propagation path is parallel to the rods because this only requires the rupture of hydrogen bonds. The skin was said to exhibit a more continuous structural integrity in the fibre direction than the core, and the core to fail more readily by transverse crack propagation. Any damage to the skin during fabrication or low-stress-level deformation of the composite was said to weaken the Kevlar fibre[15].

Panar et al[16] extended the chain-end model and proposed a fibrillar morphology for PPTA fibres with the individual fibrils having a high proportion of extended chains passing through periodic defect layers. A pleated structure is said to be superimposed on this. They attribute the superior

properties of Kevlar fibres, as compared with other organic fibres, to the high level of extended chains passing through the defect layers in the Kevlar fibre structure, see Figure 2.7(a). They suggest that the surface fibrils are uniformly axially oriented, whereas the fibrils in the core are imperfectly packed and ordered, see Figure 2.7(b).

Li et al[171] proposed that the Kevlar fibre structure was composed of a skin-core structure. The core was said to be characterized by a layered structure with layers stacked perpendicular to the fibre axis. The layers were reported to be composed of rod-shaped crystallites with an average diameter of about 50nm with the length showing a molecular weight dependence. The strength of the fibre was said to be due to the extension of some of the crystallites through two or more layers, see Figure 2.8.

The effects of impurities in Kevlar fibres as a result of the manufacturing process and its effect on the failure modes were discussed by Prueda[173]. They concluded that the major impurity in Kevlar fibres was Na_2SO_4 which was said to reside between fibrillar crystals and in microvoids formed during fibre fabrication, see Figure 2.9.

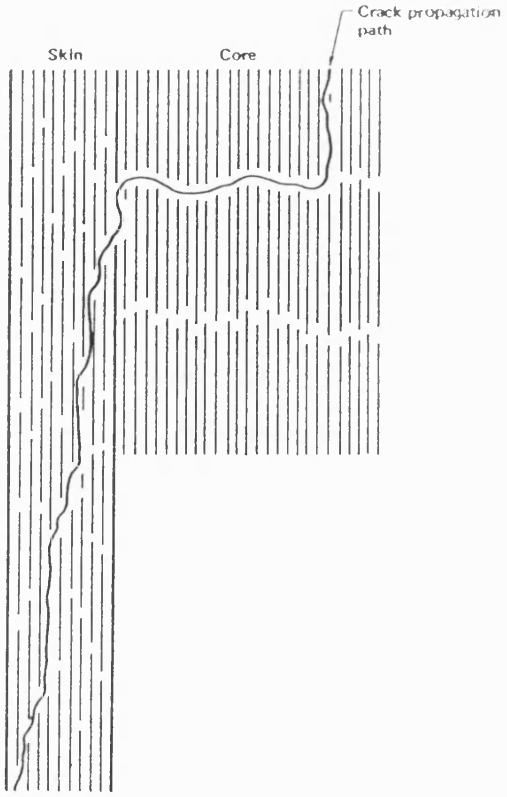

Figure 2.6(b) Crack Propagation path in 2-D through macro-molecular chain ends in fibre skin and core in Kevlar fibres. (Reference no.14)

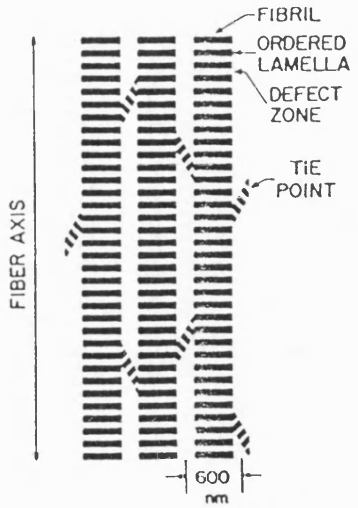

Figure 2.7(a) Schematic illustration of the fibrillar structure of Kevlar fibres. Proposed by Panar et al[16]

Pruneda et al[173] also carried out a detailed investigation into the deformation modes and failure of Kevlar fibres and composites. They concluded that Kevlar fibres fail in tension by axial splitting 20 to 50 times their diameter along their length. Hydrolytically degraded Kevlar fibres were reported to exhibit a lower fibre split length and a correlation was observed between the percentage of fibres that exhibited transverse failure without splitting and the composite strength. They observed skin deformation bands in the fibres under tensile loading and these features were apparently different to those reported for compression induced kink bands (no details were reported). Figure 2.10 illustrates a schematic failure path for the Kevlar fibre as reported by Pruneda et al[173].

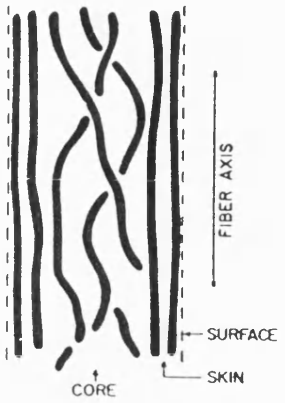

Figure 2.7 (b) Schematic of the fibrillar orientation in the skin and core. Reference no.16.

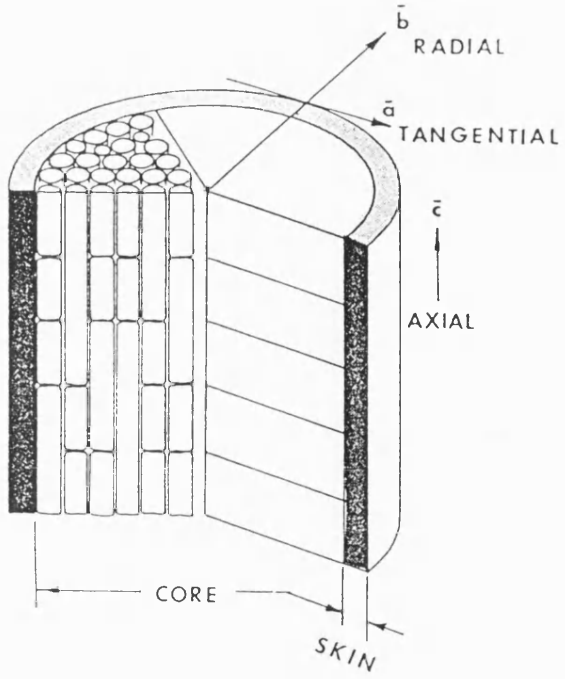

Figure 2.8 A model for polyamide fibre structure, proposed by Li et al[171].

Pruneda et al[172] stated that the drying process during the manufacture of the Kevlar fibres can result in severe skin deformations. Apparently, the shrinkage upon drying causes skin-core radial and hoop stresses and this causes longitudinal kinking of the fibrillar crystallites.

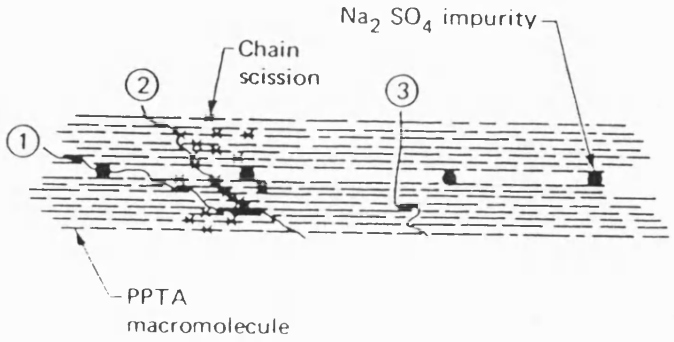

Figure 2.9 Modes of crack propagation through aligned aggregates of PPTA macromolecules. (1) Crack propagation through hydrogen bonds and original macromolecular chain ends. (2) Crack propagation path is modified by chain scission. (3) Crack propagation across chain ends. (Reference 15).

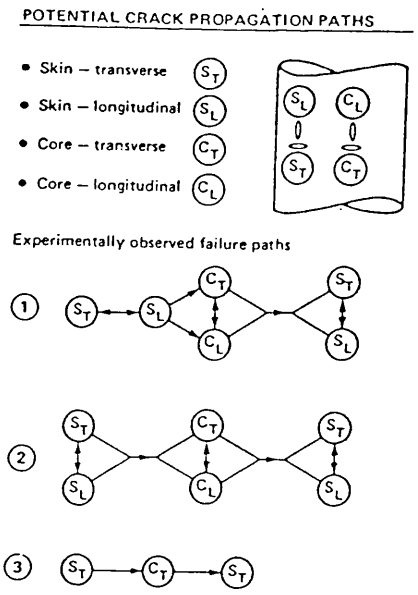

Figure 2.10 Schematic of Kevlar 49 single filament failure paths. (Reference 173).

2.2. THE MATRIX

2.2.1 Resin System

The correct selection of resin systems for composites is as important as the choice of fibre type for a specified application. The main difficulty in the selection of a matrix resin is that matrix mechanical properties do not transfer to composite mechanical properties in a parallel manner[17].

The resin system used in this programme was BSL 914 as supplied by Ciba-Geigy. This resin was a based on a blend of Ciba-Geigy MY 720. BSL 914 has been selected for the British Aerospace demonstrator program. The disclosed composition of MY 720 blend is reported to consist of the following

constituents :

(a) Tetraglycidyl methylenedianiline (TGMDA) (~37%)

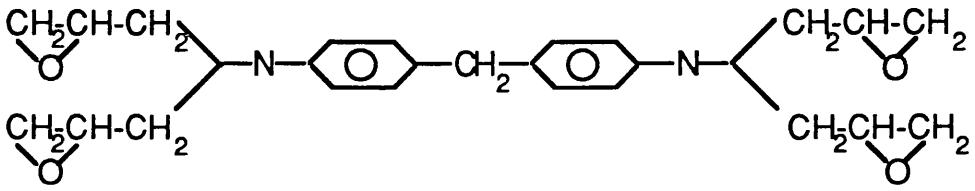

(b) Triglycidyl p-aminophenol (TGAP) (~36 %)

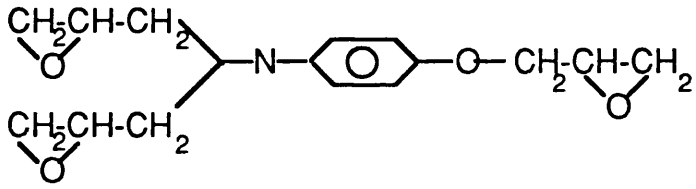

(c) Polyether sulphone (PES) (~22 %)

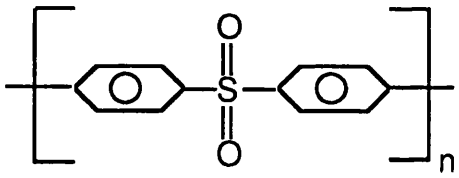

(d) Dicyandiamide (DICY) (~5 %)

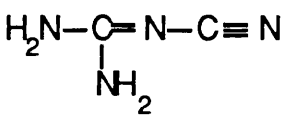

The tetrafunctional epoxy, TGMDA is one of the main constituents of MY 720 along with (TGAP). The viscosity characteristics of the resin system are obtained by chemical formulation and not by B-staging the resin [175-177]. The

viscosity modifier is a thermoplastic component, Polyether sulphone (PES). PES is insoluble in TGMDA; however, it is soluble in TGAP. On curing, the PES is thrown out of solution and appears as a fine second phase network. The trifunctional epoxy, TGPA, also acts as the reactive diluent in the resin system and forms an integral part in the crosslinked structure.

The curing agent in the BSL 914 was DICY. It was present as fine crystalline particles dispersed in the epoxy resin. DICY dissolves in the epoxy resin at around 120^{o}C, hence at room temperature it is relatively inactive as far as reacting with the epoxy groups are concerned.

2.2.2 Curing

Epoxy resins are a general class of materials characterized by a chemical structure containing the epoxide ring or oxirane ring. This ring structure is highly strained and will readily react with proton donors.

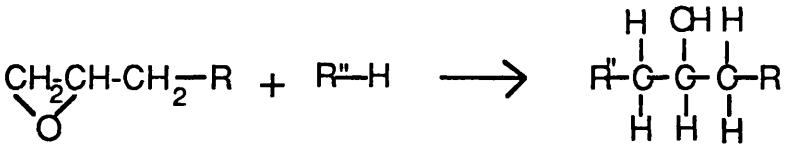

The curing of the resin begins by the formation and linear growth of chains which then branch out and crosslink. As the reaction proceeds, the molecular weight increases rapidly and eventually several chains become linked together to yield a highly crosslinked structure. This irreversible

transformation from a viscous liquid to an elastic gel and then to a glass begins to occur as the Tg of these growing chains becomes coincidental with the cure temperature.

The cure chemistry of epoxy/DICY resin systems is very complex and has been the subject of many investigations. Saunders et al[174] proposed a two-part cure mechanism. The first part of the cure mechanism involved 2 exothermic reactions where the epoxy ring is opened and crosslinked through the active hydrogens of the amine ($-NH_2$) and imino (=NH) groups in the DICY curative. Esterification or self-polymerisation was also said to be possible.

(A) N-Alkyl Cyanoquanidine formation

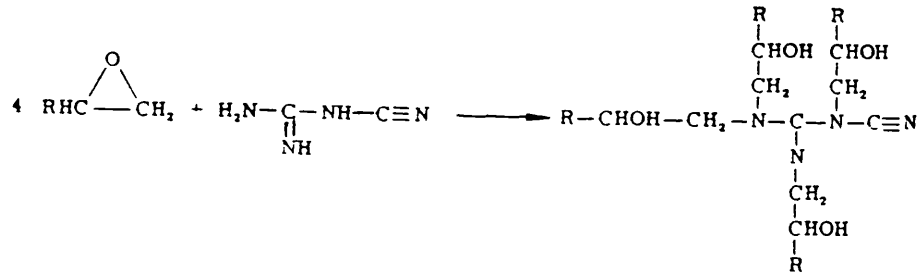

(B) Esterification

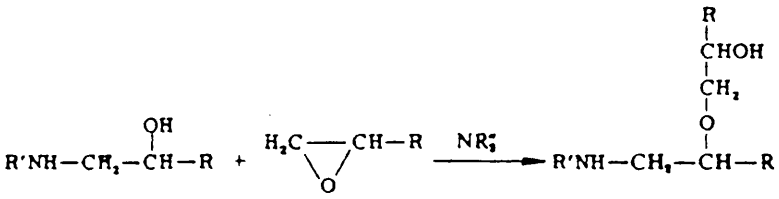

The second part of the cure mechanism takes place at temperatures above 180°C and involves the addition of hydroxyl hydrogens across the nitrile triple bonds to produce

guanyl urea.

(C) Guanyl Urea From Post Cure Reaction

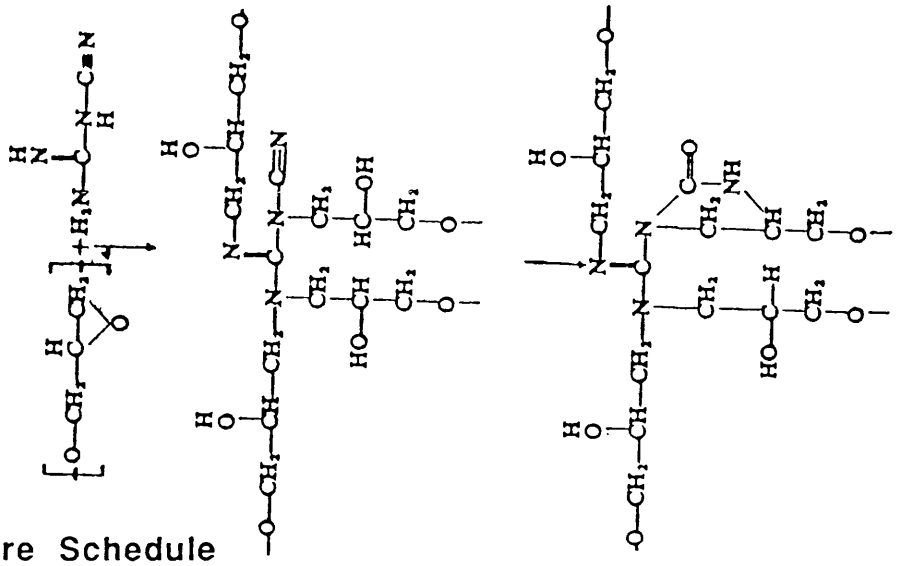

2.2.3 Cure Schedule

The recommended cure schedule for BSL 914 is as follows:

(1) Heat from ambient to 120°C at 2°C per minute under vacuum;

(2) Apply a pressure of 80 PSI and resume heating to 180°C;

(3) Hold at this temperature for 4 hours;

(4) Post cure for 8 hours at 190°C;

(5) Cool to ambient prior to removing cured composite panels.

The T_g of fully cured BSL 914 resin was evaluated in this programme to be approximately 175-180°C, this agrees with the T_g quoted by the manufacturer of the resin.

2.3 HYBRID FIBRE COMPOSITES - LITERATURE REVIEW

2.3.1 Hybrid Composite Classifications

A hybrid fibre composite is defined as a composite material composed of more than one fibre type in a specified resin matrix. Hybrid composites can be classified into four main categories:

(A) Intraply Hybrids - This class of hybrids consists of two or more types of fibres intimately mixed in the same ply. Only short fibres are normally utilized in this category of hybrids.

(B) Interply Hybrids - In these hybrids, the individual plies are of one fibre type. The composite is built up by stacking plies of other fibre types in a required stacking sequence.

(C) Fibre Skin and Core Hybrids - These hybrids consists of outer skins of one or more types of fibre laminates applied to a core made of another fibre laminate.

(D) Fibre Skin, Non-Fibre Core Hybrids- These consists of fibre skins applied to a core of foam, filled resin, honeycombe etc..

2.3.2 The Hybrid Effect

Apart from the economic and design advantages offered by

hybrid composites, hybrids have provoked a considerable amount of research aimed at answering two basic questions: does the "Hybrid Effect" exist and if so, what are the reasons for it? There are two schools of thought with regards to the definition of the hybrid effect. Some researchers define the hybrid effect as the enhancement of the failure of the low elongation fibre, (in a low elongation/high elongation hybrid composite), compared to the failure strain of the low elongation mono-fibre composite. The percentage difference in the failure strains is referred to as the hybrid effect. The assumption made here is that the low elongation fibre in the hybrid composite behaves in a similar manner to that of the low elongation mono-fibre composite. The other school of thought uses the rule of mixtures (ROM) as the basis for establishing the existence of the hybrid effect. The assumption made here is that the hybrid property in question follows a parallel rule of mixtures and any positive deviation from this is taken to represent the hybrid effect.

2.3.3 Evidence For The Hybrid Effect

Hayashi[24] has been credited with the discovery of the hybrid effect. He found that the first fracture stress and strain for unidirectional carbon/glass hybrid composite was 37% and 45% higher respectively than that predicted by the ROM. He attributed this increase to retardation of the fracture of the carbon fibres as a result of the carbon fibres being surrounded by a material of greater ducility, i.e. the glass fibres.

Kalnin[27] evaluated carbon/glass hybrids with varying fibre volume fractions. He found that the failure mode changed from a catastrophic mode for hybrids with a high volume fraction of carbon to a non-catastrophic mode for hybrids with a high volume fraction of glass. Kalnin also found that the initial fracture strain of the carbon fibres in the hybrid was greater than that of the carbon fibres in the mono-fibre composite and this effect was seen to increase with increasing ratio of glass to graphite. In contradiction to Hayashi's findings, Kalnin found that the elastic modulus in the high glass volume fraction hybrid was higher than predicted by the ROM.

Hancox and Wells[28] found that the impact energy for a 50:50 carbon fibre-glass core sandwich structure was between 2.5-5 times higher than that of an all carbon fibre composite of the same volume fraction. They attribute this to the extra strain energy that can be stored in the glass fibre core and to the extensive delamination and resin failure that can occur in the area.

Bunsell and Harris[29] reconsidered Hayashi's work and found that for a carbon/glass hybrid, the initial modulus was in agreement with the ROM upto the fracture of the carbon fibres in the hybrid, and likewise they found that the failure strain of the carbon fibres in the hybrid at this point was greater than that of the carbon fibre failure strain in the all carbon composite. They attributed the hybrid effect in part to the residual compressive stress induced in the carbon fibres during manufacture of the hybrid composite. Bunsell and Harris estimated the residual strains to be (- 0.029) %

and (+ 0.05) % in the carbon and glass respectively.

Even under conditions of no external load, stresses can build up in a composite as it is cooled down from the post-curing temperatures. These thermal stresses originate from the mismatch in the coefficients of thermal expansion (cte) between the two components. The magnitude of the thermal stress will depend on the; (i) difference between the expansion coefficients, (ii) the difference between ambient and the cure temperature (ΔT), and (iii) the proportion and relative stiffness of the two components. The thermal strain (ε^t) is equal to the product of the coefficient of thermal expansion and the difference between the stress free and service temperatures.

$$\varepsilon^t = \alpha \Delta T \qquad [2.1]$$

Consider the case when a hybrid is cooled from the post-cure temperature: As the hybrid cools, the component with the lower cte will be put into compression, and the other component will be put into tension, the result is shear stress generated at the interface[30,31]. A force balance for equilibrium conditions, with no external load (P) on the composite is given by equation [2.2].

$$P = P_H + P_L = \sigma_H A_H + \sigma_L A_L \qquad [2.2]$$

Where: (σ) is the tensile or compressive stress; (A), is the fractional cross sectional area and the subscripts H and L represent the components with the higher and lower CTE, respectively. Equating strains per unit length gives equation [2.3]

$$\frac{\sigma_H - \sigma_L}{\frac{}{E_H} - \frac{}{E_L}} = (\alpha_H - \alpha_L)\,\Delta T \qquad [2.3]$$

Solving for (σ_L) gives equation [2.4]

$$\sigma_L = -(\alpha_H - \alpha_L)\,\Delta T \frac{E_L V_H E_H}{E_L V_L + E_H V_H} \qquad [2.4]$$

The effective temperature at which the resin fully solidifies may not necessarily be the maximum cure temperature, and furthermore some degree of relaxation may be possible during the early stages of cure.

Aveston and Sillwood[32] found a 100% increase in effective fibre strength for the carbon fibres in a carbon/glass hybrid composite. They adopted an energetic argument to account for the observed increase in strength of the carbon component as a result of hybridisation. Aveston and Sillwood derived expressions for the failure strains of the low elongation component in a unidirectional hybrid assuming (a) the existence of a perfect fibre/matrix bond and (b) the presence of a sliding frictional bond. In the first case they calculated the minimum fibre strain at which sufficient work of fracture will be available to allow the fibres to fail; equation [2.5].

$$(e_{le})^2 = 2\partial_f / E_f(1+1/\alpha)\, rf * (G_m/E_f)^{0.5} * V_f^{0.25}/(1-V_f^{0.5})^{0.5} \qquad [2.5]$$

Where; (e_{le}) is the minimum strain at which the low elongation component can fracture, (G_m) is the shear modulus

of the matrix; (α) was defined as $(E_m V_m)/(E_f V_f)$. ∂_f is the surface work of fracture of the fibre and r_f is the fibre radius.

For the second case they calculated the strain to failure of the low elongation component making an assumption that a sliding frictional bond was present between the fibre/matrix; equation [2.6].

$$(e_{le})^2 = 6\partial_f \alpha V_m/(X' E_c) \qquad [2.6]$$

Where X' is the critical fibre length, ie. the distance from the crack needed for the stress in the fibre to build up to its original value. The shear strength (τ) was assumed to be constant.

$$X' = e_{le} E_f r_f/2 \tau \qquad [2.7]$$

According to equation [2.5] and [2.6], for a maximum hybrid effect the brittle fibres have to be as thin as possible; present in low quantities and be distributed evenly throughout the matrix. Aveston and Sillwood define the failure strain as the strain at which the low elongation component undergoes multiple fracture with a defined crack spacing. Good agreement was found between the experimental results for a unidirectional carbon/glass hybrid and the debonded theory. They also speculated that the intervening glass fibres enhanced the failure strain of the low elongation component by inhibiting catastrophic crack propagation as a result of the failure of a few of the low elongation fibres.

Zweben[36] proposed a statistical model to describe the tensile strength of unidirectional hybrid composites consisting of two-dimensional arrays of alternating low elongation and high elongation fibres in a common matrix. The influence of statistical fibre tensile strain characteristics, and fibre extensional moduli and cross-sectional areas were analysed and the differences between failure mechanisms in hybrids and mono-fibre composite were also considered. The approach taken by Zweben was essentially similar to that previously developed for mono-fibre composites by Rosen and Zweben[33-35]. Zweben limited his model to hybrids with a volume ratio of one to one in which the two fibre types were fully dispersed. As the fibres are loaded, failure was said to occur at points of imperfections along the fibres; it was assumed that at a given load there would be more broken low elongation fibres compared to high elongation fibres because the low elongation fibres have significantly lower ultimate failure strains. It was also assumed that the fibre break propagation in the low elongation fibres would be arrested when the crack reached the high elongation fibres. Each individual fibre in Figure 2.1 was treated as an impregnated yarn.

Zweben stated that, when an low elongation fibre breaks at a strain level (ε), the two high elongation fibres immediately adjacent to it are subjected to a strain concentration of intensity $k_h\varepsilon$, where k_h is the strain concentration factor for the hybrid material associated with a single broken low elongation fibre. Therefore, the stress in the high elongation fibres next to a broken low elongation fibre increases from $E_{he}\varepsilon$ to $k_h E_{he}\varepsilon$ due to the break. Now this strain concentration on the high elongation fibres (in the immediate vicinity of the failed low elongation fibre)

increases its probability of failure. As the strain is increased, the number of scattered low elongation fibre breaks increase along with the strain level in the over stressed regions of the high elongation fibres in the vicinity of low elongation fibre breaks. Finally, the high elongation will start to fail at the points of these strain concentrations. Zweben postulated that failure resulted from the propagation of fibre breaks caused by localized strain concentrations. Therefore, the strain at which the first over-stressed high elongation fibre is expected to break is a lower bound on the ultimate strain of the hybrid composite.

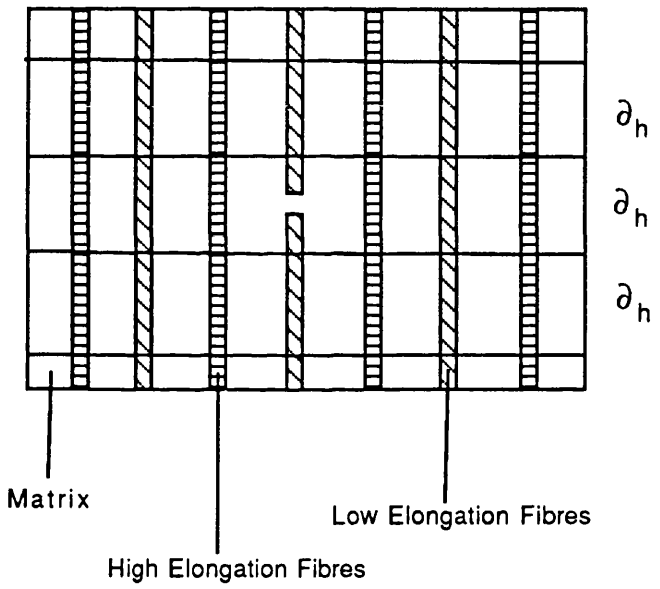

Figure 2.1 Model For Tensile Strength Analysis Of Hybrid Composites [36].

Zweben derived expressions which approximate the ratio of the lower bounds on the failure of a hybrid to that of a composite that contains only low elongation fibres, equation [2.8].

$$R_e = \frac{\left[prL\partial_h \left(k_h^{s} - 1\right)^{-1/(q+s)} \right]}{\left[2p^2 L\partial \left(k^{q} - 1\right) \right]^{-1/2q}} \qquad [2.8]$$

Where p,q and r,s are Weibull parameters of the low elongation and high elongation fibres respectively. L represents the specimen length, ∂ and ∂_h are the ineffective lengths and k and k_h are the strain concentration factors of the low elongation fibres in the mono-fibre composite and the hybrid respectively.

$$\partial = 1.531 \left((E_{le} A_{le} d) / gh\right)^{0.5}$$

$$\partial h = (2 / p^{0.5}) \left((E_{le} A_{le} d)/Gh\right)^{0.5} (m^2_{he} - m^2_{le}) / m_{le}(2-m^2_{le}) - m_{he}(2-m^2_{he})$$

$$k = 1.293$$

$$k_h = 1 + (m_{he}-m_{le}) / m_{le}(2-m^2_{le}) - m_{he}(2-m^2_{he})$$

Zweben pointed out that the expressions for ∂_h and k_h can be greater or less than the corresponding values for a low elongation mono-fibre composite, depending on whether the ratio of fibre extensional stiffness, p, is greater or less than one. Since p is independent of fibre strength properties, in principle, it is possible to construct hybrids with lower bounds on failure strain that are higher or lower than that of a low elongation mono-fibre composite. The ratio derived in equation [2.8] depends on the mean breaking strain of the fibres and therefore, the result is for the mean breaking strain of the hybrid. Zweben does not address the question of the initial failure strain of the low

elongation fibres in the hybrid composite. He readily admits the need for a more refined model for hybrids.

Fukuda[41] advanced Zweben's analysis on hybrid composites and obtained good agreement with various researchers' experimental data. As discussed previously, Zweben considered the failure of a high elongation fibre immediately adjacent to a broken low elongation fibre. Fukuda argued that when one low elongation fibre is broken under the applied load, the next failure is expected on the adjacent low elongation fibres and not on the adjacent high elongation fibre because the failure strain of the high elongation fibres is much greater than that of the low elongation fibres. Fukuda defined the hybrid effect as the enhancement of the initial failure strain of the low elongation fibres.

Manders and Bader[37-39] carried out a systematic and detailed investigation into the static strength and fracture behaviour of hybrid composites. Like Zweben, they too adapted a statistical approach in trying to model the strength of hybrid composites. They defined two parameters for hybrids, namely the hybrid ratio and the state of dispersion. The hybrid ratio was defined as the proportion of a specified fibre type to the total amount of fibre in the hybrid composite. Dispersion was defined as the reciprocal of the smallest repeat unit of the laminates. Their definition of the hybrid effect was; the apparent increase in the failure strain and hence the strength of the low elongation fibres in the hybrid when compared to the mono-fibre low elongation composite. The hybrid effect was expressed as the percentage increase of the failure strain of the low elongation component in the hybrid compared with that of an all-low

elongation composite. However, in adopting the Manders and Bader's approach, careful consideration needs to be paid to the mono-fibre low elongation composite failure strain.

Like previous researchers, they found that a greater hybrid effect was observed in a carbon/glass hybrid when the carbon (low elongation) was more finely dispersed and occupied a lower proportion of the volume. In the all-glass composites, failure was initiated by longitudinal splitting which progressed to disintegration at final failure. However, the all-carbon composites failed by the propagation of a single transverse crack with limited longitudinal splitting. The failure modes observed in the carbon core glass sandwich hybrids included principal transverse cracks in the carbon plies which ran across the whole width and thickness. A delamination crack was also produced at the intersection of the transverse crack with the outer glass plies. The extent of delamination varied according to the specimen geometry, and was greater when the carbon ply was thicker and/or the glass plies were thinner. In the hybrids, catastrophic failure mode of the all-carbon composite was avoided.

An interesting observation from Manders and Bader's work was that both the all-carbon controls, ie. mono-fibre composites, showed a relationship between the composite thickness and first failure strain. The thicker laminates failed at higher strains; about 20% higher for each doubling of laminate thickness up to 12 plies.

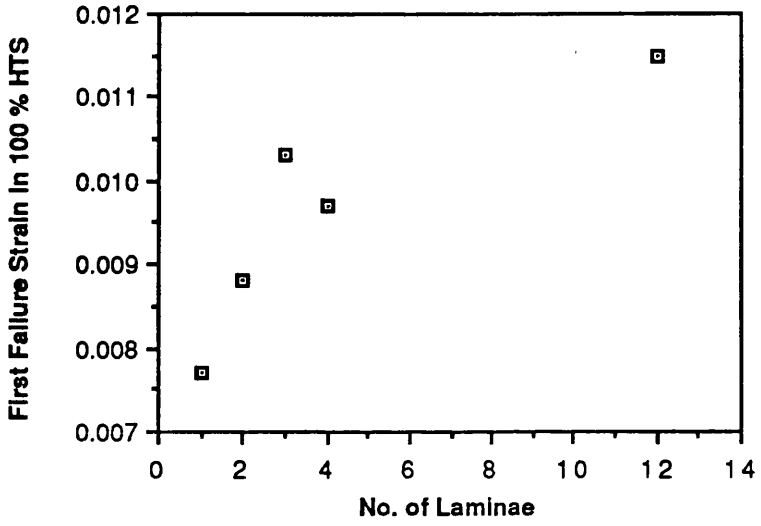

Figure 2.2 Observed relationship between the first failure strain of a HTS/epoxy composite versus number of plies. Data were obtained from reference number 37.

Manders and Bader reported that this relationship between the composite thickness and the first failure strain could not be explained; however, they proposed that the dependence of the first failure strain on the composite thickness may be due to imperfect fibre alignment in the prepregs. Obviously, the first failure strain dependence on laminate thickness should have been investigated further because the all-carbon composite was used as the baseline in their definition of the hybrid effect.

Manders[39] concluded that the hybrid effect arose from the inability of the mono-fibre carbon composite to attain its full tensile strength rather than from an enhancement of the carbon fibre strength in a hybrid composite.

Xing et al[42] proposed a dynamic explanation for the hybrid effect. They pointed out that various researchers had observed acoustic emission activity during the failure of the low elongation component. They stated that it is the dynamic stress state that should be considered instead of the static stress state. They evaluated the dynamic stress concentration factor in a hybrid composed of high elongation and low elongation fibres. For the low elongation fibre in a hybrid, it was shown that the stress concentration factor (k_{Hy}) was less than or equal to the stress concentration factor of the all-low elongation fibre composite, (k_{LE}). Therefore, in the latter case, at the level of uniform fibre axial stress of ∂_a, the local stress next to a fibre fracture could be magnified to the ultimate tensile strength resulting in fibre failure propagation. In the case of the low elongation fibre in the hybrid, the stress magnification may not reach the ultimate tensile strength because $k_{Hy} \leq k_{LE}$. As a result of this, fibre failure does not propagate as readily in hybrids as in the parent composite and the hybrid effect is realized.

2.3.4 Rule of Mixtures (ROM) - Elastic Properties

Under tensile loading, the ROM for the initial Young's Modulus (E) for a unidirectional monofibre composite is described by equation [2.9], where c,f and m represent the composite, fibre and matrix respectively.

$$E_c = E_f V_f + E_m (1-V_f) \quad .....[2.9]$$

The assumptions made in deriving equation [2.9] are:

(a) A perfect interfacial bond strength is assumed;

(b) Both the fibres and the matrix behave elastically;

(c) The Poisson's ratio for the fibre and matrix are the same;

In the case of a two-fibre, eg. Carbon(c)/Kevlar(k), unidirectional hybrid composite tested in tension in the fibre direction, both the fibres will experience the same strain level. Therefore, both the fibres will contribute to the hybrid modulus in proportion to their respective fibre volume fractions, equation [2.10], where HY,c and k represent the hybrid, carbon and Kevlar respectively. The matrix contribution is ignored.

$$E_{HY} = E_C V_C + E_k V_k \quad .....[2.10]$$

Various researchers have found that the primary modulus of hybrid composites is reasonably predicted by equation [2.10] and graphical illustration of equation [2.10] is presented in Figure 2.3.

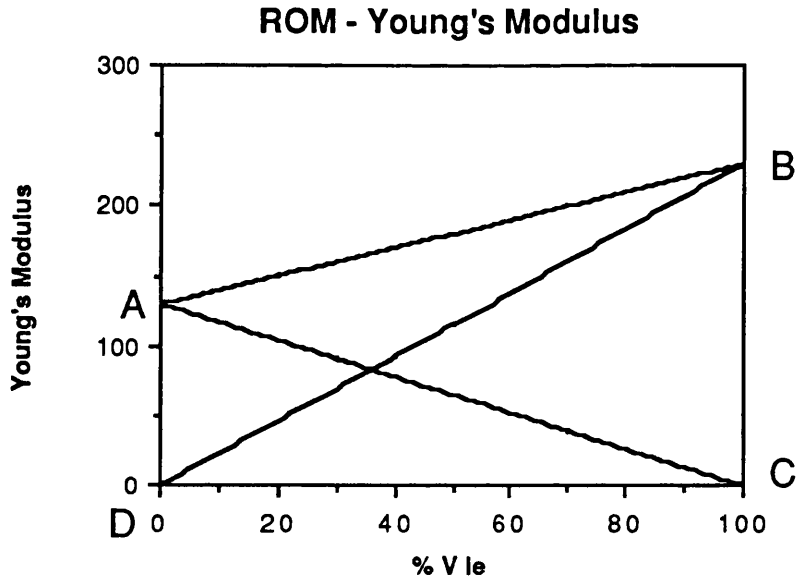

Figure 2.3 Graphical representation of the rule of mixtures equation.

2.3.5 Rule of Mixtures (ROM) - Tensile Strength

The rule of mixtures can be applied to unidirectional, continuous fibre hybrid composites to estimate their ultimate tensile strengths [25]. From here on, until otherwise stated, carbon fibres shall be referred to as the low elongation component (LE) and Kevlar or glass fibres shall be defined as the high elongation component (HE) in the hybrid composite.

Consider the case where HE fibres are mixed with LE fibres in a hybrid composite. For a 100% HE composite, the tensile strength from the ROM can be described by equation [2.11], the matrix contribution is ignored.

$$\sigma_{HY} = \sigma_{HE} V_{HE} \qquad [2.11]$$

The introduction of LE fibres into the HE fibre composite can have two possible outcomes on the tensile strength of the hybrid composite depending upon the relative volume fractions of the fibres. At high V_{HE} the extra load imposed on the HE fibres when the LE fibres fail is not sufficient to cause failure of the HE fibres and the hybrid tensile strength can be represented by equation [2.11]. On the other hand, at relatively high V_{LE} fibres when the LE fibres fail, the load is transferred to the HE fibres, but they are incapable of supporting this extra load, and therefore the HE fails. The tensile strength under these circumstances can be described by equation [2.12].

$$\sigma_{HY} = \sigma_{LE} V_{LE} + \sigma_{HE}" V_{HE} \quad [2.12] \quad \text{or} \quad \sigma_{HY} = \sigma_{LE} V_{LE} + e_{LE} E_{HE} V_{HE} \quad [2.13]$$

Where σ_{HY} represents the tensile strength of the hybrid

composite, V_{LE} and V_{HE} are the volume fractions of the low elongation and high elongation fibres respectively. σ_{HE}" is the stress on the high elongation fibres at the failure of the low elongation fibres. The relationship between ROM and equations 2.11 and 2.13 are illustrated graphically in Figure 2.4.

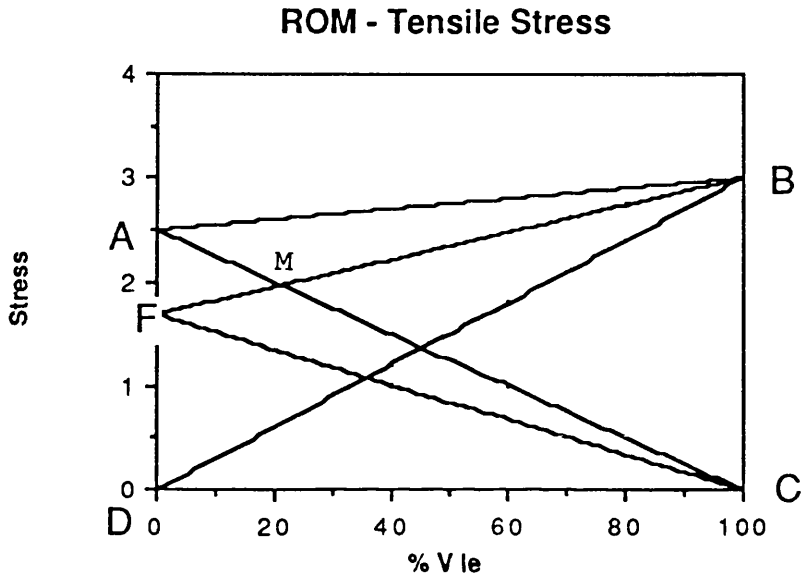

Figure 2.4 The rule of mixtures prediction for the tensile strength of hybrids. See text for explanation.

The ROM prediction for the failure stress is represented by the line (AB). In other words, (AB) is the sum of the stress contributions from the LE component (BD) and the HE component (AC). Now, if we assume that the LE fibres fail at a constant strain value, the initial failure stress of the hybrid will be described by the sum of the stress contribution from the LE fibres (BD) and the stress contribution from the HE fibres at failure strain of the LE fibres, E_{HE} $e_{LE}V_{HE}$, (FC). The ultimate tensile strength of the hybrid is then given by the line (AMB). The point (M) represents the critical LE volume fraction below which multiple fracture may occur. The line (BM), represents the

ultimate tensile strength of the hybrid composite; here the volume fraction of the high elongation fibre is not present in sufficient quantity to bear all the applied load when the low elongation fibres fail and hence a catastrophic failure will be observed. However, to the left of point (M), the line (AM) describes the situation where the high elongation fibres are present in sufficient quantity to bear all the applied load when the low elongation fibres fail[26].

$$AB = AC + BD = \sigma_{HE}(1-V_{LE}) + \sigma_{LE} V_{LE} \qquad [2.14]$$

$$BF = FC + BD = e_{LE} E_{HE}(1-V_{LE}) + \sigma_{LE} V_{LE} \qquad [2.15]$$

The transition composition (V_{LEcr}) can be obtained by solving lines (AC and BF).

$$\sigma_{HE}(1-V_{LE}) - e_{LE} E_{HE}(1-V_{LE}) - \sigma_{LE} V_{LE} = 0 \qquad [2.16]$$

$$V_{LEcr} = \frac{\sigma_{HE} - e_{LE} E_{HE}}{\sigma_{HE} - \sigma_{LE} - e_{LE} E_{HE}} \qquad [2.17]$$

$$V_{HEcr} = \frac{\sigma_{LE}}{\sigma_{HE} + \sigma_{LE} - e_{LE} E_{HE}} \qquad [2.18]$$

From equation [2.17], it can be predicted that below the critical volume fraction ,V_{LEcr} , multiple fracture of the low elongation fibres is possible. For multiple fracture to occur the load must be transferred back onto the low elongation fibres at a distance away from the vicinity of the fracture. In the above discussion it was assumed that there was no stress concentration on the high elongation fibres in

the vicinity where the low elongation fibres failed.

2.3.6 Mono-Fibre Composites - Strength Models[3]

A brief review of the tensile strength models for mono-fibre composite materials are presented in the following section.

2.3.6.1 Weakest-Link Failure

As discussed previously, on loading the composite, scattered fibre breaks can occur within the gauge length of the composite. One of these fibre breaks can trigger a stress wave or initiate a crack in the matrix;this results in a localized stress concentration which causes fracture of one or more adjacent fibres. This process can repeat itself resulting in a catastrophic mode of failure which is associated with the occurrence of one or a small number of isolated fibre breaks. The lowest stress at which this type of fracture can occur is considered to be the stress at which the first fibre will break.

2.3.6.2 Cumulative Weakening Failure

This applies in cases where the weakest-link failure mode is not observed. Instead, it is assumed that flaws in the fibres are distributed randomly and that the statistical information for the strength of single fibres are applicable. The basic principle is that when a fibre breaks, there is a stress redistribution in the vicinity of the fibre fracture site. A length of the fibre from the fractured tends not to support the full load and as discussed previously, this is

taken to represent the ineffective length. In this instance, the function of the matrix is to localize the reduction of fibre stresses when a fibre breaks. In the cumulative weakening failure model, failure is considered possible when a single layer across the section of the laminae is weakened to the extent that it can no longer sustain the applied load. The effect of stress concentrations in fibres adjacent to broken fibres is not considered.

2.3.6.3 Fibre Break Propagation Failure Model

In this model, stress concentrations on fibres in the vicinity of broken fibres are considered. When a fibre breaks, equilibrium requires that the net load on the cross section containing the broken fibre is unchanged, this means that the average load on the remaining fibres must increase. This in turn must increase the probability of fracture in fibres in the immediate vicinity of broken fibres, and this fibre break propagation can escalate leading to final failure. The probability of this mode of failure occurring is increased with the average fibre stress because of the increased number of scattered fibre breaks and the increased stress levels in the over stressed fibres.

2.4 COMPRESSIVE BEHAVIOUR OF COMPOSITE MATERIALS - LITERATURE REVIEW

Compared to the wealth of information available on the tensile behaviour of composites, there is relatively little information available in the public domain on the static

compressive and fatigue behaviour of composites. Furthermore, data on the compressive fatigue behaviour of hybrid composites is even more scarce. The experimental difficulties involved in generating reliable compressive data for composites even under static loading conditions are quite considerable because the measured properties are extremely sensitive to the mode of load application, specimen geometry and type of loading fixture deployed[164,165,179-182].

A brief summary of some of the commonly used test fixtures for determining the compressive properties of composite materials are presented in the following section.

2.4.1 Compressive Properties - Test Methods

Whitney[179] classified compression test methods for composites into three main classes:

(A) Type I - Specimens having a test gauge length that is relatively short and completely unsupported. Examples of such compression loading fixtures include the Celanese, IITRI and the Northrop test fixtures. These test fixtures require that the test specimens be fabricated such that the edges and/or the tab surfaces are very close to perfect parallelism[179].

(B) Type 2 - This test fixture is characterized by a relatively long test gauge length which is fully supported. Examples of such test fixtures are the SWRI (Southwestern Research Institute) and Lockheed-California Company. The Lockheed method utilizes side supports only over the test gauge length and the mode of load application is via

compression at one end (end-loading) and shear loading at the other end via the grips. The RAE (Royal aircraft Establishment) test fixture used in this programme is described in the experimental section.

(C) Type 3 - Here the test method involves the loading of straight-sided coupons bonded to a honeycomb core. The loading is applied either via edge wise compression or via a four-point bend test.

In compression tests where the gauge length is unsupported, it is important to ensure that the specimen does not fail by Euler buckling[164,165,183].

The critical load (P_C) for buckling of a column[184] is given by equation [2.19],

$$P_C = (k \pi^2 E I) / L^2 \qquad [2.19]$$

where;
E=compression Young's modulus;
I=moment of inertia about the neutral axis, for a rectangular column of breadth (b) and thickness (t), I=(b*t^3)/12,
L=length of column,
k=constraint factor, =1 for free ends and =4 for clamped ends.

Lee[164] stated that when dealing with unidirectional composites, additional deflections occur because of the relatively low ratio of shear to axial modulus, (~ 0.04). This was said to give rise to further significant reductions in the Euler buckling loads and proposed the following

correction factor:

$$P_{corrected} = P_c / (1+(n\ P_c / AG)) \qquad [2.20]$$

where; n= 1.2 for rectangular columns;
A= cross-sectional area;
G= shear modulus.

2.4.2 Composite Compression Strength Models

Rosen[66] treated the composite as a two-dimensional fibre-matrix system and derived equations for predicting the external loads at which fibre microbuckling takes place. Two failure modes were considered: (a) fibre microbuckling in extensional mode and (b) fibre microbuckling in shear mode, See Figure 2.5.

In the extensional mode, the transverse deformation of the fibres are out of phase relative to each other, and the resulting strains in the matrix are predominantly extensional. In the second case, the transverse deformations of the fibres are in phase, and the resulting strains in the matrix are predominantly shear strains.

The compressive strength (s_c) for the extensional mode, equation [2.21] and the shear mode, equation [2.22], according to Rosen:

$$s_c = 2\ V_f\ [\ V_f\ E_f\ E_m\ /\ 3(1-V_f)]^{0.5} \qquad [2.21]$$

$$s_c = G_m\ /\ (1-V_f) \qquad [2.22]$$

Where:

s_c = mean composite longitudinal compressive strength;

G_m = matrix shear modulus.

In general, microbuckling in the extension mode is said to take place when the fibre volume fraction is low, ≤ 0.1 and the shear mode predominates[67] at $V_f \geq 0.01$. Various researchers have reported that the above equations predict too high a value for s_c compared to that obtained from experiments, and that they do not describe accurately the variation of compressive strength with fibre volume fraction. Furthermore, equations [2.21 & 2.1] have an unreasonable feature in that as $V_f = 1$, s_c becomes infinite.

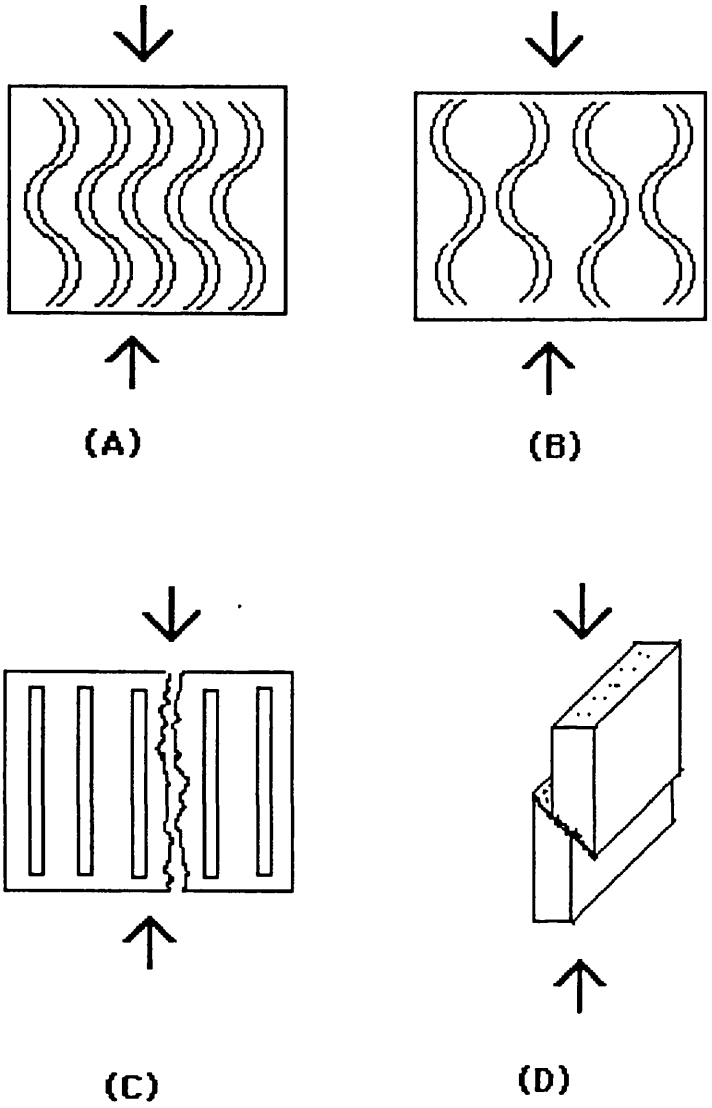

Figure 2.5 Longitudinal compressive failure modes in unidirectional composites subjected to longitudinal compression: (A) fibre microbuckling in the shear mode, (B) fibre microbuckling in the extensional mode, (C) transverse tensile failure and (D) shear failure.

Agarawal and Broutman[18] proposed that failure under compressive loading in a unidirectional composite may occur when the transverse strain exceeds the ultimate transverse

strain capability of the composite. The following expression was proposed:

$$s_c=[(E_f V_f + E_m V_m)(1-V_f^{1/3})e_{mu}]/(v_f V_f v_m V_m) \qquad [2.23]$$

Hayashi[68] derived a ROM equation for s_c, where the critical parameter was the shear instability limit of the matrix. He proposed that the matrix yield stress could be used instead of the shear instability value, because (a) the shear instability value of the matrix material is usually greater than the matrix yield stress and (b) it would give a more conservative estimate of s_c.

$$s_c = s_f V_f + s_{my} (1-V_f) \qquad [2.24]$$

where

s_{my} = matrix yield stress

s_f = fibre compressive stress at the same strain as the matrix yield strain.

Greszczuk[69] used an energy based method to derive microbuckling equations for unidirectional fibre composites. Good agreement between experimental results and the derived equations were obtained for aluminium and steel fibre composites. Microbuckling, equation [2.25], was the predominant mode of failure for composites made with low modulus resin. As the Young's and shear moduli of the resin was increased, the mode of failure changed to non-microbuckling compression failure, equation [2.26]. However, these equations were also found to over-estimate the compressive strength of carbon fibre composites. Greszczuk proposed that the initial failure mode may be via transverse

tensile failure or fibre-matrix debonding prior to microbuckling. The transverse tensile stresses (normal to the direction of the fibres) were said to originate as a result of the difference between the Poisson's ratio of the fibre and the matrix. Other factors which were said to influence the load at which microbuckling took place were the inelastic and nonlinear behaviour of the matrix, fibre misalignment and non-linearity, twisted yarns and the interfacial bond strength.

$$s_c = G_c + \pi^2 E_f V_f (r/l)^2 \qquad [2.25]$$

$$s_c = s_f V_f + \partial (1-V_f) \qquad [2.26]$$

Where,

G_c = shear modulus of composite;

s_f = compressive strength of fibre;

∂ = compressive stress in the matrix corresponding at a strain equal to the fibre failure strain; r=fibre radius; l= length.

Ewins and Ham [70] carried out a detailed investigation into the nature of compressive failure in unidirectional HMS and HTS carbon fibre reinforced composites. They proposed an upper-bound for the longitudinal compressive strength which was said to be brought about by shear failure across the fibres and the matrix. The microbuckling mode of failure was only observed for tests carried out at above 100°C; a decreasing s_c was observed with increasing temperature, reflecting the dependence of the shear modulus on this mode of failure. The compressive strengths of these composites approached 90% of the tensile strength values. On the basis of this they proposed that increases in the compressive strength of carbon

fibre composites can be realized through increases in the tensile strength.

The shear stress (τ) due to compressive load was given by equation [2.27]

$$\tau = s_c \sin \phi \cos \phi \qquad [2.27]$$

The rule of mixtures expression for s_c due to shear failure [57] was given by equation [2.28].

$$s_c = 2[V_f t_f + (1-V_f) t_m] \qquad [2.28]$$

where, t_f and t_m are the shear strengths of the fibre and matrix respectively.

Kulkarni et al[71] carried out a detailed investigation into some of the factors which they thought significantly influenced the compressive strength of Kevlar composites, namely:

(a) addition of lateral reinforcement;
(b) pre-tensioning and pre-twisting of fibres;
(c) increasing fibre diameters, effect of moisture ;
(d) alteration of the mechanical and physical properties of the matrix.

They also derived expressions for (σ_c) as a function of the fibre constituent properties and the interfacial bond strength, equation [2.29].

$$s_c = G_m \left[(1-(1-k) V_f)/(1-(1-G_m/G_f k)V_f\right]^2 * [1-(1-G_m/G_f)V_f] \qquad [2.29]$$

Where;

k = 1 for perfect interfacial bonding and for the case where no bonding is present, $k = -[(1-V_f) / V_f]$.

K was restricted such that $-[(1-V_f) / V_f] \leq K \geq 1$.

However, the the limitations observed for equation [2.19] also apply here. Kulkarni et al[71] highlighted an interesting fact with regards to the interaction between the Kevlar fibres and the matrix during cure. The radial thermal expansion coefficient for Kevlar is 205 * $10^{-6}/^{o}C$, whereas the expansion coefficient for the resin system used was 25-40 * $10^{-6}/^{o}C$. These values indicate that during curing, the shrinkage in the Kevlar fibres will be greater than that for the matrix. They point out that, unless the load transfer between the resin and the fibre is high enough, formation of a good interfacial bond may not be possible. This fact along with the anisotropy of Kevlar fibres was attributed to its low compressive behaviour. Kulkarni et al obtained significantly superior compression strength values by using a carbon/Kevlar hybrid construction, unfortunately no further details were given. Post-failure surface analysis revealed extensive kinking on the fibre surface and fibre surfaces were smooth and devoid of the matrix. Extensive fibre splitting was also observed. The compressive failure surfaces of carbon and glass fibre composites exhibited distinct fibre breaks with no evidence of intra-fibre splitting.

Figure 2.6 illustrates the fibres undergo in-phase buckling. With brittle fibres such as carbon, final failure may occur by brittle fracture in the tensile region of each fibre followed by crushing or shear failure in the compressive region. With Kevlar fibres, various researchers have observed

that fibres do not fracture in the kinked zone. Kinking during axial compression of unidirectional carbon fibre composites has been described as the mechanism of transverse deformation whereby shear takes place initially parallel to the loading direction[72]. Kinking has also been described as 'compressive creasing' due to local shear instability or microbuckling [75].

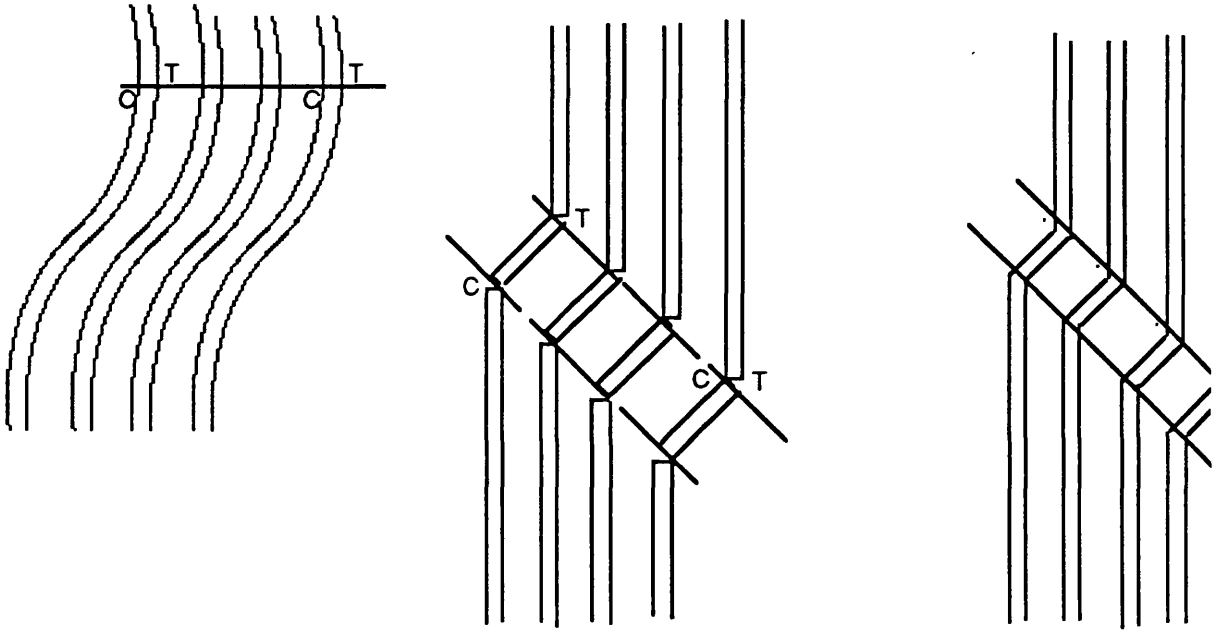

Figure 2.6 Schematic illustration of kink band formation in a unidirectional composite subjected to compressive loading in the fibre direction. Reference number 57.

Piggott and Harris et al[76-82] carried out a detailed study of the compressive behaviour of resins and composites. Piggott[76] considered the work of Harris et al and proposed a theoretical framework for the compressive properties of aligned fibre composites. In his review, Piggott considered the following factors as having an important influence on composite compressive strength:

(a) Fibre compressive strength;

(b) Matrix yield strength;

(c) Fibre/matrix bond strength;

(d) Degree of fibre linearity or fibre waviness.

Fibres that were relatively weak in compression were said to yield low composite compressive properties; Kevlar fibres were cited as an example. Theses fibres were reported as exhibiting a compressive strength of only about 0.17GPa, compared with a tensile strength of approximately 3.5GPa. The Young's modulus in compression was said to be as low as -21 GPa compared with a tensile Young's modulus of 130 GPa[185].

Piggott[185] emphasized that fibre composites can not be made with perfectly straight fibres and considered a model (which had been previously considered by Swift[83]) for the compressive stress in a fibre due to initial curvature;

$$s_c = (2\lambda^2)/(\pi^3 a)*(V_f - V_m E_{m/E_f})*s_{my} \qquad [2.30]$$

where;

λ=wavelength of the sine wave, divided by the fibre diameter;
a=amplitude of fibre waviness, divided by the fibre diameter;

The composite modulus (E_c) was derived as:

$$E_c = V_f(1/E_f + 1/E_{fl}) + V_m E_m \qquad [2.31]$$

where;

$$E_{fl} = \lambda^4 E_m/\pi^5 a^3$$

Piggott concluded as follows:

(a) When the fibres are ductile, the strength of the composite is usually dominated by the fibre compressive strength;

(b) When the matrix is very soft, it controls the compressive strength and modulus probably as a result of built-in fibre curvature that causes lateral stresses;

(c) High composite compressive strengths and moduli can be obtained by the utilization fibres which do undergo ductile failure and by minimizing fibre curvature;

(d) The splitting mode of composite failure can be retarded by having a high interfacial bond strength and a high matrix tensile strength;

(e) The transverse mode of composite failure can be retarded by utilizing a matrix with high compressive strength and yield strength;

(f) Hybridisation can be used to improve the compressive strength of composites containing ductile fibres such as Kevlar.

2.5 FATIGUE RESPONSE OF FIBRE REINFORCED COMPOSITES - LITERATURE REVIEW

2.5.1 Introduction and Terminology

Tensile fatigue of mono-fibres composite materials has received substantial coverage in the literature. This reflects the concern and interest among researchers and design engineers in trying to understand and predict the fatigue response of composite materials. However, only a limited amount of research has been reported on compressive fatigue and fatigue of hybrid composites.

Characterizing the response of composites to repeated load applications is of great importance because most aerospace and automotive structures and components are subjected to numerous load cycles during their life-times. The action of this repeated cyclic loading on composite structures induces various form of damage in the material leading to loss in structural performance and integrity. The typical forms of damage observed in composites are: fibre breaks, matrix cracking, fibre pull-out, debonding and delaminations. Factors which effect the fatigue life of composites include:

(a) Type of loading or wave-form;
(b) Materials properties;
(c) Mean stress, stress amplitude and stress ratio (R);
(d) Strain rate and frequency effects;
(e) Stress concentrations;
(f) Environmental effects; and
(g) Specimen geometry.

Historically, fatigue test results have been presented graphically in the form of S-N curves[45]. The variable component (σ_1) is usually the stress amplitude, σ_a, or the peak applied stress, (σ_{max}) and the constant component (σ_2) is the minimum stress, (σ_{min}), mean stress, (σ_m) or the ratio of the minimum stress to the maximum stress, R. The definition of these terms and a graphical illustration of the wave-form is presented in Figure 2.7.

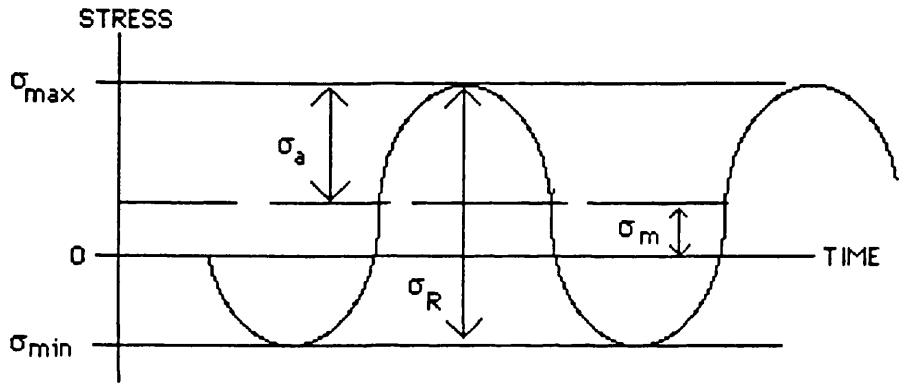

Figure 2.7 Key stress variables associated with cyclic loading. Reproduced from reference number 132.

σ_{max} = Maximum applied stress - the highest algebraic value of the stress in the stress cycle; tensile stress is defined as positive and compressive stress is defined as negative.

σ_{min} = Minimum applied stress - the lowest algebraic value of the stress in the stress cycle, tensile stress is defined as positive and compressive stress is defined as negative.

σ_N = Fatigue strength - the stress which produces fatigue failure at a number of stress cycles.

σ_R = Stress range = $(\sigma_{max} - \sigma_{min})$.

σ_m = Mean stress = 0.5 (σ_{max} + σ_{min}).

σ_a = Stress amplitude = 0.5 (σ_r) = 0.5 (σ_{max} - σ_{min}).

R = Stress ratio = σ_{min} / σ_{max}.

σ_e = The fatigue strength for N => ∞.

σ_u = The fatigue strength for N => 0. This value is not necessarily equal to the ultimate tensile (σ_t) or compressive strength (σ_c) of the composite. The data is usually plotted in terms of log Cycles to Failure (Nf) versus Peak Stress (σ).

2.5.2 Tension/Tension Fatigue

Dharan[43] reported that the fatigue response of fibre reinforced composites could be divided into three distinct life ranges, see Figure 2.8. In Region I, <200 cycles, the dependence of the fatigue life on the cyclic behaviour was said to be small. Observations of the specimen during fatigue showed that in addition to a progressive increase in matrix microcracking with stress, the peak stress was high enough to precipitate a large number of fibre failures within the material. The behaviour in this region was stated to be governed by the fibre mean strength and fibre strength distribution. Failure occurred by the coalescence of local fibre breaks which then propagate within a few cycles to connect with other such regions until the specimen fails catastrophically in a manner similar to tensile fracture.

In Region II, 200-10^6 cycles, failure was said to occur by the growth of matrix micro-cracks which lead to preferential fibre failure followed by interfacial shear failure. A similar mechanism to that observed in Region I was observed in Region II; however, the fibre and crack density was much lower. As cycling progressed, the surface microcracks were

seen to propagate perpendicular to the loading direction breaking the fibres in their path. When these cracks were large enough; shear-type failure parallel to the fibres was observed after which, delamination was observed, leading to a loss in the apparent modulus and eventual failure. An illustration of Dharan's model for the sequence of fatigue failure in Region II is presented in Figure 2.9.

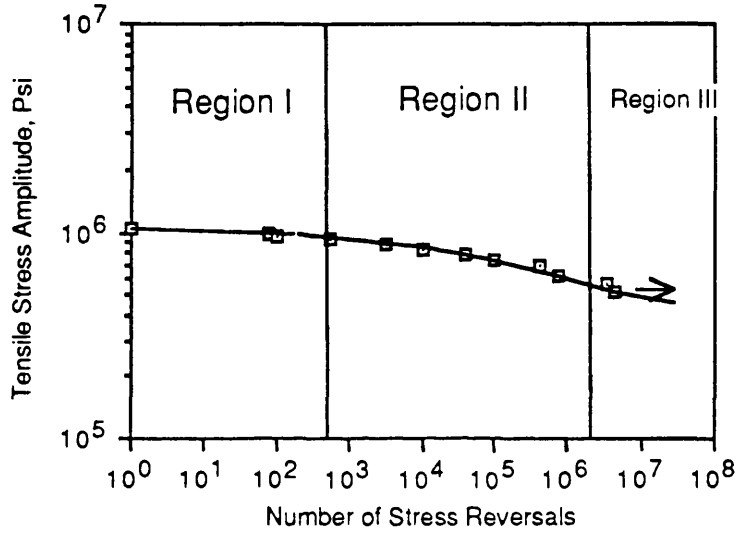

Figure 2.8 Illustration of the three life ranges in fatigue of a glass fibre composite as defined by Dharan[44]. (Reproduced from reference number 44).

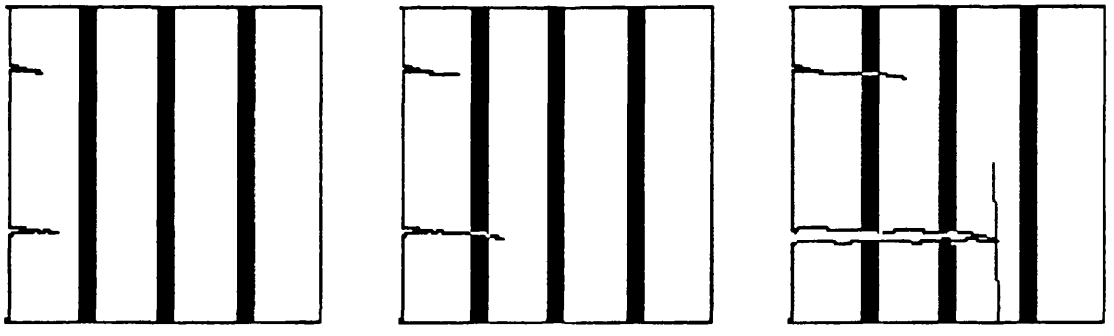

Figure 2.9 Schematic of the sequence of fatigue failure in Region II. Copied from reference number 44.

The third region, > 10^6-10^7 cycles, the applied stress was said to be below the microcrack initiation stress and hence no failures were observed. (The fatigue limit is defined as the stress below which no fatigue failures are observed within the time scale of the experiment).

Dharan[43] also investigated the fatigue behaviour of a carbon fibre composite under four-point loading. Fatigue failures were always observed on the compression surfaces. Progressive fatigue failure was observed to occur in four stages:

(a) Initiation of a zone of fibre buckling;
(b) Localized delamination at the failure zone;
(c) Formation of a surface transverse crack with a width that depended upon the applied stress, and subsequently propagation of the crack into the specimen; and
(d) Delamination parallel to the fibres.

Hahn[46] investigated the fatigue response of a quasi-isotropic glass reinforced epoxy composite. The temperature rise in the specimen during fatigue testing was reported to be proportional to the cyclic frequency. The fatigue strength did not show any dependence on the frequency as it was changed from 10 Hz to 4 Hz. The maximum recorded temperature rise at the surface was about $8^{o}C$. Hahn et al also investigated the effect of specimen thickness on the static and fatigue properties of the glass fibre composite. They observed a reduction in the tensile strength and elastic modulus with increases in sample thickness; the correlation coefficients were 0.65 and 0.68 respectively. The scatter in

the fatigue lives did not permit any conclusions to be drawn.

Hahn[47] discussed the fatigue behaviour of unidirectional composites in terms of the ductility and failure strains of the constituent materials in the composite. Hahn stated that the composite fatigue behaviour is best correlated to that of the constituents in terms of fatigue strains rather than fatigue stress because, in the fibre direction both the fibres and matrix are subjected to almost the same strain. He assumes that the fibres fail before the matrix. The subsequent crack growth was said to depend on the rate of stress application and at the level of the applied stress at which the fibres break. The results of previous researchers were quoted to justify the claim that the cracks created by a fibre break tend to grow into the matrix at higher loading rates, thereby giving lower composite strength with increasing loading rates. The reference quoted by Hahn were for compressive loading and may not necessarily apply to tensile loading conditions.

Awerbuck and Hahn[54] found that ud CFRP, under cyclic loading, failed abruptly in a mode typical of static failures at maximum cyclic stresses within the scatter band of the composite. At cyclic stresses slightly below this level, fatigue damage was in the form of longitudinal matrix cracks between fibres near the edges of the specimens. Most of the specimens survived between 10^5 and 10^6 cycles without any measurable reduction in strength.

Talreja[55] expanded the ideas proposed by Dharan and discussed mechanisms of damage in matrix, fibre and interface caused by tensile fatigue of ud composites. Two forms of damage growth

processes in the matrix were identified; dispersed matrix failure modes and localized matrix failure modes.

The dispersed failure mode was defined as the situation where cracks initiate when the applied cyclic strain exceeds the matrix strain limit and grow until they strike an interface whereupon further growth was delayed (if the stress at the crack tip was insufficient to break the fibre). At sufficiently low strains the cracks were said to be confined to the matrix alone, increasing only in numbers with fatigue cycling, see Figure 2.10(A). However, at high applied strains, the stress at the crack tip exceed the strength of the fibre, leading to fibre failure, see Figure 2.10(B). The matrix crack can now propagate under fatigue loading until it encounters another fibre. If the shear stress at the crack tip of this crack was high, then occurrence of interfacial failure or debonding was said to be likely. see Figure 2.10(B). A simple representation of the principle stress states at a crack tip are illustrated in Figure 2.11. If the stress (σ_1) at the tip is greater than the fibre strength, it would result in fibre fracture. The transverse stress (σ_2) in turn can lead to tensile separation at the interface along with the shear stress causing shear failure at the interface[57]. The failure modes that can now occur depend on the critical stresses for these failure processes. The following situations are considered with reference to Figure 2.11: (a) When the ratio of the ultimate longitudinal tensile strength (σ_0), to the ultimate transverse tensile strength (σ_{90}), is greater than the ratio of the maximum longitudinal and transverse stress at the crack tip, tensile cracking to the interface will occur before fibre fracture. The maximum tensile stress, (σ_{1max}), at right angles to the crack occurs

at the tip of the crack and the maximum tensile stress, (σ_{2max}), parallel to the crack occurs just ahead of the crack tip. (b) When $\sigma_o / \tau_o > \sigma_{1max} / \tau_{max}$ shear fracture will occur before fibre fracture. τ_o is the interlaminar shear strength parallel to the fibres. (c) When $\tau_o / \sigma_{90} > \tau_{max} / \sigma_{90\ max}$, tensile cracking at the interface will be preferred to shear cracking.

Talreja next discussed fibre damage in composites. Here the consequence of a single fibre failure was considered in relation to the state of the matrix. In the first case the matrix was considered to remain intact when the fibre broke at its weakest cross-section under an applied load. The fibre failure can cause a shear stress concentration at the interface leading to debonding of the fibre from the matrix, Figure 2.12 (A). The void created in the matrix could then enhance the tensile stresses locally leading to a transverse crack. The second situation considered was where a fibre failure is observed near the vicinity of a matrix crack in the dispersed mode. The failure of a fibre here would increase the crack length thereby imposing a stress concentration on neighboring fibres, Figure 2.12 (B). The final case considered was where the matrix exhibited a multiple fracture mode. Apparently, here the load that was previously carried by the matrix is transferred and shared equally by the bridging fibres Figure 2.12 (C). The bridging fibres can then be treated as lose bundles with the weakest fibre failing first and the load is then shared equally by the remaining fibres.

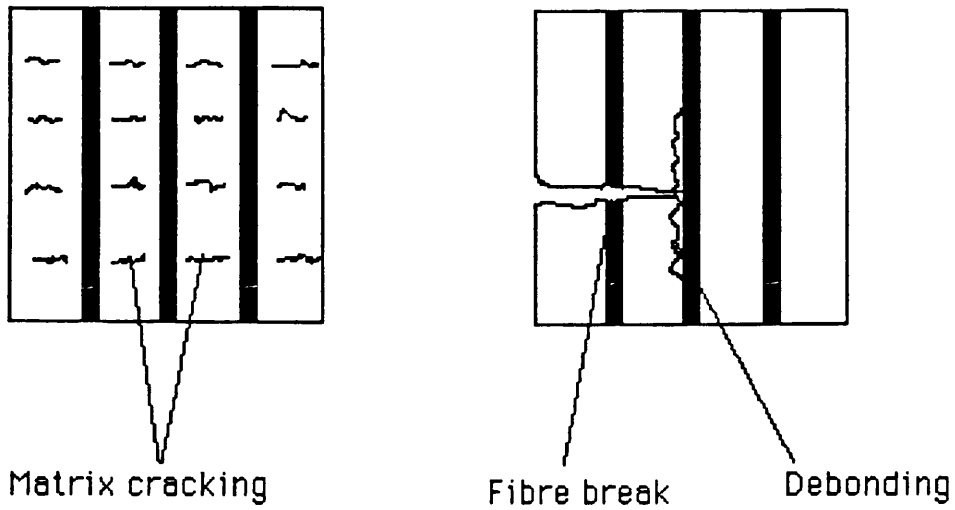

Figure 2.10 Matrix damage modes in composite materials: (A) Dispersed failure mode - cracks confined to matrix only. (B) Localized failure mode - cracks grow by fibre breaks followed by debonding. Reproduced from reference number 55.

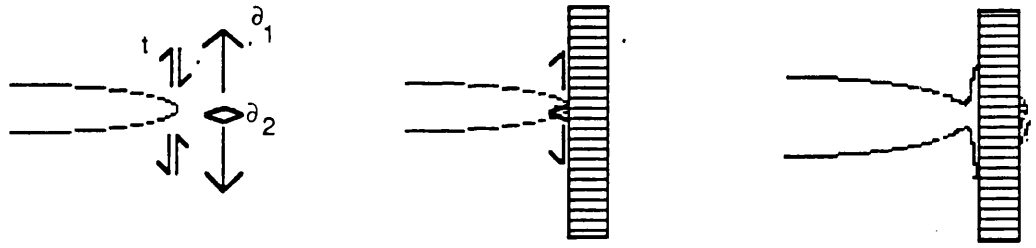

Figure 2.11 (A) Schematic representation of ∂_1, ∂_2 and t at the crack tip, (B) Crack tip at the fibre interface and, (C) Interfacial splitting and crack opening when the crack intersects the fibre. Reproduced from reference number 57.

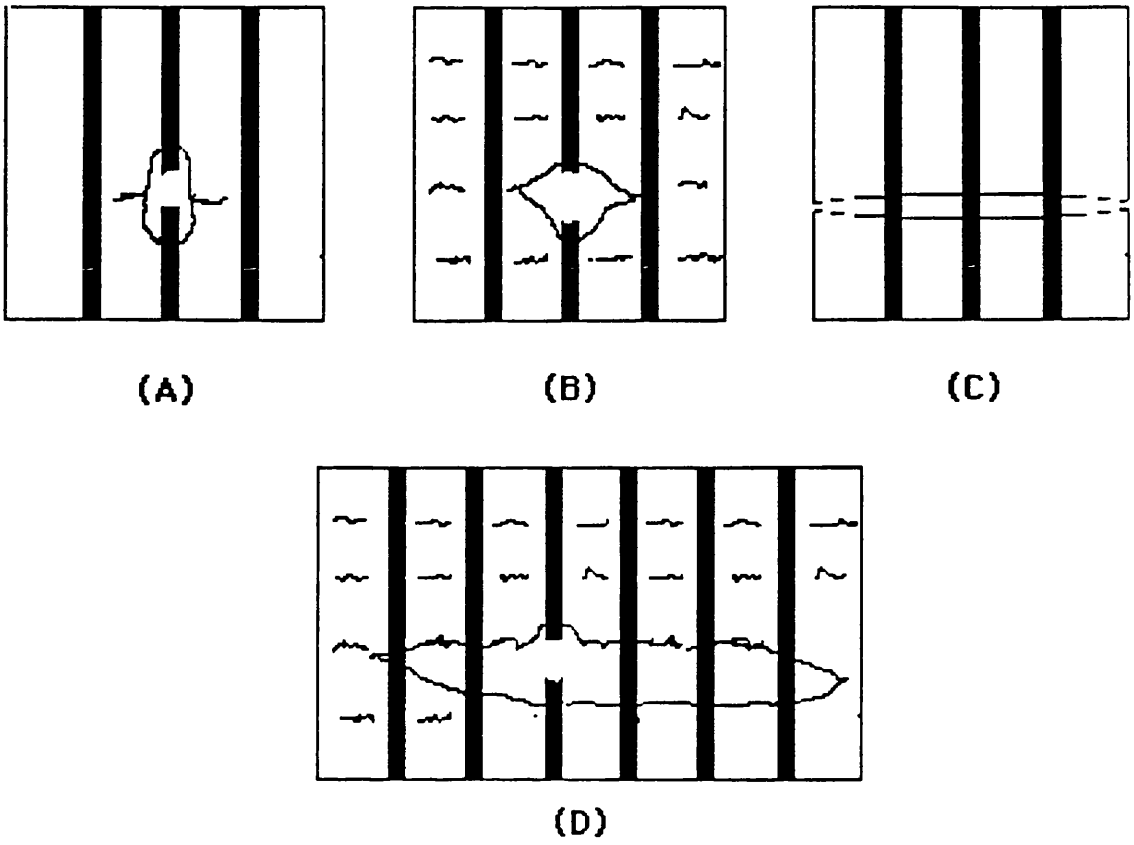

Figure 2.12 Schematic illustration of Fibre damage modes in composites: (A) Fibre break causing interfacial debonding; (B) Fibre break increasing matrix cracks; (C) Fibres bridging a matrix crack; (D) Combination of (A,B and C).

Figure 2.12(D) represents a combination of the three previous failure modes previously. Talreja postulated that these failure modes may have a region of dominance dependent on the range of the applied cyclic strain.

Talreja next considered fatigue life diagrams and like Dharan, he divided the fatigue life diagram into three distinct regions, see Figure 2.13.

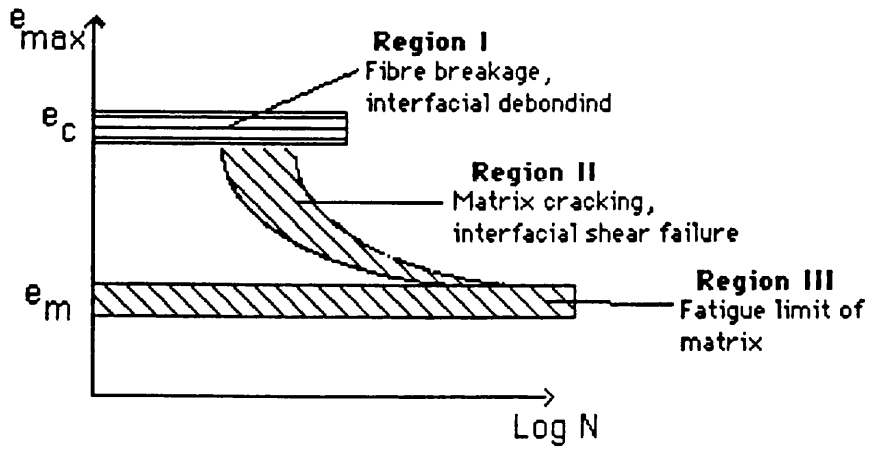

Figure 2.13 A schematic fatigue life diagram for tensile fatigue of ud composites. Reproduced from reference number[55].

The predominant failure modes in Region I were said to be fibre breakage and interfacial debonding. The fibres break within the static ultimate scatter band and the damage was considered to be non-progressive in the sense that a zone of damage growing from an early stage of the fatigue life to the final failure could not be readily identified. The fibre break propagation failure was proposed as the mechanism of ultimate failure. In Region II progressive damage was said to occur and the damage was stated as being cycle-dependent. In Region II the failure modes were said to be matrix-dependent. Region III was defined as the strain below which no cracks or only non-propagating cracks were initiated in the matrix.

Using the ideas presented by Hahn, Talreja also discussed the fatigue behaviour of composites in terms of its constituent properties, Figure 2.14.

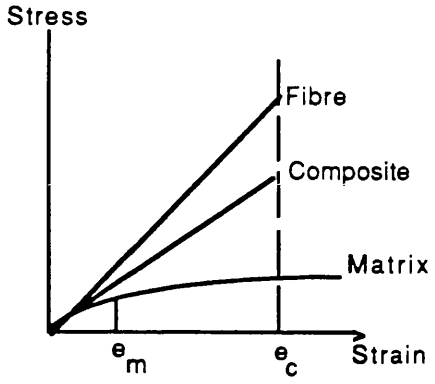

(A)

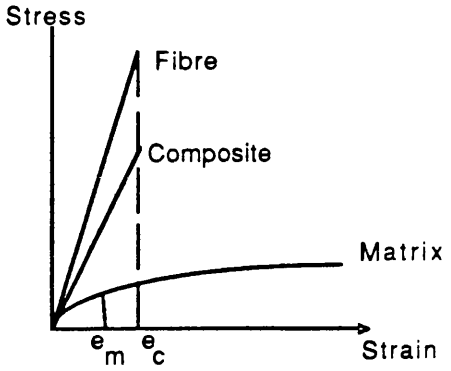

(B)

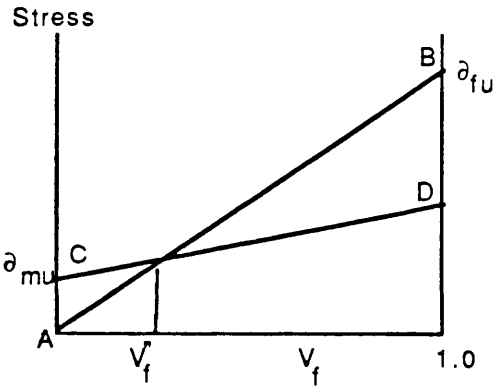

(Ai)

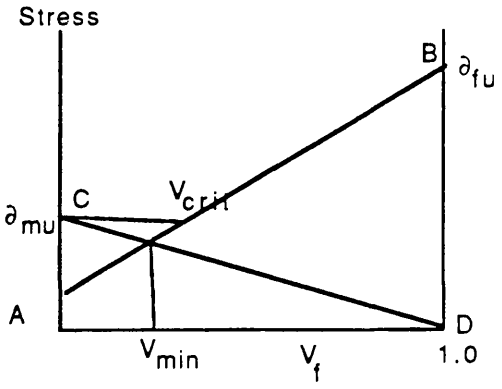

(Bi)

Figure 2.14 Stress-strain characteristics of unidirectional composites: (A) Low stiffness, high elongation fibres (GFRP); (B) High stiffness, low elongation fibres (CFRP).

The basic idea proposed by Taljera was that the fatigue behaviour of composites depended on the relative values of composite failure strain, e_c, and the matrix fatigue limit, e_m. The higher the difference between e_c and e_m, the greater will be the observed progressive damage in the matrix. This would result in a pronounced three-staged fatigue curve as discussed previously. As the difference between e_c and e_m is reduced, (for example, using stiffer fibres with a low

failure strain) would result in a greatly reduced Region II. This is because the applied strain is now only slightly lower than the matrix fatigue limit but is close to the strain limit of the fibres. The predominant failure modes will then be fibre breakage and interfacial debonding.

Gouda et al[49] postulated that fatigue crack growth processes along the interface occur as the result of debonding along the interface. The extent of growth per cycle was considered to be proportional to the relative displacement of the fibre and the matrix at the crack tip. They stated that the nature of the crack path would have a strong influence on the overall fatigue behaviour of composites. In the case where the interface between the fibre and matrix is relatively weak, a crack would grow along the interface between the fibre and the matrix. This was considered damaging only when a weak site in the fibre was encountered. In the case where a strong interface is present, the cracks were said to grow transverse to the fibre and the loading direction.

Stinchcomb et al[58] studied the effect of ply constraint on fatigue damage in composites. When plies of some other orientation are bonded to the ud plies, they were said to constrain the response of the ud material. The magnitude of the constraint is controlled by the orientation of the plies in a given laminate and can manifest itself in-plane stresses and through-thickness stresses. An example of a ud and 90/0 composite was cited to show the influence of in-plane (σ_y) stresses in damage development. In the ud composite, longitudinal splitting along the fibres was the predominant damage mode. Final fracture was by transverse fibre breakage. The transverse fracture was nearly always

discontinuous with regions separated by longitudinal splitting. In the case of the 90/0 composite, the application of a load in the zero degree ply, the Poisson's effect causes the transverse dimensions to change in proportion. As the plies are bonded, this will result in a tensile transverse constrain strain in the 0^{o} ply; this will result in increased longitudinal splitting.

The through-thickness stresses were said to develop due to interlaminar stresses that resulted from the different response of each laminae in the laminate. A major effect of the through-thickness stresses was on the fatigue response via delamination growth along laminae boundaries. Another important effect of these through-thickness constraints was said to be the creation of a characteristic damage state (CDS). This state consists of a regular array of cracks in the off-axis plies of an angle-ply laminate. The CDS was defined as a laminate property, controlled by the properties of each laminae and the stacking sequence of the laminae in the composite. The crack spacing was controlled by the constraint of the laminate on the cracked plies. Their model assumed that the constraining layers transferred stresses back into the broken ply on either side of the cracks until the stress that created the first crack was reached again. They concluded that the constraint situation which produced the greatest static strength did not minimize the extent of damage that developed during fatigue.

Reifsnider et al[52,53,187] have made a significant contribution to the understanding of damage processes in composite materials during fatigue testing. They developed techniques such as edge replication, stereo radiography, deplying and

monitoring damage development via stiffness reduction.

Schulte[186] provided an excellent review of damage development in composite materials under cyclic loading. He investigated the fatigue response of unidirectional continuous carbon fibre composite, aligned short fibre composite and a woven carbon fibre composite. Like previous researchers, only a very small reduction in the stiffness was detected for Region I of the fatigue curve. A small but progressive reduction in the stiffness was observed in Region II of the fatigue curve. Increasing fibres fracture and fibre matrix debonding was said to contribute to the observed stiffness reductions. A stepwise decrease in the stiffness reduction was observed for Region III of his fatigue curve. This stepwise decrease in the stiffness was attributed to the failure of fibre bundles. The aligned short fibre composite showed a comparatively shorter Region I compared to the continuous fibre composite and flatter Region II. The damage development in this Region was characterized by the growth of existing cracks and to a small extent by the initiation of new cracks. The formation and growth of delaminations was not observed for the aligned short fibre composite. Compared to the continuous fibre composite, Region III in the aligned short fibre composite was less steep, i.e. a sudden death type phenomenon was not observed.

So far the discussion has been on the response of fibre reinforced composites to tensile fatigue loading. The effect of tension/compression and compression/compression fatigue loading on composite materials has not received the same degree of attention in the literature as tension/tension

fatigue loading. The following section summarizes some of the literature on the response of fibre reinforced composites subjected to tension/compression fatigue loading.

2.5.3 Tension/Compression Fatigue

Bakis et al[188] investigated the fatigue response of quasi isotropic carbon/epoxy and carbon/PEEK composites under reversed cyclic loading. The tests were carried out on unrestrained specimens, ie. antibuckling jigs were not used. They argued that most compression test fixtures eliminate buckling effects by constraining the specimen and that this was not representative of loading of structural components in real life. Bakis et al reported that the stiffness reductions as a result of tension/compression fatigue response could be describe by three stages (Regions). Region I comprised the first 5 to 15% of the fatigue life and was characterized by rapid but slowing rates of stiffness changes and damage growth. Region II comprised the majority of the fatigue life and was found to be the slowest period of damage growth and stiffness reduction. Region III comprised the last 5 to 15% of the fatigue life and was characterized by rapid delamination growth and consequent loss of compressive strength. The residual tensile strength of the notched fibre-reinforced composite was found to increase in Regions I and II.

They concluded that under constant amplitude, R=-1, the damage modes included matrix cracking, delamination and fibre fracture which led to the observed changes in the tensile and compressive stiffness and strength. Their results of the

mixed amplitude tests revealed that an increased tensile load amplitude increased the rate of material degradation of the carbon/epoxy laminate such that compressive fatigue failure was precipitated. The effect of decreasing the compressive load was to extend the fatigue life, but the failure in the notched laminates were still limited by the reduced compressive strength.

Ramkumar[189] investigated the effect of imbedded delaminatons on the compression fatigue behaviour of quasi isotropic carbon/epoxy laminates. The fatigue life was found to depend on the location of the inclusion with respect to the surface plies. Inclusion away from the first ply interface resulted in neglible delamination growth until failure. Delamination growth was monitored by enhanced x-Ray radiography with holes being drilled to permit the penetrant to reach the internal inclusions. No control experiments were carried out to investigate the effect of these holes on the fatigue response of the material. Furthermore, the relevance of simulating impact damage by placing inclusions on the first ply interface is questionable because no fibre damage was incorporated.

Saff[190] provided an excellent review on the fatigue life behaviour and damage models for composite materials. The following discussion is based on the review presented by Saff.

Damage development was said to start with interlaminar matrix cracking. The matrix cracking was said to initiate as debonding of the fibre-matrix interface at fibre discontinuties after a few load cycles. Intralaminar

cracking was then said to progresses along fibres in a manner which was said to reduces in-plane stress concentrations. This reduction in the in-plane stress concentrations was said to contribute to increased residual strength in some laminates subsequent to fatigue loading. Delaminations and interlaminar cracking were said to interact and lead to rapid degradation of the matrix. The reduced fibres support then leads to fibre microbuckling or fracture leading to overall failure of the composite. Intralaminar cracking was said to occur very early on in life regardless of the stacking sequence of the plies, but the time required to initiate delaminations was said to be very much dependent upon lay-up and stacking sequence.

2.5.4 Fatigue of Hybrid Composites

There is very little information available in the literature concerning the fatigue response of hybrid composites. Phillips[191] and Hofer et al[192] showed that fatigue response of the hybrid composite was dependent on the relative volume fractions of the two constituent fibres. These two research groups found that, the higher the carbon content in a carbon/glass hybrid, the greater was the fatigue resistance of the composite.

At the time of writing this thesis, the author was not aware of any reported research work on the effect of ply stacking sequence on the fatigue response of hybrid composites. This is in contrast to the vast amount of information that is available on the static tensile properties of hybrid

composites. The intention of this current programme is to generate some information on the damage mechanisms and fatigue response of hybrid composites. A convenient starting point in the understanding of hybrid composite behaviour is to consider the failure processes of the individual fibre systems in the hybrid composite. A discussion on the various strength models was discussed previously; the following section outlines the fatigue failure models of composites[190,193].

2.5.5 Fatigue Life Models[190]

The following discussion is based on the literature review presented by Saff[190]. He classified the current fatigue life models into the following categories: Empirical methods; degradation models and fatigue damage models.

2.5.5.1 Empirical Methods

Empirical techniques are still widely used due to the lack of confidence in and verification of analytical fatigue life prediction techniques. These empirical methods require a large data base to impart sufficient confidence in the analysis.

2.5.5.2 Degradation Models

(A) Cumulative damage models - are used to correlate and predict fatigue life in a structure when no measurable damage occurs before failure or when information in relation to damage growth and applied stress is not available. The basic

assumption in the cumulative damage model is that a predictable portion of the structural life is consumed with each stress cycle.

(B). Linear residual strength degradation model - is based on the assumption that a portion of the residual strength is depleted with the application of each stress cycle.

(C). Wear-out models - assumes that the damage growth rate can be determined by residual strength testing after cyclic loading for a given number of cycles.

(D). Sudden-death model - assumes that the damage produced by each cycle does not necessarily effect the residual strength. Furthermore, the model also assumes that there is a unique relationship between the static strength of the composite and the fatigue life, ie. the stronger the specimen the longer it would last.

2.5.5.3 Fatigue Damage Models

These models are based on: (a) Determining the mechanisms which drive the damage growth in composite materials and thus control the fatigue life, (b) Characterizing the the damage state thus permitting the residual strength and fatigue life to be assessed.

2.6 MOISTURE ABSORPTION IN EPOXY RESINS AND COMPOSITES - LITERATURE REVIEW

2.6.1 Diffusion

Numerous studies have shown that the combined effects of absorbed moisture and elevated temperatures can cause significant changes in the mechanical response of composites[194-199]. An understanding of the response of composites to hydrothermal conditioning is essential if predictions of the short and long term durability of these materials are to be made.

Listed below are some of the material property changes that can be induced by absorbed moisture:

i) Lowering of the glass-transition temperature (Tg);
ii) Reduction in the resin modulus over a wide temperature range;
iii) Swelling stresses induced by sorbed moisture;
iv) Resin degradation and leaching, especially at high temperatures and prolonged exposure.

The response of resins to moisture is affected by several factors including:

i) exposed area, thickness;
ii) diffusivity;
iii) temperature, relative humidity
iv) crosslink density, morphology, free volume, functional groups present and the resin-hardener system used.

Eckstein[200] investigated a number of epoxy formulations and their moisture absorption characteristics. The trend in his results showed that moisture absorption was a function of the resin polarity. Higher equilibrium moisture contents were found in resin formulations with higher polar functional groups. BF_3 complexes are common catalysts which are used to facilitate lower curing temperatures (e.g. 913 resin system). Resin systems with BF_3 complexes gave a higher equilibrium moisture content compared to resins without this catalyst system. It was suggested that the use of BF_3 catalyst resulted in the formation of ether linkages in the crosslinked structure rather than pendant OH groups, resulting in a more polar resin.

Conflicting reports have been published on the relationship between degree of cure and sorption behaviour of epoxy resins. Eckstein[200] found that the moisture up-take was not very sensitive to the cure schedule provided the samples were fully cured. Enns et al[201] found a higher equilibrium moisture content and higher diffusivity with increasing cure time. However, Illinger and Schneider[202] observed a decrease in the rate of moisture uptake for post-cured samples as compared to specimens that had not undergone post-curing, but post-curing did not eliminate the high final sorption levels. They proposed that during post-curing additional polar groups (C=0) are formed which could account for the higher equilibrium values. Contrary to Eckstein's findings, Moy et al [203] found that the equilibrium moisture content in the epoxy resin was markedly affected by the curing conditions. A decrease in the rates of sorption with increasing cure temperature was observed. SEM micro-graphs revealed the formation of coarser grain structures with increasing cure

temperature.

Mikols et al[204] varied the hardener content to obtain different crosslink densities. They observed an increased resistance to moisture sorption for samples cured with a higher hardener content, this also gave a higher crosslink density. However, the equilibrium moisture contents were found to increase with increasing hardener content. They suggested that for systems with greater hardener content the mobility of chain segments in the curing resin is impaired as the gel point is approached. This causes an increased fraction of the molecular constituent species to become trapped in the unreacted state. Mikolas et al assume that these trapped species could occupy the free volume in the polymer network, consequently impairing moisture absorption. The higher equilibrium moisture content in samples with higher hardener concentrations was not discussed. In another study[205], the same authors highlighted the importance of stoichiometry. Once again systems with a high hardener content showed a higher M_m value. They attributed this to the presence of unreacted amine (hardener) which facilitated an increased number of hydrogen-bonded sites.

Goodrich et al[206] found that brominated TGDDM derivatives showed a reduction in the equilibrium moisture (M_m) content by 50% and a corresponding reduction in the rate of moisture uptake. The change in the Tg and hence the crosslink density was only slight. The authors did not understand the mechanism by which the presence of bromine reduced the M_m values. Morphological changes introduced by the presence of bromine was suggested as a possible explanation.

It is quite evident from the previous discussions that the formulation and cure schedule determine the sorption behaviour of epoxy resins. In composites, the importance of using a consistent cure schedule cannot be over emphasized. Charriere[207] found a significant difference in the sorption behaviour of autoclaved samples as compared to hot-pressed composite samples. The mechanical properties and absorption resistance was better for the autoclaved samples.

Unfortunately the control over resin formulations lies with the manufacturer. Researchers are often unaware of compositional variations which originate at the manufacturing level. In light of these considerations, it is hardly surprising that researchers investigating the same resin/fibre systems have come to different conclusions.

The correlation between the sorption response of neat laminating resins and that of composites with the same resin should be reasonable. This was indeed the case with the findings of Deiasi et al[208]. They also investigated the sorption behaviour of a hybrid construction consisting of a Boron/carbon/epoxy composite and found that the sorption behaviour of the hybrid was between sorption behaviour of the mono-fibre composites. The major differences between the neat resin and the resin in the composite are the stress states in the resin and the presence of interfaces i.e. resin/fibre and ply interfaces.

Marom et al[209] proposed that the diffusion mechanism depended on the free volume within the resin system. The application of an external load was said to affect both the rate of diffusion and the equilibrium moisture content through

changes in the free volume. They found that the moisture uptake under an external load increased with the loading angle. Various researchers have also found that increasing the external stress resulted in higher diffusivities and higher initial absorption rates. Fahmy et al[213] utilized a free volume model to predict the dependence of the diffusion coefficient on stress. The free volume is the difference between the specific volume of the polymer and the actual volume of its molecules. The model predicted that a sample under tension will exhibit a greater free volume than when under compression. Hence, the diffusion coefficient would increase when the sample was subjected to a tensile stress.

Gillat and Broutman[210] observed significant increases in diffusivities for carbon/epoxy laminates subjected to stresses greater than 45% of the UTS. The diffusion process under these conditions was adequately predicted by Fickian diffusion. The increased diffusion under external loading was attributed to transverse ply cracking. Marshall et al [211] utilized radio-labelled diffusants to study the diffusion of liquids into GRP using a vinyl ester resin system. Damaged specimens showed a five-fold increase for the diffusion coefficient in the vicinity of the damage zone, the application of an external load was also found to increase the rate of diffusion. No evidence was found to suggest that moisture wicks along the fibres. Kasturiarchchi[212] found that the moisture distribution of a sample subjected to 3-point bending was greater on the tensile side as compared to the compressive face.

Hahn et al[214,215] investigated the swelling of composites as a result of absorbed moisture and derived expressions to

calculate the swelling strains in composites induced by absorbed moisture. An interesting feature of the analysis was that residual stresses were shown to be compressive during absorption and tensile during desorption. They suggested that this was the reason for the absorption initially being slower than the desorption. Swelling stresses were said to lead to the creation of microvoids in the composite. However, these swelling stresses were said to be beneficial in relieving the residual thermal stresses that are set up on cooling from the cure-temperature.

2.6.2 Diffusion Models

2.6.2.1 Fickian Diffusion[215-217]

The one-dimensional Fickian model by Shen and Springer[216] has been a popular one amongst most researchers, primarily because of its ease of application. The Shen and Springer equations are obtained from solving Fick's second law equation [2.32] with the following assumptions and boundary conditions:

i) The analysis was for a plate of thickness, (h), exposed on two sides to the same moist environment; the plate is taken to be finite in the Y and Z directions, see Figure. 2.15. The moisture content and temperatures vary only in direction perpendicular to the face of the plate.

ii) Initial temperature and moisture distribution are uniform inside the material.

iii) Temperature inside the material approaches equilibrium

faster than the moisture content.

iv) The ambient temperature, T_a, and moisture concentration, C_a, are constant and equal on both sides of the plate.

v) The diffusion coefficient depends only on temperature and is independent of moisture concentration and stress levels inside the material.

vi) The plate is made of a single layer and is quasi-homogeneous. Variations of density, (ρ), moisture concentration, (c), and the diffusion coefficient (D_x) with position inside the material are neglected.

Under these conditions the concentration is described by Fick's second law:

$$dc/dt = D_x \, d^2c / dx^2 \qquad [2.32]$$

The solution for eqn. [2.32], with the appropriate boundary conditions obtained by Springer was:

$$\frac{c - c_i}{c_m - c_i} = 1 - \frac{4}{\pi} \sum_{j=0}^{\infty} \frac{1}{(2j+1)} \sin \frac{(2j+1)\pi x}{h} \exp\left[-\frac{(2j+1)^2 \pi^2 D_x t}{h^2}\right] \qquad [2.33]$$

They derived an expression for the total weight of the moisture in the material by integrating equation [2.33] over the plate thickness, with the appropriate boundary conditions and substituting (m) for (c):

$$\frac{m - m_i}{m_m - m_i} = 1 - \frac{8}{\pi^2} \sum_{j=0}^{\infty} \frac{\exp\left[-(2j+1)^2 \pi^2 ((D_x t)/h^2)\right]}{(2j+1)^2} \qquad [2.34]$$

where;

m_i = initial weight of moisture in the material.

m = moisture in the material at time (t).

m_m = weight of moisture when equilibrium has been attained.

For when time (t) is sufficiently large, equation [2.34] can be approximated by the first term in the series:

$$\frac{m - m_i}{m_m - m_i} = 1 - \frac{8}{\pi^2} \exp\left[-\frac{\pi^2 D_x t}{h^2}\right] \qquad [2.35]$$

For a short time (t), the following approximation was found to hold;

$$\frac{m - m_i}{m_m - m_i} = 4\left[\frac{D_x t}{\pi h^2}\right]^{0.5} \qquad [2.36]$$

Equation [2.36] can be used to determine the diffusivity, (D_x), for the material. (D_x) is obtained from the initial (linear portion) slope of a plot of moisture content versus √time, see Figure 2.16.

$$D_x = \pi \left[\frac{h}{4 M_m}\right]^2 \left[\frac{M_2 - M_1}{\sqrt{t_2} - \sqrt{t_1}}\right]^2 \qquad [2.37]$$

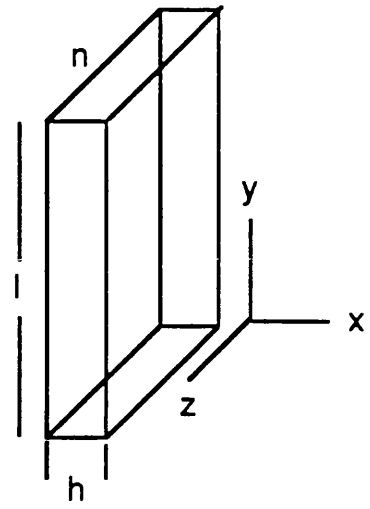

Figure 2.15 Geometry of test specimen

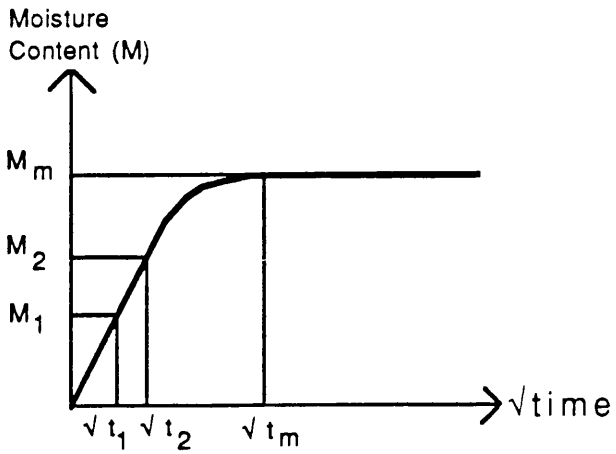

Figure 2.16 Illustration of the change of moisture content with the square root of time.

The temperature dependence of the diffusion coefficient can be expressed by an Arrhenius type relationship.

$$D_x = D_0 \exp(- E_a / RT) \qquad [2.38]$$

where;

D_0 = permeability index,

E_a = activation energy for diffusion,

R = universal gas constant and

T = temperature.

From equation [2.38], a plot of Ln D_x vs 1/T should give a straight line with the slope yielding E_a and the intercept giving D_0.

2.6.2.2 Non-Fickian Diffusion

The diffusion behaviour of many polymers, glassy or crosslinked, cannot be adequately described by a

concentration independent Fick's law with constant boundary conditions. This is especially true when the penetrant is coupled with molecular relaxation and morphological modifications of the polymer are involved. Deviations from Fickian behaviour are considered to be associated with the finite rates at which the polymer structure may change in response to the sorption of penetrant molecules. In general, sorption behaviour in polymers can be described by one of the following classifications, see Figure 2.17.

a) Fickian:

(Discussed previously) In the early stages, the amount of absorbed moisture is directly proportional to $\sqrt{t}$. Therefore, a plot of concentration versus $\sqrt{t}$ime will be initially linear and then concave towards the $\sqrt{t}$ axis to a final equilibrium value.

b) Pseudo-Fickian:

A plot of concentration versus $\sqrt{t}$ shows a small initial region that resembles Fickian behaviour but departs from Fickian behaviour on thickness scaling.

c) Sigmoid:

The sorption curves are sigmoid in shape with a simple point of inflection at about 50% equilibrium sorption. The initial rate of desorption exceeds that of sorption but desorption soon becomes slower and the curves cross.

d) Two Stage Sorption:

After an initial rapid uptake the sorption curve as a function $\sqrt{t}$ approaches a quasi-equilibrium followed by a slow approach to a final true equilibrium.

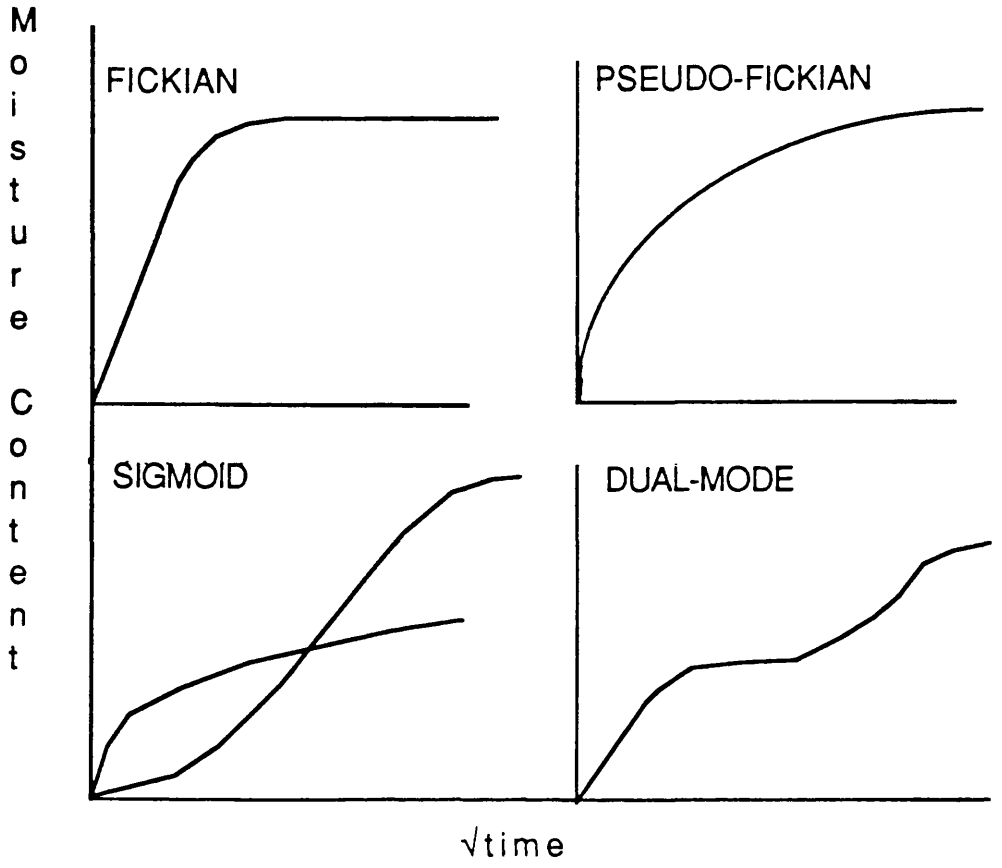

Figure 2.17 Typical sorption behaviour exhibited by polymeric materials. Copied from reference number 217.

Several authors have attempted to account for the non-Fickian sorption behaviour in polymers.

Bragly and Long[218] postulated that the dual sorption behaviour may be due to time dependent surface concentrations. A quasi-equilibrium is said to be rapidly reached first at the polymer surface and then by a simple diffusion through the polymer section. The second state of sorption is associated with an increase in surface concentration which occurs slowly as compared with the diffusion process and is the rate-determining factor for sorption.

Newns[219] stated that at the end of the first stage, the elastic forces in the swollen polymer network increased the

chemical potential of the absorbed penetrant to such an extent that no further sorption occurred. On standing, the elastic forces slowly relaxed which resulted in a decrease in the chemical potential and more penetrant being absorbed to establish equilibrium again. This process continued until the elastic forces had decayed away completely or when equilibrium was reached.

Berens and Hopfenberg[221] postulated that sorption by an initially penetrant free polymer sample is dominated by a rapid Fickian diffusion process, while incremental sorption show large relative contribution from slow relaxation processes. Expressions were derived describing the individual contributions from the diffusion and relaxation processes.

Smith and Fisrier[222] assumed a single diffusion coefficient coupled with a stress relaxation contribution. They obtained good agreements for sorption of melamine formaldehyde resins. Vinson[220] proposed a trapped species mobility hypothesis. As absorbed water swells the matrix, mobility of the penetrant species is altered as a result of changes in the internal structure of the network. Such changes modify the time-dependent behaviour of moisture transport and the result is an apparent concentration dependence of the diffusion coefficient. The Langmuir and BET absorption equations have been used with some success for water vapour sorption at low partial pressures.

In dealing with the Langmuir and BET models a new criterion is introduced to the diffusion process, namely, specific

absorption sites for the penetrant in the resin/composite. The exact nature of these sites are not fully understood. However, the functional groups present in the resin system and the cured resin morphology may offer specific absorption sites for the penetrant.

The functional groups present in the 914 resin system include OH, C=0 and O=S=0 groups, unreacted epoxy groups and unreacted or partially reacted DICY. In composites the resin fibre interface would also be a possible attraction site for sorbed moisture. The type of fibre in use can have a contribution to the diffusion process, for example, Kevlar fibres are known to absorb significant amount of moisture. `Holes' or irregular cavities in the matrix have also been proposed as possible absorption sites for the penetrant[223]. It was proposed that these holes formed when the crosslinked resin was cooled below its Tg, and the loss of segmental motion froze `holes' in the resin. Due to the nature of the crosslink density in these epoxy resins, the regions of low crosslink density could exhibit a preferential site for sorbed penetrant[223].

There is some evidence to indicate that sorbed moisture in polar resins does not exist in two phases[224]. Moy et al[203] showed that at low moisture concentrations the penetrating species was immobilised. On increasing the moisture concentration the secondary water layers exhibit mobility. Carter and Kibler [225] and Gurtin and Yatomi [226] proposed a Langmuir type absorption model which involves mobile and immobile phase for the diffusing penetrant.

2.6.2.3 Langmuir Type Absorption Model [226]

The model is based on the assumption that absorbed moisture consists of a mobile and bound phase. Molecules of the mobile phase diffuse with a concentration and stress independent diffusion coefficient (D), and are absorbed with a probability per unit time (γ). Molecules are emitted from the bound phase, thereby becoming mobile with a probability per unit time (β).

The percentage, by weight, of moisture uptake after a time (t), in an initially dry specimen is given by equation [2.39].

$$M_t = M_m \left[\frac{\beta}{\gamma+\beta} e^{-\gamma t} Y(t) + \frac{\beta}{\gamma+\beta}(e^{-\beta t} - e^{-\gamma t}) + (1 - e^{-\beta t}) \right] \quad [2.39]$$

where,

$$Y(t) = 1 - \frac{8}{\pi^2} \sum_{j=0}^{\infty} \frac{\exp\left[-(2j+1)^2 (Kt)\right]}{(2j+1)^2} \quad [2.40]$$

The terms representing Y(t) are the same as those which determine Mt in Fickian diffusion mode when $\gamma = 0$. When the exposure time is small enough such that Kt is less than about 0.7, equation [2.39] yields the approximation

$$M_t = \frac{4}{\pi^{1.5}} \left[\frac{\beta}{\beta+\gamma} M_m \right] \sqrt{Kt}$$

$$2\gamma, 2\beta < K, \tau < 0.7 / K \quad [2.41]$$

where

$$K = \frac{\pi^2 D}{h^2}$$

If the exposure time is long enough such that Kt is large compared to 1, the following approximation was said to hold;

$$M_t = M_m\left[1 - \frac{\gamma}{\gamma+\beta} e^{-\beta t}\right] \qquad \begin{matrix} 2\gamma, 2\beta > K \\ t > 1/K \end{matrix} \qquad [2.42]$$

Using the nomenclature defined previously, equation [2.42] can be rewritten as follows;

$$\frac{M - M_i}{M_m - M_i} = 1 - \frac{\gamma}{\gamma+\beta} e^{-\beta t} \qquad [2.43]$$

Rearranging equation [2.43] and taking the natural logarithm on both sides of the equation yields the following expression;

$$\ln\left[1 - \frac{M - M_i}{M_m - M_i}\right] = \ln\frac{\gamma}{\gamma+\beta} - \beta t \qquad [2.44]$$

A plot of Ln $(1-(M-M_i)/(M_m-M_i))$ versus time will give the value of γ and β, with β being the slope and γ being the intercept value at time (t)=0.

The diffusivity, D_2, for the dual mode sorption model is related to the diffusitivity for the one phase model by the

following relationship [215];

$$D_{DM} = D_F \left[\frac{\gamma + \beta}{\beta} \right]^2 \qquad [2.45]$$

In this programme the both the Fickian model and the Dual-Mode Sorption models were applied to the diffusion of moisture into the 914 epoxy resin system.

2.7 Effect of Absorbed Moisture on Tg

As mentioned previously, sorbed moisture can result in the plasticisation of the matrix and can lower the Tg. The extent to which the Tg is lowered is important as this factor determines the operating temperature range for the material. The values reported in the literature for the lowering of Tg by sorbed moisture varies between 50° - 150°C for tetrafunctional crosslinked epoxy resins[227-232].

The Tg is viewed as a transition from an equilibrium to a non-equilibrium state which is the result of insufficient molecular or segmental motion in the material. As a polymer is heated it undergoes a transition similar to a classical thermodynamic second order transition. For example, in thermodynamics a first order transition involves a discontinuity in a primary thermodynamic quantity such as entropy (S) and the enthalpy (H). A second order transition involves a change in the slope of the first derivative of the primary thermodynamic quantity e.g. heat capacity (cp) and the coefficient of thermal expansion.

An excellent review on the various models for predicting the lowering of Tg by diluents was presented by Moy[233].

Gordon et al[234] derived an expression relating the Tg of a polymer-diluent mixture to the Tg of the components. Their derived expression was also obtained from a classical thermodynamic argument by Couchman and Karasz [235]. The expression was given as:

$$T_{g_{12}}(\phi) = \frac{\phi_1 T_{g_1} + (1 - \phi_1) T_{g_2} K}{\phi_1 + (1-\phi_1) K} \qquad [2.46]$$

where;

$T_{g_{12}}$ = glass transition temperature of the mixture.

$\phi_{1,2}$ = volume fraction of the polymer and diluent respectively.

$T_{g_{1,2}}$ = glass transition temperature of the polymer and diluent respectively.

K is a parameter initially adjustable to yield a best fit curve for the experimental data. However, K may also be formally identified with the ratio $\Delta Cp_1/\Delta Cp_2$ where $\Delta Cp_{1,2}$ is the heat capacity discontinuity at $Tg_{1,2}$ respectively [234].

Carter and Kibler [236] derived a configurational entropy model for the Tg in wet resins and composites. The model is particularly applicable to cases where the diluent is absorbed primarily by localization at strongly polar molecular groups. This model is of particular interest because it utilizes some parameters which are determined by the chemical structure of the crosslinked network. The

Carter and Kibler equation is given as:

$$Tg_{12} = Tg_1 [1 - (R / \Delta C_p M_s) Y(r)] \qquad [2.47]$$

where;

$$Y(r) = r \ln (1/r) + (1+r) \ln (1/(1-r))$$

$$r = [M_s/M_w]f$$

M_s (gm / mol)= effective formula weight of a hydrogen bonded site.

ΔC_p (cal / gm/ K) = specific heat change on passing the Tg of the dry resin.

R (Cal / gm K) = universal gas constant.

M_w (gm.mol) = formula wt of water.

f = moisture fraction.

The Tg measurements that were carried out in this programme for the neat 914 epoxy resin system were fitted to the Carter and Kibler model and the results are discussed in a subsequent section.

3. EXPERIMENTAL

3.1 Composite Manufacture

3.1.1 Materials and Laying-Up

The prepreg materials used in this programme were continuous XAS/Fibredux 914 and Kevlar/Fibredux 914 as supplied by Ciba-Geigy in the form of zero-bleed prepregs. The resin content of the prepregs was 34% and 48% for the carbon and Kevlar respectively. Prior to cutting and laminating, the prepregs were removed from -18°C cold storage and allowed to equilibrate to ambient temperature. The prepregs were then cut into one-meter lengths and stacked-up using a vacuum chuck which was designed and built for this purpose, see Figure 3.1. The hybrid laminates were made by stacking individual Kevlar and carbon plies in the required sequence. In addition to the 100% unidirectional carbon and 100% unidirectional Kevlar composites, three unidirectional intra-ply hybrid constructions were also made; the stacking sequences were as follows:

100% Kevlar	16 plies
50% Kevlar	(K,C,K,C,K,C,K,C)s
37.5% Kevlar	(K,C,C,K,C,C,K,C)s
25% Kevlar	(K,C,C,C,C,K,C,C)s
100% carbon	16 plies

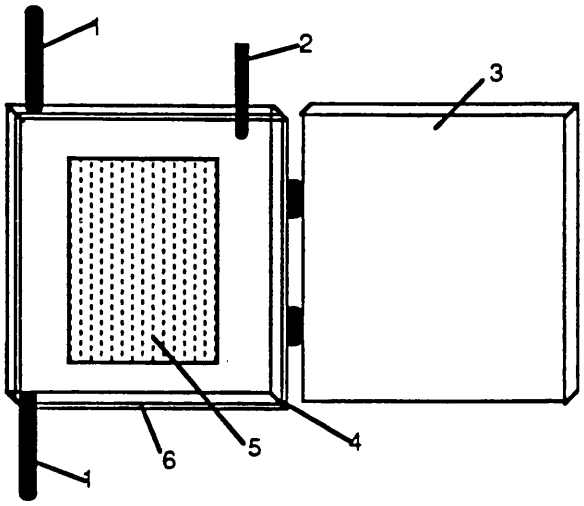

(1) Handle
(2) Vacuum I let
(3) Base Frame
(4) 2 Layered Persplex Frame
(5) Top Persplex Sheet with Perforations
(6) Base perplex Sheet

Figure 3.1 Illustration of vacuum chuck used in to lay-up prepregs. (Built by R. Jones and J. Hayward).

As a result of time constraints and in order to keep the research programme within manageable bounds, the number of compositional variations were limited to the above mentioned. The investigation was based on the effect of 'diluting' a 100% carbon composite and characterizing the subsequent fatigue response. The outer layers of the hybrids were Kevlar plies to mimic real life situations where Kevlar is placed on the outer layers to give the structure impact protection.

A portion of the initial research programme was dedicated to the processing and quality control of aligned short fibre interply hybrid composites. Details of this work were reported in a previous publication[40].

It is worth mentioning that a simple but effective method for hand laying of prepregs was developed, see Figure 3.2. This method ensured that the alignment and orientation of the

fibres was better controlled and reproducible. A template was used to cut out the required shape and size from the prepreg sheet, see Figure 3.2(A). Two strips of double sided adhesive tape were then placed on the template and the cut-out prepreg, with the backing paper still in place, was then stuck on to the template. This whole unit was then laid down onto two strips of double-sided adhesive tape which had been previously placed on the laying-table, see Figure 3.2(B). Alignment was achieved via a right-angle piece, see Figure 3.2(C). The template was then eased off and the prepreg was rubbed down to get rid of trapped air. The top release paper was removed and the process repeated until the required number of prepregs had been laid.

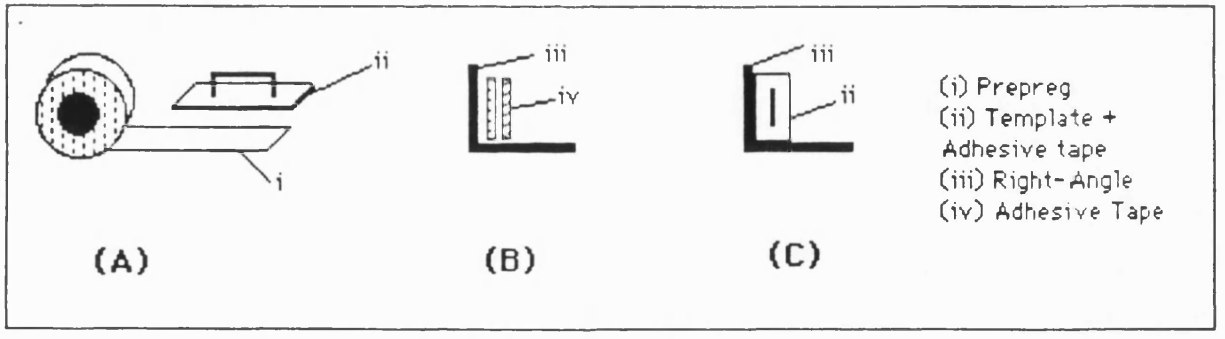

Figure 3.2 Schematic illustration of the improved hand-laying-up procedure for prepregs: see text for explanation.

3.1.2 Curing of Prepregs

The stacked prepregs were sealed in polyethylene bags with a sachet of silica gel and dispatched to the Royal Aircraft Establishment for cold storage and subsequent autoclaving. The cure schedule used was as follows[86].

(a) Heat under vacuum to 120 °C at ~ 2 °C per minute;

(b) When component reaches 120 °C apply 700 kN/m^2 pressure and vent component to atmosphere. Continue heating to 175 °C;

(c) Cure for 1 hour at 175 °C;

(d) Post-cure for 4 hours at 190 °C. Cool to 60 °C before pressure removal and component ejection.

3.2 Specimen Preparation

3.2.1 Tensile - Static and Fatigue Test Samples

The cured panels were C-scanned at RAE for quality, dried and then dispatched back to Bath. A diamond saw, with water as the lubricating medium was used to cut strips from the panel; defective regions identified from the C-scan were excluded. The dimensions of the specimens used in this program are illustrated in Figure 3.3.

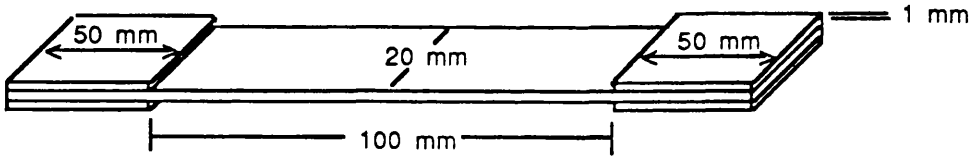

Figure 3.3 Specimen dimensions and profile utilized in this programme for static and fatigue testing.

Only straight edged specimens were used in this program. This was primarily due to the ease of production of straight edged specimens compared to profiled or waisted edged specimens. Furthermore, previous researchers had found no advantage in using profiled specimens[84,87].

The edges of the samples were polished using 320-grit number abrasive paper. This was particularly necessary for composites which contained Kevlar since it burred quite extensively at the edges. Subsequently, panels were dispatched to British Hovercraft for water jet cutting. The edge finish on the Kevlar composite from water jet cutting was excellent. However, in the carbon composite and in the hybrids, this cutting process tended to induce edge delaminations at the carbon/Kevlar interface and carbon fibre breaks at the edges. Hence, edge polishing was once again necessary to remove these defects. The specimens were dried in an air circulating oven at 60 ^{o}C for about two days prior to end-tabbing.

3.2.2 End-Tabbing

The optimum sample preparation and bonding conditions were arrived at by a process of trial and error, especially in the case where the outside plies were Kevlar. Aluminum sheets, 0.5X0.5m were first sand blasted on one side and cut into 21mm wide strips and then into 50mm long pieces. These were then immersed in acetone and placed in an ultrasonic cleaner for about 30 minutes. The process was repeated for the same length of time in a fresh supply of acetone. After the immersion, the acetone was decanted and the end-tabs were dried off under a stream of hot air and stored in an air-circulated oven until required.

The composite samples were first subjected to light surface abrasion over the intended tab-bonding area. The abraded regions were then wiped clean with acetone and the flamed,

i.e. the abraded ends were whisked past the flame of a bunsen burner to evaporate off the solvent and to possibly increase the surface polarity of the fibres. Flaming is used in the polyethylene packaging industry to improve the materials' bonding and dye receptive properties. Samples prepared in this manner proved satisfactory even under compressive loading.

The aluminum end-tabs were bonded on using a two-part epoxy resin; Ciba-Geigy Redux 403 adhesive. A limited amount of work was carried out to investigate the fatigue response of specimens which had been previously subjected to 100% RH conditioning. It was previously established that for these conditions, Ciba-Geigy Araldite 2004 resin proved satisfactory[88,89]. The resin was mixed just prior to end-tabbing. A thin film of the adhesive was applied onto the sand-blasted side of the aluminum tab and the abraded composite sections, these were then stuck together. Initially the tabbed specimens were placed in an alignment jig (three specimens at a time) to prevent tab movement during curing of the resin. Using this method of end-tabbing, the through-put was low and it was not possible to obtain a consistent glue-line. Furthermore, copious amount of mould release aerosol had to be sprayed onto the jig to prevent the resin from adhering to it.

Subsequent trials showed that it was possible to carry out end-tabbing without the use of the alignment jig. This involved placing the assembled specimens on a flat aluminum base plate (0.5X0.5m) which was covered with release paper. Another sheet of release paper and a flat metal plate was

placed on top of the assembled specimens and the whole assembly was then transferred to a hydraulic press. A contact was applied for one minute and the pressure then released. The top aluminum plate and release paper was removed and the specimens were inspected visually to check for tab misalignments. Significant movement was observed only if excess resin was initially applied. After making the necessary adjustments to the tabs the release paper and top aluminum plate were placed on top of the assembled specimens. A contact pressure was once again applied and the resin was cured at ambient temperature for 24 hours after which the temperature was raised to 45 ^{o}C for a further 24 hours[90].

3.3 Tension-Compression Fatigue And Static Compression

3.3.1 Tension-Compression Fatigue Testing

The jaw configuration of the fatigue test machine did not permit the use of short gauge length specimens and hence standard length tensile specimens were used in conjunction with the RAE anti-buckling guide. An illustration of the antibuckling guide used in the programme is presented in Figure 3.4. Two such jigs were built and were used to carry out all the tension-compression fatigue testing reported in this programme. This jig was designed by the Royal Aircraft Establishment-Farnborough.

3.3.2 Static Compression Testing

As mentioned previously, the jaw configuration of the fatigue test machine did not permit the use of small gauge length specimens. However, static compression testing using the RAE rig was also not attempted because of the possibility of damage to the compression jig. The static compression tests were carried out on a jig developed by Dr. A. Barker, Department of Chemical Engineering, University of Birmingham. The following description of the jig was reproduced from reference number 91. The jig consists of two steel blocks into which either end of the specimen is inserted. It is gripped over a 40mm length by the side face clamps. All surfaces of mutual contact between the jig and the specimen are smoothed in order to prevent damage to the specimen by gripping. The blocks themselves are placed within a high precision die set which is used to ensure axial loading. The upper block is fixed but the lower block floats within the die set. Most of the load is transferred to the specimen directly through its ends which are in contact with hardened steel inserts in the pressure plates. However, about 10-20% of the load is transferred through the side face clamps. The level of side face loading is controlled by the use of a torque wrench on the allen-head screws.

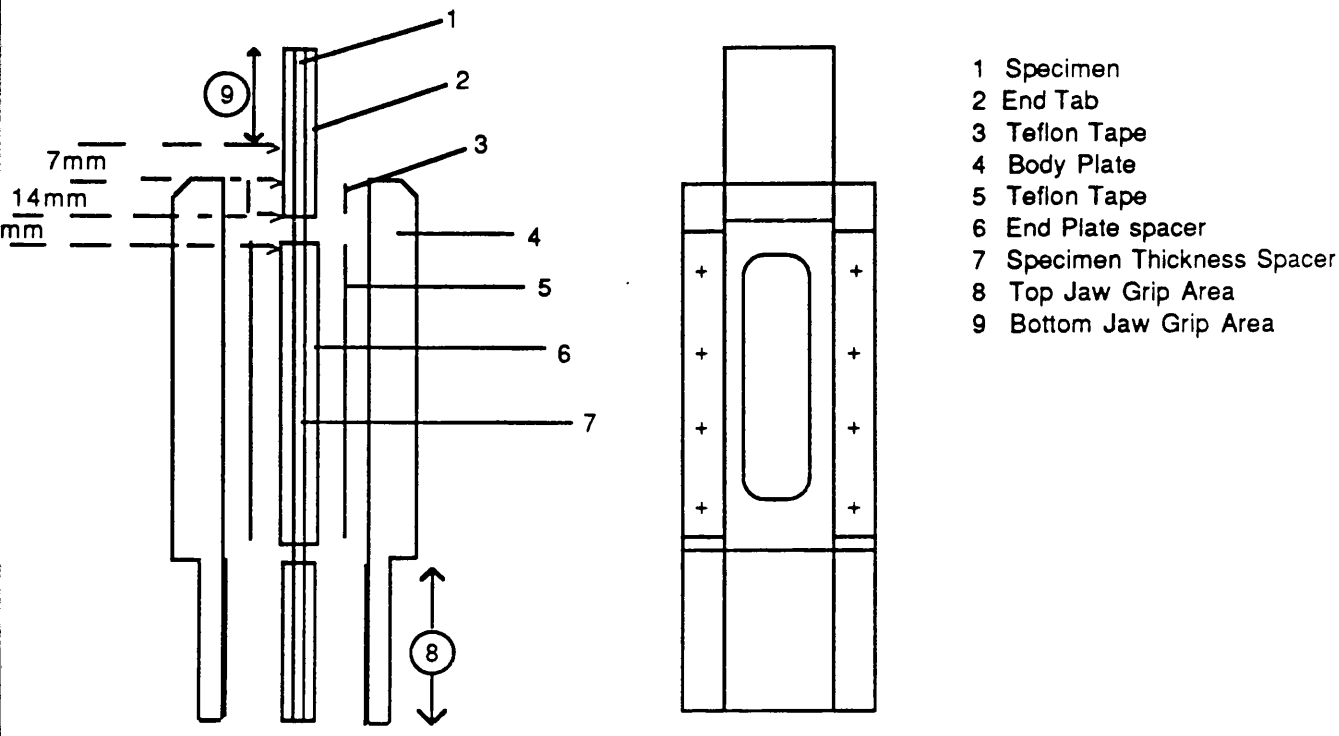

Figure 3.4 RAE Anti-buckling Guide: Reproduced from reference number 85.

The dimensions and specimen profiles are illustrated in Figure 3.5. A great deal of care and attention was in preparing samples for use in this jig. All the edges and end faces of the specimens were ground parallel and perpendicular to ensure that the overall dimensions were maintained within defined tolerance. This was done to ensure that a precise fit of the specimens within the jig was achieved.

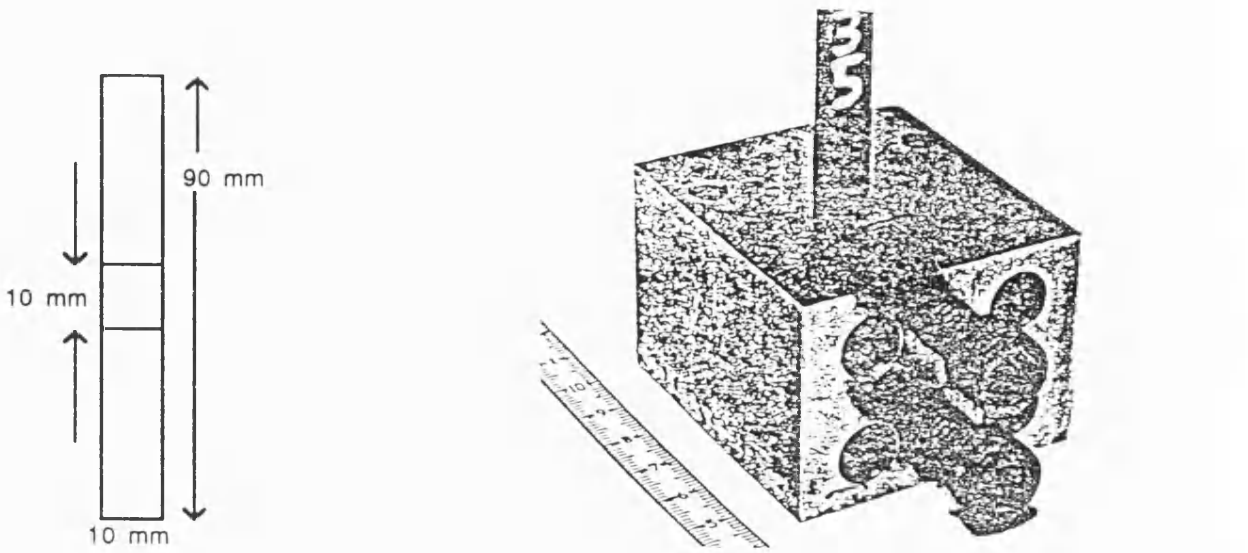

Figure 3.5 (A) Illustration of specimen dimensions and profile; (B) Static compression jig copied from reference number 91.

3.3.3 Static and Fatigue Testing Machines

All the static tensile and compression tests were carried out on an screw-driven Instron 1195, (100KN) machine at a constant cross-head speed of 0.5mm/minute. The tensile specimens were always instrumented with an extensometer and when required the samples were strain gauged.

The fatigue tests were carried out on a pair of servo-hydraulic Instron 1332 and 1342 (100KN) machines under load control. The tests were carried out initially at a constant rate of load application (RLA) of 200KN/second. However, while generating the first S-N curve, it was realized that the RLA had to be increased if all the the hybrid compositions were to be tested within the time scale of this

programme. Hence the RLA was raised to 500KN/second. Both static and fatigue tensile tests carried out at the two frequencies did not show any significant differences in the measured tensile or fatigue behaviour. Furthermore, it was also previously established[88,89] that at the RLA under discussion, neither Kevlar nor carbon composites exhibited any rate dependence on strength.

3.3.4 Elevated Temperature Fatigue

A furnace was designed and built to investigate the effect of temperature on the fatigue response of the composite materials used in this programme. An illustration of the furnace is presented in Figure 3.6. The installation procedure for the specimen was as follows: the specimen was clamped in the usual way into the top jaw of the fatigue machine; a plumb line or a right-angle piece was used to ensure that the specimens were clamped vertically. The furnace was then bolted onto the top jaw assembly of the fatigue machine via the asbestos disk. A clearance of approximately 10mm was allowed between the furnace and the bottom jaw assembly; this region was covered with glass wool to minimize the heat loss from the specimen. The specimens were allowed to stand for 20 minutes in this assembly at the required temperature prior to commencing the fatigue testing. Surface temperature measurements of the specimens were obtained during the fatigue testing by the use of thermocouples. This confirmed that the specimen surface temperatures were within two degrees of the furnace air temperature.

The surface temperature of the composites and hybrids specimens was also monitored on occasion for the period of the fatigue testing. This was achieved by attaching a thermocouple to the mid-section of the specimen. A reference thermocouple was also included in the circuit to monitor the

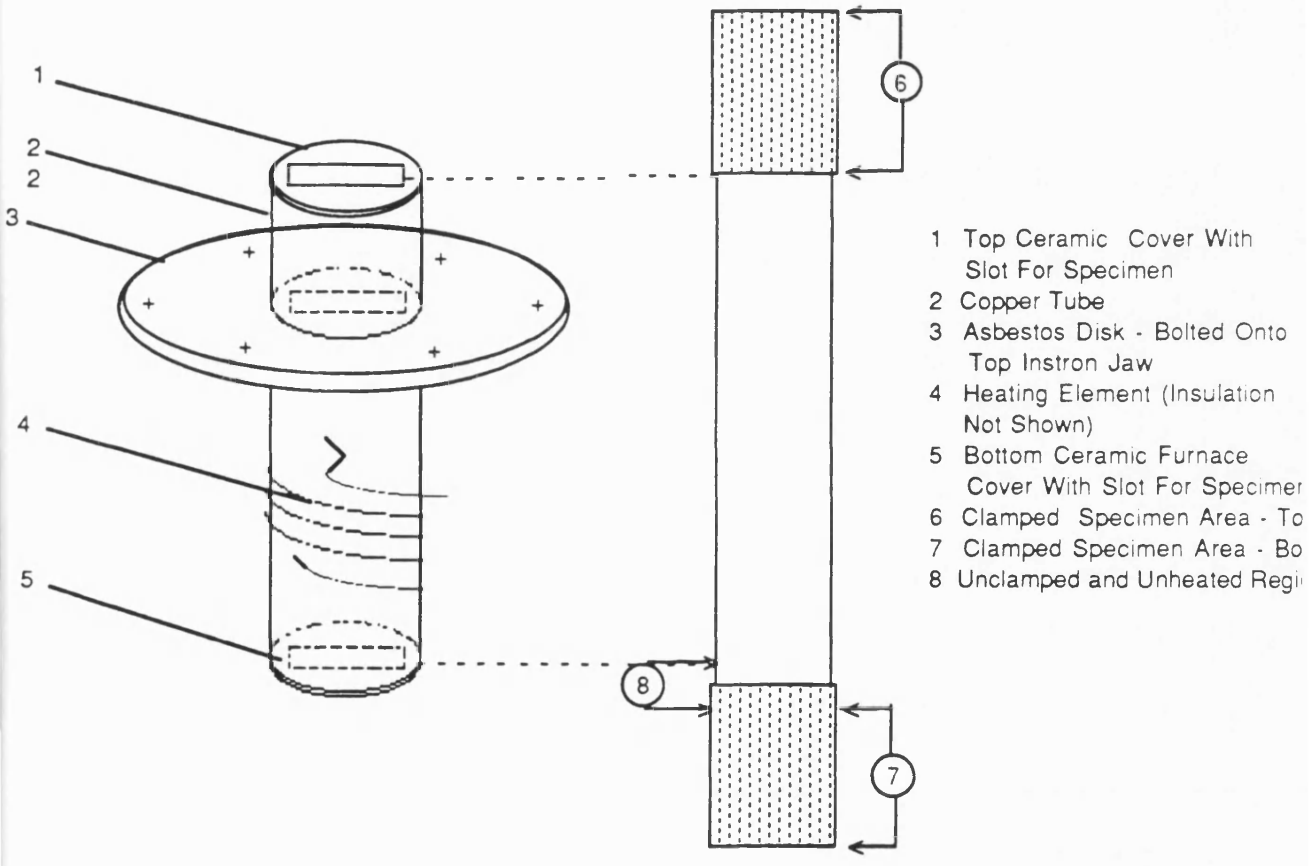

Figure 3.6 Illustration of 'oven' used in elevated temperature fatigue studies in this programme.(Built by Mr. P. Taylor).

temperature of the immediate surroundings, i.e. laboratory temperature. The thermocouple was attached at the centre of the specimen via a bulldog clip and was shielded from the laboratory atmosphere with a piece of expanded polystyrene.

3.4 Damage Monitoring And Fatigue Testing

Three of the following methods were employed in an attempt to monitor the progress of damage build-up in the composite materials during fatigue testing.

3.4.1 Enhanced X-Ray Radiography

Initial trials were carried out on dental x-ray unit at Bath University Medical Centre using pre-fatigued 0/90 Kevlar/ code 69 composites. A zinc iodide/isopropyl solution was used as the penetrant. Excellent x-ray radiographs were obtained showing transverse and longitudinal cracking and delamination sites, confirming the observations of previous research[88]. As a result of this, an x-ray unit was designed to facilitate in-situ radiography during fatigue testing. This simply consisted of an x-ray unit mounted in a mobile 'split-cabinet' which was clipped around the Instron jaws. The stringent requirements of the University's radiological requirements were complied with. This unit gave good results with cross-plied and angle-plied continuous and short fibre composites. However, unfortunately the damage modes observed for the unidirectional composites made this technique inapplicable.

3.4.2 Optical Microscopy

Composite sections were cut, mounted in resin and polished using standard techniques. Fibre volume fraction determinations were carried out on these sections using an image analyser. Pre-fatigued composite specimens were always

mounted in resin prior to sectioning and polishing for optical microscopy.

3.4.3 Scanning Electron Microscopy (SEM)

Post failure investigation of the composites and resin were carried out on a Jeol 35C. Sections for SEM were obtained from failed composite sections of interest and were sputter coated with a fine film of gold using standard techniques.

3.5 Diffusion Studies On 914 Resin And Carbon/Kevlar Composites

The experiments in this section were divided into two sections:

(a) Characterization of the diffusion behaviour of neat 914 resin and;

(b) Characterization of the diffusion behaviour of carbon and Kevlar composites and their interply hybrids. Due to specimen availability and time limitations it was not possible to carry out a comprehensive investigation into the fatigue response of environmentally conditioned specimens; however, a limited number of such experiments were conducted.

3.5.1 Neat 914 Resin Specimens For Diffusion Studies

The neat resin samples used in this programme were supplied by Ciba-Geigy as solid resin. Neat resin film was also

initially evaluated but was later abandoned since it was not as convenient a process as the solid resin samples.

A moulding technique was developed to produce neat resin samples using similar procedures implemented in the manufacture of composites At first, neat resin samples were made via silicone moulds, however controlling the void content and specimen profile proved difficult. A moulding technique using a frame and a hot-press was developed and it overcame the problems encountered with using silicone moulds. Surface profiles similar to that of the composites were obtained using the same make of release cloth material. The thickness of the frame determined the specimen thickness; two frame thicknesses were used, namely, 1.1mm and 1.5mm. The cure schedule used was identical to that used to process composites. Vacuum application was carried out in a vacuum oven and then the assembly was transferred to the hot-press. After post-curing the plaques were cooled to room temperature prior to removal from the press. These were then cut into 20mm wide strips and the edges were polished on 800 grip abrasive paper. Following this the specimens were cut to give the required length, washed and dried to constant weight. Once this was achieved the samples were transferred to the appropriate distilled water baths.

3.5.2 Composite Specimens For Diffusion Studies

The composite specimens used for these experiments were obtained from panels from which the tensile and fatigue samples were obtained, ie. those autoclaved at RAE. The following fibre orientations and hybrid compositions were

used in this study:

(a) 0^{o} & 90^{o} ud carbon composites
(b) 0^{o}, 90^{o} & 45^{o} ud Kevlar composites
(c) 0^{o} & 90^{o} ud 25%, 37.5% and 50% Kevlar/carbon interply hybrids.

The composite specimens were prepared in a similar way to the tensile specimens except that the length was 10cm, Figure 3.7. The edges were first polished and cleaned and then dried to constant weight at $60^{o}C$ in an air circulated oven. A moisture resistant lacquer was then painted along the edges and the specimens were returned to the oven for a further two weeks, reweighed and then placed into the relevant conditioning tanks.

3.5.3 Environmental Conditioning

The diffusion response of the neat resin and that of the composites was investigated under the following environmental conditioning treatments:
(a) 65% RH, $23^{o}C$;
(b) 100% RH $23^{o}C$;
(c) 100% RH $50^{o}C$;
(d) 100% RH $75^{o}C$;
(e) 100% RH $100^{o}C$.

The 100% RH $100^{o}C$ conditioning was carried out in a round bottom flask under reflux conditions. Individual specimens were suspended in the flask via copper wires to avoid

bunching. The rest of the environmental conditioning was carried out in water baths at the appropriate temperatures. The samples were removed periodically from their conditioning environments, dried between absorbent tissue, weighed and then returned back to their conditioning environments. The moisture uptake values quoted are the average of four or five individual specimens uptake values.

The test specimens for the neat resin were coded as follows: i) 25C; ii) 75CR; and iii) 100TS. The numeral in front of the letters represents the conditioning temperature. The letters (C) and (TS) after the numerals represent a sample thickness of approximately 1.1mm and 1.5mm respectively. The letters (CR) represent a series of tests where the specimens were removed more frequently from their conditioning environment to monitor the initial weight increase in the specimens due to moisture absorption.

3.5.4 Glass Transition Temperature Measurements (T_g)

The T_g of the resin samples was also measured as a function of progressive moisture uptake with time for the various environmental conditions investigated. The T_g were carried out on a Perkin Elmer DSC-1B machine. The T_g is defined as the mid-point of the region where a change of slope was observed in the DSC trace. Samples for the T_g measurements were obtained by snapping off pieces of neat resin plaques which were immersed in the various environments along with the diffusion specimens. The specimens were shaped using a pair of wire cutters, weighed and then placed into the standard aluminum pans; an aluminum lid was crimped on. The

results quoted are the average of 2-3 individual specimens and each of these was subjected to three consecutive temperature scans from ambient to 200°C under a nitrogen flow of approximately 10cc per minute. The instrument was periodically calibrated using indium and tin[92].

Specimen preparation for DSC analysis of composites proved difficult and furthermore, attempts to obtain T_g from composite specimens was not successful.

4. RESULTS AND DISCUSSION - NEAT RESIN AND STATIC PROPERTIES

The following abbreviated coding system was used to make reference to the composite materials used in this programme.

100% XAS=(XAS Composite)-Carbon mono-fibre composite;
25% Kevlar=(25% Hybrid)-25% Kevlar/75% XAS hybrid composite;
37.5% Kevlar=(37.5% Hybrid)-37.5% Kevlar/62.5% XAS hybrid composite;
50% Kevlar=(50% Hybrid)-50% Kevlar/50% XAS hybrid composite;
100% Kevlar=(Kevlar Composite)-Kevlar mono-fibre composite.

4.1 Neat Resin Properties

4.1.1 Fiberdux 914 Neat Resin - Tensile Properties

A summary of the tensile properties of moulded neat 914 resin samples tested in this programme are presented in Table 4.1. The stress-strain curves for the neat resin were essentially linear to failure, see Figure 4.1.

	Failure Strain (%)	Tensile Strength (MPa)	Modulus (GPa)	
Min	0.68	34.51	2.92	
Max	1.26	39.43	5.45	
Mean	1.06	37.25	3.71	No. of observations = 6
SD	0.27	1.9	1.04	
CV(%)	25.29	5.10	28.05	

Table 4.1 Summary of tensile properties for neat 914 resin.

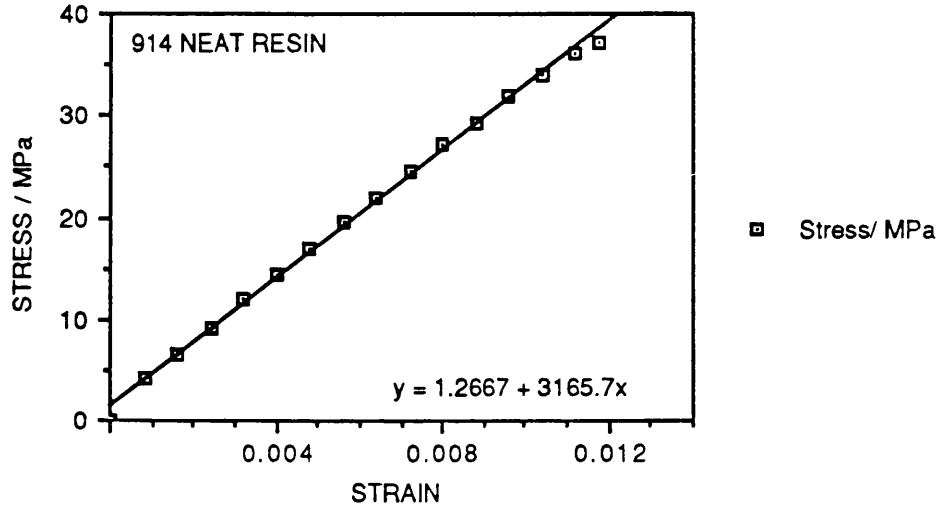

Figure 4.1 Stress-Strain Trace For Moulded 914 Neat Resin

The values quoted in reference number 117 were 1.4 % for the failure strain at ambient temperature and, 51 MPa and 3.96 GPa for the tensile strength and modulus respectively. The measured tensile properties in this programme are in good agreement with those obtained by Woolstencroft[118], who obtained values of approximately 1.2 %, 48 MPa, and 3.9 GPa for the neat resin failure strain, tensile strength and modulus respectively. The measured properties of resin systems are very sensitive to the initial quality of the resin components and in particular to the processing route taken in its production.

4.2 Fibre Volume Fractions

A typical distribution of fibre volume fractions for the XAS and Kevlar mono-fibre composites are illustrated in Figures 4.2 and 4.3 respectively. As described previously, an image

analyser was used to measure the fibre volume fractions. The average fibre volume fraction for the XAS composite was found to be 60.3%. The Kevlar fibre volume fraction on the other hand gave an average value of 55%. The Kevlar fibre volume fibre distributions showed a greater spread compared to the XAS fibre distribution. Clustering and the incidence of touching fibres was greater for the Kevlar plies.

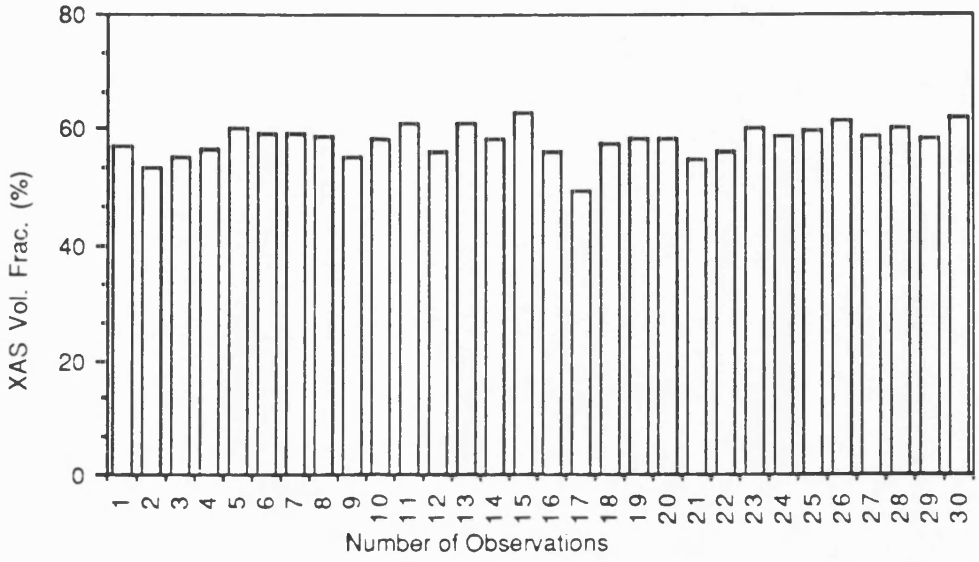

Figure 4.2 A typical XAS fibre distribution for the XAS/914 composite.

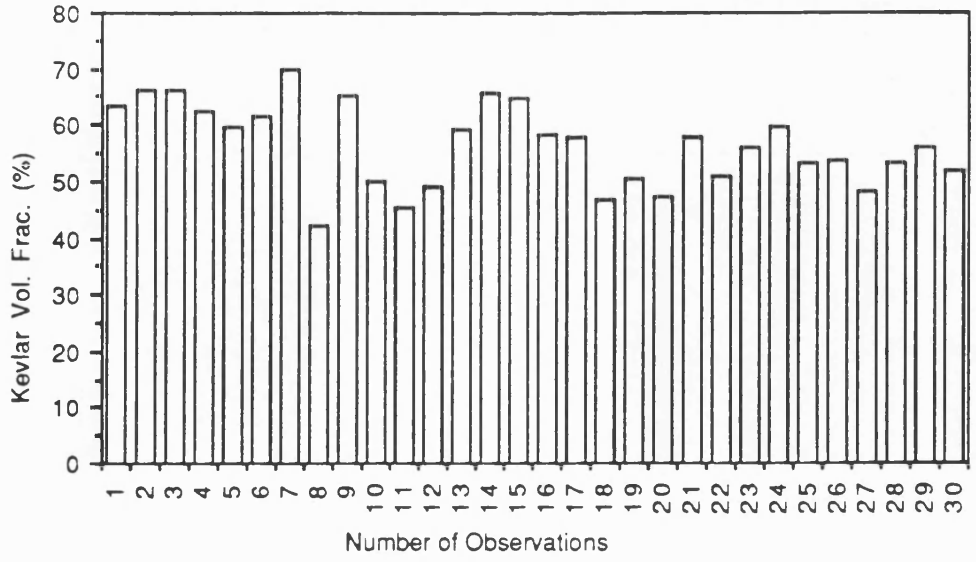

Figure 4.3 A typical Kevlar fibre distribution for the Kevlar/914 composite.

4.3 XAS Mono-Fibre Composite - Tensile Properties

A selection of typical stress-strain curves for the XAS mono-fibre composite are reproduced in Figures 4.4-4.6. Three representative XAS stress-strain curves are illustrated in Figure 4.4. These figures were reproduced from the load-displacement traces from the Instron test machine. A statistical summary of the tensile test data is presented in Table 4.2. The range of failure strains obtained from twelve specimens was between 1.30-1.48% with a mean of 1.37%. The failure strains quoted by the manufacturers for XAS fibres was 1.3 - 1.5%[111]. Specimen number 4.1 recorded a failure strain of 1.48 %, this specimen was strain gauged in addition to the use of an extensometer to monitor strain. Specimen number 2.3 showed the highest non-linear behaviour and specimen number 2.7 displayed the highest secondary modulus (modulus at failure). It is evident from Figure 4.4 that the stress-strain response of this material was not linear, an apparent increase in the modulus was observed with increasing strain and stress. The strain gauged specimens also showed a similar behaviour. Figure 4.5 illustrates the comparison between the strain gauge output to that of the extensometer. Both sets of data displayed an increase in the slope of the stress-strain curve, however, the strain gauge data displayed a higher slope. The gauge length of the strain gauge utilized was 10mm and that of the extensometer was 25mm. This may account for some of the differences observed as the strain gauge measures a relatively local strain. Manders[39] found that the strain output was extremely sensitive to the location of the strain gauge.

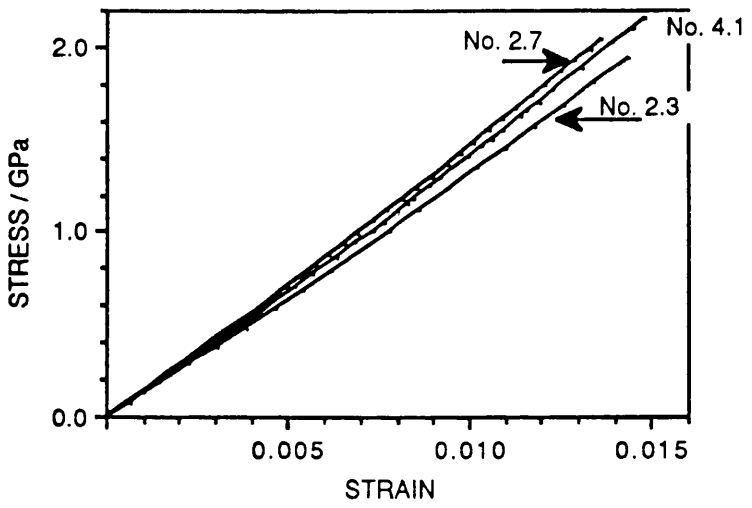

Figure 4.4 A selection of stress-strain curve for 100% XAS fibre composite. Note the non-linear behaviour.

	Failure Strain (%)	Tensile Strength (GPa)	Primary Modulus (GPa)	Secondary Modulus (GPa)
Min	1.304	1.84	121.61	145.52
Max	1.48	2.15	141.28	159.72
Mean	1.37	1.98	135.34	151.99
SD	0.05	0.11	5.34	4.11
CV(%)	3.65	5.46	3.94	2.71

No. of observations = 12

Table 4.2 Summary of Tensile Properties for the XAS Mono-Fibre Composite. (Note: Primary Modulus=Initial Modulus And Secondary Modulus= Modulus At Failure).

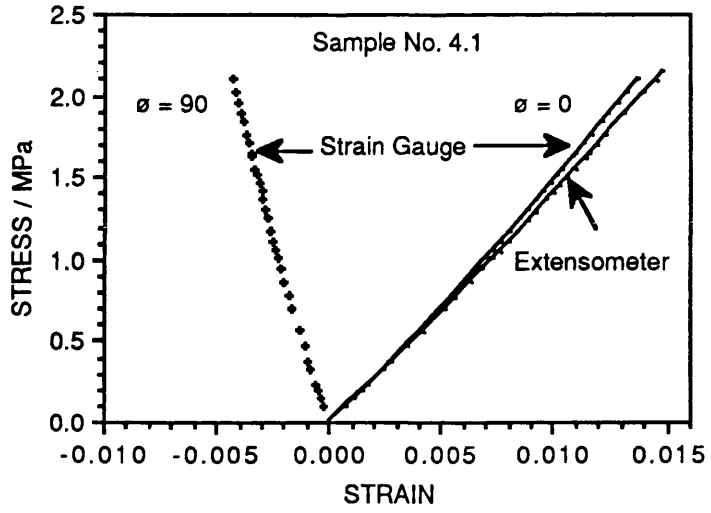

Figure 4.5 A typical stress-strain response for the XAS mono-fibre composite. Both the strain gauge and the extensometer responses were non-linear.

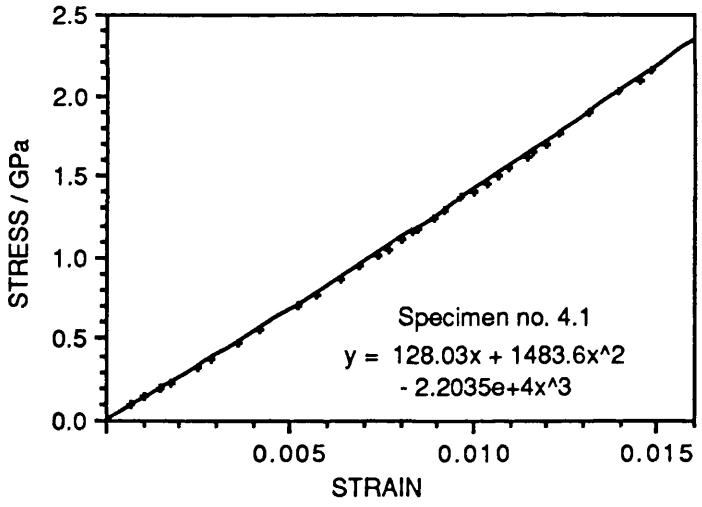

Figure 4.6 Specimen number 4.1 stress-strain response was fitted to a cubic function.

The observed non-linear response of the XAS composites and the inherent variability of the failure strains poses a problem in defining a mean modulus value for this composite. Sample number 4.1 best approximated the average primary and

secondary modulus values quoted in Table 4.2. A cubic function was fitted to sample number 4.1, and is illustrated in Figure 4.6.

Various researchers[104-108] have reported that the stress-strain curves for carbon fibres exhibit non-linear behaviour; i.e., the slope increases with applied stress and strain. Hughes[106] and Curtis et al[108] presented stress-strain data to show that the unimpregnated fibres themselves exhibited an increasing modulus with increasing stress or strain. Curtis et al obtained modulus increases of up to 30% for HTS carbon fibres and no hysteresis effects were observed on repeated loading and unloading. It was proposed that the stiffening of the fibre was associated with a change in the crystallite orientation.

Lagace[104] also reported a non-linear stress-strain response for unidirectional AS/3501 carbon epoxy composites. This composite did not show any significant variation in the fracture stress or moduli between specimens which were directly loaded to failure as compared to those which had been pre-fatigued (loaded and unloaded 100 times). Lagace also found that for [± ø] laminates where ø=0°-15°, overall stiffening of the composite of up to 12% was observed. The measured initial modulus values compares favourably with those predicted using laminate plate theory.

Zweben et al[116] stated that to overcome material and load eccentricity when tensile testing, two strain gauges should be used on both sides of the specimen to detect the effect of

bending stresses.

From the previous discussion, there is sufficient evidence to conclude that carbon fibre and their composites exhibit strain induced stiffening behaviour. However, this stiffening of carbon fibres was not observed/reported by previous researchers of hybrid composites. For example, Manders et al[37] presented a typical load-extension plot for interply carbon/glass hybrid and an observable increase in modulus with increasing strain was evident for the higher carbon volume fraction (Figure 7 of reference number 37), but this increase in modulus was not discussed.

The significance of this observed modulus increase with stress or strain on hybrid composites will depend on the mode of analysis of the stress-strain data. The first obvious conclusion that can be reached is that any calculations based on the initial modulus will underestimate the stress on the carbon fibres especially at high strains. Furthermore, utilization of the initial modulus will overestimate the strain experienced by the fibres especially at high stresses. The summary of XAS mono-fibre composite data presented in Table 4.2 indicates that the modulus increase ranged between 6-21% with an average of 12.5%.

The number of specimens tested (12) did not permit any conclusions to be drawn with regards to the position of the specimen in the composite panel and the observed modulus increase. It is implied here that in addition to the inherent non-linear behaviour of carbon fibres, the processing of the prepregs may introduce a degree of waviness

to the fibres. It is conceivable that this waviness may also contribute to the non-linear behaviour of composites.

The hybrid effect is defined as the enhancement of the initial failure strain of the low elongation fibres in a hybrid composite; therefore it is critical to establish the statistics for the failure strain for the low elongation fibres (carbon). Furthermore, the location and measurement of this initial failure strain from the stress-strain curve of the hybrid composite also needs to be precise - this is not always easily accomplished. The strain outputs obtained from this programme indicated that it was sensitive to the measurement technique used, ie. extensometer or strain gauge. Manders[37] found that the measured strain was sensitive to the location of the strain gauges on the test specimen surface.

The first (initial) failure strain of the carbon fibres in a hybrid composite is taken as the load-drop in the load-displacement trace, and it is assumed that this load drop is entirely due the fracture of the carbon fibres. After the failure of the carbon fibres, the load is transferred to higher elongation fibres, and the subsequent events after this depend on the relative volume fractions of the two fibres as discussed previously. The volume dependence on the failure strength of low elongation fibre composites needs further investigation. For example, Manders[37] et al found that the failure stress and strain increased with thickness of the mono-fibre low elongation composite; this is contrary to what is expected from the statistical treatment of strength. This is also in agreement with the findings of Zweben et al[116]. They proposed that further work should be

carried out to investigate the effect of the number of plies on the tensile and flexural modulus of composite materials. The implication is that the volume dependence of the failure strain needs to be established when considering hybrid composites with varying number of carbon plies.

The details of the predominant failure modes observed under static tensile testing for XAS fibre composites are discussed in a subsequent section. Although there was a steady increase in audible sound emission with increasing applied strain, the final failure was sudden and catastrophic. The failed specimens exhibited extensive longitudinal splitting and transverse fractures. An interesting observation was that specimens in which the transverse fracture was partly within the gauge length tended to give failure strains which were on the high-end of the failure strain range for XAS fibre composites.

4.4 Kevlar Mono-Fibre Composite - Tensile Properties

The summary of the tensile test data for the Kevlar mono-fibre composite are presented in Table 4.3. A representative sample of stress-strain traces obtained for this unidirectional composite are presented Figure 4.7 and 4.8. Unlike the failure mode observed for XAS composites, the Kevlar composite exhibited extensive longitudinal splitting from about 1.5% applied strain. The outcome of this longitudinal splitting was two-fold. Firstly, the longitudinal splitting in some instances tended to 'shift' the extensometer, making the final failure strain

measurements difficult. Secondly, in some cases the splitting resulted in a load drop-off in the stress-strain trace with no apparent change in the strain; this is shown in Figure 4.7.

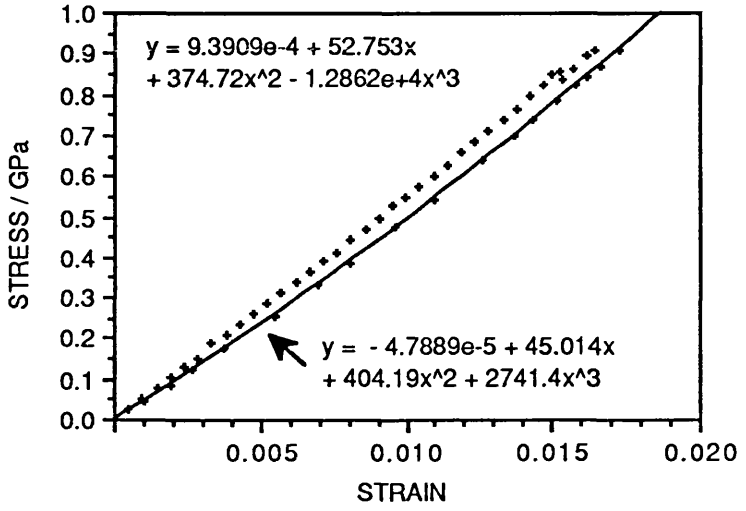

Figure 4.7 Stress-strain output for unidirectional Kevlar/914 mono-fibre composite.

Caution obviously needs to be exercised when analyzing the stress-strain traces for hybrid composites, especially with the Kevlar fibres on the outside because the early longitudinal splitting of the Kevlar can be misinterpreted as the failure of the carbon fibres. The strain-gauge readings were also sensitive to the location of the resistance gauges, in most instances it was not possible to obtain the final failure strain values because the longitudinal splitting either damaged or caused the gauges to delaminate from the surface. From Figure 4.8 it is evident that the surface strain measurements using strain gauges were higher than those obtained using an extensometer.

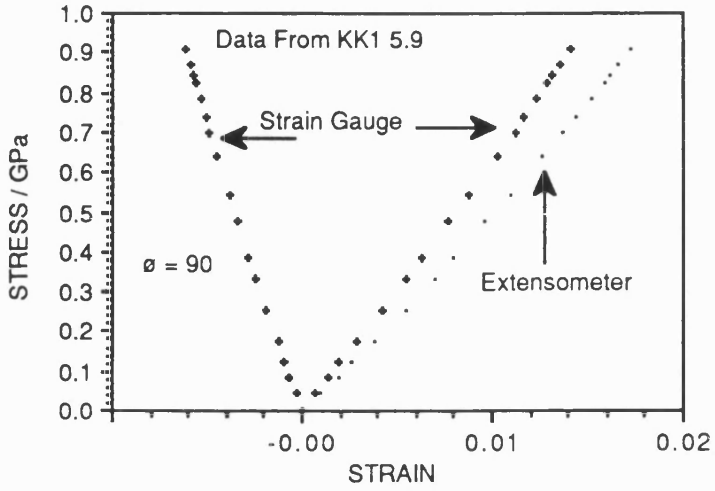

Figure 4.8 Comparison of stress-strain behaviour for strain-gauge and extensometer outputs.

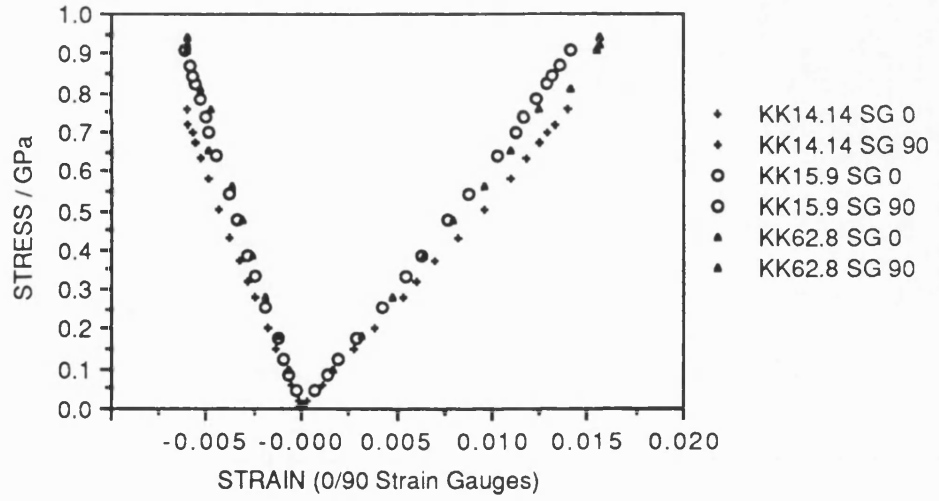

Figure 4.9 Representative stress-strain outputs for specimens instrumented with strain gauges.

The stress-strain behaviour for the Kevlar 49/914 resin composite was essentially linear, however, a stiffening of about 5% on average was observed. This increase in the Kevlar modulus has also been observed by other researchers, eg. Bunsell[114] (Kevlar fibres), Roylance et al[112,125] (composite

static test), Konopasek et al[113], Howard[115], Hahn et al[127] (under fatigue loading).

	Failure Strain (%)	Tensile Strength (GPa)	Primary Modulus (GPa)	Secondary Modulus (GPa)
Min	1.60	0.878	49.48	53.43
Max	1.71	1.179	61.45	66.11
Mean	1.65	0.963	56.12	59.15
[CV] (%)	[2.25]	[10.58]	[7.31]	[64.26]

No. of observations = 10

Table 4.3 Summary of tensile properties of unidirectional Kevlar 49/914 mono-fibre composite.

	Failure Strain (%)	Tensile Strength (GPa)	Primary Modulus (GPa)	Secondary Modulus (GPa)	V_f [Resin]	(Ref)
	1.65	0.963	56.12	59.15	55%	(Current)
CV(%)	*2.25*	*10.58*	*7.31*	*64.26*	[914]	
	1.6	1.241	76.67	89.64	70%	(112)
CV(%)	*0.5*	*6.3*	*6.8*	*7.4*	[934]	
	-	1.1-1.25	65	75	50%	(57)
CV(%)			[Not Specified]			
	-	1.24	75.83	-	60%	(71)
CV(%)			[Not Specified]			

Table 4.4 Selection tensile test data for unidirectional Kevlar composites quoted in the literature.

The measured Kevlar volume fraction for the composites used in this programme was approximately 55%. Using the rule of mixtures equation for the modulus, with a fibre modulus of 130 GPa and resin modulus of 3.71 GPa the expected composite modulus is 73.17 GPa.

From Table 4.3, it is seen that the mean primary and secondary modulus values were 56 GPa and 59 GPa respectively with a range of 49-61 GPa for the primary modulus and a range of 53-66 GPa for the secondary modulus. Roylance et al[112] using a similar resin system with unidirectional Kevlar obtained modulus values of 60 Gpa and 70 GPa for the primary and secondary modulus respectively (V_f normalized to 0.55). The fibre volume fractions obtained by using an Image Analyser were also verified by 'fibre counting' using micrographs of polished Kevlar composite sections. As discussed previously, the volume fraction measurements showed that there was significant variation in the fibre distribution in the Kevlar composites and this may partly account for the range of modulus values observed. In addition to this, it is possible that two other factors may have contributed to the low modulus values observed for these composites, namely; (a) undulating (waviness) profile of the plies and fibres after curing; and (b) the effect of the cure temperatures, residual stresses and resin shrinkage stresses imposed on the Kevlar fibres and thus possibly damaging the fibres. Furthermore, it is also possible that these effects may be partly responsible for the observed non-linear stress-strain behaviour of unidirectional Kevlar composites. These points are further discussed in a later section.

4.4.1 Effect of Fibre Waviness

The Kevlar and carbon composite and their hybrids used in this programme showed a degree of waviness and this is illustrated in Figures 7.18, 7.25, 7.38 and 7.39. Although

the affect of fibre waviness was not investigated in this programme, a brief consideration is given to this topic as fibre waviness can have an effect on both the tensile and especially the compressive properties of composites. Some researchers have speculated that the observed increase in the modulus with strain may be due to the fibres achieving a greater degree of alignment at the higher loads. Various reasons can be speculated upon as to the sources of origin of the observed waviness, and these include: (a) Waviness introduced at the manufacturing stage of the prepregs and subsequent storage; (b) waviness and fibre misalignment could be introduced during the laying-up process; (c) residual stresses may also contribute to fibre curvature. According to Lifshitz, (as quoted by Roylance[125]), the fibres are slightly warped in the cured specimen since they are not under constant tension during cure of the laminate. As a result of this, it was proposed that some of the fibres are not fully effective in load bearing until they are stretched and become straight. DeTeresa[120,128] showed that pre-compressed Kevlar fibres on subsequent tensile loadings displayed a highly non-linear stress-strain curve for the first load cycle and then a linear response with subsequent tensile loadings.

4.5 HYBRID COMPOSITES - TENSILE BEHAVIOUR

A summary of the mean tensile results for the unidirectional Kevlar/carbon composites used in this programme are presented in Table 4.5. In order to facilitate ease of comparison, the results for the mono-fibre composites have been reproduced.

	100% XAS	75% XAS	62.5% XAS	50% XAS	100% Kevlar
Failure Strain (%)	1.372	1.34	1.39	1.32	1.65
[CV] (%)	[3.65]	[3.78]	[3.11]	[1.14]	[2.25]
Tensile Strength (GPa)	1.975	1.594	1.426	1.272	0.963
(CV %)	[5.46]	[7.16]	[5.16]	[2.74]	[10.58]
Primary Modulus (GPa)	135.34	112.94	103.62	94.22	56.12
(CV %)	[3.94]	[7.19]	[2.45]	[2.49]	[6.86]
Secondary Modulus (GPa)	151.99	124.65	113.50	102.88	59.15
(CV %)	[2.71]	[5.79]	[2.96]	[2.99]	[7.31]
No. of Samples	12	12	12	6	10

Table 4.5 Summary of tensile properties for unidirectional mono-fibre and hybrid Kevlar/carbon composites, tested in the fibre direction.

The rule of mixtures equation was found to adequately predict the primary longitudinal tensile modulus of the hybrid composites investigated in this study. Good agreement was also obtained between the mean secondary modulus and the ROM prediction. The mean primary modulus values for the Kevlar composite with the mean secondary modulus for XAS was used in calculation of the ROM equation for the mean hybrid secondary modulus, (line (2) in Figure 4.10).

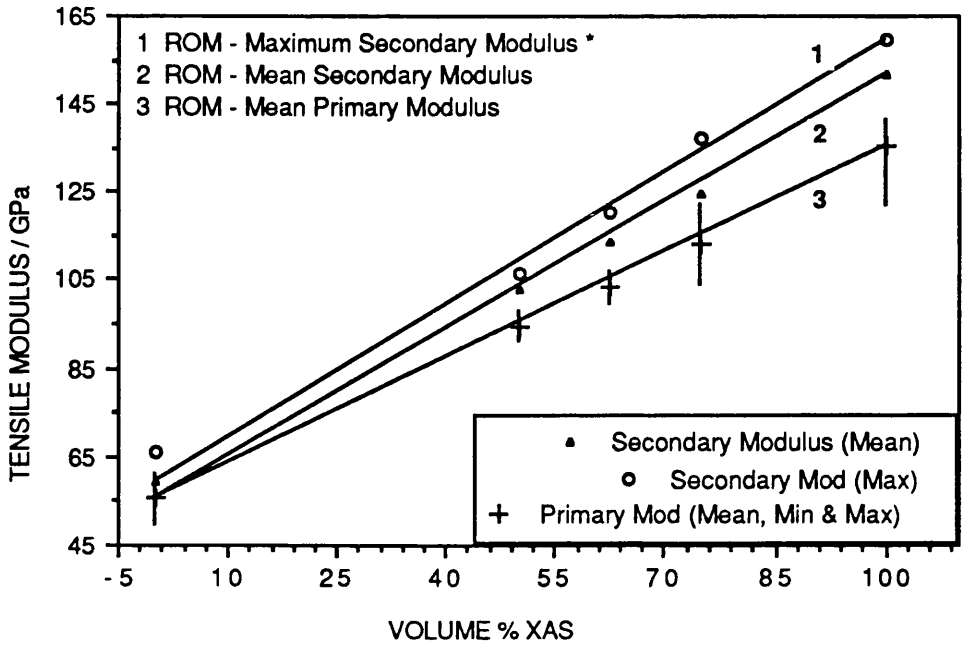

Figure 4.10 Experimental and ROM prediction for the uniaxial tensile modulus for Kevlar/XAS/914 hybrids.

This is reasonable as the corresponding modulus for the Kevlar composites at this strain level in the carbon fibres on average, correspond to the primary modulus. Likewise, the mean Kevlar secondary modulus values and the peak XAS modulus values were used in the ROM, (line (3), in Figure 4.10), calculation of the secondary hybrid modulus. The increase in the secondary modulus values were seen to be in proportion to the volume fraction of XAS present. Like the findings of previous researchers, it was concluded that the ROM equation adequately described the tensile modulus for Kevlar/XAS hybrid composites.

Figure 4.11 illustrates the tensile strength for the mono-fibre and hybrid composites versus the hybrid composition. The ROM prediction is represented by the line AB, this is the sum of the contributions from the mono-fibre Kevlar composite

(A) and the mono-fibre XAS composite (B). The point (F) represents the stress on the Kevlar fibres at the failure strain of the XAS fibres, this is because the failure strain of the Kevlar composite is 1.65% and that of the XAS composite is 1.37%. Assuming that all the XAS fibres fail at a constant strain value, then the additional stress carried by the Kevlar at the first failure of the XAS is given by (FC). Therefore, the hybrid stress at the failure of the XAS (BF), is the sum of the stress contributions from the XAS (BD) and the stress contribution from Kevlar at the failure strain of the XAS (FC). The significance of the point (M) is that to the left of it, there are sufficient Kevlar fibres present to bear the additional imposed stress when the XAS fails. To the right of (M), the Kevlar is not present in sufficient quantity to bear the load when the XAS fails and hence when the XAS fails, catastrophic failure of the composite will take place. The stress on the Kevlar at the failure strain of the XAS, (E_k $e_c V_k$), was obtained using the average primary modulus of the Kevlar (line FB).

The effect of using a lower Kevlar composite modulus value (minimum value from experiment) is illustrated by the line (iB). The data in Figure 4.11 seems to suggest that the contribution to the tensile strength of the hybrid composites is primarily derived from the XAS component. In fact if a lower Kevlar composite modulus of 0.5 GPa is used to calculate the point (F), then a good agreement is obtained with experimental results. However there is no justification for using this lower value unless it can be shown that the Kevlar modulus was lower in the hybrid compared to the mono-fibre Kevlar composite. The effect of fibre curvature or waviness was mentioned previously as a possible cause for the observed low modulus for the Kevlar mono-fibre composite used in this programme. Micrographs depicting the extent of

curvature in the Kevlar fibres are presented in a later section. Another factor that has to be considered when dealing with hybrid composites is the extent of residual stresses present in the individual components.

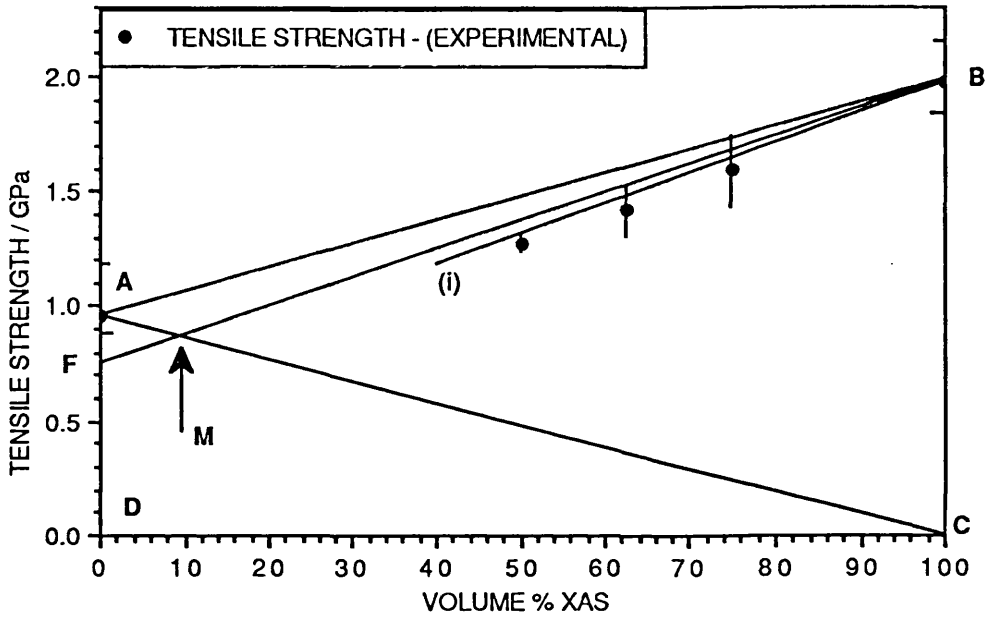

Figure 4.11 Tensile strength of unidirectional mono-fibre and Kevlar/carbon hybrid composites as a function of hybrid composition. See discussion above for explanation of the various lines.

4.6 HYBRID COMPOSITES - RESIDUAL STRESSES

Bunsell and Harris[29] pointed out that residual stresses in hybrid composites could arise as a result of the mismatch between the two fibre components on cooling from the cure temperature. With reference to Table 4.6 it is seen that the axial thermal expansion coefficient of Kevlar composite is negative and lower than that of the XAS fibres composite by an order of magnitude. On cooling down from this gel-

temperature back to ambient the material with the lower coefficient of thermal expansion will be held in compression.

	Longitudinal CTE	Radial CTE X 10^{-6} $^{o}C^{-1}$	Reference [ ]
XAS Fibres	-0.3	17	[118]
Kevlar	-3.6,(-2)*	206, (59)*,	[71,119*]
914 Resin	30	-	[118]

Table 4.6 Thermal properties of constitutive composite properties.

It was previously discussed that the compressive stress on the Kevlar component can be described by the following expression:

$$\sigma_k = -[\,(\alpha_c-\alpha_k)\,\Delta T\,E_k V_c\,]\,/\,[\,V_k(E_k/E_c-1)+1\,] \qquad [4.1]$$

Figure 4.12 illustrates the calculated Kevlar ply stress versus the hybrid composition. The ambient temperature was taken as 20^{o}C and the stress free temperature of 170^{o}C was used along with the relevant values quoted in Table 4.6.

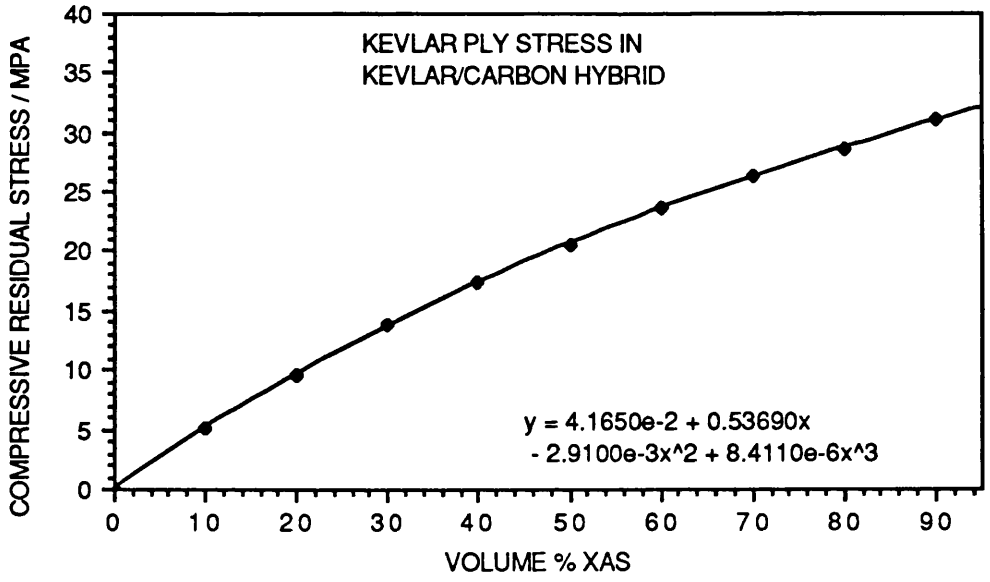

Figure 4.12 Calculated compressive residual stresses in the KFRP plies of a KFRP/CFRP ply.

With reference to Figure 4.12, for a 50/50 hybrid composite, the maximum indicated stress level in the Kevlar plies can be as high as 20 MPa which for a ply containing about 60% of fibres, amounts to a Kevlar fibre compression stress of about 35 MPa. Various researchers have found that the compressive properties of Kevlar fibres are much lower compared to its tensile properties. For example Piggott and Harris[76] found that the effective limiting strength of Kevlar fibres in compression was 10% (0.28 GPa) of its tensile failure stress. Greenwood et al[67] estimated that the Kevlar fibres yielded at a bending strain of about 0.7%. DeTeresa et al[120,121] found a marked difference in the stress-strain response of Kevlar fibres which had previously been compressed. The compression on the Kevlar was achieved by casting the fibre in a nylon/formic acid solution. Evaporating the solvent resulted in the nylon solidifying and shrinking around the Kevlar fibre. They[120] reported a value of 0.53% strain as the

critical compressive strain for kink formation in Kevlar 49. However, this value has to be considered as an upper bound value as it was calculated from the appearance of permanent and visible kinking after the test. The tensile stress-strain curve for pre-compressed Kevlar fibres obtained by DeTeresa et al showed that the fibre extends at a near constant and low stress to approximately 2% elongation. With further extension there was a large upturn in the curve as the apparent fibre modulus increased. Unloading the fibres after 75% of the failure load and reloading, the stress-strain behaviour resembled that of virgin Kevlar fibres but with a slightly reduced tensile strength. The implication was that once the kinks in the Kevlar fibres (skins) are unfolded and the fibre segments realigned, the initial as-received fibre properties can be regained. This means that the poor static compression strength of Kevlar fibres may not necessarily translate into poor tension/compression fatigue properties.

It is difficult to accurately estimate the thermal stresses because of the non-linear response of the thermal expansion coefficients of the carbon and Kevlar phases[119] and inaccuracies in the measured fibre volume fractions. Furthermore, the location of the stress-free temperature is assumed to be slightly below the gellation temperature. In the 914 resin system, on heating from ambient, the hardener melts at about 120^{o}C, from then on the crosslinking process takes place. This temperature also corresponds to the maximum viscosity of the resin (manufacturers literature[86]). As the temperature is increased, the rate of reaction between the resin and the hardener increases and the minimum resin

viscosity is achieved at a temperature of about 170°C and this is assumed to be the stress free temperature. However, accompanying the curing reaction is an associated volumetric shrinkage of the resin as the crosslinking proceeds. It is possible that as a result of resin shrinkage and as the curing reaction carries on at the post-cure temperature of 190°C, additional stresses may be built up in the hybrid.

As regards the effect of residual thermal strains contributing to the "hybrid effect"; Zweben[36] and Manders[39] concluded that the residual stresses only contributed approximately 10% of the enhancement of the carbon fibres in a carbon/glass hybrid composite. Zweben[36] found a hybrid effect in a Kevlar/carbon hybrid composite although the residual thermal strains for the carbon in this case were positive.

5. RESULTS AND DISCUSSION - FATIGUE

5.1 Fatigue Test Frequency

The fatigue data for the unidirectional (ud) mono-fibre and hybrid composites were plotted in terms of peak stress versus log cycles to failure (Nf), see Figure 5.1. The mean ultimate tensile strength (UTS) was represented (where appropriate) in the fatigue curve (S/Log Nf) at 0.5 cycles.

Initially, the fatigue tests were carried out at a constant loading rate of 200KN/seconds, however, it soon became apparent that the loading rate had to be increased to accommodate the fatigue testing of all the composite compositions that were intended for use in this programme within the time scale of the research programme. Therefore, the loading rate was increased to 500KN/sec. The main concerns with regards to performing fatigue tests at high frequencies are the strain rate sensitivity of the composite constituents and autogeneous heating of the specimen.

Jones [88] had previously shown that ultimate tensile strength of cross-ply Kevlar/HTS/Code 69 composite did not show any rate dependence for loading rates between 0.01 to 200KN/Sec. Other researchers have also found the UTS of Kevlar and carbon fibres to be independent of the loading rate. The fatigue testing in this programme was carried out under load control at a constant rate of load application. Therefore, a lower frequency was used at higher loads relative to samples fatigued at lower stresses. For example, using a loading

rate of 500KN/sec for a peak cyclic stress corresponding to 90% of UTS for Kevlar composite, the cycling frequency was 6Hz and at 50% of UTS the cycling frequency was 11 Hz. From Figure 5.1 it is apparent that there was no obvious or significant differences in the fatigue response at the two rates of loading. However, it will be shown later that a three stage representation of the fatigue life lines for the Kevlar mono-fibre composite may not be valid.

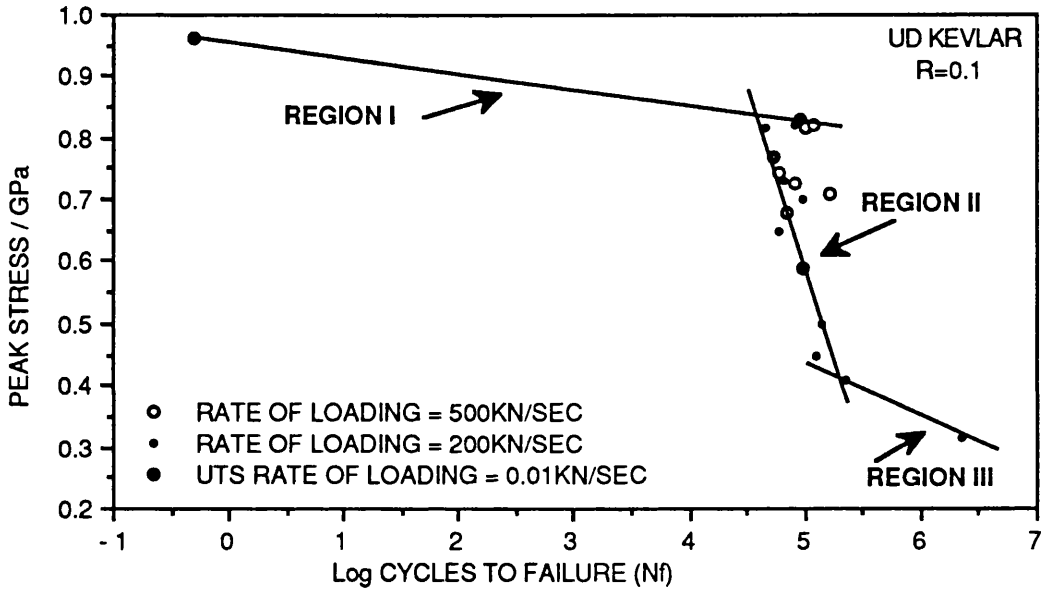

Figure 5.1 Fatigue response of ud Kevlar/914 composite fatigue tested at loading rates of 200 and 500 KN/sec at a stress ratio (R) of 0.1.

5.2 Presentation of Fatigue Data

With reference to Figure 5.1, it was assumed that the S/Log Nf curve for this composite could be represented by three regression (least squares) lines corresponding to Regions (I, II and III).

Region (I) represents the data for the mean UTS and all peak stresses corresponding to greater than approximately 90% of UTS. Region (II) represents the best fit line for peak stresses corresponding to less than 90% and greater than approximately 35% of UTS respectively. Region (III) represents the lowest point from Region (II) and any other points that do not follow the slope of Region (II).

The justifications for representing the fatigue data in the above prescribed manner are as follows: (a) It was previously discussed in the Introduction that a change in the slope of the S/Log Nf represented a change in the relative predominance of the various failure mechanisms in the composite material; microscopic examinations of the composites fatigue tested in this programme lent support to this hypothesis. (b) The primary aim of this programme was to investigate and compare the fatigue response of the mono-fibre Kevlar and XAS composites versus the performance of their inter-ply hybrid composites. Hence, a consistent method of representing the fatigue data points was required, instead of drawing the line 'by eye'. The least squares regression line adequately fulfilled this requirement.

5.3 Fatigue Response Of UD Kevlar/914 Mono-Fibre Composite

5.3.1 Tension-Tension Fatigue

Representing Region (I) in Figure 5.1 by a straight line is questionable since no fatigue data was generated for peak

stresses above 87% of the UTS for this composite. This was because the initial strategy was to first generate fatigue data in the medium and high cycle regions and then to turn to the low cycle region. However, it was subsequently decided that an investigation on the fatigue response under tension-compression be carried out. Other researchers [88,125,129] have shown that fatigue response in Region (I) for mono-fibre Kevlar composites can be represented by a straight line for peak stresses greater than approximately 85% of the UTS under T/T fatigue loading, see Figure 5.2.

The regression line for Region (I) in Figure 5.1 was calculated from the mean UTS and six fatigue data points where the peak cyclic stress was greater than 85% of UTS; the correlation coefficient was 0.98. It is apparent from Figure 5.1 that these six points exhibit slightly superior fatigue lives compared to the fatigue data points in Region (II) although the latter were tested at lower peak stresses. As discussed previously, the static tensile tests response of the ud Kevlar/914 composite exhibited a modulus increase of upto 10% prior to failure and other researchers have shown that the fibres themselves exhibit this stiffening behaviour on approaching the ultimate failure strain of the Kevlar fibre. Therefore, it is reasonable to expect a higher reinforcing effect by the Kevlar fibres for high peak stresses in a fatigue test. Ericksen[160] reported the creep rate to be greater at lower stresses compared to high stress loading. The enhanced fatigue life and reduced creep rates at relatively high stresses for Kevlar composites must mean that the rate of fibre strength degradation was also reduced. The regression equation for Region (I) is $Y=0.95-0.027$ Log Nf

with a correlation coefficient of 0.979. Further research is required to establish the true fatigue response for the Kevlar mono-fibre composite in Region (I).

Region (II) in Figure 5.1 represents fatigue points generated for peak stresses corresponding to between 40-80% of the UTS. The regression equation for this region is given by Y = 3.58 - 0.6 Log Nf with a correlation coefficient of 0.824. Manufacturers' literature on the fatigue data for Kevlar fibre reinforced composites do not indicate any downturn in the fatigue behaviour after about 10^4 cycles. Jones et al[126], and Hahn et al[127,129] however did observe a down-turn in the fatigue response of Kevlar fibre reinforced composites irrespective of environmental conditioning. It has to be pointed out that comparison of fatigue data quoted in the literature is difficult because: (a) Resin/fibre systems are different; (b) No standard environmental conditioning exist; (c) Initial condition of the composite materials are not known; and (d) Differences in the presentation and analysis of fatigue data. For example, Jones [88] re-plotted the data presented by Roylance and Miner et al and found that the fatigue response of the respective Kevlar composite was better represented by a two stage process; Regions (I and II). The original fatigue data was represented by a single line which included the fatigue and UTS data points. The down-turn was observed for peak stresses approximately below 80% of the ultimate tensile strength.

Figure 5. 2 illustrates the comparison between fatigue data obtained in this programme to that obtained by previous researchers. For ease of comparison, the data are plotted in

terms of normalized tensile strength vs Log cycles to failure. Region (I) in Hahn's[129] data coincides with the result obtained in this study, however, his composite seemed to indicate a better Region (II) performance - only one datum point was generated in Region (II) in Hahn's study. Roylance's[125] composite displayed a steeper Region (I) but the down-turn seemed to occur at 10^5 cycles - only three data points were presented for Region (II). Hahn obtained fatigue run-outs at stress levels below 70% of UTS whereas, Roylance did not obtain any run-outs even at 60% of UTS. It has to be reiterated that comparisons of this nature will only be of real use if there was a means of standardizing test procedures and materials composition.

It is apparent from Figure 5.1 that Region (III) for ud Kevlar/914 does not represent the fatigue limit; no run-outs were recorded at 10^6 cycles. Unfortunately, due to time constraints it was not possible to identify the fatigue limit for this composite. This also helps to point out the dilemma in defining a termination time for fatigue testing. For example, if tests were terminated on reaching 10^6 cycles then the lowest point in Figure 5.1 would have represented a run-out. Although testing to failure at low stresses is desirable, it is very time consuming. The regression equation for Region (III) was defined as $y = 0.867 - 0.086$ Log Nf.

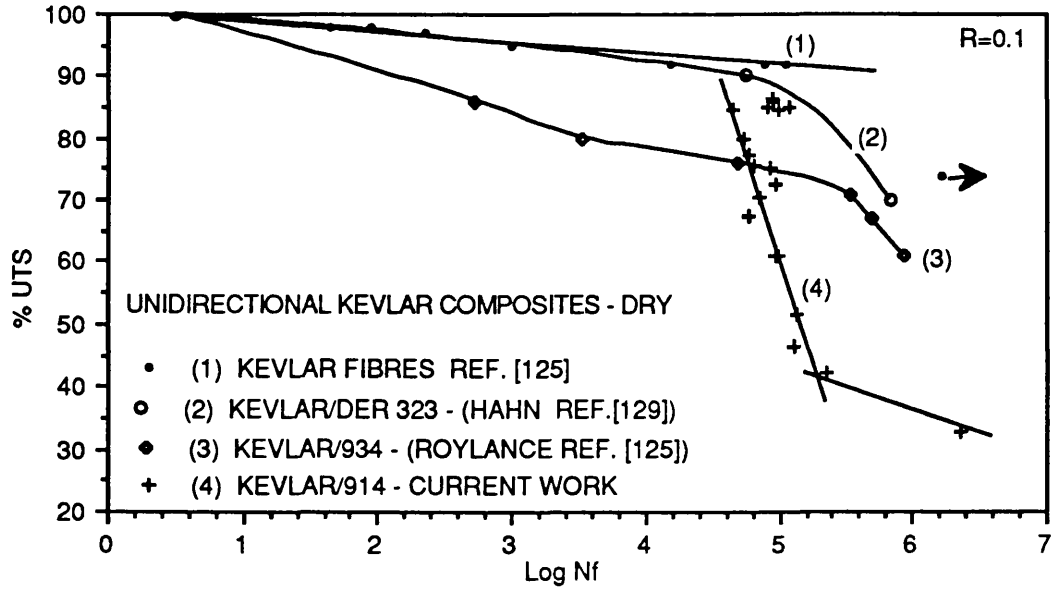

Figure 5.2 Comparison of fatigue data for unidirectional Kevlar fibre reinforced composites from four sources obtained in the literature.

Having established that the down-turn in the fatigue curve of Kevlar reinforced composites was indeed a real effect, the possible causes of this phenomenon are considered in the light of what has been reported in the literature.

Bunsell[114] investigated the tensile and fatigue behaviour of Kevlar fibres. Under fatigue loading he found that there was a definite trend for the fibres to survive longer when the minimum load was raised with the peak stress being held constant. The findings of Jones[88] and the data generated in this programme found that raising the minimum stress and holding the peak stress constant for Kevlar/epoxy composites does indeed result in fatigue life times of greater than 10^6 at 80% of the ultimate tensile strength. Roylance[125] found that the fatigue response of the Kevlar fibre itself was excellent, with a strength loss of approximately 1.7% of UTS

per decade of fatigue loading. On comparing fibre fatigue performance to that of the composite fatigue response, see Figure 5.2, it is seen that the fatigue response for the Kevlar composite is worse than that for the fibres alone. Morgan et al[14] and Chiao[94] presented stress rupture data for Kevlar/epoxy strands which indicate that for a given stress, the life times were about 5 orders of magnitude longer than the corresponding tests under fatigue loading. It has to be pointed out that even under static loads of 50% of UTS, the Kevlar strands fail after about 5 years.

Bunsell [114] reported that the creep in Kevlar fibres was very low and that it stablised after the first few cycles and no measurable change in the modulus was observed after 10^6 cycles. Hahn et al[127] observed that under tensile loading a modulus increase of 13% was observed and upon unloading a hysteretic effect was obtained which partly recovered with time. Under fatigue loading they observed that the hysterisis loop disappeared with fatigue cycles and was accompanied by an increase in modulus. Modulus increases of between 10-20% were recorded for fatigue peak stresses of 70-80% of UTS. Knopasek and Hearley[113] reported an increase in the maximum attainable peak stress after the initial cycle at relatively lower stress in fatigue. Howard[115] observed that Kevlar yarns after prolonged and repeated loading also exhibited recovery of creep and an increasing modulus. Erickson[160] found the creep rate to be lower at relatively high imposed loads whereas the creep rate was greater than that of the neat epoxy resin at low imposed loads.

The implication of the above discussion are as follows:

(a) Kevlar fibres are sensitive to the applied stress amplitude under tension/tension fatigue loading. Reducing the stress amplitude results in an improved fatigue performance. This implies that the damage mechanism for Kevlar fibres under fatigue loading is influenced by the applied stress amplitude.

(b) The fatigue response of Kevlar fibres can be influenced by the surrounding material, i.e. the resin and neighbouring fibres. This implies that the resin shrinkage, residual fabrication stresses, touching-fibres and resin morphology can influence the fatigue response of the Kevlar composites.

(c) The modulus increase and creep recovery may possibly be due to molecular rearrangement/alignment within the Kevlar structure. Structural rearrangement of this nature have been reported for carbon fibres as discussed previously and hence, it is reasonable to expect similar behaviour for Kevlar fibres.

Another factor which has to be considered with regards to the fatigue response of Kevlar composites is the effect of temperature due to autogenous heating and elevated temperature fatigue. Surface temperature increases of 100^{o}C have been reported by Roylance[125] during fatiguing of Kevlar composites, unfortunately, Roylance did not monitor surface temperature during fatigue testing of Kevlar fibres. Bunsell[114] wrongly inferred from the small hysterisis loop on fatiguing Kevlar fibres at 50Hz that autogenous heating was not significant. Results and discussions on the surface temperature measurements made on the Kevlar/914 mono-fibre

and hybrid composites in this programme are presented in a following section.

5.3.2 Elevated Temperature Fatigue Testing of Kevlar/914

A limited number of fatigue tests were carried out at 100°C on the mono-fibre Kevlar/914 composite and the results from this study are presented in Figure 5.3. The regression equation for Region (II) for the elevated temperature fatigue tests was Y=3.24-0.544 Log Nf with a correlation coefficient of 0.74. Whereas the regression equation for the ambient temperature tests in Region (II) was Y=3.58-0.597 Log Nf, this indicates a slight reduction in the fatigue life for the elevated temperature fatigue tests compared to the ambient temperature tests.

DuPont's trade literature for dry Kevlar fibres indicate that both the tensile strength and modulus decreased linearly with temperature. Approximately a 10% drop in the tensile strength and modulus was reported for fibres tested at 100°C. Only a 2-3% reduction in tensile strength was observed for fibres conditioned at 150°C in air for 81 hours.

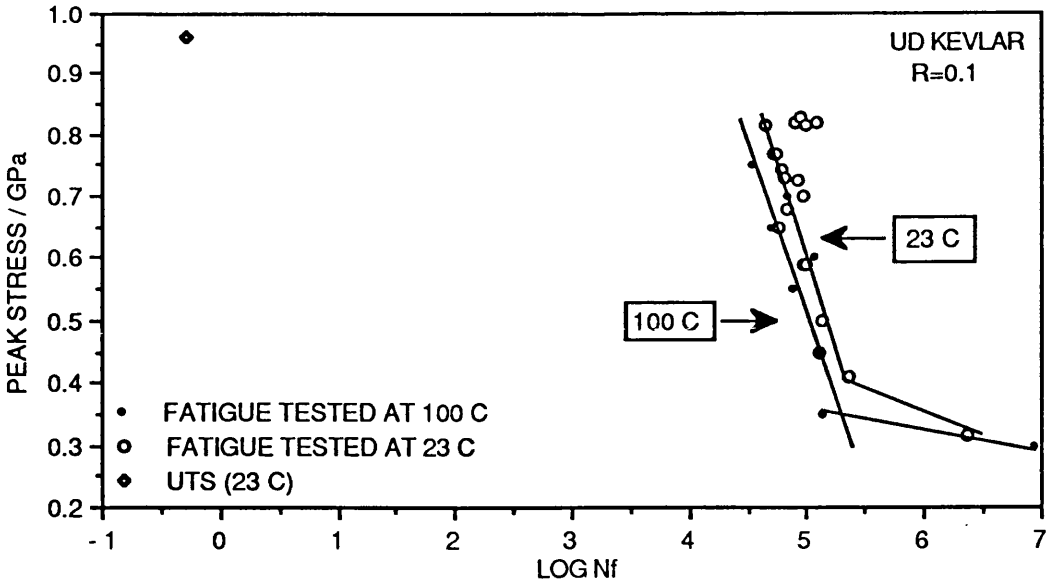

Figure 5.3 Comparison of Kevlar/914 fatigue data at 23°C and 100°C.

The measured glass transition temperature for the dry 914 thermoset resin system was approximately 180°C. Therefore, it is unlikely that the test temperature of 100°C would have significantly affected the matrix tensile properties. It is probable that the observed slight decrease in the elevated temperature fatigue performance of the Kevlar/914 composite was due to the deterioration in the mechanical properties of the Kevlar fibres itself. However, SEM inspection of the elevated temperature fatigue tested samples showed that the fracture surfaces were littered with polyethersulphone particles. The reason for this is not understood and is worthy of further investigation.

5.3.3 EFFECT OF STRESS RATIO (1> R >0) ON THE FATIGUE RESPONSE OF UD KEVLAR/914 COMPOSITE

Figure 5.4 illustrates the fatigue response of ud Kevlar/914 composite tested at stress ratios of 0.1, 0.01 and 0.5. Although only two data points were generated for R=0.5, is is seen that increasing the stress ratio from 0.1 to 0.5 does indeed result in a significant improvement in the fatigue life of this composite. It would have been useful to generate a fatigue curve at this stress ratio but since a run-out was obtained at a peak stress corresponding to 86% of UTS, it was decided that generating a full S/N curve would have taken an unacceptably long time. However, other researchers, for example, Jones and Bunsell have conclusively shown that raising the minimum stress in a T/T fatigue test significantly enhances the number of cycles to failure compared to instances where a lower minimum stress was used.

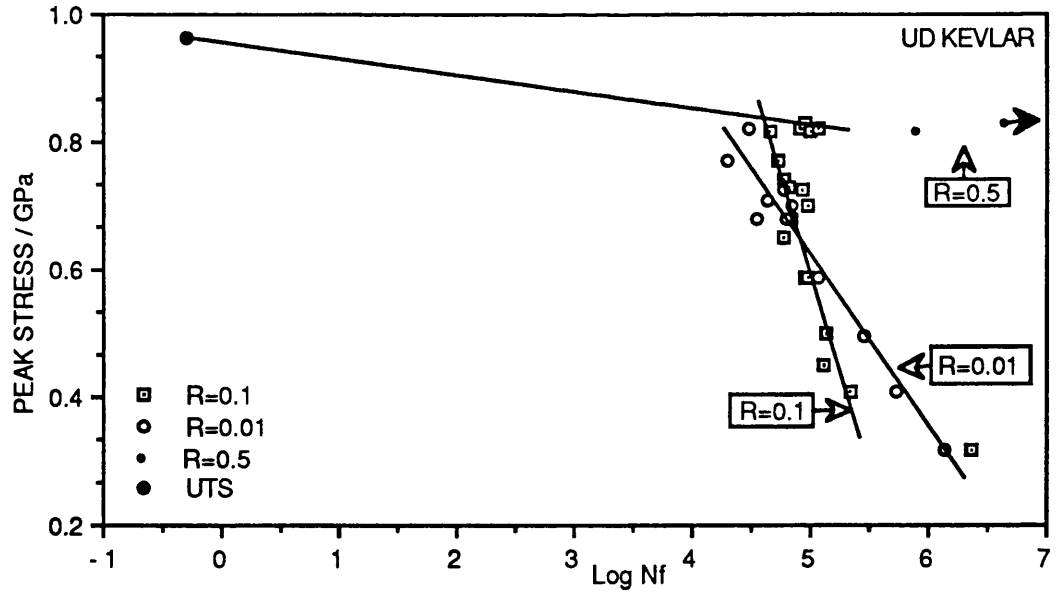

Figure 5.4 Comparison of ud Kevlar fatigue data for test carried out at stress ratios of R=0.1, 0.01 and 0.5. The regression equation for Region (II) for R=0.1 and 0.01 are Y=3.58-0.597 Log Nf (correlation coeff.=0.824) and Y=1.96-0.269 Log Nf (correlation coeff.=0.948) respectively.

The observed differences in the fatigue response of the ud Kevlar/914 when tested at R=0.1 and 0.01 are difficult to account for since both regimes are tension/tension tests with the latter having a slightly larger stress range for a given peak stress value. It will be seen later that the fatigue response of the 50% Kevlar/XAS hybrid composite fatigue response for R=0.1 and 0.01 are clearly distinguishable, with the fatigue life of R=0.01 being slightly worse than that observed for R=0.1. Furthermore, the cross-over observed for the R=0.1 and 0.01 was not observed for any of the other composite materials tested in this programme. Therefore, it is conceivable that the fatigue response of the ud Kevlar composite is best represented by a two-stage regression line - Regions (I) and (II), rather than by three Regions as discussed previously. Jones's fatigue data for 0/90, Kevlar/Code 69 is presented in Figure 5.5 as a further comparison. His data is also best represented by a two-stage fatigue curve since he too did not observe any run-outs. In Figure 5.5, the regression line for Region (II) for the Kevlar/914 was calculated by treating the data for the two loading rates at R=0.1 as a single data-set.

The uncertainty in the fatigue response of the R=0.1 fatigue curve is made worse by the fact that for the 500KN/sec loading rate, see Figure 5.1, no fatigue data points were generated below 0.589 GPa and the regression line was drawn by including the data points from the 200 KN/sec series.

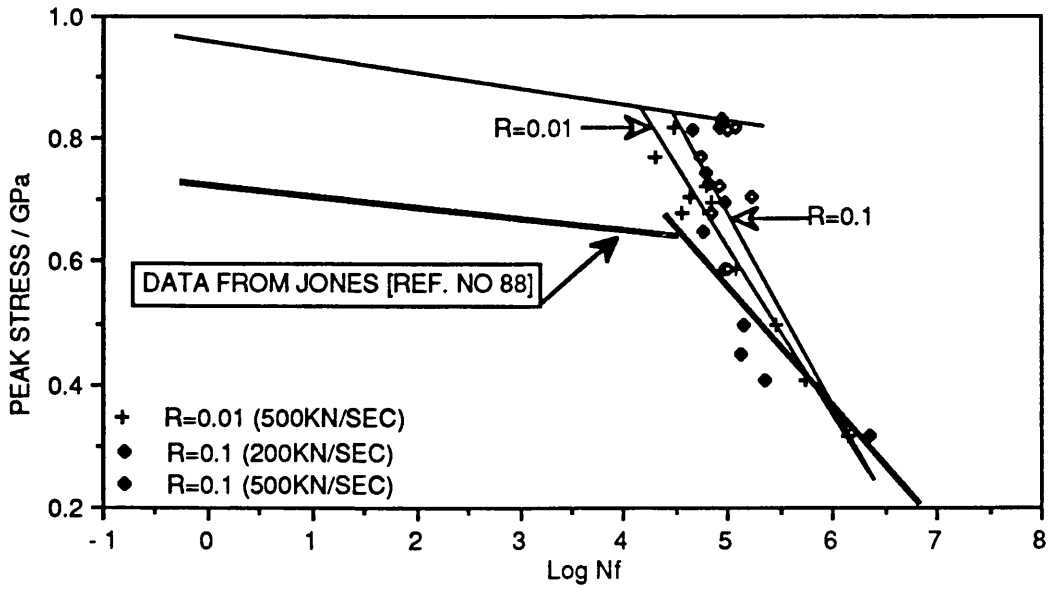

Figure 5.6 Comparison of fatigue data from Jones[88] and data from current work. The regression lines for the ud Kevlar/914 were calculated by assuming a two-stage fatigue behaviour and all the R=0.1 data points were treated as a single data-set.

5.3.4 TENSION/COMPRESSION FATIGUE RESPONSE OF UD KEVLAR/914 MONO-FIBRE COMPOSITE

The tension/compression fatigue tests were carried out using the anti-buckling jig described previously. Figure 5.7 illustrates the fatigue response of ud Kevlar/914 mono-fibre composite tested at stress ratios of 0.0, 0.01, -0.3 and -0.6. It is apparent that increasing the negative stress component (or decreasing the minimum stress) results in the worsening of the fatigue performance of this composite material for a given peak stress. No significant difference was observed in the T/C fatigue response of the ud Kevlar/914

tested at loading rates of 200 and 500 KN/seconds for R=-0.3. A change in the macroscopic failure mode was observed as the stress ratio was reduced from +0.1 to -0.6, details of which are discussed later.

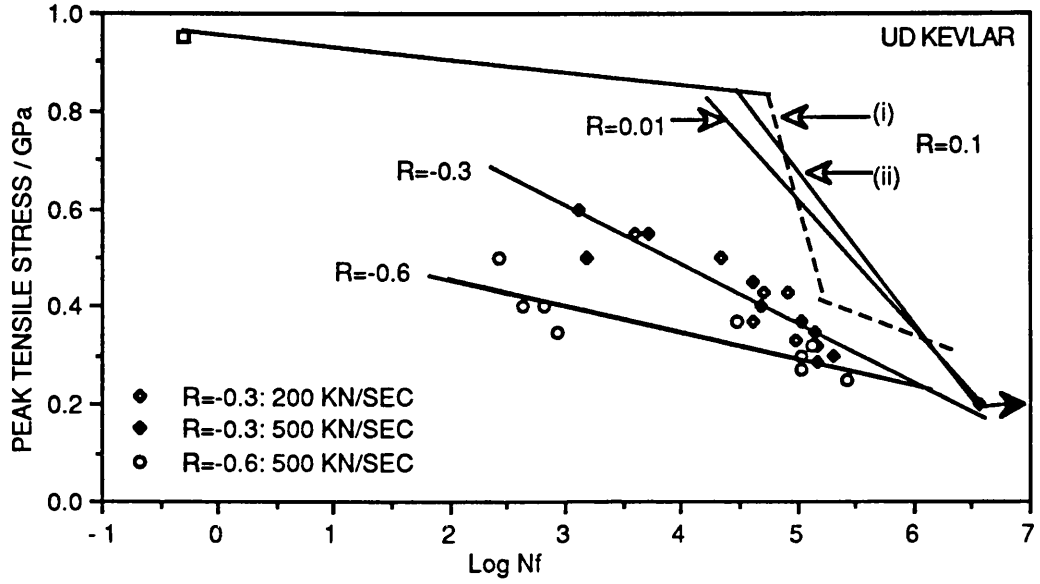

Figure 5.7 Fatigue response of ud Kevlar/914 composite fatigue tested at stress ratios of R=0.1, 0.01,-0.3 and -0.6. (i) Three stage fatigue curve representation and (ii) Two stage fatigue curve representation; for R=0.1.

The regression equations for the the data presented in the above figure are listed below:

R=0.1* Y=3.58 - 0.597 Log Nf (cd.=0.82)
R=0.01 Y=1.96 - 0.268 Log Nf (cd.=0.95)
R=-0.3 Y=0.966 - 0.121 Log Nf (cd.=0.81)
R=-0.6 Y=0.563 - 0.053 Log Nf (cd.=0.75)
R= 0.1** Y=2.23 - 0.312 Log Nf (cd.=0.53)

(*) Three stage fatigue curve. Region (II) as defined previously for R=0.1.

(**) Data for R=0.1 was treated as a single data-set.

In Figure 5.8 the slopes of the regression lines (for "Region II") from the previous graph were plotted in terms of their respective stress ratios.

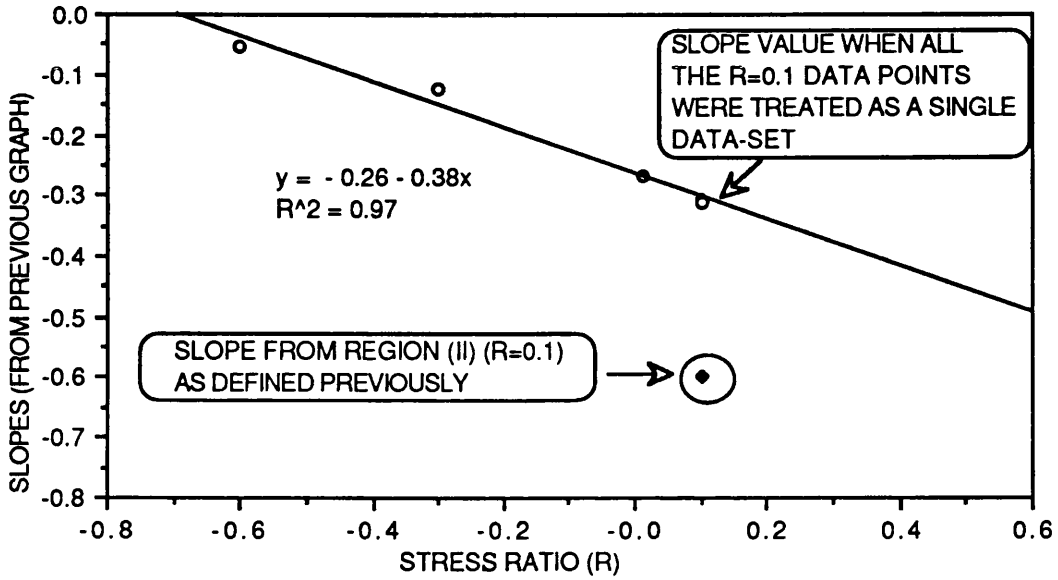

Figure 5.8 The slopes from the previous graph have been replotted in terms of their respective stress ratios.

It is seen from Figure 5.8 that when the fatigue data for R=0.1 is treated as a single data-set (i.e. assuming a two stage fatigue life line), an apparent linear relationship was observed between the stress ratios and the slopes of the S/Log Nf curves for the ud Kevlar/914 mono-fibre composite. The slope from the previous definition of Region (II) for this composite is also represented in Figure 5.8 but was excluded from the calculation of the regression line; Y= - 0.261 - 0.377(R) and coefficient of determination was 0.97.

If this apparent linear relationship between the various stress ratios and the slopes of the S/Log Nf curves for this composite exists, then it will be possible to predict the fatigue response for this composite at any stress ratio

between 0.1 and -0.6; however, a further reference point for each of the stress ratios would need to be defined.

With reference to Figure 5.7, it is proposed that it may be reasonable to assume that the R=0.1 and 0.01 regression lines merge to a common point on the fatigue curve at a relatively low peak tensile stress value. Solving the R=0.1 and 0.01 equations, the intersection is defined by Log Nf=6.07 and peak tensile stress = 0.336 GPa. Similarly the intersection for R=-0.3 and -0.6 is give by Log Nf=5.93 and peak tensile stress=0.249 GPa. It is reasonable to expect a different convergence point for the T/T and T/C fatigue results since the failure mechanisms are dissimilar for the two cases. However, further work is necessary to confirm the range of stress ratio values where convergence is observed under T/T and T/C fatigue testing.

It was previously discussed that for Kevlar composites subjected to T/T testing, the fatigue behaviour exhibited a Region (I) and a Region (II). Comparison of fatigue data from other researchers and post-failure inspection carried out in this programme also provided evidence for the presence of the two Regions. Post-failure inspection of the T/C tested samples showed that the predominant failure mode of this composite was dependent on the magnitude of the peak stress. At high compressive stresses failure was via a predominant transverse crack and at intermediate compressive loads, failure was due to longitudinal splitting, inter and intra-ply delaminations and a fibre abrasion mechanism. Therefore even under T/C loading, the fatigue response of this composite can be represented by Regions (I and II).

Since an apparent linear relationship exists between the slope of the S/Log Nf curves and the stress ratio for ud Kevlar/914, the fatigue response at any stress ratio can be predicted if a reliable reference point can be identified for each (R) ratio. Assuming for the moment that the fatigue life lines for R=-0.3 and -0.6 ratios converge at 0.25 GPa and Log 5.93 cycles, and assuming that the convergence point for R=0.1 and 0.01 is at 0.34 GPa and Log 6.07 cycles; fatigue life lines can be drawn radiating from these points. This is illustrated with the aid of Figure 5.9.

In Figure 5.9 the locus (BG) is taken to represent the failure envelope distinguishing Region (I) from Region (II). This was based on the macroscopic failure modes exhibited by these samples. For the T/T case, the samples to the left of (BG) exhibited a macroscopic fracture mode that was similar to those observed for the static tensile test samples. Similarly, in the T/C cases, the samples to the left of (BG) failed via the propagation of a predominant transverse crack, whereas, to the right of (BG) extensive longitudinal splitting and delaminations were observed. The actual profile for this locus can be determined by obtaining fatigue data in the very low cycle region (this should be readily achieved with computer controlled fatigue machines).

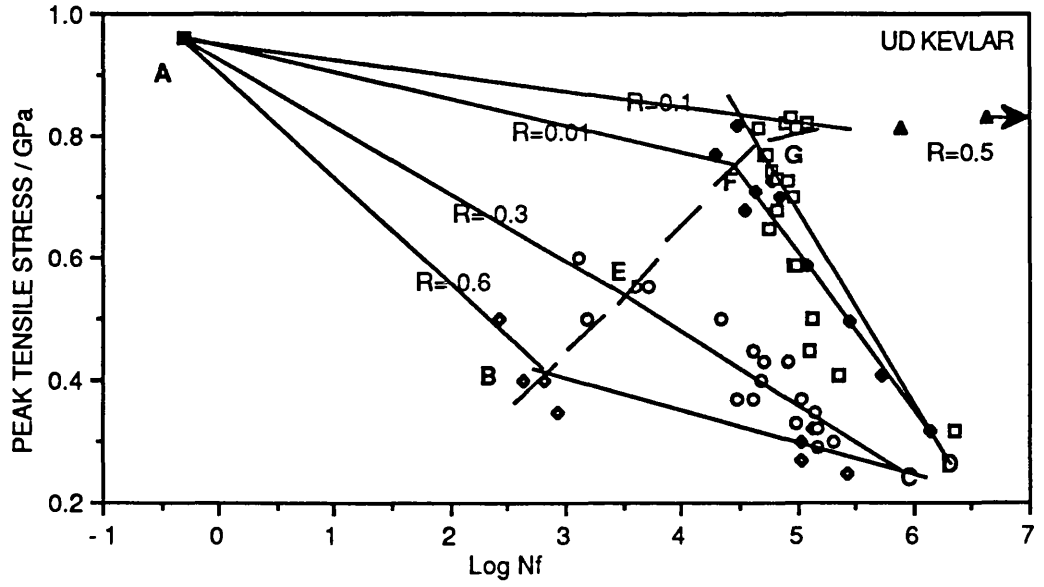

Figure 5.9 Proposed S/Log Nf fatigue curves for ud Kevlar/914 mono-fibre composite. See text for explanation.

In Figure 5.9, the UTS was represented by point (A). The regression lines for R=-0.6,-0.3,0.01 and 0.1 were represented by the lines (BC), (CE), (CF) and (DG) respectively. The line (BG) represents the observed change in failure mechanism from Region (I) to Region (II), i.e. lines (AB, AE, AF, and AG represent Region (I) type failures. It may be reasonable to suggest that the convergence points (C and D) are best represented by a line (CD), this implies that the 'fatigue stress limit' for T/C is lower than that for T/T tests and furthermore, that the fatigue stress limit is unique to a particular stress ratio (R). Further work is necessary to confirm this.

The implications of plotting T/C fatigue results in terms of the peak tensile stress versus Log Nf are worth considering. The line (AGD) is taken to represent the tensile strength degradation of the test specimen with number of cycles

relative to the mean ultimate tensile strength. Similarly the line (ABC) represents the tensile strength degradation with number of cycles under a tension/compression loading regime. Convention was followed in the representation of the UTS at 0.5 cycles (Log -0.30).

5.4 FATIGUE BEHAVIOUR OF UD XAS/914 CARBON FIBRE REINFORCED COMPOSITE (CFRP)

5.4.1 Tension-Tension Fatigue

The results for the tension/tension fatigue of XAS/914 composite are illustrated in Figure 5.10. It is apparent that S/Log Nf for this composite system is relatively flat. Previous researchers have also consistently reported that the fatigue curve for ud CFRP composites to be relatively flat, for example; Sturgeon[137], Owen[138], Dharan[43,44], Talreja[55], Gerhart[139] and Beaumont and Harris[140].

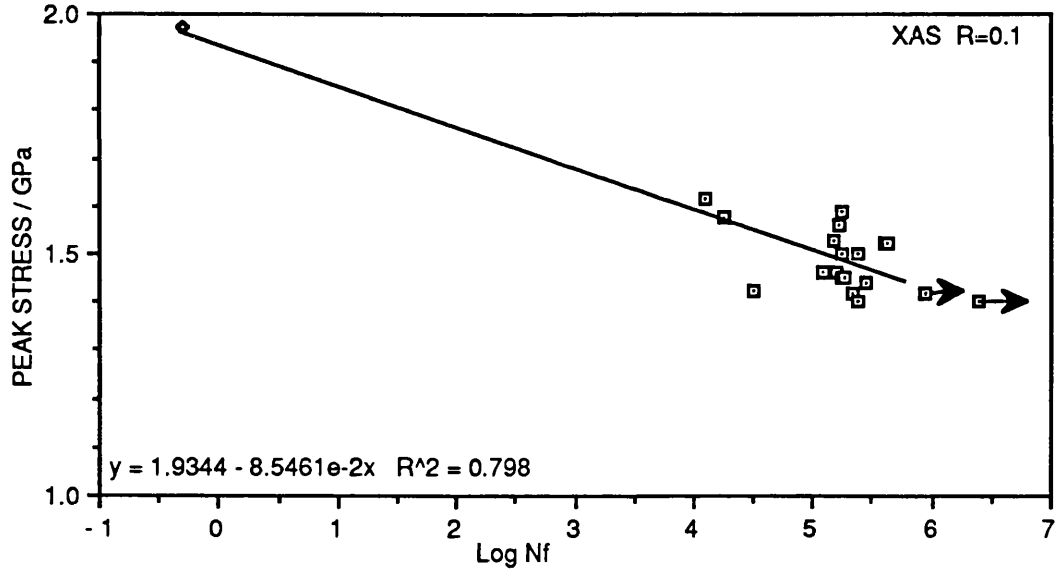

Figure 5.10 Fatigue curve for ud XAS/914 composite tested at R=0.1.

In Figure 5.10, the static UTS was included in the calculation of the linear regression line, whereas for ud Kevlar/914 composite a straight forward extrapolation to the UTS was not possible. The slope of the S/Log Nf curve for

the ud XAS/914 composite was -0.0854 , which corresponds to fatigue strength reduction of 4.3% per decade of cycling, this is in agreement with values reported by other researchers. It is apparent from Figure 5.10 that run-outs were obtained at 10^6 cycles for peak stresses below 71% of UTS. Inspection of the run-out samples revealed extensive surface ply delaminations and some longitudinal splitting. It is probable that these specimens would have failed eventually if the fatigue test was continued beyond 10^6 cycles.

As a consequence of this an alternative representation of Figure 5.10 is presented in Figure 5.11 as a discussion point. Here a three stage fatigue curve for the ud XAS/914 composite is proposed. Region (II and III) in Figure 5.11 are fairly well defined, however, this is not so for Region (I). One reason for this was that it was not possible to achieve the required peak load on the fatigue machine at the loading rate of 500KN/seconds. Furthermore, specimens that failed during loading-up were not included in the fatigue curve. The validity of representing the fatigue curve for this composite as depicted in Figure 5.11 will be discussed further when the fatigue performance of the mono-fibre composites are compared with those of the hybrid composites. The T800/6376 composite system [136] was reported as exhibiting a down-turn in the fatigue performance after about 10^5 cycles.

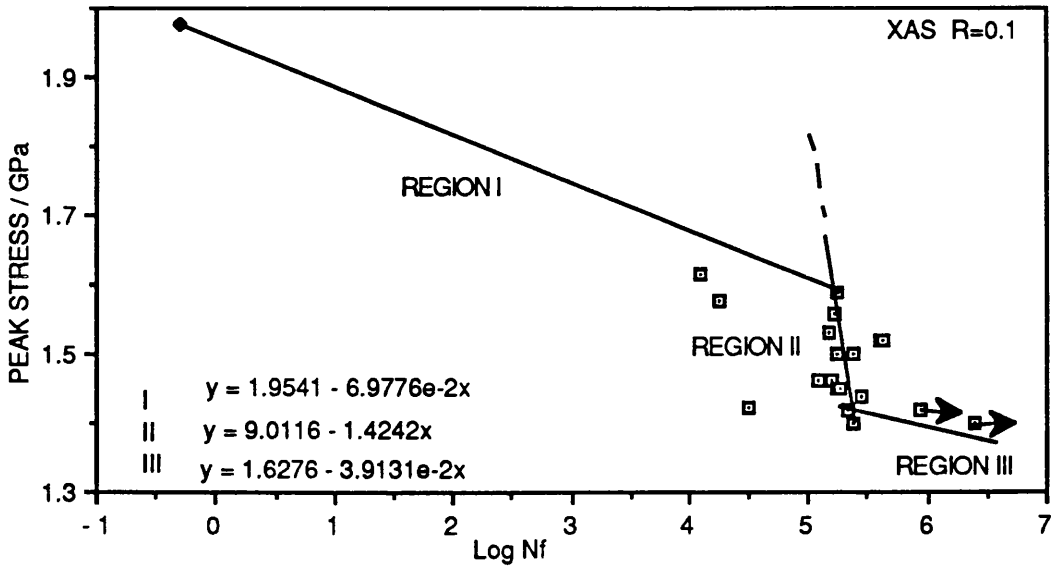

Figure 5.11 An alternate representation of the data from Figure 5.10; data for ud XAS/914 composite fatigue tested at a stress ratio of R= 0.1.

5.4.2 TENSION-COMPRESSION FATIGUE TESTING OF UD XAS/914 COMPOSITE.

The effect of introducing a compressive stress component into the fatigue response of us XAS/914 composite is illustrated in Figure 5.12, the data for R=0.1 has been replotted for ease of comparison. It is seen that the effect of the compressive stress component is to lower the operating peak stress of the ud/XAS composite as the stress ratio is reduced from 0.1 to -1.2.

In the first instance, the regression lines from the three stress ratios were calculated by excluding the UTS in the data-set. However, including the UTS in the regression calculation gave a superior fit. This is illustrated in Figures 5.12 and 5.13.

In Figure 5.13 the regression line for the three stress ratios was calculated by including the ultimate tensile strength in the calculation. A better correlation coefficient was obtained by including the UTS in the calculation of the regression lines for R=-0.6 and -1.2.

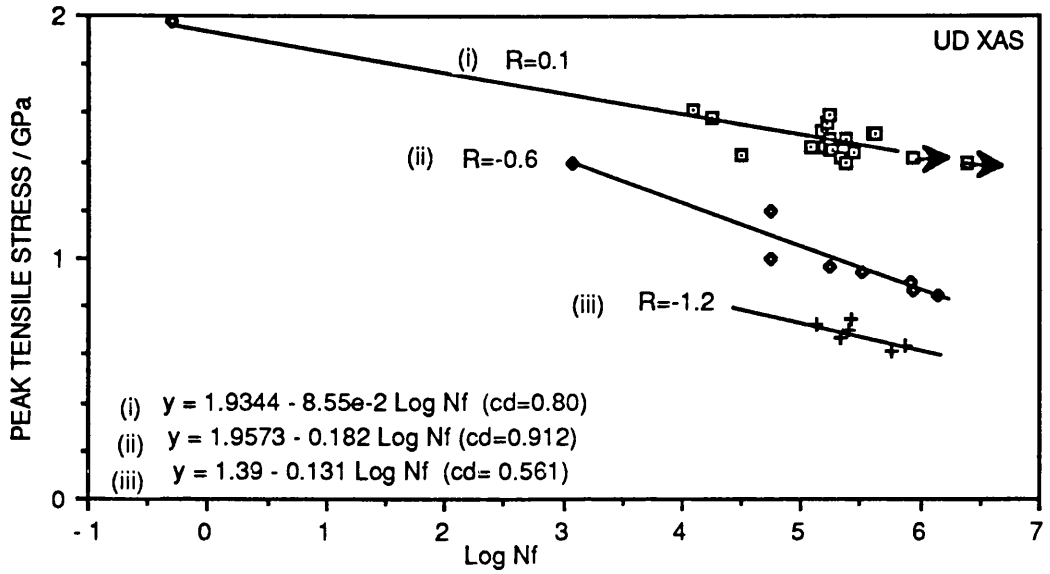

Figure 5.12 Effect of introducing a compressive stress component on the fatigue response of ud XAS/914 mono-fibre composite. The UTS was not included in the regression line calculations for R=-0.6 and -1.2.

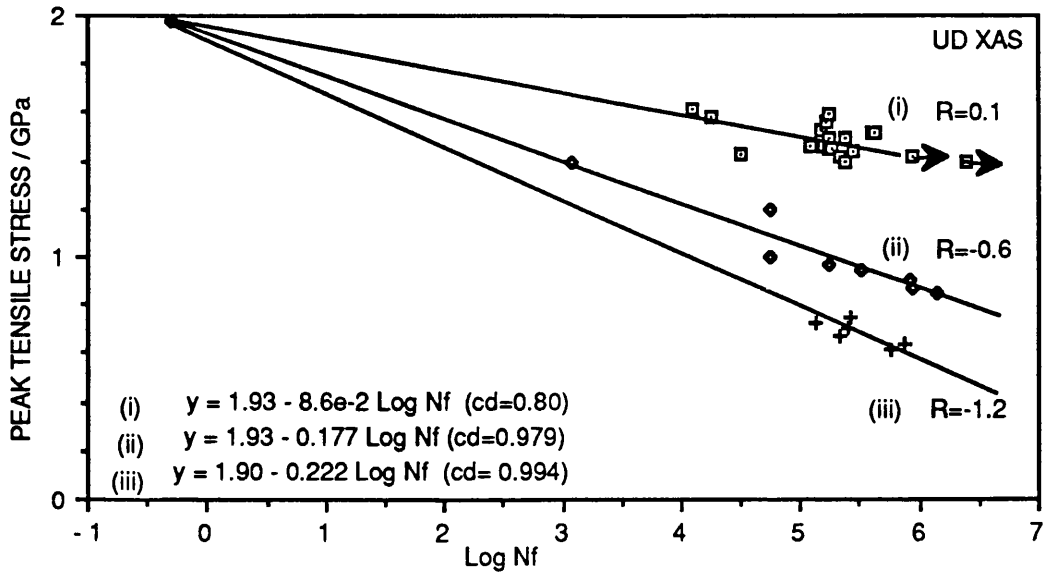

Figure 5.13 Fatigue response of ud XAS/914; the regression lines for R=0.1, -0.6 and -1.2 were calculated by including the ultimate tensile strength in the data-set.

A summary of the regression equations for the ud XAS/914 mono-fibre composite with and without the inclusion of the UTS are listed below.

	UTS excluded form the regression calculations	UTS included in the regression calculations
R=0.1	Y=1.79-0.059 Log Nf (cd=0.16)	Y=1.93-0.086 Log Nf (cd=0.80)
R=-0.6	Y=1.96-0.18 Log Nf (cd=0.91)	Y=1.93-0.18 Log Nf (cd=0.98)
R=-1.2	Y=1.39-0.13 Log Nf (cd=0.56)	Y=1.79-0.22 Log Nf (cd=0.99)

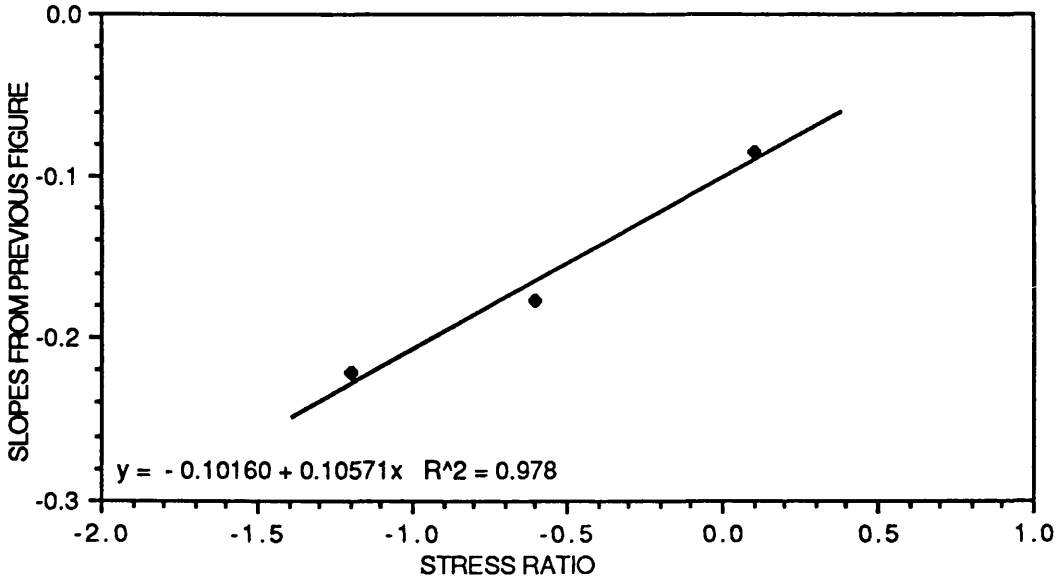

Figure 5.14 A plot of slopes from previous figure versus their respective stress ratios, the UTS was included in the original regression line calculations.

In Figure 5.14, the slopes for the XAS/914 mono-fibre composite where UTS was included in the regression calculations, were plotted against the corresponding stress ratio. Although only three stress ratios were performed for the XAS/914 composite, if the apparent linear relationship between the slopes of the S/Log Nf curves for this composite is an accurate representation of the true fatigue behaviour, then the fatigue response of any stress ratio between 0.1 and -1.2 can be accurately predicted. In other words the predicted fatigue life line can be drawn radiating from the UTS with the slopes being defined by the equation y(slope)=-0.102+0.1057(R) for the stress ratios of interest.

It was previously shown that the fatigue response of the ud Kevlar/914 mono-fibre composite also showed an apparent linear relationship between the slopes of the fatigue life

line and the stress ratio. However, in the XAS composite the reference point was the UTS and for the Kevlar composite it was the fatigue stress limit. A discussion on the general fatigue response of the composites tested in this programme are presented in the following section.

As mentioned previously, representing the T/C results in terms of peak tensile stress does not give a direct indication of the true range of stress to which the sample was subjected. Some researchers[138] represent both positive and negative stress ratios on the same S/Log Nf graph by plotting the maximum stress without regard to the sign (tensile or compressive). Such a representation where the ordinate of the S/Log Nf curve is plotted in terms of peak stress (regardless of the sign) will be identical to plots of peak tensile stress versus Log Nf except when 1<R>-1.

5.5 FATIGUE RESPONSE OF 25% UD KEVLAR/XAS HYBRID COMPOSITE

5.5.1 Tension-Tension and Tension-Compression Fatigue Response

The fatigue response of the 25 % Kevlar/XAS hybrid composite subjected to T/T and T/C loading are presented in Figures 5.15 and 5.16. The regression line in Figure 5.15 were calculated by including the ultimate tensile strength value for the 25% hybrid composite. An alternate representation of the fatigue data for the 25% hybrid is presented in Figure 5.16 where the UTS was excluded from the regression. A

summary of the regression equations along with the coefficient of determination are listed below for the respective stress ratios.

	UTS included in the regression calculations.	UTS excluded in the regression calculations.
R=0.1	y=1.56-0.049 Log Nf (cd=0.84)	y=1.54-0.046 Log Nf (cd=0.74)
R=-0.3	y=1.51-0.109 Log Nf (cd=0.94)	y=1.18-0.045 Log Nf (cd=0.83)
R=-0.6	y=1.47-0.123 Log Nf (cd=0.93)	y=1.20-0.068 Log Nf (cd=0.86)
R=-1.0	y=1.55-0.171 Log Nf (cd=0.98)	y=0.90-0.054 Log Nf (cd=0.45)
R=-1.2	y=1.33-0.189 Log Nf (cd=0.80)	y=0.78-0.052 Log Nf (cd=0.98)

The correlation of determination (cd) is an estimate of how well the estimated regression line fits the data and the correlation of determination for linear regression is the square of the correlation coefficient[133].

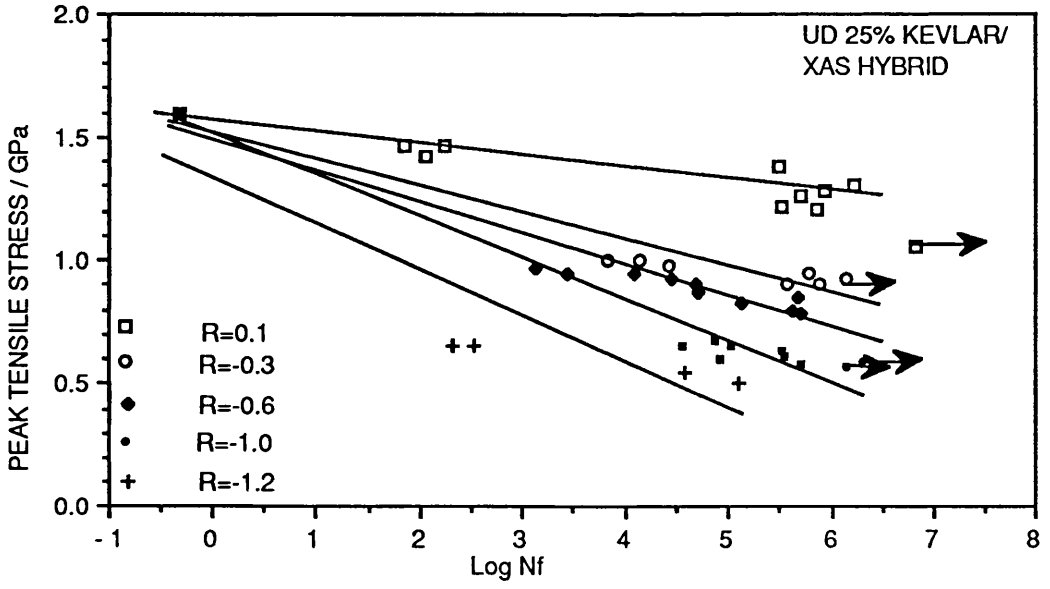

Figure 5.15 Fatigue response of the ud 25% Kevlar/XAS/914 hybrid composite. The ultimate tensile strength was included in the regression line calculations.

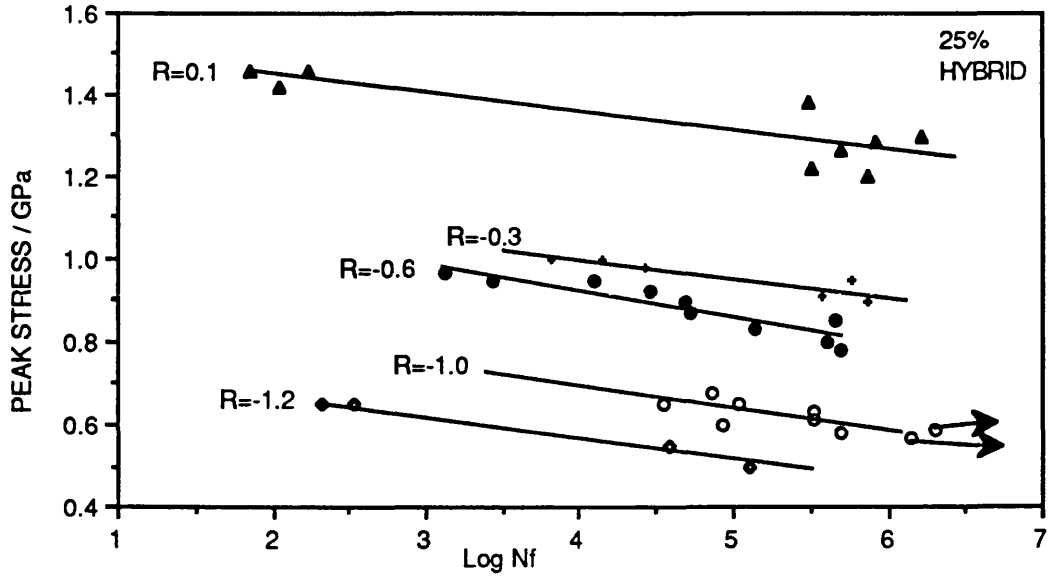

Figure 5.16 Fatigue response of the ud 25% Kevlar/XAS/914 hybrid composite, the ultimate tensile strength was excluded from the regression line calculations.

As in the case for the XAS composite, including the UTS in the regression line calculation gave a superior regression fit to the experimental data. Furthermore, the trend observed for the 25% hybrid composite was similar to the XAS mono-fibre composite. It was previously shown that an apparent linear relationship exists between the slopes of XAS mono-fibre composite and the corresponding stress ratio. The results of a similar operation for the 25% hybrid composite fatigue data are illustrated in Figure 5.17. Once again, a linear relationship is observed and in this case 5 different stress ratios were used and the coefficient of determination was 0.98.

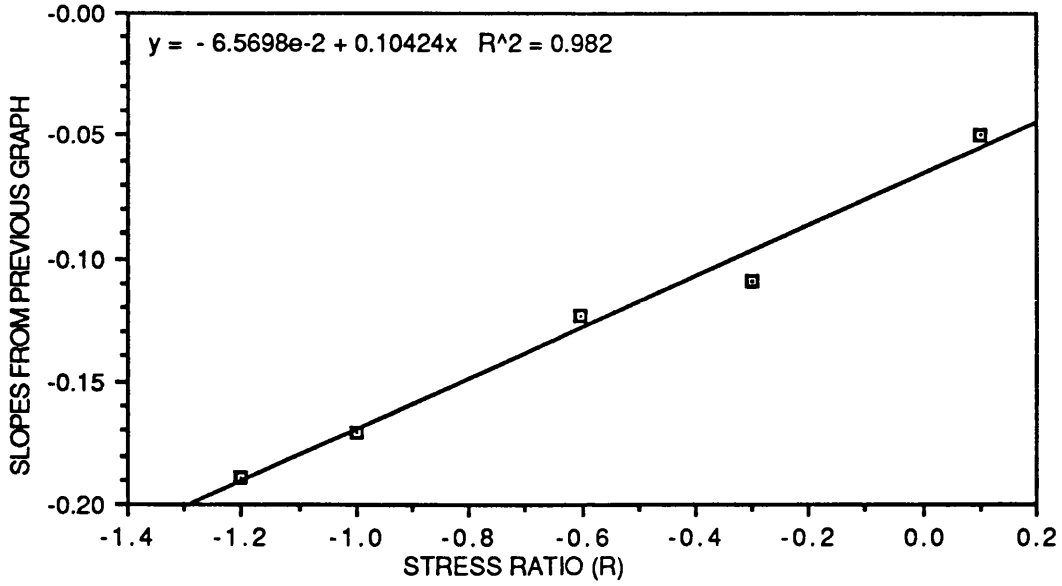

Figure 5.17 The values of the slopes for the 25% hybrid (where the regression line was calculated by including the UTS) have been plotted versus their respective stress ratios.

Because of this apparent linear relationship between the slopes of the fatigue life lines and the stress ratio for the 25% hybrid composite; the fatigue behaviour at any stress ratio between 0.1 and -1.2 can be made using the UTS as a reference point. The regression fit to the R=-1.2 is not as good as that observed for the other (R) values. This may be due to the fact that only four samples were tested at this stress ratio. It is also possible that extrapolating the fatigue life line to the UTS may not be valid for R=-1.2. This is discussed further in a later section.

5.6 FATIGUE RESPONSE OF 37.5% UD KEVLAR/XAS HYBRID COMPOSITE

5.6.1 Tension/Tension and Tension/Compression Fatigue Response

The fatigue life data for the 37.5% Kevlar/XAS hybrid composite was analysed in a similar manner to the 25% hybrid composite. A summary of the regression analysis with and without the inclusion of the UTS in the data-set are presented below.

	UTS included in the regression line calculation	UTS excluded from the regression line calc.
R=0.1	y=1.49-0.055 Log Nf (cd=0.58)	y=2.02-0.148 Log Nf (cd=0.80)
R=-0.3	y=1.39-0.095 Log Nf (cd=0.95)	y=1.40-0.096 Log Nf (cd=0.83)
R=-0.6	y=1.37-0.11 Log Nf (cd=0.92)	y=1.30-0.094 Log Nf (cd=0.62)
R=-0.8	y=1.35-0.136 Log Nf (cd=0.98)	y=1.15-0.094 Log Nf (cd=0.88)
R=-1.2	y=1.33-0.175 Log Nf (cd=0.96)	y=0.67-0.032 Log Nf (cd=0.70)

With the exception of the R=0.1 data-set, including the UTS gave a superior fit to the calculated regression lines. The behaviour of the R=0.1 data set was different to that observed for the XAS mono-fibre and 25% hybrid composites, but was similar in trend to that observed for the Kevlar mono-fibre composite i.e. a two-stage fatigue response.

The fatigue response of the 37.5% Kevlar/XAS/914 hybrid

composite are illustrated in Figure 5.18. The regression lines were calculated by including the UTS values in the data-set for each of the stress ratios investigated. The fatigue response of this hybrid exhibited a similar trend to that observed for the XAS mono-fibre and 25% hybrid composites for stress ratios of R=-0.3, -0.6, -0.8 and -1.2; the fatigue life lines at these stress ratios converged at the UTS for this composite. An apparent linear relationship was once again obtained on plotting the slopes against the respective stress ratios for this composite, see Figure 5.19.

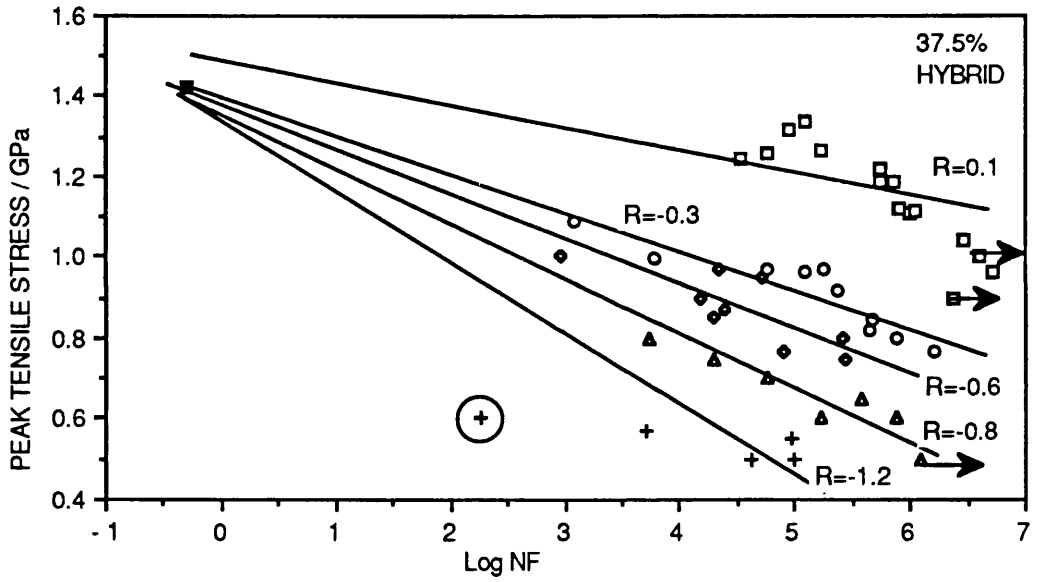

Figure 5.18 The fatigue response of the 37.5% Kevlar/XAS hybrid composite when tested at stress ratios of R=0.1, -0.3, -0.6, -0.8 and -1.2. The UTS was included in the calculation of the regression lines. The encircled datum point for R=-1.2 was omitted from the regression calculation.

Therefore, like the XAS mono-fibre composite and the 25% hybrid composite, predicting the fatigue life lines for the 37.5% hybrid composite is relatively straightforward for any stress ratios between -0.3 and -1.2. Predicting the fatigue

life line for R=0.1 is discussed next. On comparing the regression lines for R=0.1, a better fit to the experimental data was obtained when the UTS was excluded from the regression line calculation. However, experimental data points were only obtained between log cycles 4.5 and 6.5, hence a description for Region (I) is required for this hybrid composite at R=0.1. The following two methods to define Region (I) for the 37.5% hybrid are considered.

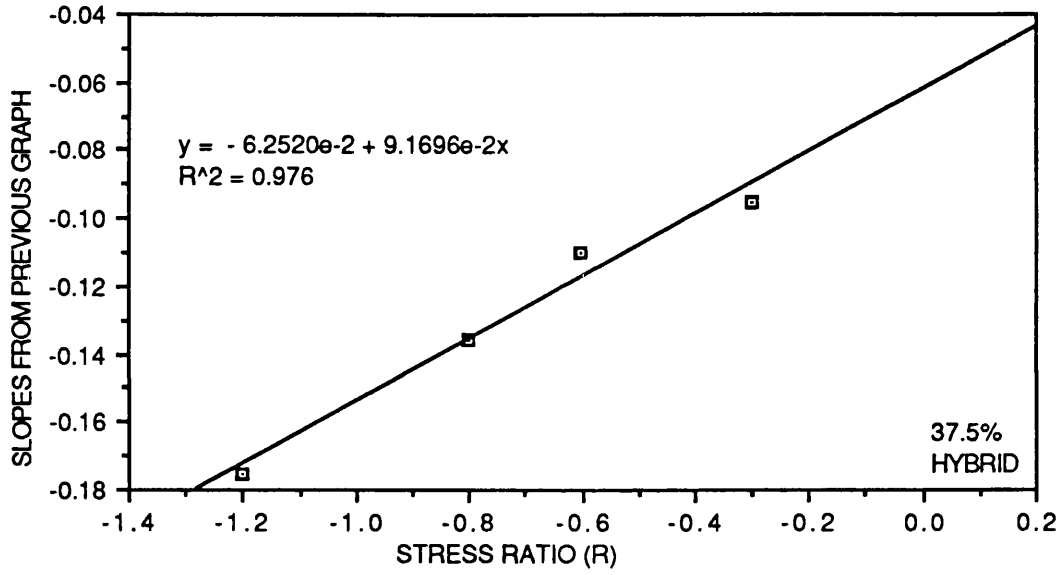

Figure 5.19 The slopes from the previous figure were plotted against the respective stress ratio for the 37.5% hybrid composite. The slope for the R=0.1 was not included in this plot.

In the first method Region (I) is defined by examining the macroscopic failure modes for the fatigue tested samples and to identify all the samples that exhibited a 'static tensile test' like the macroscopic failure mode. The regression line for Region (I) is then calculated by including the UTS in the data-set. In the second method, the equation that was

derived by plotting the slopes of the fatigue life lines versus the stress ratios for this composite can be used to define Region (I). An illustration of using both these methods to define Region (I) for the 37.5% hybrid are presented in Figure 5.20.

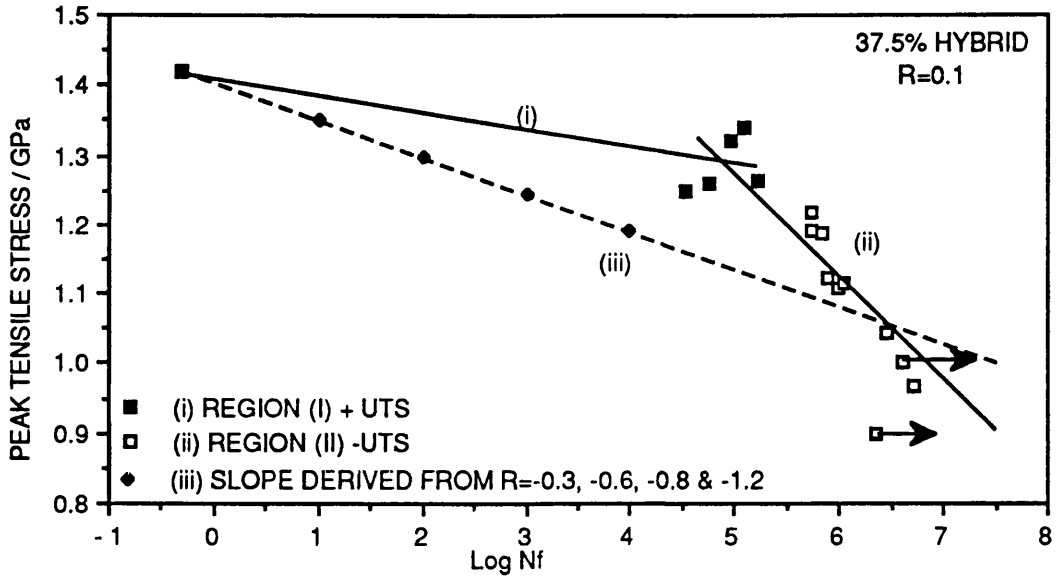

Figure 5.20 Illustration of two possible ways of defining Region (I) for the 37.5% hybrid composite. See text for explanation.

In Figure 5.18, it was shown that the fatigue life lines for the 37.5% hybrid at stress ratios of R=-0.3, -0.6, -0.8 and -1.2 are accurately described by the linear regression lines; the UTS was included in the regression line calculation. An apparent linear relationship was also shown in Figure 5.19 where the slopes of the fatigue life lines were plotted against the above mentioned stress ratios. Using this linear relationship (y=-0.0625 + 0.0917(R)) gives a slope of 0.0534 for R=0.1. However, as seen in Figure 5.20, using the UTS as a reference point and the slope of 0.0534 does not describe the data for R=0.1; it underestimates the fatigue life lines

for both Regions (I and II).

Recalling that the fatigue life lines for the XAS mono-fibre composite and the 25% hybrid composite were accurately described by the regression lines with the inclusion of the UTS in the data-set for all the stress ratios investigated (including R=0. 1). A similar linear relationship was also observed for the 37.5% hybrid composite for all the stress ratios with the exception of R=0.1. This implies that the fatigue performance of the 37.5% hybrid under T/T testing shows a relatively improved performance compared to the T/C fatigue series. The possibility that the Kevlar fibres in the 37.5% hybrid composite may somehow delay the catastrophic (premature) failure of the composite will be addressed in the next section. Figure 5.21 illustrates the case where the UTS was excluded from the regression line calculation for the 37.5% hybrid composite. This mode of representing the fatigue life line will be compared with the case where the UTS was included in the regression line calculation.

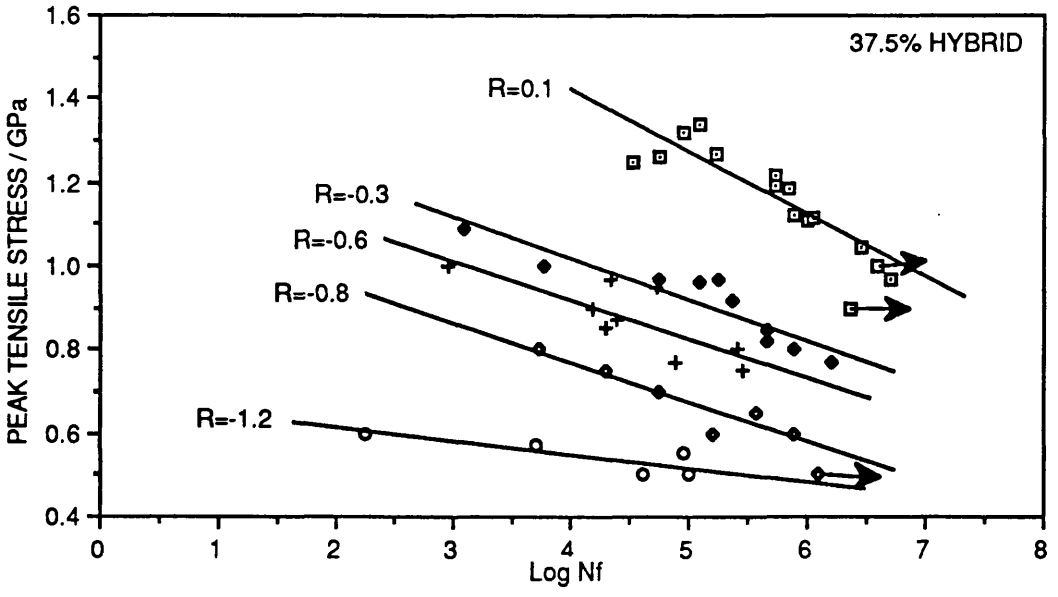

Figure 5.21 An alternate representation of the 37.5% fatigue life lines; the UTS was excluded from the regression line calculation.

5.7 FATIGUE RESPONSE OF 50% KEVLAR/XAS/914 HYBRID

5.7.1 Tension/Tension Fatigue Behaviour

A summary of the regression equations for the 50% hybrid composite along with the respective coefficient of determination are presented below.

	UTS excluded from regression line calculations.	UTS included in the regression line calcul.
R=0.1	Y=1.98-0.164 Log Nf (cd=0.70)	Y=1.34-0.044 Log Nf (cd=0.52)
R=0.01	Y=1.63-0.111 Log Nf (cd=0.53)	Y=1.29-0.046 Log Nf (cd=0.61)
R=0.01*	Y=1.65-0.119 Log Nf (cd=0.84)	Y=1.28-0.049 Log Nf (cd=0.78)

R=0.1 REGION (I) Y=1.26-0.021 Log Nf

On inspecting the regression equations for R=0.1, it is apparent that a better fit to the experimental was obtained when the UTS was excluded from the data-set. As in the case for the Kevlar mono-fibre composite and the 37.5% hybrid this was taken to represent a two stage fatigue response. Region (I) for R=0.1 was defined, as before, by including the UTS and the specimens that exhibited a macroscopic failure mode that was similar in appearance to the static tensile test failure mode.

The scatter in the R=0.01 data-set was quite considerable as seen in Figure 5.22. Two pairs of regression equations were calculated for this stress ratio; the first pair consisted of the UTS included and excluded from the data-set. In the second pair two of the encircled points in Figure 5.22 were

excluded from the regression line calculations. Although no real justification can be offered for excluding the two selected data points; a better fit to the other data points was obtained in doing so for the R=0.01 data set. However, it is clear that the fatigue response of the hybrid composite T/T fatigue tested at R=0.1 exhibits a superior performance to R=0.01. The three data points were generated using R=0.5 at peak stress corresponding to approximately 90% of the UTS, run-outs were recorded for two of the specimens at 10^6. Therefore, as in the case for the Kevlar mono-fibre composite, increasing the stress ratio form 0.1 to 0.5 resulted in an enhanced fatigue performance in the high-cycle region. Further work is necessary to establish the fatigue life lines at stress ratios greater than 0.1.

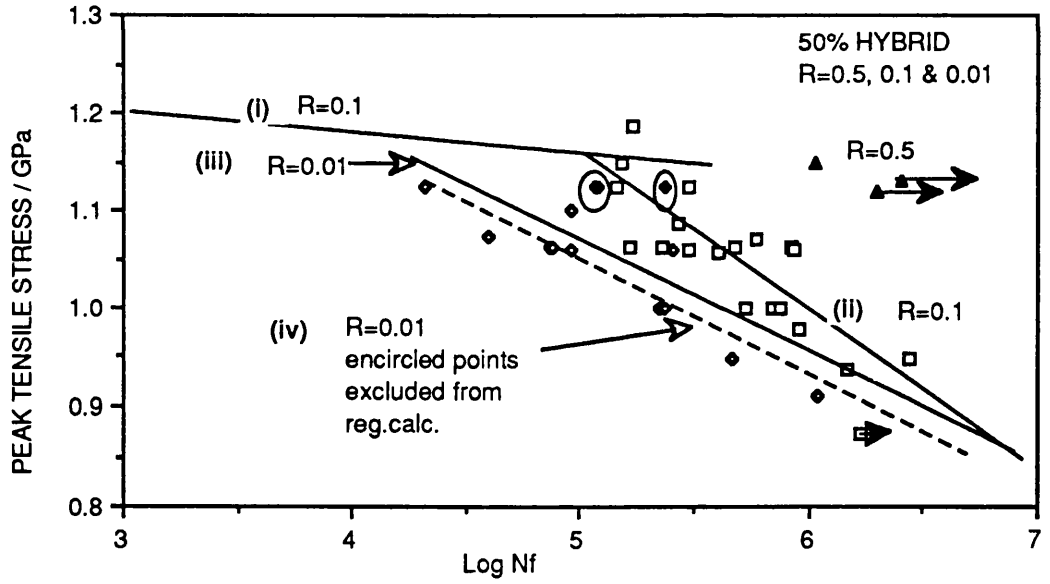

Figure 5.22 The fatigue response of the 50% Kevlar/XAS/914 hybrid composite, T/T fatigue tested at stress ratios of 0.5, 0.1 and 0.01.

The uncertainty in the fatigue response of the R=0.01 data-

set is unfortunate as it makes comparisons with the other stress ratios and the other hybrids difficult. However, the 50% hybrid shows a similar trend to that observed for the Kevlar mono-fibre composite. In addition to the two stage fatigue behaviour, the R=0.1 and 0.01 fatigue life lines converge. For the unmodified data-set for the 50% hybrid this convergence according to the regression equations takes place at, Y=0.85 5GPa, X=6.86 Log Nf and for the modified data-set the convergence is at, Y=0.78 5GPa, X=7.33 Log Nf. Assuming that the modified data-set is the more appropriate since the modified regression line describes the data points for R=0.01 more accurately; a similar procedure to that adopted for the Kevlar mono-fibre composite can be used to predict the fatigue life line for the 50% hybrid for R=0.1 and 0.01. Interestingly, the fatigue life line for R=-0.1 also shows an apparent convergence in the vicinity of the R=0.1 and 0.01 convergence point.

5.7.2 TENSION/COMPRESSION FATIGUE RESPONSE

The effect of introducing a compressive cyclic stress component on the fatigue response of the 50% hybrid composite is illustrated in Figures 5.23 and 5.24; the fatigue life lines for R=0.1 and 0.01 are also represented in these figures to facilitate ease of comparison. The modified regression line was used for R=0.01. Figure 5.23 illustrates the case where the UTS was included in the regression line calculation and Figure 5.24 illustrates the case where the UTS was excluded from the regression line calculation. A summary of all the regression equations for the 50% hybrid

are listed below.

	UTS excluded from the regression line calculations.	UTS included in the reg. line calculations.
R=0.1	Y=1.98-0.164 Log Nf (cd=0.70)	Y=1.34-0.044 Log Nf (cd=0.52)
R=0.01*	Y=1.65-0.119 Log Nf (cd=0.84)	Y=1.28-0.049 Log Nf (cd=0.78)
R=-0.1	Y=1.49-0.10 Log Nf (cd=0.67)	Y=1.28-0.055 Log Nf (cd=0.79)
R=-0.3	Y=2.08-0.24 Log Nf (cd=0.92)	Y=1.35-0.101 Log Nf (cd=0.75)
R=-0.4	Y=1.76-0.20 Log Nf (cd=0.99)	Y=1.24-0.099 Log Nf (cd=0.98)
R=-0.6	Y=1.84-0.22 Log Nf (cd=0.92)	Y=1.28-0.114 Log Nf (cd=0.89)
R=-1.2	Y=0.55-0.023 Log Nf (cd=0.60)	Y=1.98-0.164 Log Nf (cd=0.70)

It is apparent from Figures 5.24 and 5.25 that the fatigue response of the 50% hybrid does not follow the trends observed for the mono-fibre composites. However, the general trend seems closer to the Kevlar mono-fibre composite than the XAS composite. Unfortunately, the lack of data points for some of the stress ratios and the scatter in the results for this composite makes the analysis very difficult. For example, as seen in the regression summary for the 50% hybrid, the coefficient of determination for R=-0.1 was only 0.67.

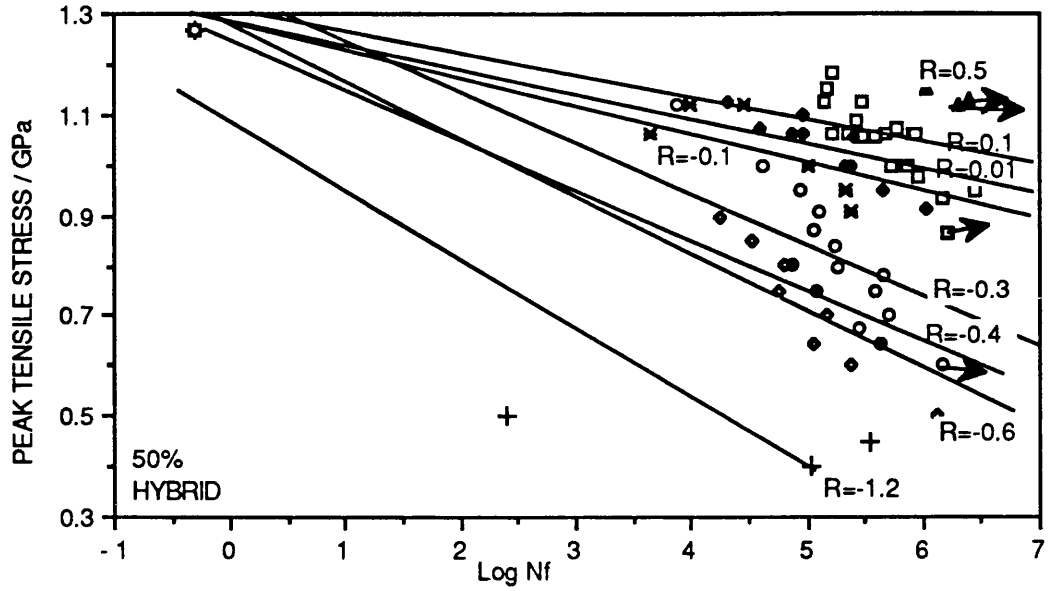

Figure 5.23 Fatigue response of the 50% Kevlar/XAS/914 ud hybrid composite fatigue tested at R=0.5, 0.1, 0.01, -0.1, -0.3, -0.4, -0.6, and -1.2. The UTS was included from the regression line calculation.

Examination of the raw data showed that the regression line was biased by one datum point, see Figure 5.25. A significant change in the slope of the fatigue life line is observed on excluding this 'stray' datum point. Once again, no real justification can be offered for excluding the single stray datum point other than to attribute it to scatter. However, it is obvious from Figure 5.25 that the highlighted datum point does not fit the general pattern observed for the R=-0.1 data-set.

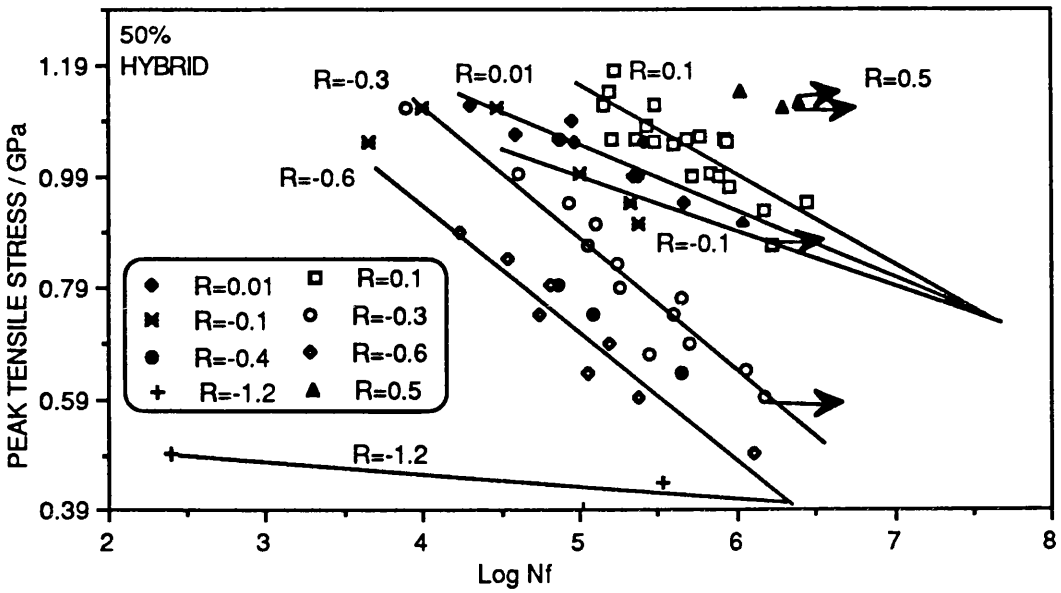

Figure 5.24 Fatigue response of the 50% Kevlar/XAS/914 ud hybrid composite fatigue tested at R=0.5, 0.1, 0.01, -0.1, -0.3, -0.4, -0.6, and -1.2. The UTS was excluded from the regression line calculation.

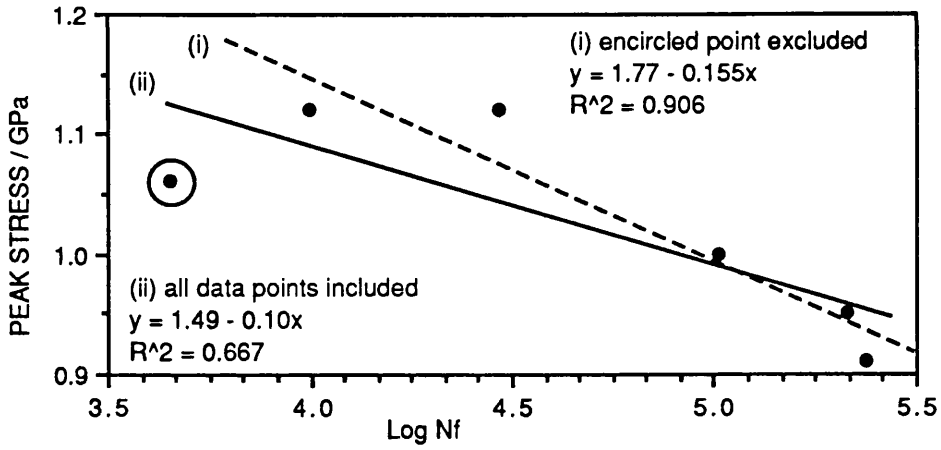

Figure 5.25 Illustration of uncertainty in the actual fatigue life line caused by scatter and lack of data points for R=-0.1 in the 50% hybrid composite.

5.7.3 ELEVATED TEMPERATURE FATIGUE - 50% KEVLAR/XAS HYBRID

A limited number of fatigue tests were carried out on this hybrid composite at 100°C to facilitate comparison with the elevated temperature fatigue performance of the Kevlar mono-fibre composite. The results from this investigation are illustrated in Figure 5.26, the data for the room temperature tests are also presented for ease of comparison.

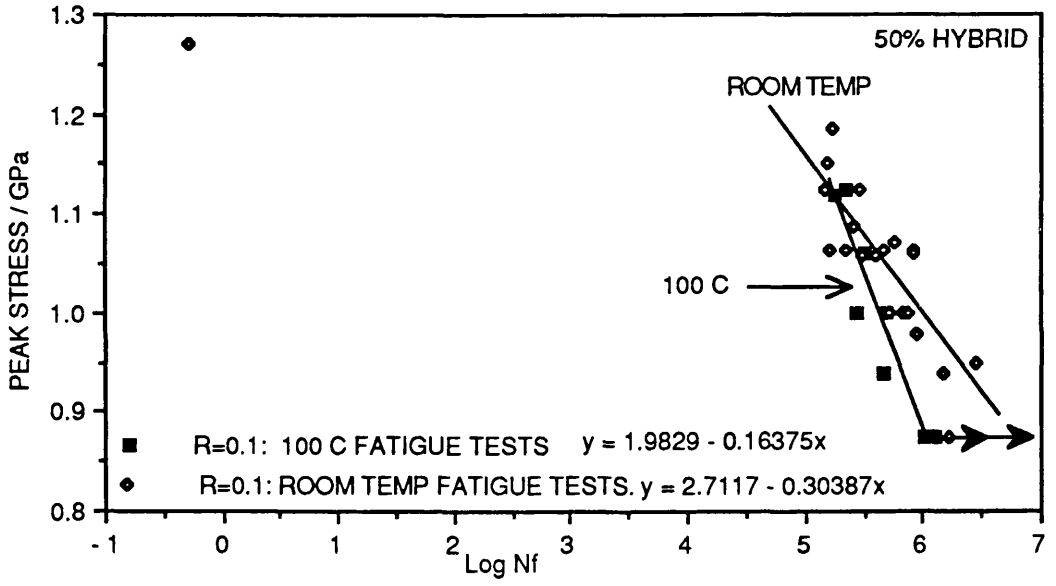

Figure 5.26 Comparison of the fatigue response of fatigue tests carried out at ambient and 100°C for 50% Kevlar/XAS hybrid composite.

As seen in Figure 5.26, there seems to be a small reduction in the fatigue response of this material at 100°C compared to ambient temperature fatigue tests. The response of the mono fibre Kevlar composite showed a similar trend. The deviation from ambient behaviour seems to be greater at lower values of peak stress, however it has to be pointed out that this

observation is based on a limited number of data points. The failure mode for the 50% hybrid fatigue tested at 100°C exhibited a different failure mode compared to the ambient temperature fatigue tests. The failed samples had an appearance best described as brush like failures and this was most prominent for the samples fatigue tested at relatively lower peak stresses.

5.8 Anti-Buckling Jig

These tension/compression fatigue tests were tests were carried out using the anti-buckling jig which was described in the experimental section. A brief discussion on the anti-buckling jig is presented in this section prior to discussing the results obtained using the jig.

The legitimacy of comparing data generated under different 'environments' needs to be considered first prior to drawing any conclusions. For instance, all the positive stress ratio fatigue tests were carried out without the use of the anti-buckling device. With hind-sight this should have been carried out to ensure that the jig itself did not contribute in any way to the fatigue response of the test specimen[135]. The use of anti-buckling guides can result in heating due to friction between the jig and the specimen. In this programme, Teflon™ strips were used to minimize the friction between the specimen and the jig. A more serious consequence of using anti-buckling guides is the possibility that the mode of damage development and propagation may be affected. There is very little information on this in the literature. Gerharz[134] reported a marked difference in the fatigue life of

specimens depending on the extent of surface covered by the anti-buckling jig. His results showed that unsupported edges resulted in reduction by a factor of 5 for fatigue lives greater than 10^4 compared to specimens where edge support was provided. It was suggested that by providing edge support, the growth of fatigue damage initiated at the edges was retarded. Gerharz also reported the findings of another researcher who found that for centre-holed specimens, the use of a windowless jig across the hole gave fatigue lives greater than a factor of 30 compared to 'holed' specimens with a window across the hole.

The mode of load application and bending effects when conduction compression tests were discussed in a previous section. The intention of the present investigation was to study the effect of compressive loading on the fatigue behaviour of Kevlar, XAS and their hybrids. It was assumed that any influence by the anti-buckling jig would have had a similar effect on the Kevlar and Kevlar/XAS hybrid composites.

5.9 COMPARISON AND PREDICTIONS OF FATIGUE PERFORMANCE OF MONO-FIBRE AND HYBRID UD KEVLAR/XAS/914 COMPOSITES

Fatigue tests on the XAS/914 composite were carried out using stress ratios of R=0.1, -0.6 and -1.2. An excellent fit to the linear regression lines was obtained at each of the stress ratios when the UTS was included in the regression line calculation. It turned out that the regression

equations took the form

$$\sigma = UTS - B \log Nf$$

Where

σ = peak tensile stress during each cycle,

UTS = mean ultimate tensile strength,

B = slope of the fatigue life line,

Nf = cycles to failure.

The above form of the regression equation is in fact identical to that given by Mandell[163]. He defined the ratio UTS/B as a normalised measure of the steepness of the fatigue life line and the ratio B/UTS as the fractional loss in tensile strength per decade of cycles. The UTS/B ratios was found to be close to 10 for a series of E-glass in various matrices. However, his conclusion that the tensile fatigue to be a fibre property independent of matrix or interface is debatable.

In this programme, it was previously shown that, an apparent linear relationship existed between the slopes of the fatigue life lines against their respective stress ratios for the XAS/914 composite. A similar trend was observed for the 25% hybrid and in the 37.5% composite for negative stress ratios. The fatigue behaviour of the Kevlar mono-fibre composite was different in that there was an apparent convergence point for the stress ratios in the high cycle region. The general fatigue trends for the 50% hybrid were different to that observed for the other two hybrids.

The XAS/914 composite fatigue life lines illustrated in Figure 5.27 were generated using an equation that described the relationship between the slope and the stress ratio for the XAS/914 composite. A square fit was found to describe the experimental data better than the linear relationship previously calculated; Y(slope) = -0.1015 + 0.1512 (R) + 0.0426 (R^2).

The non-linear relationship between the slopes and the stress ratio is worthy of further discussion. The slopes obtained experimentally and using the above equation are presented in Figure 5.28.

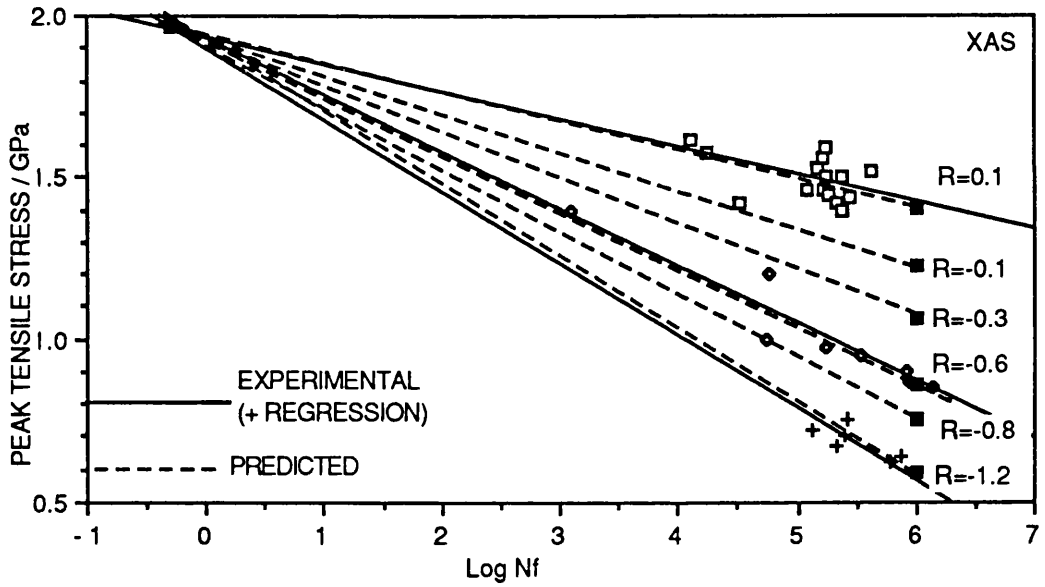

Figure 5.27 Experimental and predicted fatigue life lines for the XAS/914 mono-fibre composite at different stress ratios.

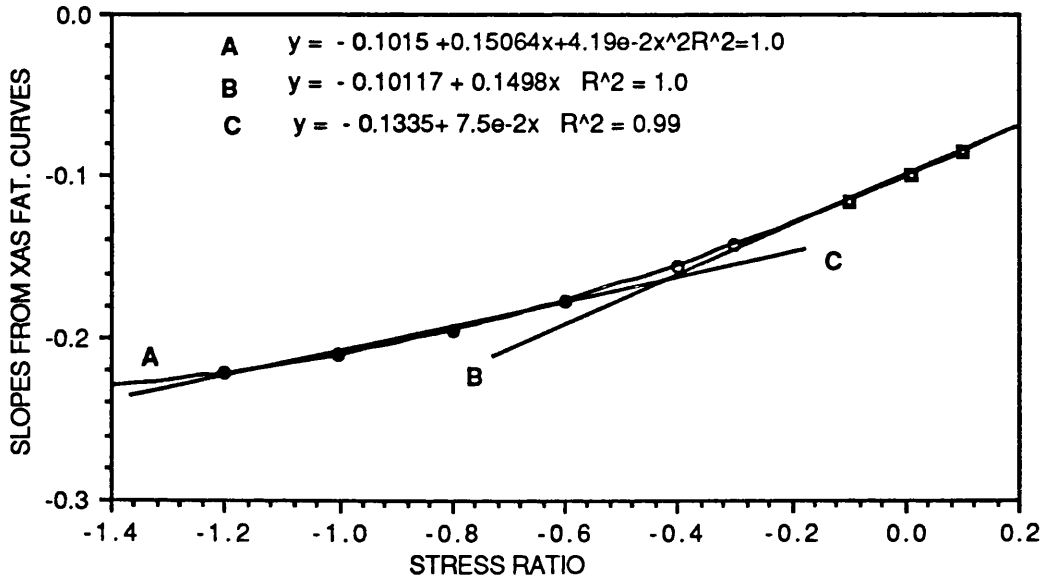

Figure 5.28 Illustration of the relationship between the experiment and predicted slopes versus their respective stress ratios for the XAS mono-fibre composite.

It is apparent from Figure 5.28 that the slopes of the fatigue life lines from R=0.1 to R=-0.1 can be approximated by a linear relationship, and that the slopes for R=-1.2 to -0.6 can also be approximated by another linear relationship. Therefore, presumably the effects of the cyclic compressive stress become significant for stress ratios greater than -0.1 in the XAS/914 composite. These results also suggest that a progressive change in failure mechanism occurs in going from R=0.1 to R=-1.2; this was confirmed from post-failure inspections of the specimens.

In order to compare the fatigue life line of the hybrids with that of the XAS and Kevlar mono-fibre composite, a normalization procedure is necessary. The method proposed by Mandell[163] where the normalization was achieved by dividing the slopes of the fatigue life lines at the respective stress

ratios by the UTS. The relevance of the proposed normalization need to be considered, since T/C data are involved here whereas Mandell discussed the general trends in T/T fatigue tested composites.

A S/Log Nf for T/T fatigue is a measure of the rate of degradation of the tensile properties with number of cycles. Normalising the data to the ultimate static strength provides a common starting point for all the fatigue life lines of interest and their rates of strength degradation with cycles can then be carried out. However, for T/C fatigue tests, normalising the fatigue life lines to the UTS only takes care of the tensile component and ignores the compressive cyclic contribution. This is acceptable as it is the rate of degradation of tensile properties with the number of cycles that are of interest. Fatigue life lines that extrapolate to the UTS, imply that the predominant failure mechanism that control the static strength, play a predominant role in the strength degradation during fatigue - provided that other failure (new) mechanisms do not become predominant, for example, the degradation of interfacial properties with number of cycles. Curtis[166] carried out a detailed investigation on the mechanical properties of carbon fibre composites and clearly showed that the fatigue response of a given carbon fibre type was dependent on the fibre/matrix combination.

The general fatigue behaviour of the 37.5% hybrid is considered next. Figure 5.29 illustrates the normalised slopes for the XAS mono-fibre composite and the normalised slopes for the 37.5% hybrid composite. It is clear that the

rate of tensile strength degradation for the hybrid composite is marginally superior to that of the XAS mono-fibre composite for stress ratios between R=0.1 to R=-1.0. Careful consideration was given to the actual mode of representing the data in Figure 5.29 and three cases were considered in fitting an equation to the data.

Firstly, a cubic regression analysis on the raw fatigue data was carried out by 'forcing" it to pass through the UTS, this was achieved by including two further data points corresponding to the UTS (i.e. X=-0.3 and Y=1.42GPa) in the data-set. This is a reasonable operation because (a) a high correlation coefficient was obtained by including a single UTS/Log 0.5 cycles pair in the data-set; (b) the data showed a tendency to converge at the UTS/Log $_{0.5}$ cycles.

Secondly, a linear fit was performed on the raw normalised data and the following equation was derived Y=-0.0447-0.0638(R); cd =0.989. The linear regression line was not included in Figure 5.29 for clarity. Thirdly, a 'normal' cubic fit was performed on the normalised slopes versus stress ratio i.e. only one UTS/Log 0.5 cycles pair was included in the original data-set. The linear regression line adequately represented the cubic fit for stress ratios between R=0.1 and -1.0.

With reference to Figure 5.29, the fatigue response of the 37.5% hybrid does seem to be superior to that of the XAS mono-fibre composite for stress ratios greater than R=-0.1. The differences in the regression lines at R=0.1 for the 'normal' and 'forced' fit curves for the 37.5% hybrid have

been attributed to the following reasons. (a) The fatigue data for the 37.5% hybrid indicated that the fatigue response was best represented by a regression line where the UTS was not included in the data-set; hence a two stage (Regions I and II) description of the fatigue response was required at R=0.1. However, experimental data points were only obtained between Log cycles 4.5 and 6.5, hence an accurate description for Region (I) was not possible, this is illustrated with the aid of Figure 5.30.

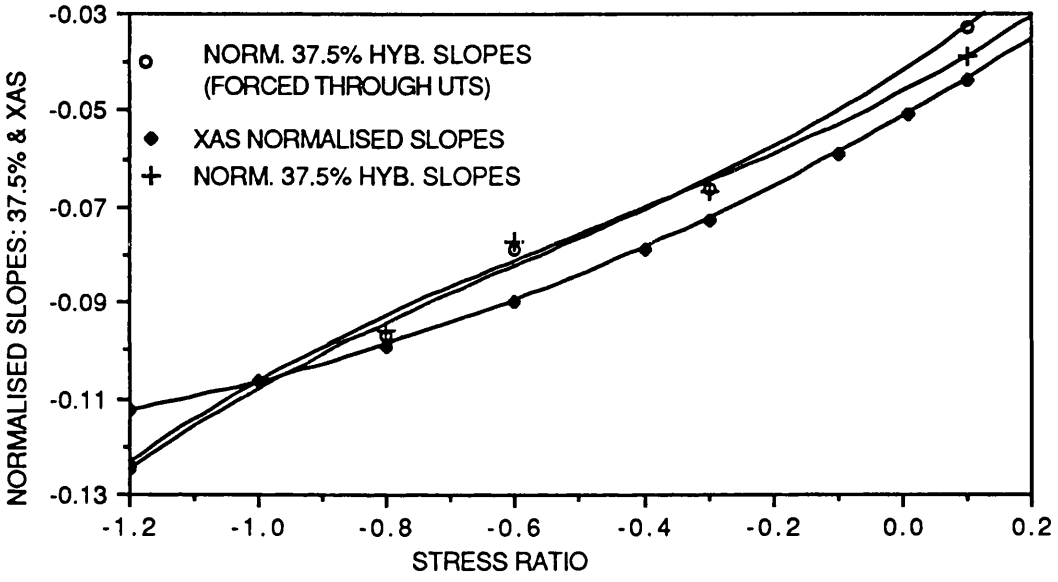

Figure 5.29 Comparison of normalised slopes for the 37.5% Kevlar/XAS hybrid and that of the XAS mono-fiber composite as a function of stress ratio.

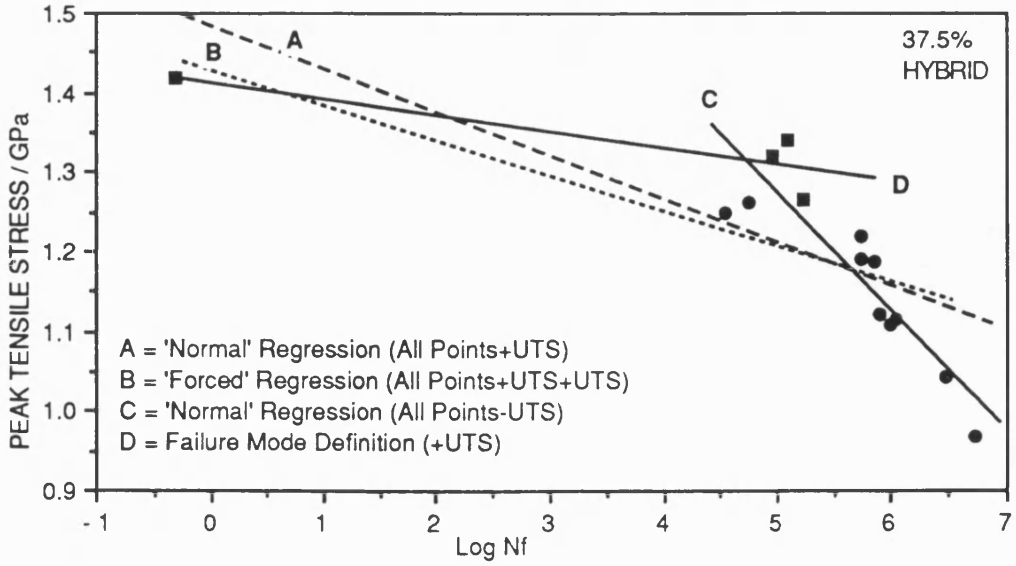

Figure 5.30 Illustration of the possible representation of Region (I) for the 37.5% hybrid composite.

With reference to Figure 5.30, the regression line (A) was calculated by including the UTS in the data-set. Line (B) was calculated by 'forcing' the regression line to pass through the UTS. Regression line (C) represents the normal way of calculating the fatigue life regression lines and the UTS was not included in the regression line calculation. The calculation of line (D) was subjective in that samples which exhibited a static tensile type failure mode were included in the data-set along with the UTS. It is apparent from Figure 5.30 that representing the R=0.1 by regression lines (A or B) will underestimate the fatigue resistance upto about 10^5 cycles and then overestimate the fatigue performance of this composite for cycles greater than 10^5. A similar behaviour was also observed for the 50% hybrid composite.

A further consideration of the R=0.1 fatigue life line representation for the mono-fibres and hybrids is presented

in Figure 5.31; the peak tensile stresses (Y-axis) were normalised to the UTS of the respective composites.

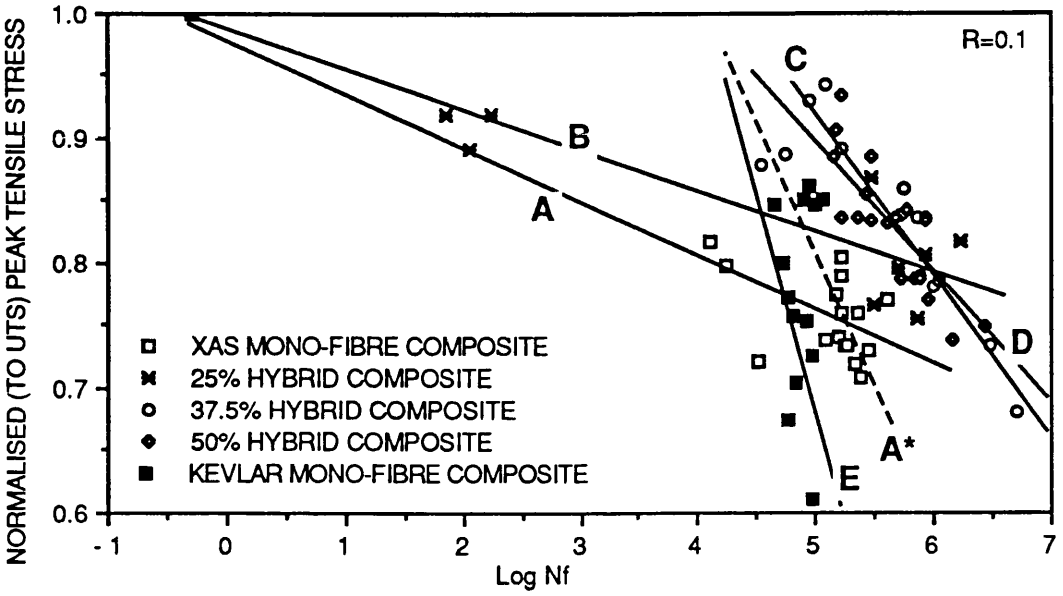

Figure 5.31 Fatigue data for R=0.1 normalised to the respective UTS values. See text for explanation.

With reference to Figure 5.31, the line (A) represents the regression line for the XAS mono-fibre composite where the UTS was included in the calculation. The fatigue life line for the XAS composite is typical of fatigue life lines reported in the literature for carbon reinforced plastics. However, inspecting the fatigue data for the XAS composite does indicate the possibility that the fatigue performance may be represented by a two stage life line, i.e. Regions (I and II). Another way of representing Region (II) for the XAS/914 is illustrated in Figure 5.31 as line (A*). The fatigue data presented by Curtis[166] and Schultz[167] were indeed presented as a two stage fatigue process.

The fatigue T/C fatigue data presented by Schults also showed a similar trend to that observed in this study - on reducing

the stress ratio (from R=0.1 to R=-5), a progressive deterioration in the fatigue performance relative to the R=0.1 case was observed.

The line (B) represents the fatigue life regression line for the 25% hybrid. It can be argued that even this hybrid exhibits a two stage fatigue response and the three low cycle data points bias the regression line through the UTS. Lines (C and D) represent the fatigue life regression lines for the 50% and 37.5% hybrid composites respectively. It is clear that regardless of how the fatigue data for the mono-fibre composites are represented, the normalised fatigue data for the hybrids show a superior fatigue performance to the mono-fibre composites.

The above discussion, in effect, has introduced uncertainty in the interpretation of the R=0.1 fatigue data for the XAS mono-fibre composite and the 25% hybrid. The fatigue life data for these two composites can be interpreted in two ways: (a) a single regression line which includes the UTS and the fatigue data points; (b) a two stage fatigue life line. These two representations are illustrated in Figure 5.32 and 5.33 and are used as the basis for comparison of the unnormalised fatigue data as a function of composite composition, see Figure 5.34.

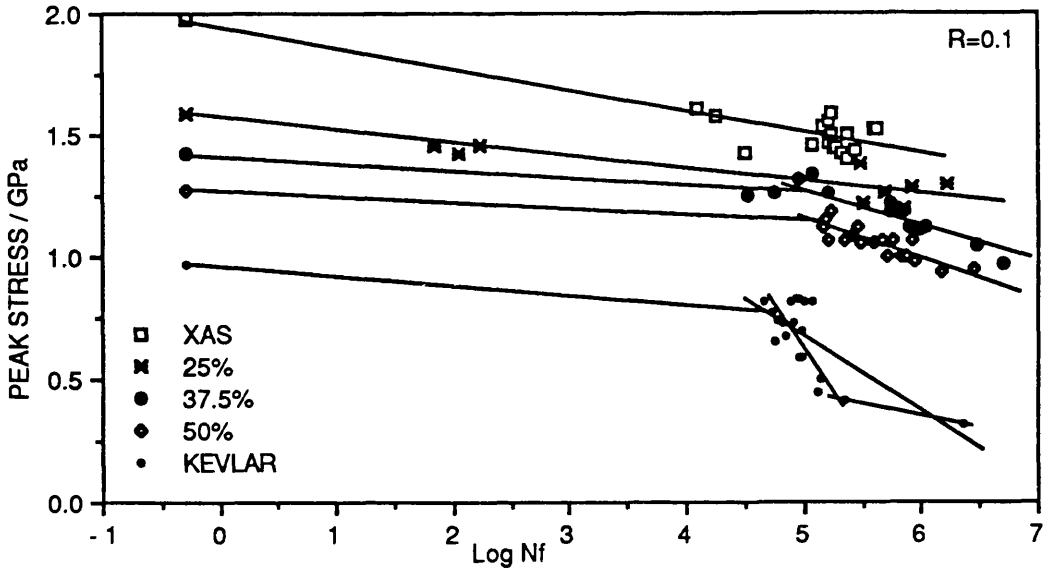

Figure 5.32 Representation of the fatigue life lines (R=0.1) by: one-stage for XAS and 25% hybrid; two-stages for the 37.5% and 50% hybrids; and both two-stage and three-stage for the Kevlar composite.

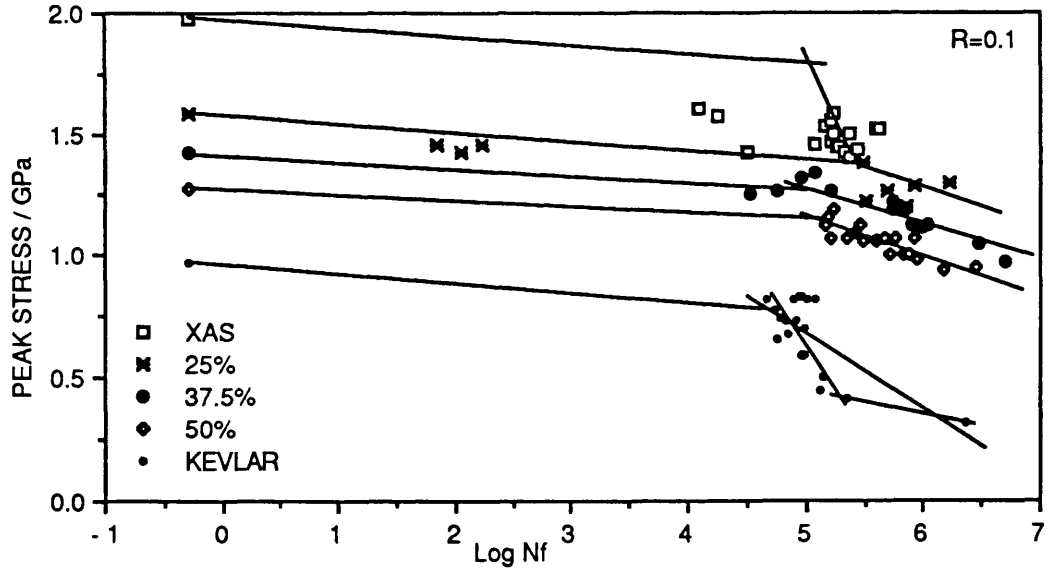

Figure 5.33 Representation of the fatigue life lines (R=0.1) by: two-stages for XAS and 25% hybrid; two-stages for the 37.5% and 50% hybrids; and both two-stage and three-stage representation for the Kevlar mono-fibre composite.

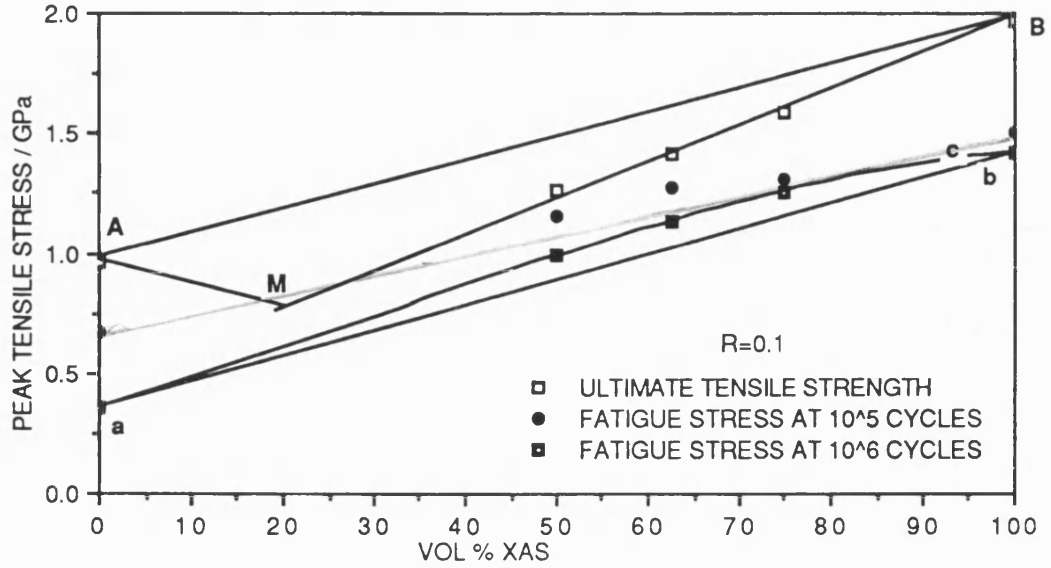

Figure 5.34 Representation of the fatigue tensile stress at 10^5 and 10^6 cycles as a function of mono-fibre and hybrid compositions. The ultimate tensile strength values for the respective composites are also represented.

In Figure 5.34, the line (AB) is the ROM description of the UTS for the mono-fibre and hybrid composites, as discussed previously. The regression line (MB) describes the ultimate strength of the hybrids and the XAS mono-fibre composites; it was previously discussed that in order to obtain the line (MB), a lower modulus value for the Kevlar fibres (i.e., lower than that quoted by the manufacturers) had to be assumed. It was also speculated that the lower Kevlar fibre modulus may have been due to induced compression loading on the fibres as a result of thermal stresses from processing the prepregs. The possibility that the Kevlar fibres were of an inferior quality can not be ruled out. This serves to highlight the need to have a standard quality control procedure for both the fibres and the matrix prior to processing the prepregs.

With reference to Figure 5.34, the line (ab) represents the ROM at 10^6 cycles under fatigue loading for the two mono-fibre composites. The line (ac) represents the fatigue stress at 10^6 cycles for the mono-fibre and hybrid composites. An apparent improvement in the fatigue performance in the hybrids over their mono-fibre composites is evident. A similar trend was also observed at 10^5 cycles, see Figure 5.34.

The relative displacement of the hybrid fatigue stress at 10^6 relative to the mono-fibre composites will obviously be sensitive to the values attributed to the mono-fibre composite. The two fatigue life line representations presented for the Kevlar composite (two-stage and three-stage fatigue life lines) illustrated in Figures 5.32 do not differ significantly at 10^5 and 10^6 cycles.

However, when considering the XAS mono-fibre composite, if a two stage fatigue life line was used, then the fatigue stress at 10^6 would have yielded a significantly lower value, see Figure 5.32, thus indicating a greater apparent improvement in the fatigue performance of the hybrid composites. However, at 10^5, using a two stage fatigue life line for the XAS composite would have resulted in a higher fatigue stress value. This uncertainty in the interpretation of the R=0.1 fatigue data makes it impossible to come to a firm conclusion on the comparative performance of the hybrids compared to the mono-fibre composites. However, it is clear that the fatigue performance of the hybrids like the tensile strength changes in proportion to the composition. Bearing in mind the uncertainties in defining the fatigue life lines for the

composites discussed previously; the incorporation of Kevlar fibres in a XAS composite was seen to give a marginal improvement in the fatigue performance at (R)=0.1 over the mono-fibre composites as defined by the ROM.

Figures 5.35 and 5.36 illustrate the relationship between fatigue stress at 10^5 and 10^6 cycles respectively for the mono-fibre and hybrid composites in terms of their composition.

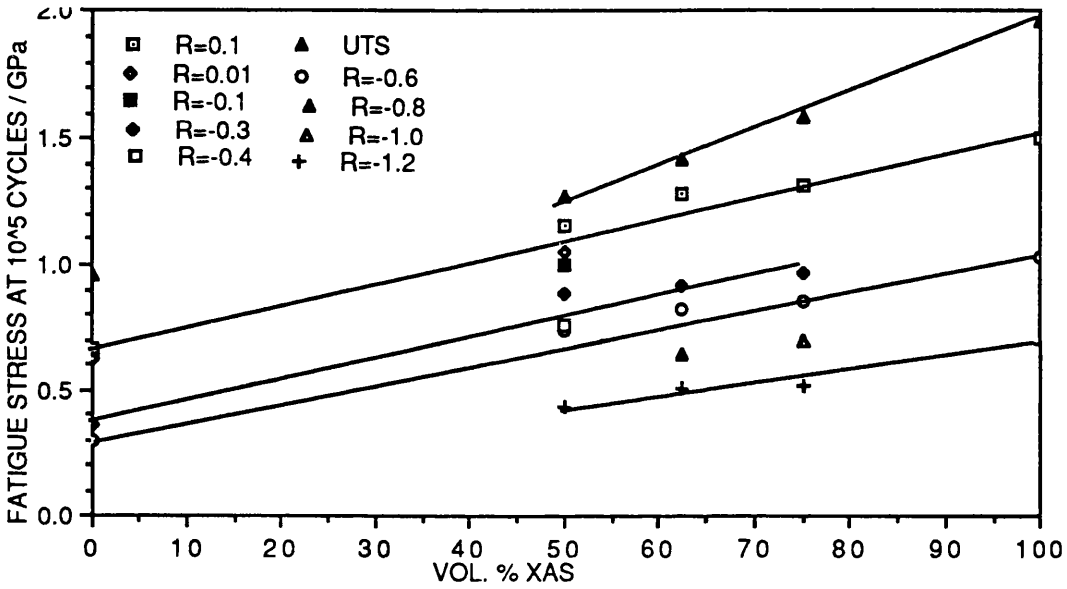

Figure 5.35 The observed relationship between the fatigue stress at 10^5 cycles and composition at the various stress ratios investigated.

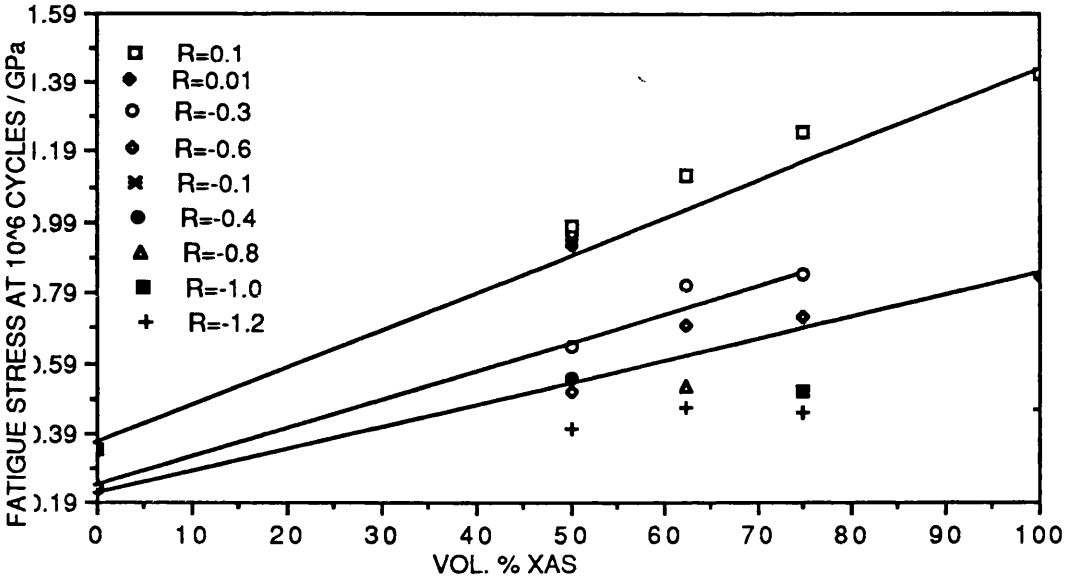

Figure 5.36 The observed relationship between the fatigue stress at 10^6 cycles and composition at the various stress ratios investigated.

The UTS values for the respective composites were represented in Figure 5.35 to illustrate that even under tension/compression cycling, the fatigue response of the hybrids changed in proportion to their respective compositions. The fatigue response of the composites were weaker under tension/compression cycling compared with tension/tension cycling.

An alternate way of representing the data from the previous two figures is illustrated in Figures 5.37 and 5.38, here the stress ratios were plotted against the fatigue ratio at 10^5 and 10^6 cycles respectively. The fatigue ratio was defined as the fatigue stress divided by the respective UTS values for the composites at a specified number of cycles. Figure 5.37 clearly illustrates that the Kevlar mono-fibre composite was most affected by tension/compression fatigue testing. It

was also evident that the fatigue response of the hybrid composites were marginally superior to that of their mono-fibre XAS composite; this improvement (at 10^5 cycles) increased as the volume fraction of the XAS decreased.

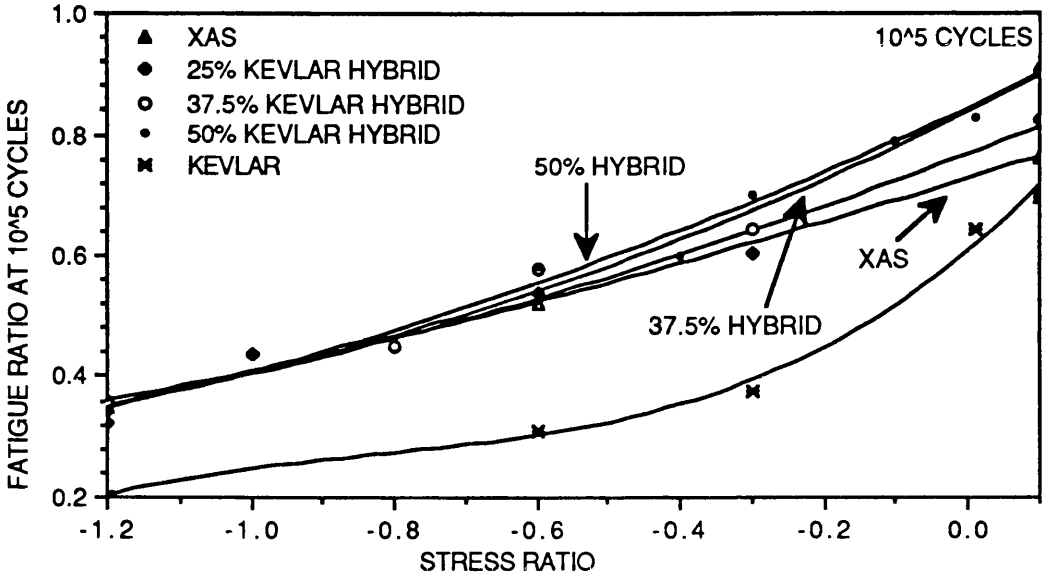

Figure 5.37 Illustration of the relationship between the fatigue ratio at 10^5 cycles and the fatigue stress ratios for the respective hybrids.

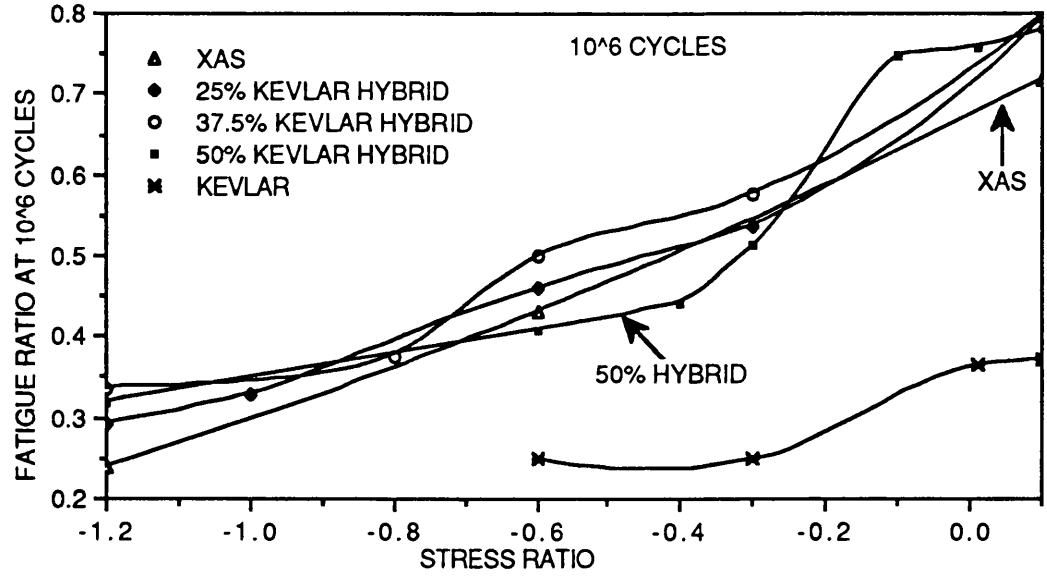

Figure 5.38 Illustration of the relationship between the fatigue ratio at 10^6 cycles and the fatigue stress ratios for the respective hybrids.

With reference to Figure 5.38, the 50% hybrid composite showed a rapid fall in the fatigue ratio when the stress ratio was reduced from (R)=0.1 to (R)=-1.2.

5.10 Master Fatigue Diagrams

The Goodman diagram (master diagram) is a convenient way of inspecting and representing the fatigue response at the various mean stresses investigated. The stress amplitude versus the mean stress is plotted at a specified number of cycles. Diagrams of this nature also permit lines of constant stress ratios to be drawn radiating from σ_a (stress amplitude) and σ_m (mean stress)=0. Various empirical curve-fitting procedures have been cited in the literature, including the following [168]:

1. Goodman's linear relationship $\sigma_a/\sigma_N + \sigma_m/\sigma_U = 1$
2. Gerber's Parabolic Relationship $\sigma_a/\sigma_N + (\sigma_m/\sigma_U)^2 = 1$
3. Elliptic Relationship $(\sigma_a/\sigma_N)^2 + (\sigma_m/\sigma_U)^2 = 1$
4. Adam's [169] Parametrics analysis - Adam[169] introduced a normalisation procedure where mean stress, stress amplitude and the static compressive stresses were divided by the static UTS:

$m = \sigma_m / \sigma_t$ m = mean, t = UTS

$a = \sigma_a / \sigma_t$ a = amplitude

$c = \sigma_c / \sigma_t$ c = UCS

He proposed an empirical interaction curve of the form

$$f = (a) / (1-m)(c+m)$$

where f is a function of alternating stress, mean stress, UTS and UCS. This has the merit of combining the various parameters into one master function.

The Master diagram for the XAS/914 composite is considered first using the 'forced' regression lines for the fatigue life lines listed below.

R=0.1 Y=1.94 -0.087 Log Nf $\sigma_{mean} = \sigma_{max}\ (1+R)/2$

R=-0.6 Y= 1.925 - 0.176 Log Nf $\sigma_{amp} = \sigma_{max}\ (1-R)/2$

R=-1.2 Y=1.906 - 0.222 Log Nf

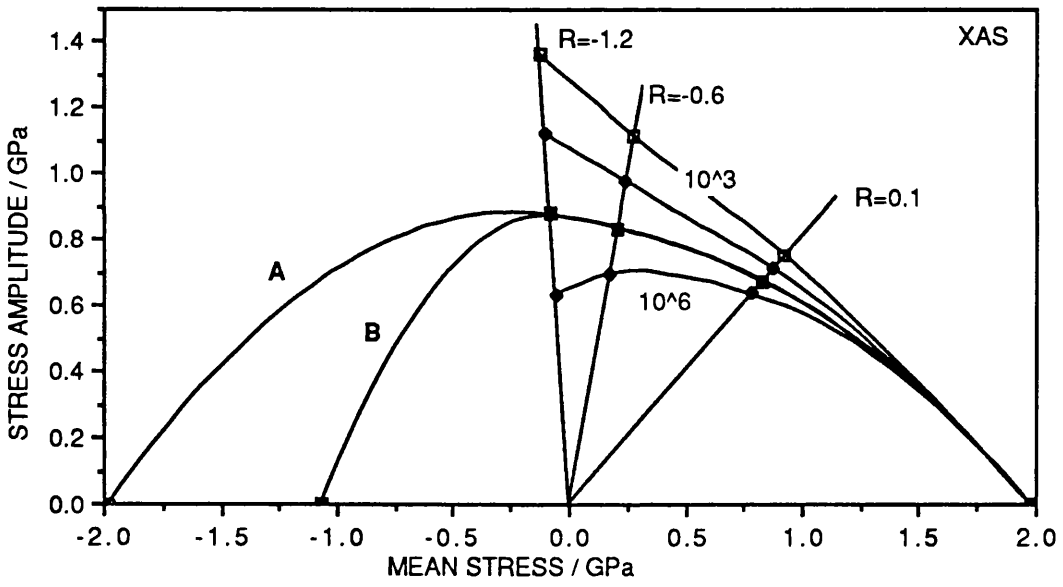

Figure 5.39 Constant life diagram for the XAS mono-fibre composite. See text for explanation.

In Figure 5.39, the line (A) was drawn assuming an equal tensile and compressive strength value. The line (B) was drawn using the experimental value for the compression strength. Lines (A and B) serve to illustrate that the choice of the UCS is important in defining the constant life

diagram. As discussed previously, the static compression strength of the mono-fibre and hybrid Kevlar/XAS composites were generated using different experimental set-up to the anti-buckling that was used in the T/C fatigue tests. Regrettably, static compression tests were not attempted using the anti-buckling jig used to generate the T/C fatigue data. The compressive strength of the XAS/914 composite system was 1.07GPa, which compares with a tensile strength of 1.97GPa for this composite. However, compressive strength values of 1.41GPa have been reported for the XAS/914 composite with V_f=0.6 by Lee [164] and Barker[165].

Figure 5.40 illustrates the constant life diagram for the mono-fibre composites and their hybrids at 10^5 cycles. A number of interesting features can be highlighted in Figure 5.40. Firstly, the peak stress amplitude values for all the composites lie in the tension/tension quadrant. This indicates that tension/compression loading is more detrimental than tension/tension fatigue loading. Secondly, the relative asymmetry (respect to a mean stress of zero) for each of the composites is seen to be dependent on their composition. The asymmetry was greatest for the Kevlar mono-fibre composite and was seen to decrease as the volume fraction of the Kevlar fibres was reduced in the hybrids.

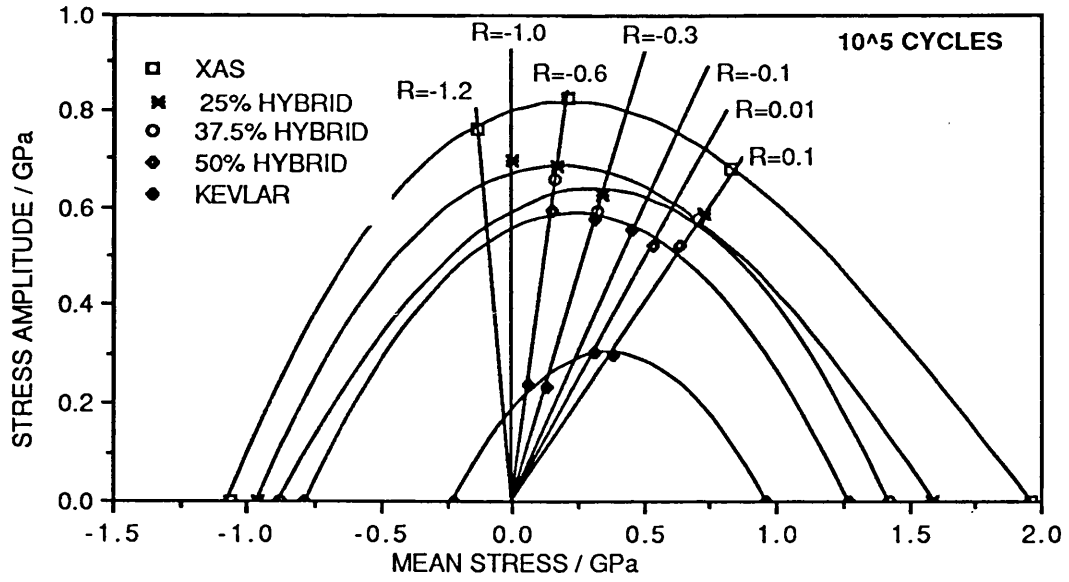

Figure 5.40 Constant life diagrams for the XAS and Kevlar mono-fibres and their unidirectional hybrid composites at 10^5 cycles.

This implies that the effect of the compressive load component was greatest for the Kevlar mono-fibre composite. The third interesting feature in Figure 5.40 is that the Kevlar fibres do not seem to exert any unexpected weakening effect on the fatigue response of the XAS in the hybrid composites. It is worth recalling that DeTeresa et al[120-122] had shown that the Kevlar fibres had displayed a strange behaviour on being subjected to uniaxial compression followed by subsequent T/T cycling; the fibre displayed the remarkable ability of almost total recovery of tensile properties subsequent to a previous compressive stress excursion. Therefore, poor compressive properties of Kevlar fibres under static loading conditions may not necessarily be reflected in their tension/compression response under fatigue loading.

6. Surface Temperature Measurements

6.1 Effect of Cyclic Frequency and Loading Rates

Surface temperatures of ud Kevlar composites were monitored by attaching a thermocouple to the surface of the specimen as previously described in the experimental section.

Figures 6.1 and 6.2 illustrate the surface temperature increases (above ambient) during fatigue testing of ud Kevlar composites for tests carried out at 200 and 500KN/sec loading rates. The surface temperature was seen to rise very rapidly at the beginning of the fatigue test up to approximately 100-400 cycles and then usually decreased and stablised until prior to failure. In almost all the samples tested, the surface temperature was seen to rise rapidly just prior to failure and the final peak temperature was always greater than the initial peak temperature. Due to the low chart-paper speeds used in recording the surface temperatures, it was not possible to identify accurately the number of cycles corresponding to this initial peak temperature; however, there were no problems in measuring the initial and final peak temperatures.

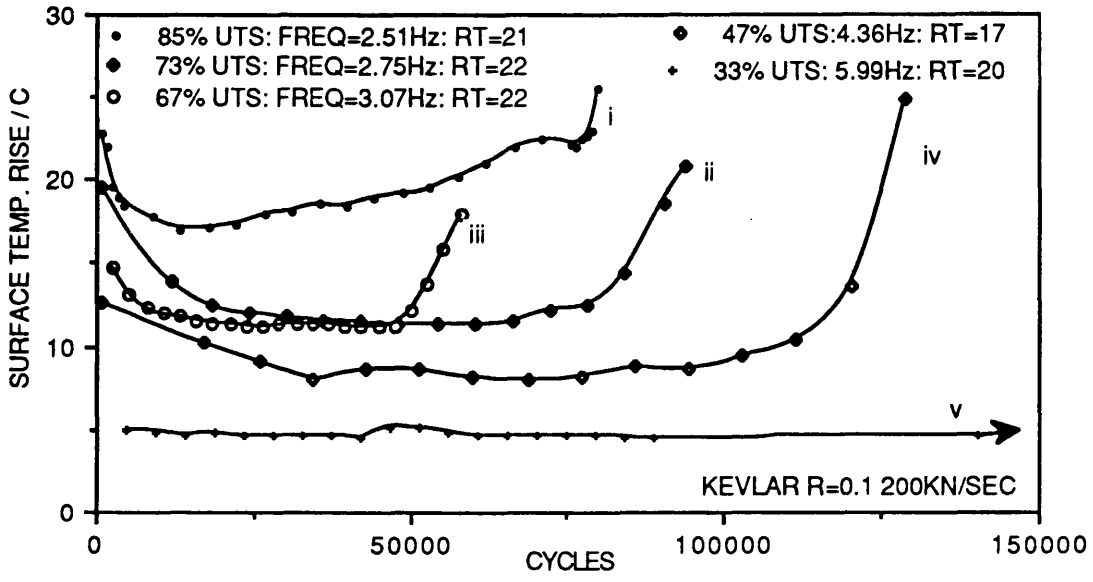

Figure 6.1 Measured surface temperature (above ambient) for ud Kevlar/914 fatigue tested at a stress ratio of 0.1 and a rate of loading of 200KN/seconds. Note: The the initial temperature rise is from ambient.

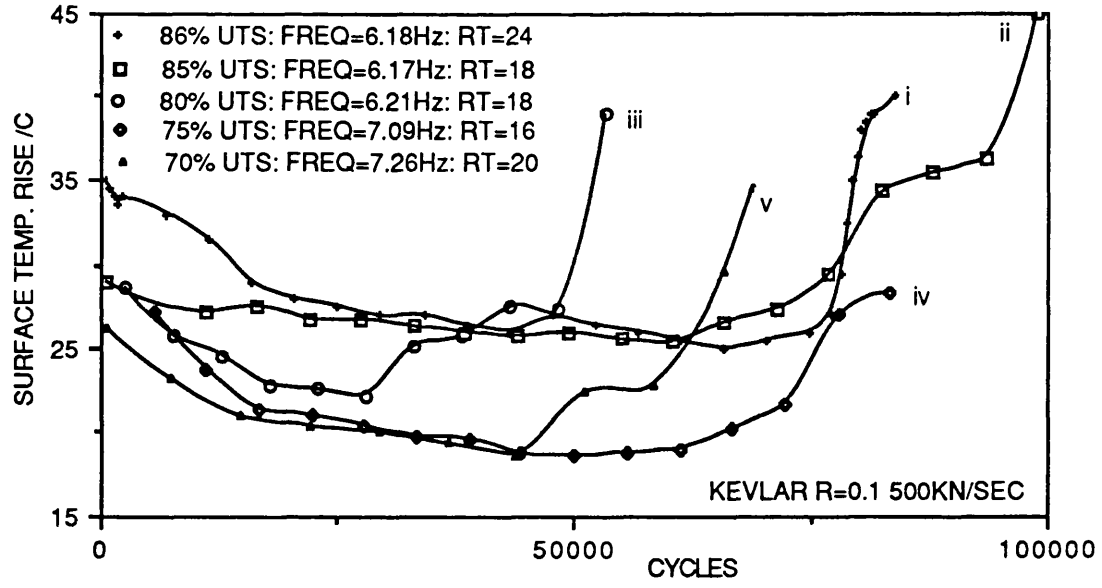

Figure 6.2 Measured surface temperature increases (above ambient) for ud Kevlar/914 fatigue tested at a stress ratio of 0.1 and a loading rate of 500 KN/seconds.

It is evident from Figures 6.1 and 6.2 that the measured surface temperature rise was a function of the applied peak stress and the cyclic frequency. For a given loading rate, lowering the peak stress resulted in lower measured surface temperature. This was inspite of the fact that the cyclic frequency increases as the peak load is decreased under constant rate of load application. For example, Figure 6.1-(i) represents a test specimen that was cycled at a peak stress corresponding to 85% of the ultimate tensile strength of the ud Kevlar composite, the cyclic frequency was 2.51Hz. The measure surface temperature at 50,000 cycles was approximately 40^{o}C. Lowering the peak stress to 33% of UTS with a corresponding increase in the cyclic frequency of 5.99Hz, yielded a surface temperature of approximately 28^{o}C at 50,000 cycles. A similar trend of lower surface temperatures with lower peak stresses were observed for loading rates of 500KN/sec. A comparison of the measured surface temperatures for ud Kevlar composites at loading rates of 200 and 500KN/second are illustrated in Figure 6.3.

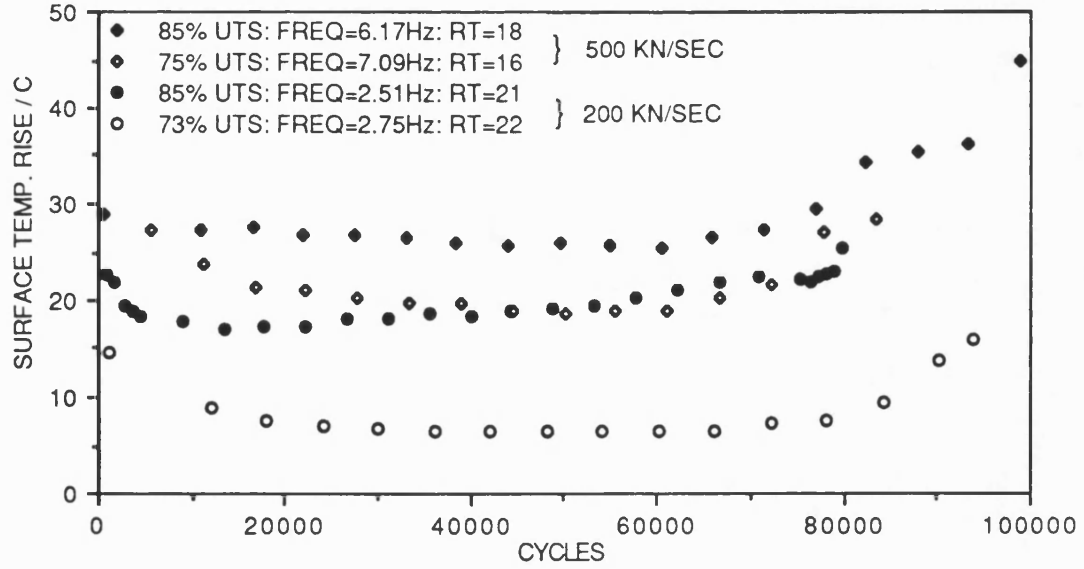

Figure 6.3 Comparison of surface temperature increases during fatigue testing of ud Kevlar composites tested at loading rates of 200 and 500 KN/second and a stress ratio of 0.1.

With reference to Figures 6.1, 6.2 and 6.3 some general comments are made on the nature of the observed surface temperature rises during tension-tension fatigue testing of ud Kevlar/914 composites.

(a) There was a very rapid rise in the surface temperature at the onset of fatigue testing. The initial peak surface temperature was seen to be a function of the cyclic frequency and the peak applied stress. This implies that the mechanism responsible for the observed surface temperature rise is influenced by the magnitude of the stress range (σ_{max}-.σ_{min}). In other words, it is proposed that for a given rate of loading or stress application, the higher the stress range, the higher would be the measured surface temperature rise. Therefore, performing fatigue tests at stress ratios ($\sigma_{min}/\sigma_{max}$) greater that R=0.1 should result in a reduction of the surface temperature rise. The effect of stress ratios on the fatigue performance and surface temperature rise of ud Kevlar composites is discussed in the following section.

(b) The surface temperature was seen to fall after the initial rise and then stablised until failure was imminent. This fall-off and stabilization of surface temperature presumably represents a stabilization of the mechanism responsible for heat generation during fatigue testing. Previous researchers had found that hysteritic heating of Kevlar during fatigue was very low. Roylance[125] proposed that a fibre abrasion mechanism may be responsible for the relatively high surface temperatures. Therefore, if fibre/matrix, inter-fibre (skin-core) or intra-fibre (fibre-

fibre) abrasion was responsible for the measured surface temperature increase during fatigue testing it is reasonable to expect a higher temperature at the onset of fatigue testing as any wear-mechanisms would be most prominent at the initial stages. The levelling-off of the surface temperature and gradual increase just prior to failure presumably corresponds to a decrease in the prominence of the initial wear mechanism but with other mechanisms such as delaminations, longitudinal splitting and progressive fibre failures and equilibrium temperature being attained with the surroundings.

With reference to the previous three Figures, it is clear that surface temperature monitoring can be used as a non-destructive testing tool in obtaining advance warning of imminent failure of the fatigue specimen. This was indeed the primary reason for embarking on surface temperature monitoring in this programme. The intention was to terminate the fatigue test just prior to failure and then to carry out a microscopic (optical/SEM) investigation of the specimen to elucidate on damage modes and damage mechanism.

(c) The measured surface temperatures were observed to be sensitive to the location of the thermocouple on the specimen surface. For example, on occasions where the thermocouple was located in the vicinity of a developing longitudinal crack, a sharp increase in the surface temperature was recorded, Figure 6.2(iii and v).

(d) In almost all the specimens in which the surface temperature was monitored, a rapid increase in the surface

temperature was observed just prior to specimen failure. A general comment can also be made on the relationship between the inherent scatter observed in these fatigue test results and the surface temperature measurements. For example, Figure 6.1(iii) corresponds to a specimen that was cycled at 67% of UTS and seen to attain the same steady temperature as a specimen that was cycled at 73% of UTS, Figure 6.1(ii), after approximately 50,000 cycles. It is reasonable to assume that the extent or rate of damage development in the former case was greater than that in the latter case and hence a lower fatigue life was observed for the specimen that was cycled at 67% of UTS. Further detailed study is needed to verify the usefulness of this simple technique.

(e) From Figure 6.3 it is apparent that for a given peak cyclic stress, the surface temperature rise is dependent on the rate of stress application during fatigue tests - the higher the rate of loading, the greater the measured surface temperature.

(f) The validity of fatigue testing of environmentally pre-conditioned (moisture) Kevlar composites is questionable because of the high temperatures that develop within the composite. Therefore, precautions need to be taken to inhibit excessive desorption during fatigue testing of Kevlar composites.

6.2 Effect of Stress Ratio (R) On Surface Temperature Rise

Surface temperatures were also monitored for the ud Kevlar/914 composite during fatigue testing at R=0.1 and 0.01 at a loading rate of 500KN/seconds. Figure 6.4 illustrates the differences observed in the measured surface temperatures for R=0.1 and 0.5 at a peak stress corresponding to approximately 85% of UTS. It is seen that for a given loading rate and applied peak stress, lowering the stress range from 0.74 GPa, (Figure 6.4-(i)) to 0.4 1 GPa, (Figure 6.4-(ii)) resulted in a surface temperature drop of approximately 30°C at 50,000 cycles. The number of cycles chosen i.e. 50,000 has no real significance other than as a convenient point for comparisons between different specimens. For most of the specimens tested, this region in the surface temperature rise vs number of cycles plots corresponded to the region where the temperature had stablised.

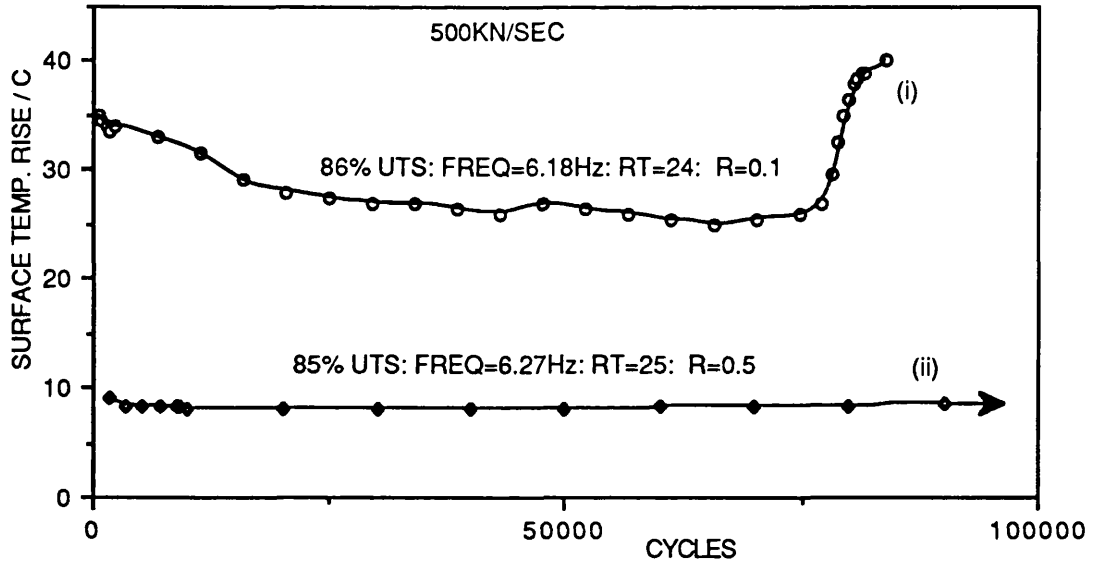

Figure 6.4 Comparison of surface temperature increases for two specimens cycled at 85% of UTS at 500KN/second loading rate and stress ratios of (i) 0.1 and (ii) 0.5 respectively.

An interesting point to note in Figure 6.4(ii), R=0.5, is that the initial peak temperature rise was only about 9°C above ambient whereas the initial peak temperature in Figure 6.4(i), R=0.1, was approximately 35°C above ambient. The final peak temperature for the specimen with R=0.5 was approximately 12°C above ambient (not shown as a failure in Figure 6.4(ii), specimen failed at 768,650 cycles), whereas the final peak temperature for the R=0.1 specimen was 45°C above ambient. The differences in the initial peak surface temperatures for R=0.1 and 0.5 may be accounted for by the (experimental) mode of load application to the fatigue test specimen. For example, in the R=0.5 test, the sample is loaded under a ramp mode to just below the required mean load, (no observed temperature rise), and then the cycling is commenced followed by adjustments to the to the peak stress and minimum stress to obtain the desired stress ratio. Therefore, the R=0.5 specimens never actually experience the load range experienced by the R=0.1 specimens. The differences in the final peak temperatures at the two stress ratios can not be explained at present.

Figure 6.5 illustrates the measured surface temperature rise for ud Kevlar composite fatigued at a stress ratio of 0.01 at loading rate of 500KN/ seconds. Once again the surface temperature is seen to rise in proportion to the applied peak stress (stress range).

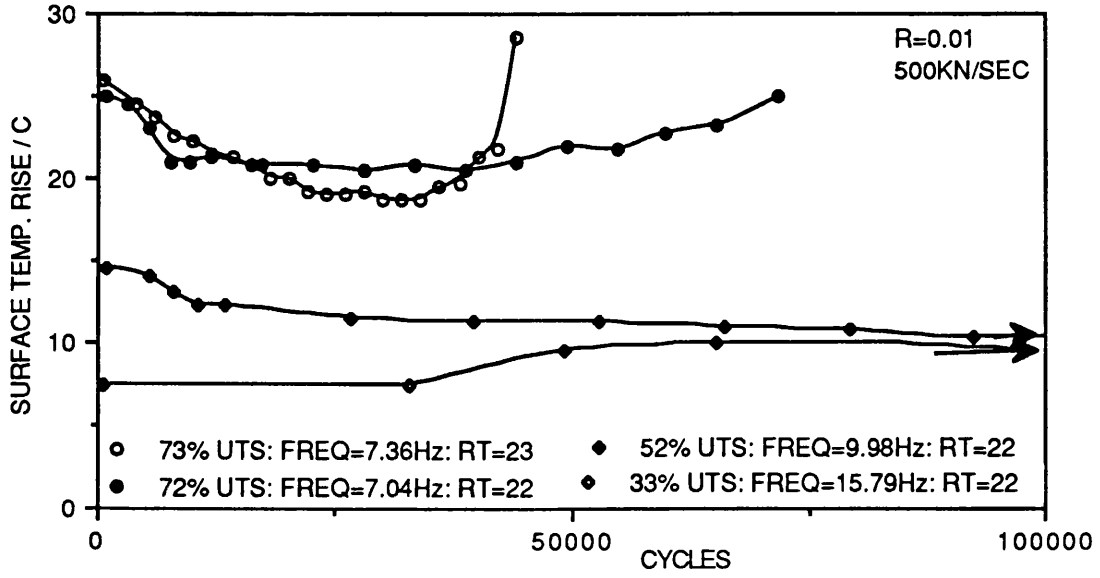

Figure 6.5 Surface temperature rises for ud Kevlar/914 fatigue tested at a stress ratio of R=0.01 and a loading rate of 500KN/second.

A plot of the initial temperatures versus stress range for the 200 and 500KN/second loading rate are presented in Figures 6.6 and 6.7. The initial peak surface temperature was chosen rather than the final peak temperature because it is reasonable to assume that the initial temperature in essence is a function of the loading conditions, whereas the final surface temperature rise is a function of the loading conditions and the extent of accumulated damage (it was previously discussed that Kevlar composites exhibit very little hysteritic heating).

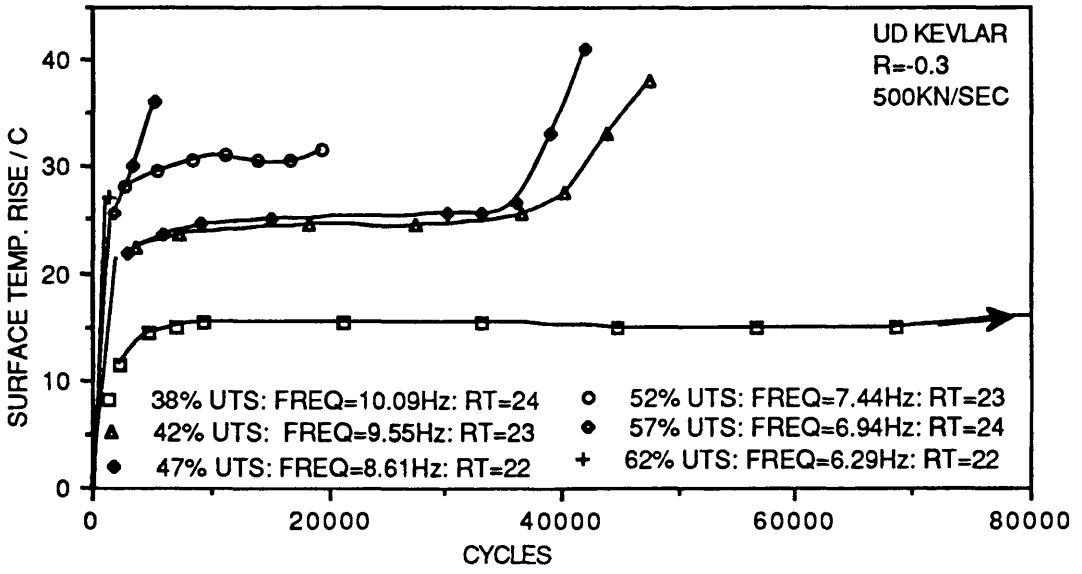

Figure 6.6 Surface temperature rises for ud Kevlar/914 composite fatigue tested at a stress ratio of R=-0.3 and a loading rate of 500KN/second.

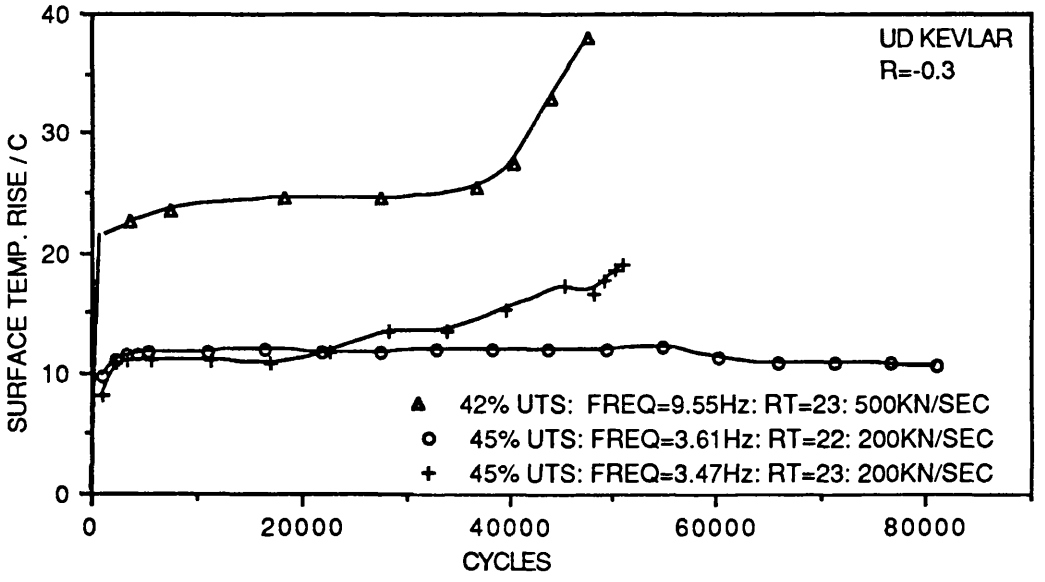

Figure 6.7 Effect of loading rate on the measured surface temperature rise during tension/compression fatigue testing.

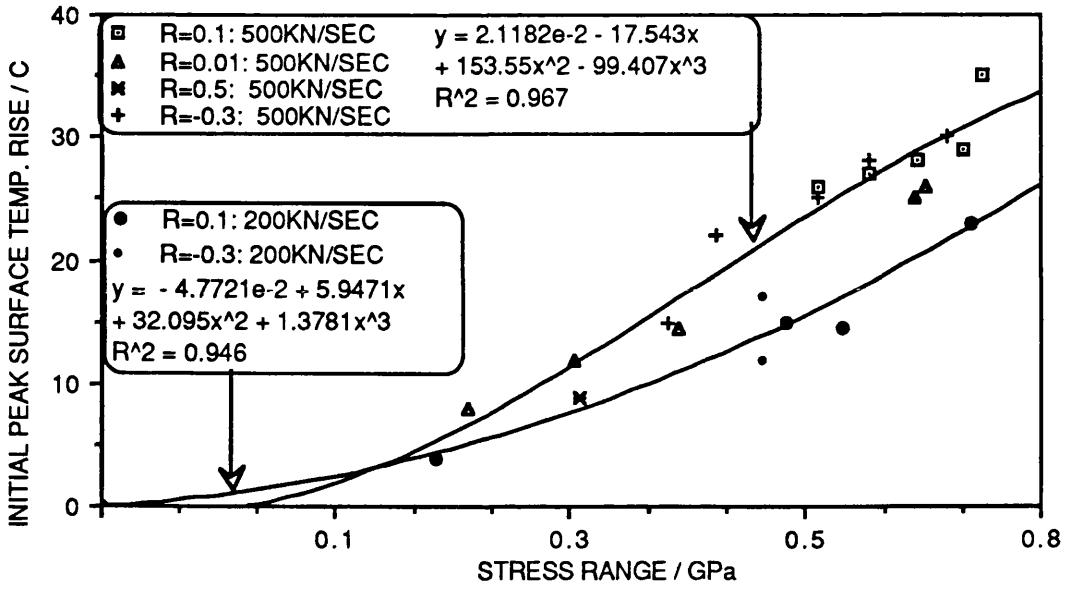

Figure 6.8 The surface temperature for ud Kevlar/914 fatigue tested at R=0.1 and a loading rate of 200 KN/seconds represented in terms of the stress range. Note: The surface temperature rises for R=-0.3 is also represented.

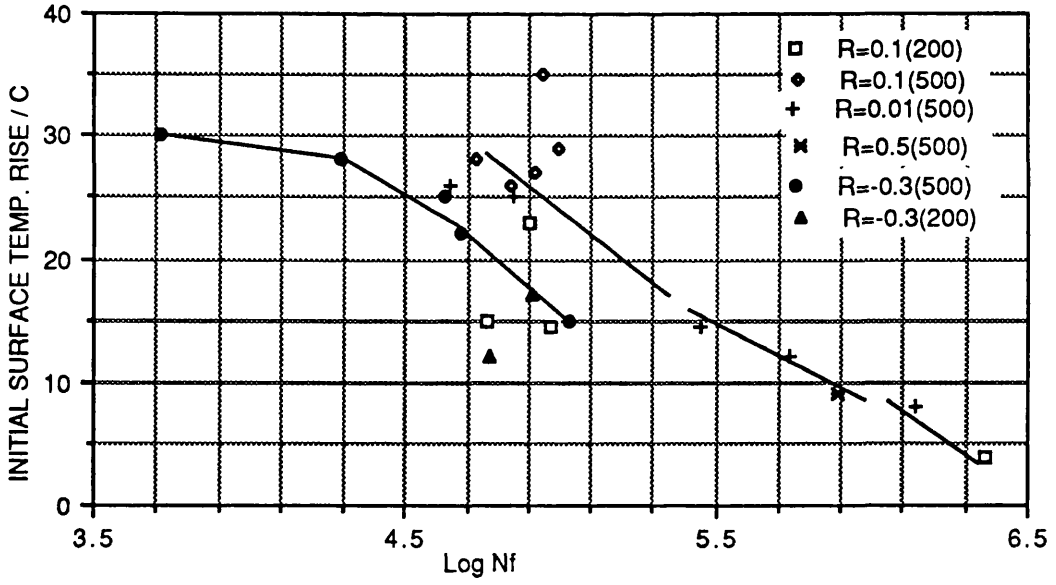

Figure 6.9 Illustration of the relationship between the initial surface temperature rise and the corresponding fatigue life for ud Kevlar/914 mono-fibre composite.

Figure 6.9 illustrates the relationship between the initial

(peak) surface temperature rise and the fatigue lives of the corresponding specimens. It is evident that the the higher the initial temperature rise the shorter is the fatigue life. Such a relationship was also observed by Roylance[125].

Considering the simplicity of the surface temperature monitoring technique used in this programme, the results are nevertheless extremely informative. Surprisingly, the surface temperature measurements for R=-0.3 are also seen to fall on the straight line in Figure 6.8. This is inspite of the fact that the tension-compression fatigue tests were carried out using a jig to prevent the specimen from buckling. Furthermore, the presence of the anti-buckling jig require the thermocouple to be mounted in a different manner to specimens fatigue tested with positive stress ratios. When anti-buckling guides were used, the thermocouple was located on the specimen surface though the window of the jig and was held in place using a block of expanded polystyrene and a rubber band. It is possible that some heat may have been generated as a result of the thermocouple rubbing onto the specimen surface. However, this would have had a greater effect at the higher frequencies but such an effect was not observed in the experimental study. Further study is necessary to establish if the temperature rise during fatigue results in a somewhat uniform temperature distribution in the specimen or if numerous local hot spots develop during testing. Other factors which need to be considered are presumably the heat loss through radiation and conduction via the fatigue machine gripping arrangements and anti-buckling jig in the tension-compression tests. In fact, the anti-buckling could have also contributed to heat generation by

friction. Obviously the ideal technique for surface temperature studies of this nature would be thermography with the aid of an infra-red video camera coupled with a facility to monitor a material property change, eg. stiffness.

A discussion on the theory of the nature of hysteretic heating and wear is beyond the scope of this study. A detailed account on the subject may be obtained from reference numbers 132 and 133. However, based on the evidence presented in the next section (which discusses the various failure modes observed for ud Kevlar composites under different loading conditions), it is speculated that fibre/matrix abrasion and fibre skin/core abrasion as a possible mechanism for heat generation during fatigue testing of ud Kevlar composites.

The following conclusions can be made based on the surface temperature monitoring of ud Kevlar undertaken in this study:

(a) The technique can be used as an NDT tool to terminate fatigue testing just prior to failure.

(b) The technique seems to be quite sensitive to sample variability (scatter). In other words, specimens which failed prematurely gave higher surface temperature readings (at a given load) compared to specimens which exhibited longer fatigue lives at the same load.

(c) An apparent linear relationship between the stress range and the initial surface temperature rise was observed for a

given rate of load application. This meant that higher surface temperatures were recorded for specimens with the larger stress ranges.

(d) For a given peak load, lowering the cyclic frequency resulted in the lowering of the measured surface temperature rise, i.e. the higher the load rate, the higher would be the surface temperature rise at the corresponding peak loads or stress ranges. This poses a problem in the sense that it was previously assumed that there was no apparent difference in the fatigue lives of Kevlar composites fatigue tested at loading rate of 200 and 500 KN/seconds. Whereas there was a significant difference in the initial peak surface temperature for similar peak stresses. This was possibly because at the lower loading rate and hence lower cyclic frequency, the heat generated within the specimen was dissipated to the surroundings to a greater extent than for samples tested at the higher loading rate. Hence resulting in a lower measured surface temperature.

(e) It is apparent from Figure 6.8 that even under tension/compression loading regime, the relationship between the surface temperature rise and stress range seems to hold. This is surprising since previous researchers have stipulated that the compressive properties of Kevlar fibres are extremely poor. However in the light of the work of DeTeresa el al[120-122] and the findings reported in this study so far it is possible that the fatigue or the repeated loading behaviour of Kevlar fibres under tension/compression loading is not as detrimental as monotonic compressive loading. It was previously discussed that Kevlar fibres are prone to

kinking and buckling when loaded in compression. DeTeresa et al have shown that the damage induced during compression was reversible, i.e. the surface kinks that are introduced in compression are 'relieved' after a few cycles of tensile loading. Unfortunately they did not report on the relationship between the level of pre-compressive stress to the rate or extent of subsequent recovery on applying a tensile stress. Therefore, unless this relationship is established, attempts to introduce compressive pre-loads on Kevlar composites followed by tensile loading may not be fruitful.

6.3 SURFACE TEMPERATURE RISE DURING FATIGUE TESTING OF XAS/914 COMPOSITES.

The surface temperature rise of the XAS composite was of the order of 3-6^{o}C above ambient for the stress ranges investigated in this programme. This is in sharp contrast to that observed for the Kevlar composites which showed that the surface temperature rise was proportional to the stress range. The low surface temperature rise for the ud XAS composite may be attributed to the higher thermal conductivity of these fibres. Furthermore, in the case of the Kevlar composite, it was proposed that fibre surface abrasion was a contributing mechanism to surface temperature increase during fatigue testing. Post-failure surface examinations did not indicate the presence of such a mechanism for the ud XAS composite.

7. FRACTOGRAPHY

7.1 Introduction

Fractography of fibre reinforced composite materials has received extensive coverage in the literature[150-159]. Post-failure surface examination can be a very useful method of obtaining information on fatigue damage mechanisms in composites. However, great care needs to be exercised in obtaining and preparing samples to avoid any further damage to the specimens. Furthermore, post-failure damage may also tend to mask the actual failure modes in the composite material.

A major draw-back of the Fiberdux 914 resin system as far as post-failure inspection was concerned was that it contained about 20% polyethersulphone which tended to mask most aspects of the resin deformation modes. Furthermore, the fibrillar fracture mode exhibited by the Kevlar fibres tended to mask the XAS fibre fracture sites in the hybrid composites. Hence, in this programme only accessible fracture sites were inspected under the SEM, i.e. no forced separation was used to obtain specimens. Admittedly, restricting the inspection of post-fractured specimens to the vicinity of the primary fracture site may not impart information of the actual degradation mechanisms in operation for a given composite composition, loading regime and environment. However, a variety of failure modes were observed for the Kevlar fibres in this programme. The failure mode of the Kevlar fibres was found to be a function of the mode of load application,

cyclic load levels and environmental pre-conditioning.

The fracture modes observed for ud Kevlar/914 composite under microscopic examination were found to be dependent on where the sample was obtained relative to the fracture zone(s). The co-ordinate system used in this discussion for scanning electron microscopy of the fractured specimens are defined in Figure 7.1.

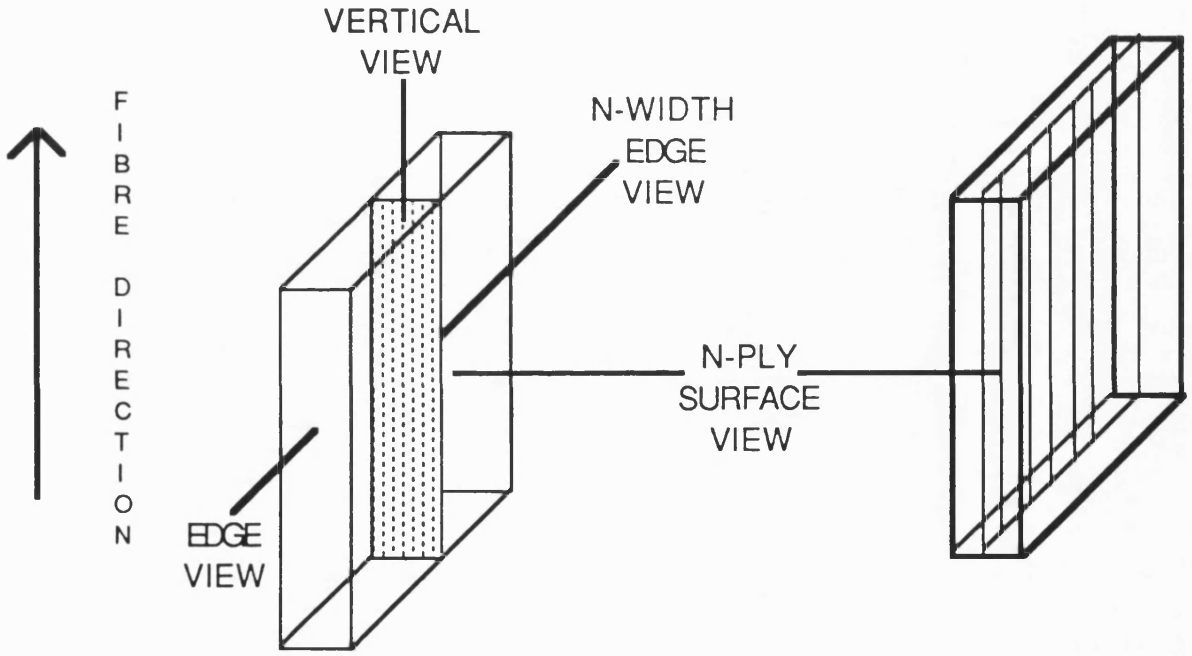

Figure 7.1 Definition of viewing directions for post-failure inspection

7.2 FAILURE MODES

7.2.1 Observed Static Tensile Failure Modes For Kevlar/914

The macro failure mode was found to depend on the peak load, minimum load and the test temperature. This is contrary to the observations made by Hahn et al[127,129] who found that all the samples exhibited a brush like failure mode regardless of test conditions under tension-tension loading.

Figures 7.2(a-c) illustrate the macroscopic failure mode observe for static tensile tested ud Kevlar/914 composite. The predominant failure modes observed for this composite were longitudinal splitting and extensive intra-ply fibre defibrillation and inter-ply separations. The longitudinal splits were observed to develop from the end-tab regions and then to propagate the length of the specimen.

Figures 7.3(a & b) illustrate typical static tensile failure modes that were observed under microscopic examination for the Kevlar composite. The main features are longitudinal fibre splitting and defibrillation of the fibre surface. This failure mode has been well documented in the literature, for example the work of Konopasek and Hearley[113] and Morgan et al[14]. Figures 7.3(a & b) indicate that the fractured fibre-ends exhibit two main types of failure modes: (a) fibre-ends which show a considerable degree of longitudinal splitting at the fractured region and (b) fibre-ends which appear as a solid piece. Konopasek and Hearley[113] proposed the following model to account for this bi-distribution of fractured ends from a tensile test.

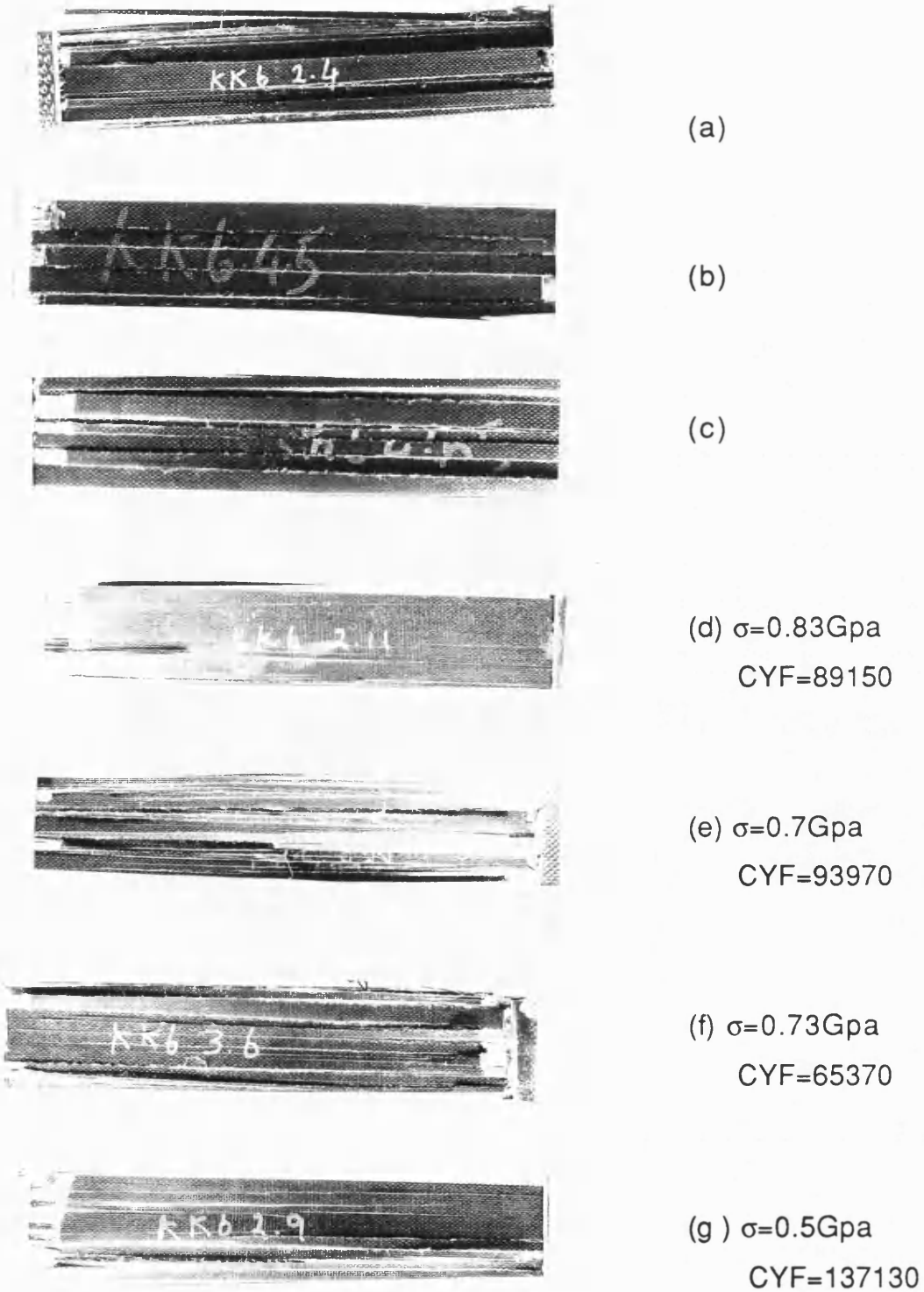

Figure 7.2 A selection of the macroscopic failure modes observed for static tensile tested (a-c) and fatigue tested (d-g) mono-fibre Kevlar/914 composite.

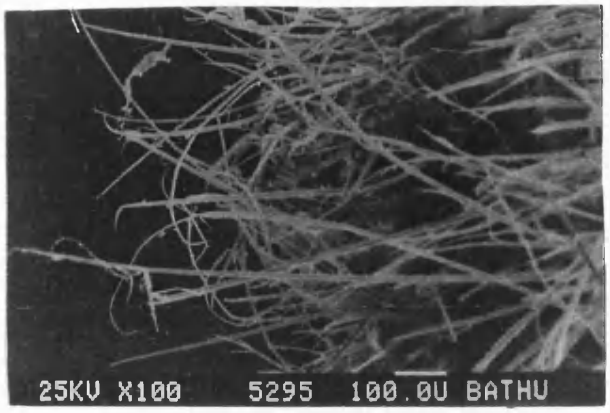

(a)

(b)

Figure 7.3(a & b) Typical microscopic failure modes observed in static tensile tested Kevlar mono-fibre composite.

Konopasek and Hearley[113] proposed that an imperfection on the fibre surface could act as an initiation point in the breakup of the fibrillar unit under increasing tensile loading, see Figure 7.4(A). The longitudinal shear stress which is introduced at the root of the initial gap then apparently causes longitudinal splitting of the first bundles of fibrils-Figure 7.4(B). After the next layer of fibrils break, a new gap is said to open up, and as a result of this, the shear stress concentration at the new root causes splitting of the next layer of fibrils, Figure 7.4(C). This process is said to repeat itself until the filament fractures into two sections as shown in Figure 7.4(D). This failure mode was proposed on the basis of a tensile test on unimpregnated fibres. However, the micrographs presented by

Morgan et al[14], Jones[88] and Hull[57] do not exhibit the failure modes described by Konopaske and Hearle. A similar failure mode to that proposed by them was observed in this programme and is shown in Figure 7.5. This failure mode was occasionally found to occur at tensile fractured intraply delaminated areas under fatigue cycling.

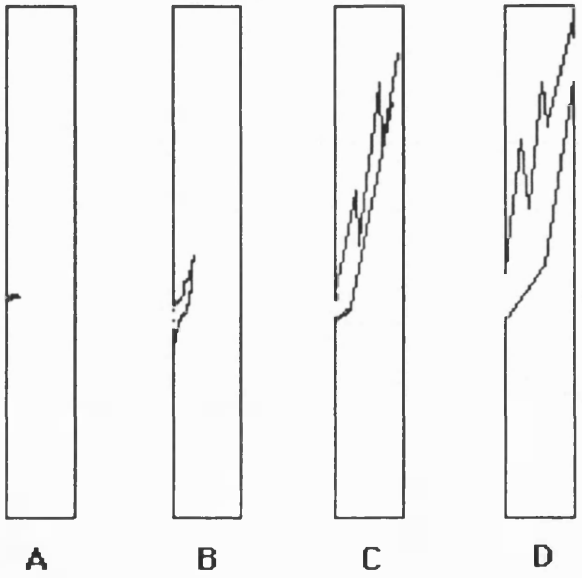

Figure 7.4 Schematic representation of tensile fracture development in ployaramid fibre - proposed by Konopasek and Hearley[113].

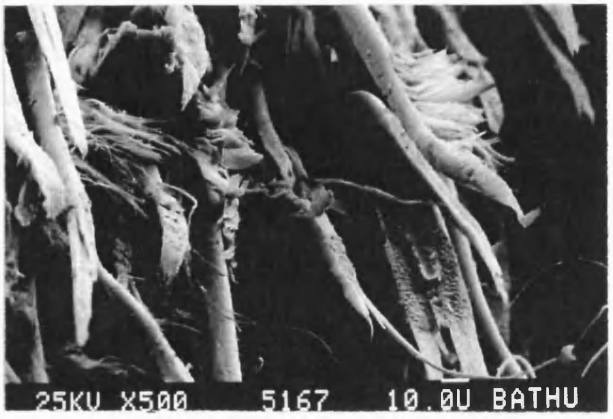

Figure 7.5 Illustration of the fracture modes described by Konopasek and Hearley as typical tensile failure modes for Kevlar fibres.

The observed tensile fracture modes for Kevlar fibres, see

Figure 7.3(a & b) may be explained in terms of the skin/core structure of this fibre. A schematic illustration of the prominent tensile failure modes observed for Kevlar fibres are presented in Figures 7.6(a) and 7.6(b).

Figure 7.6(a)-(A & B) represent a schematic illustration of a feature where the skin of the Kevlar fibre is thought to separate from the core as result of tensile fracture. In general the outer skin of the fibre exhibited a very smooth surface, whereas the core outer surface had a fibrous appearance with fine longitudinal striation. Another general observation was that the widths of the defibrillated (peel) strands were much smaller than those observed in the core. The peeled-off outer skin tended to curl inwards along the longitudinal fracture path.

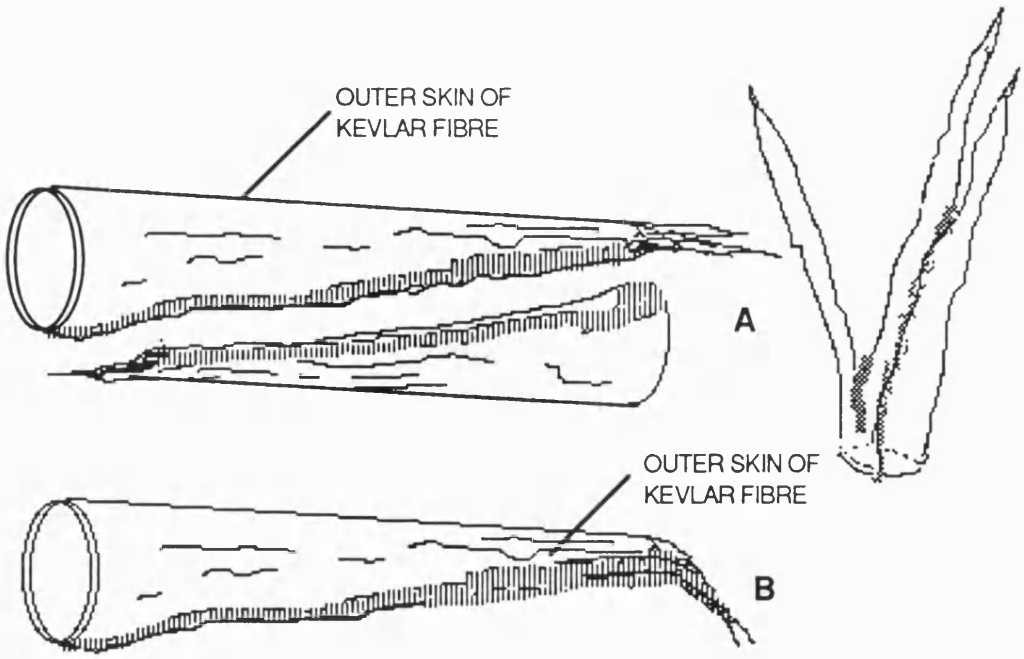

Figure 7.6(a)-(A & B) Observed failure modes for Kevlar/914 outer-skin failure under static tensile test.

Figure 7.6(b)-(A-C) illustrates a schematic representation of a fracture feature that is thought to be a section of the Kevlar fibre core. These features imparted the impression of being much more rigid than the features which have been proposed as being the fibre skin. It would be a gross over-simplification to suggest that only these two failure modes were observed for Kevlar fibres as a result of static tensile failure. In a lot of instances it was very difficult to assign with any certainty the features to either the core or the skin of the fibre. No significant differences in failure modes for the Kevlar fibres in the hybrid composite was observed compared with the mono-fibre composite.

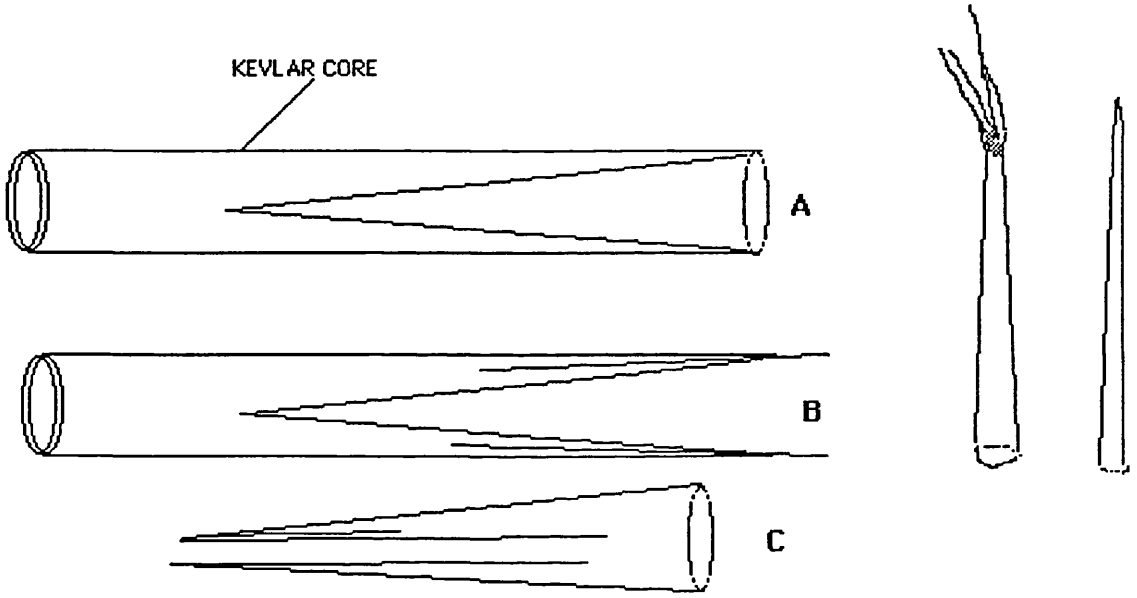

Figure 7.6(b)-(A-C) Schematic illustration of an observed failure mode in Kevlar composite. It is proposed that this feature may correspond to the fibre core.

Figure 7.7 illustrates some of the features attributed to the skin/core structure of Kevlar fibres discussed previously. With reference to Figure 7.7; the defibrillation profile on the skin was found to be finer (a) than that observed for the core (d). This defibrillation was most prominent in fatigue tested samples.

Figure 7.7 A typical tensile failure mode observed in Kevlar fibres subsequent to a tensile test. (a)-Fibre skin; (b)-Skin defibrillations; (c)-fibre core; (d)-defibrillations in the core.

7.2.2 Observed Fatigue Failure Modes For Kevlar

The macro-failure modes of Kevlar/914 under tensile fatigue loading are presented in Figures 7.2(d-g). It was seen that the extent of longitudinal splitting was dependent on the peak cycling stress. At high peak stress levels, see Figure 7.2(d), the extent of longitudinal splitting and inter- and intra-ply delaminations were limited and the macroscopic failures resembled those observed for the tensile static test samples. At intermediate cycling stress levels, see Figure 7.2(e-f), a distinct increase in the extent of delaminations and longitudinal splitting was seen.

On a microscopic scale, a wider distribution of failure modes was observed for samples tested under fatigue loading. It was found that the fracture features observed under microscopic examination were very dependent on the location from where the samples were obtained in relation to the primary fracture site.

The fracture surfaces of the fatigue samples were similar to those of the tensile tested samples; however, the extent of fibre defibrillation/tearing was more extensive and very prominent for the fatigue tested specimens. This is illustrated in Figures 7.8(a & b) (second ply surface view). Figure 7.8(b) illustrates a single fibre that had undergone extensive longitudinal splitting with what seems like a single transverse crack through the diameter of the fibre. A similar 'transverse' failure feature is shown in Figure 7.9; here a fracture path at an angle to fibre and loading direction is apparent. (The sample in Figure 7.9 was in fact

obtained from T/T fatigue test, R=0.1 at 100^{o}C, and the spherical particles are polethersulphone which has dislodged from the matrix). These transverse fractures observed in the Kevlar fibres from T/T tested samples were a prominent feature in the T/C specimens. It is not known if the Kevlar composite used in this programme had been subjected excessive compressive loading during manufacture or processing. It will be recalled that the mechanical properties of the Kevlar composite were lower than those quoted by other researchers in the literature.

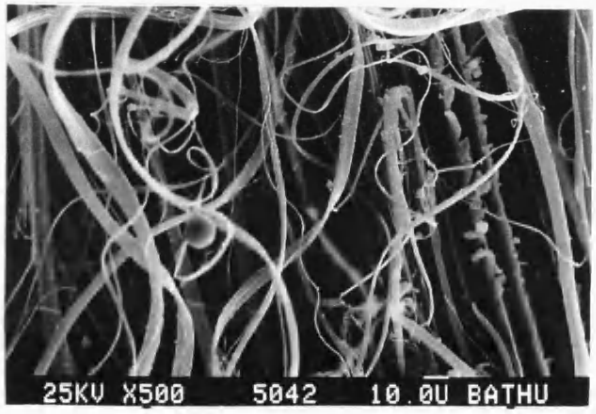

Figure7.8(a) Tensile fatigue failed Kevlar fibres from the mono-fibre composite illustrating extensive longitudinal splitting.

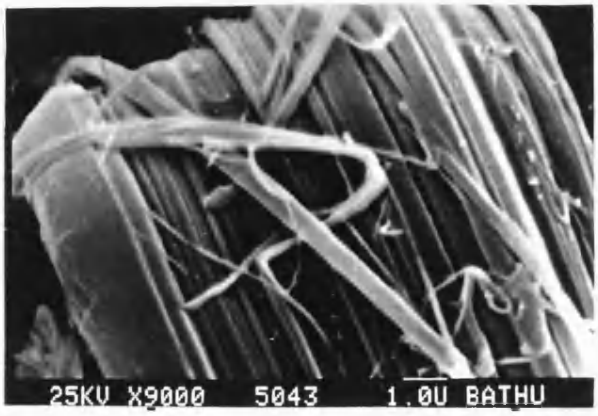

Figure 7.8(b) Magnified view of a fractured single fibre-end failed by tensile fatigue. Note the extensive longitudinal splitting and the apparent transverse failure mode.

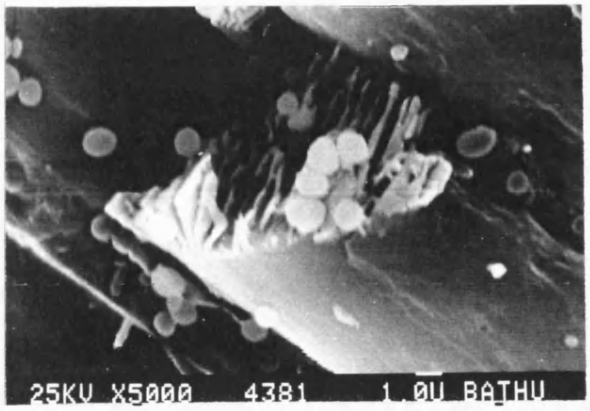

Figure 7.9 Illustration of Kevlar fibre that exhibited a transverse failure mode (subsequent to 100°C fatigue testing). The spherical particles are thought to be polyethersulphone which presumably had been dislodged as a result of the high temperature fatigue test.

Figures 7.10(a & b) represent an edge view along a longitudinal split in the ud Kevlar composite away from the fracture region - identical specimen from which Figure 7.8 was obtained. Apart from the longitudinal cracking along the fibre/matrix interface seen in Figure 7.10(b), kink bands-(i) and compression type damage features (bulges)-(ii) are observed on the fibres surface. The compression type damage on the Kevlar fibres has been previously reported by Konpasek[113] and DeTeresa[121]. It is probable that these bulges/section-swelling of the fibres are caused by the fibre snapping back on fracture[113]. However, these bulges were also common features on samples which had undergone compressive loading, such a feature is illustrated in Figure 7.11. The kink lines in Figure 7.10(b) were generally observed along longitudinal splits in the composite and are probably caused by fibre bending due to the loss of lateral support. It also seems probable that the kink bands can develop under repeated

load application to give rise to the bulges observed on the fibre surface.

Figure 7.10(a) An edge view along a longitudinal split in the ud Kevlar composite away from the fracture region - identical specimen from which Figure 7.8 was obtained.

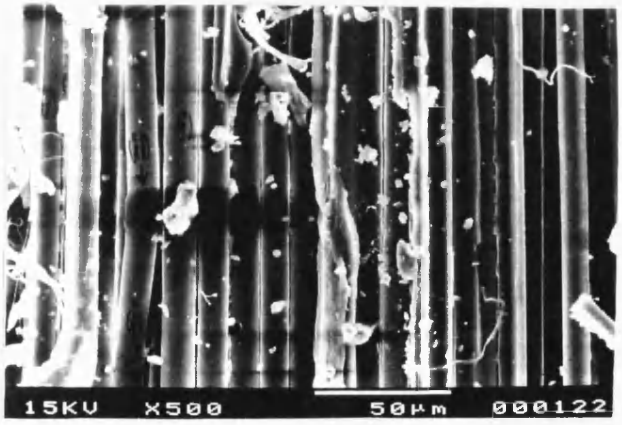

Figure 7.10(b) Note longitudinal cracking along the fibre/matrix interface and the transverse fibre fractures. Kink bands-(i) and compression type damage features (bulges)-(ii) are also present on the fibres surface.

Figures 7.12(a & b) illustrate typical features that were observed in the delaminated outer layers for T/T fatigue tested samples. Kink band formation and bulges are readily visible in Figure 7.12(a). These features-(i) originate probably as a result of bending. The failure modes for the

fibres region (ii) were somewhat different to those described previously and were most prominent where the fibres had been subjected to repeated bending, i.e. delaminated outer layers. Figure 7.12(b) clearly illustrates a failure mode where the fibre skin had peeled away from the core as a result of repeated bending.

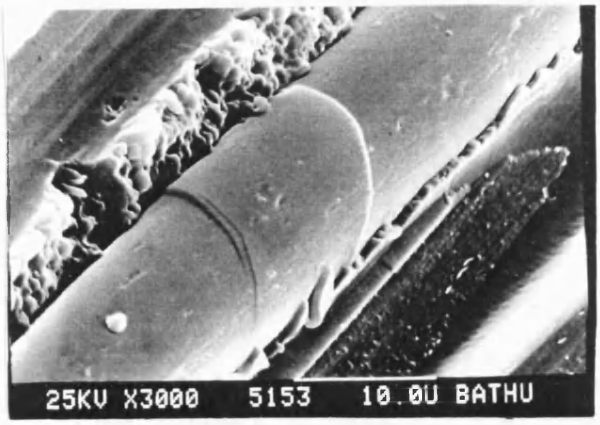

Figure 7.11 Compression induced kink zone in a Kevlar fibre.

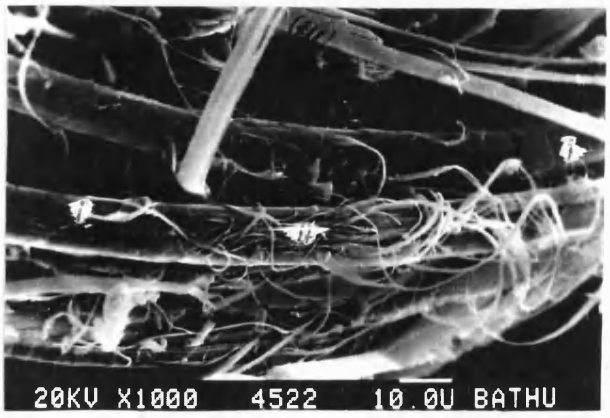

Figure 7.12(a) Illustration of the failure modes observed in the delaminated outer plies during tension/tension fatigue testing. (i)-kink zones, possibly induced by bending; (ii) typical failure mode for Kevlar fibres subjected to bending fatigue.

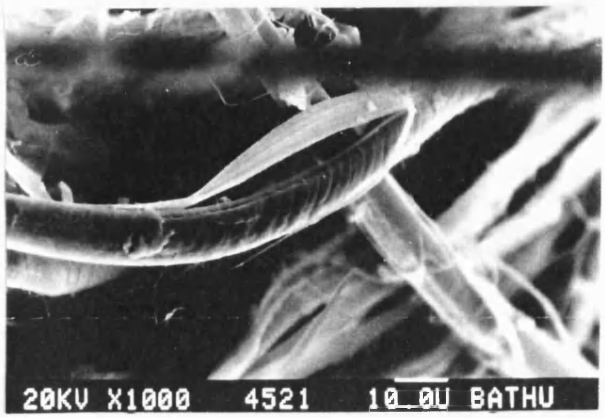

Figure 7.12(b) A magnified view of previous sample away from the main fracture site. The fibre skin has been peeled away from the core.

As mentioned previously, all the micrographs were investigated in the as-fractured state, i.e. no forced separation was carried out. Therefore the fracture modes reported only represent readily accessible sites. It would be very informative if a method can be developed to be able to expose relatively long sections of the Kevlar composite to enable study of damage development along the fibre length away from the main fracture. This would also facilitate an inspection and assessment of the virgin composite prior to any testing.

7.2.3 Observed Failure Modes for Kevlar Under Static Compression and Tension/Compression Fatigue Testing

The experimental details for carrying out these static compression tests were discussed in the experimental section. Figure 7.13 (edge view) illustrates a typical macroscopic failure profile for Kevlar/914 tested in static compression where the sample is seen to fail by kinking through the

thickness and width of the specimen.

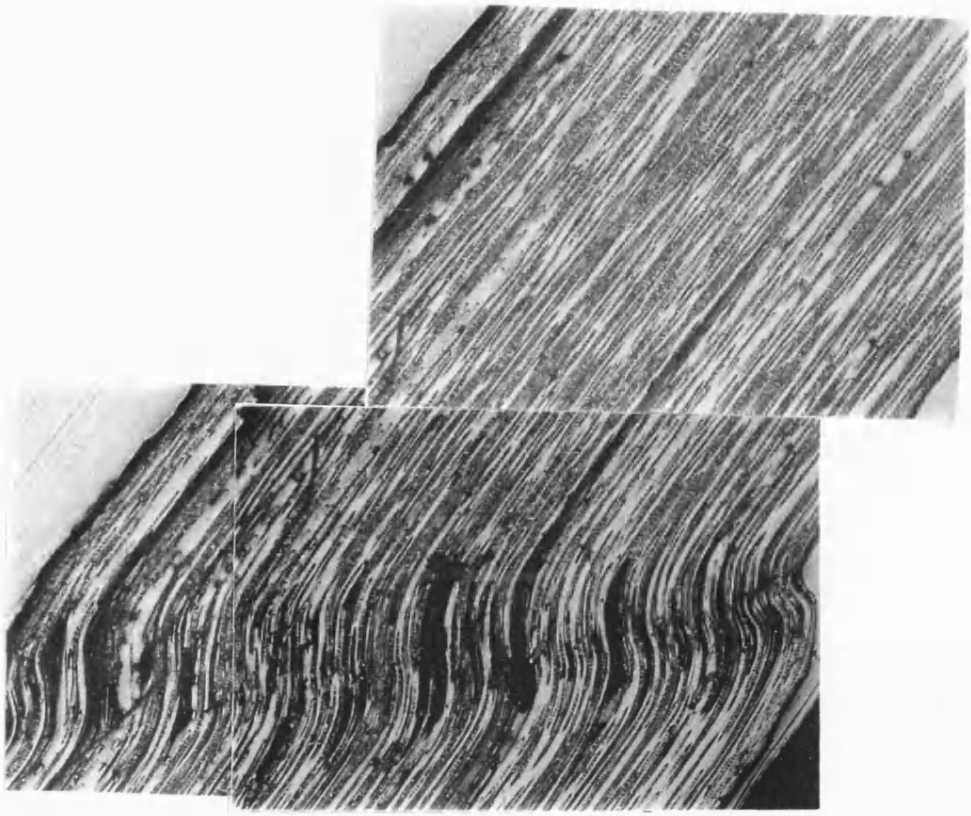

Figure 7.13 A macroscopic view of the failure mode observed in the Kevlar mono-fibre composite as a result of static compression test.

Figures 7.14 (a-c) illustrate typical macroscopic failure modes observed for unidirectional Kevlar/914 subjected to tension/compression fatigue testing. The failure mode in these specimens is best described as transverse fracture through the width of the specimens and this is quite different to the failure modes observed for the T/T fatigue tested samples discussed previously.

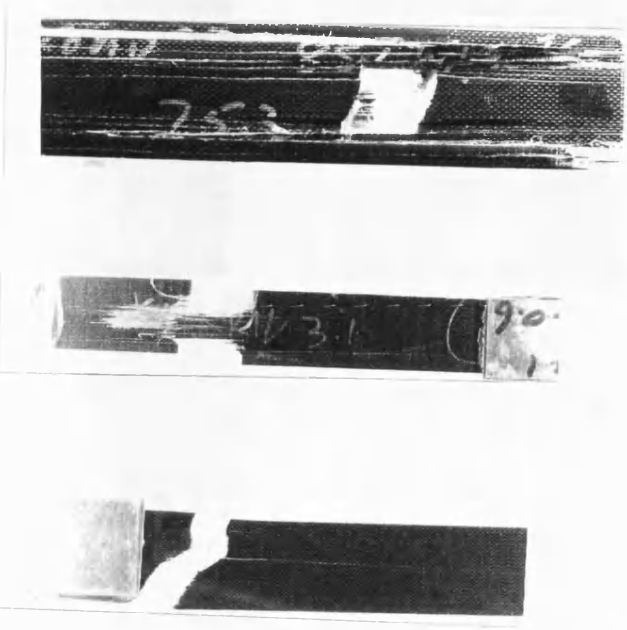

(a) $\sigma+$ =0.55GPa
CYF=5160
R=-0.3

(b) $\sigma+$ =0.5GPa
CYF=260
R=-0.6

(c) $\sigma+$ =0.35GPa
CYF=870
R=-0.6

Figures 7.14(a-c) Typical macroscopic failures of T/C fatigue tested Kevlar mono-fibre composite.

Typical surface view, (interface between first and second ply) of microscopic fracture features of tension/compression (R=-0.3) fatigue tested samples are presented in Figure 7.15(a & b). It is apparent that different failure mechanisms are in operation under T/C fatigue testing as compared to the T/T case.

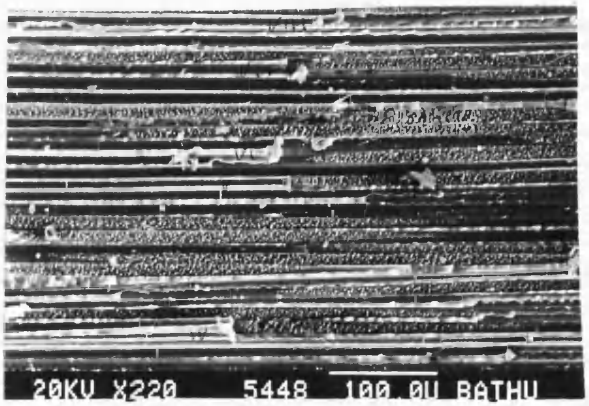

Figure 7.15(a) Typical surface view, (interface between first and second ply) of microscopic fracture features of tension/compression (R=-0.3) fatigue tested.

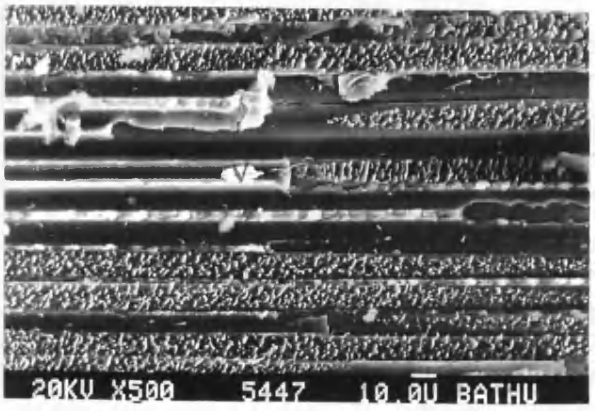

Figure 7.15(b) Magnified view of previous micrograph. Note the extensive surface marking on the Kevlar fibre surface. Fibre-(v) represents a transversely fractured Kevlar fibre; fibre-(v) seems to be the initiation point for the surface marking on the fibre below it.

The most prominent features observed in the T/C were extensive surface abrasion damage on the Kevlar fibre surface. Extensive longitudinal shear type failure was also seen in the matrix and the amount of debris in the form of resin particles and spherical polyethersulphone particles was also more evident. As in the tensile tested specimens, the Kevlar fibres exhibited very clean separation from the matrix.

It is also apparent form Figure 7.15(a) that the fibres exhibit a degree of waviness and the abrasion features appeared on the crown of the curved fibres (x-z plane). A high correlation was obtained between transverse fibre fractures and the apparent point of origin of the surface abrasion; this is shown in Figure 7.15(a)-fibres-(iv-viii). A magnified view of the vicinity of fibre (v) in Figure 7.15(a) is shown in Figure 7.15(b). Note that the surface markings are seen to originate at the surface and then

propagate longitudinally at an angle through the fibre thickness. Regrettably, deplying was not attempted with any of the failed samples; with hindsight, it may have been useful to establish the pattern of these surface markings along the gauge length of the specimen.

The mechanism responsible for the formation of these surface abrasion type markings on the Kevlar fibres subjected to T/C cycling has not been established at present. However, it is worth considering possible reasons for the formation of these surface features. These features were most prominent along sites of delaminations in the T/C tested samples away from the primary fracture site. Two mechanisms are thought to be the likely cause of the surface markings on the Kevlar fibres, the micrographic evidence for the two proposed mechanisms are discussed next.

Figure 7.16(a), fibre-(i) illustrates a section of the fibre skin that has been torn off the fibres. The exposed core-(ii) exhibits defibrillation, a magnified view of this region is shown in Figure 7.16(b) and is best described as strip of the outer skin peeling away in the fibre direction. Such features were also observed in areas where there was no evidence of the skin having peeled off. Extensive matrix shear failure modes-(iii) are also seen in Figure 7.16(a). Feature-(iv) has been attributed to a compressively failed Kevlar fibre; the nodular fracture was observed to be a common feature of compressive fracture surfaces of this fibre as will be seen later, note that the resin failure surface is somewhat similar too. The most prominent feature in the delaminated surfaces was that shown in Figure 7.16(a) fibres-

(ii) and (v), a magnified view of these fibres are shown in Figure 7.16(b & c) respectively. It is apparent that these surface features actually extend into the fibre. The following mechanisms are proposed as possible reasons to explain the above observations.

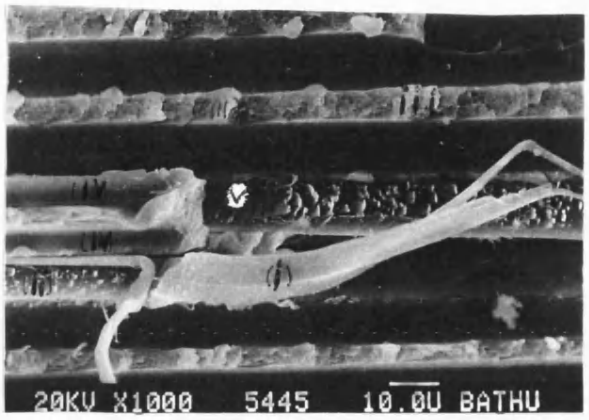

Figure 7.16(a) A magnified view of the second Kevlar ply surface subsequent to T/C fatigue testing. Fibre-(i) is an illustration where the outer skin of the fibre has torn away from the core and exposed the core-(ii). Object-(iii) is the resin matrix; the failure modes here are obscured by the presence of the polyethersulphone. Fibre-(iv) represents a fibre that has failed via transverse fracture as a result of compression loading.

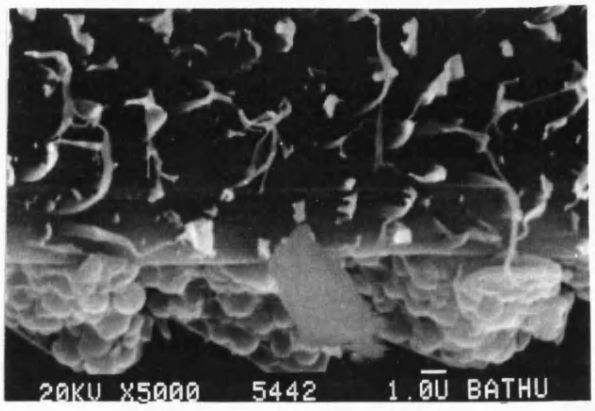

Figure 7.16(b) A magnified view of fibre-(ii) from the previous Figure.

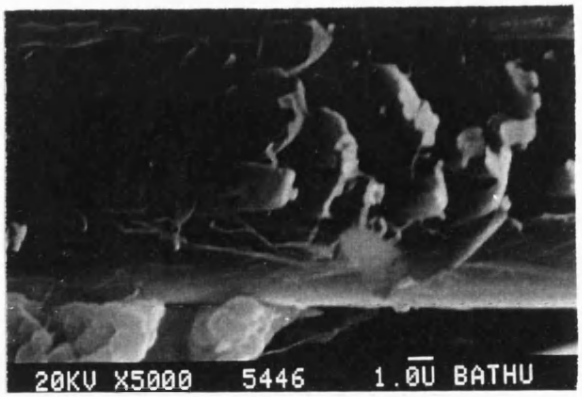

Figure 7.16(c) A magnified view of fibre-(v) from Figure 7.16(a).

(a) Fibre Abrasion

Figures 7.17(a & b) indicate the presence of extensive fibre-fibre contact in the Kevlar mono-fibre composite and Figures 7.18(a & b) show the presence of considerable fibre curvature in the mono-fibre Kevlar composite. The macroscopic profile of the surface features discussed previously are elliptical and this may possibly be due to the damaged fibre being worn down by a planar surface. It was assumed that these features were caused by the outer delaminated layer abrading against the intact inner layer. Another possible mechanism for the formation of the surface features may be that the crack or delamination path simply propagates in the longitudinal direction through the Kevlar fibre. The elliptical features may then be because the fibre had a waviness perpendicular to the crack-front or that the delamination crack-front followed a sinusoidal path. Using the co-ordinate system illustrated in Figure 7.19, a schematic illustration of the speculated mechanism are presented in Figures 7.20 and 7.21.

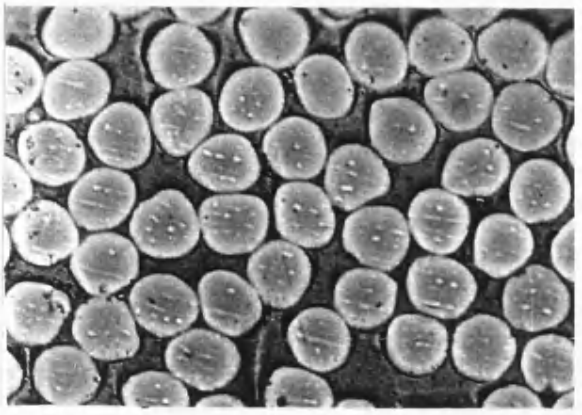

Figure 7.17(a) A transverse section of the mono-fibre Kevlar composite. Note the irregular shapes of the fibre-end profiles.

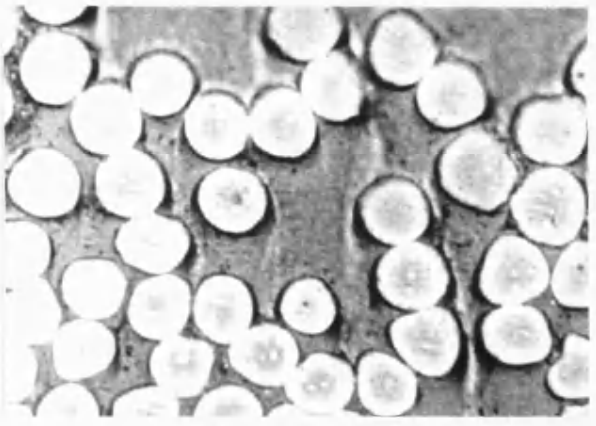

Figure 7.17(b) A transverse section of the mono-fibre Kevlar composite. Note the irregular shapes of the fibre-end profiles, the non-uniform fibre distribution and the resin rich areas.

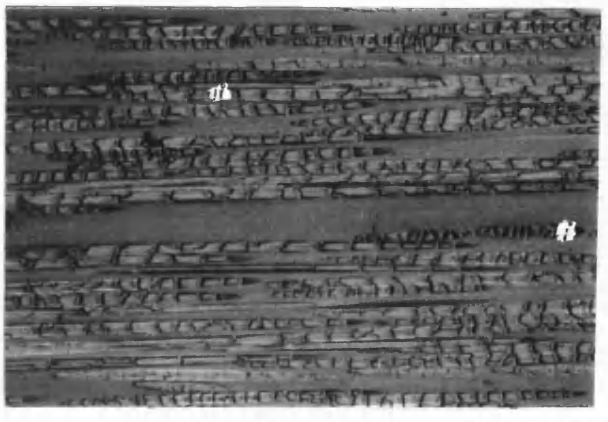

Figure 7.18(a) A typical longitudinal edge view of the

Kevlar mono-fibre composite. Extensive fibre waviness is apparent. Note also the regular markings on the fibre surface. Fibre-(i) illustrates waviness in the X-Y plane and fibre-(ii) illustrates possible waviness in the X-Z plane.

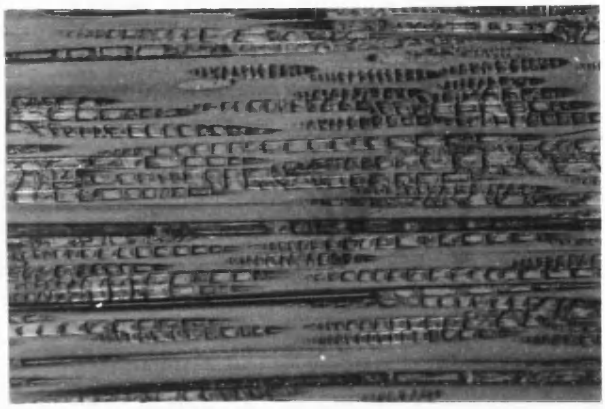

Figure 7.18(b) Another example of a longitudinal edge view of the mono-fibre Kevlar composite. As observed in the previous micrograph, extensive fibre waviness is apparent. Note also the transverse markings on the fibre surface.

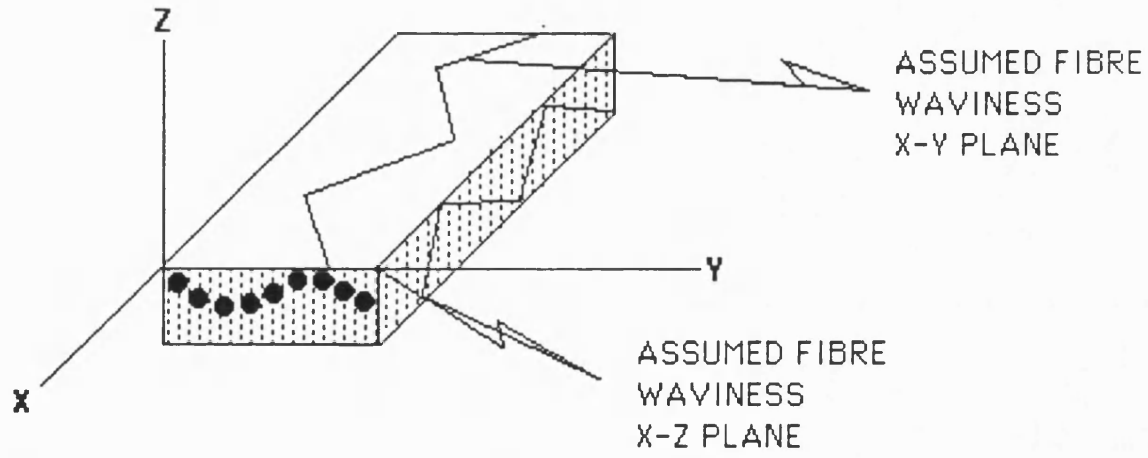

Figure 7.19 Co-ordinated system for fibre distribution in the composite. The longitudinal fibre direction is the X-direction.

Examination of a number of micrographs in the y-z plane (transverse section) showed considerable amount of ply

waviness in the z-y plane, see Figure 7.18(a & b). It not possible to deduce from Figure 7.17(a & b) if the non-circular shapes are typical of Kevlar fibres or if they are due to fibre waviness or fibre contact. Direct evidence for fibre waviness in the x-y plane is presented in Figure 7.18(a), (edge view). From the elliptical profile of fibre-(i) in Figure 7.18(a), it is apparent that this fibre exhibits waviness in the x-y plane. Waviness in the x-z plane would appear as curved profiles from an edge view. Although the edge view is probably not the best section for detecting fibre waviness in the thickness direction, Figure 7.18(a) fibre-(ii) indicates the possibility of waviness in the thickness direction too. It has to be emphasized that the observed fibre non-linearity were not just isolated cases but a consistent feature in the Kevlar plies. Extensive ply waviness were also observed in the hybrid composites.

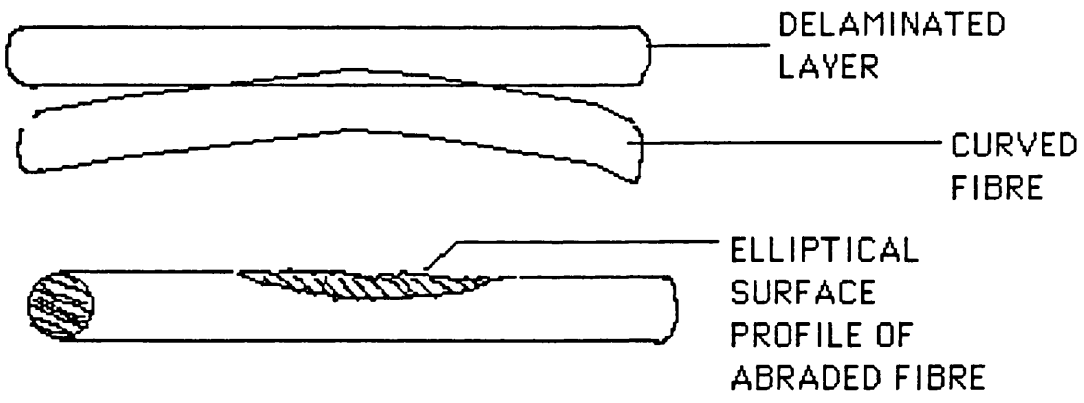

Figure 7.20 Illustration of speculated mechanism for the development of surface markings on the Kevlar fibres during T/C fatigue testing via fibre/fibre abrasion.

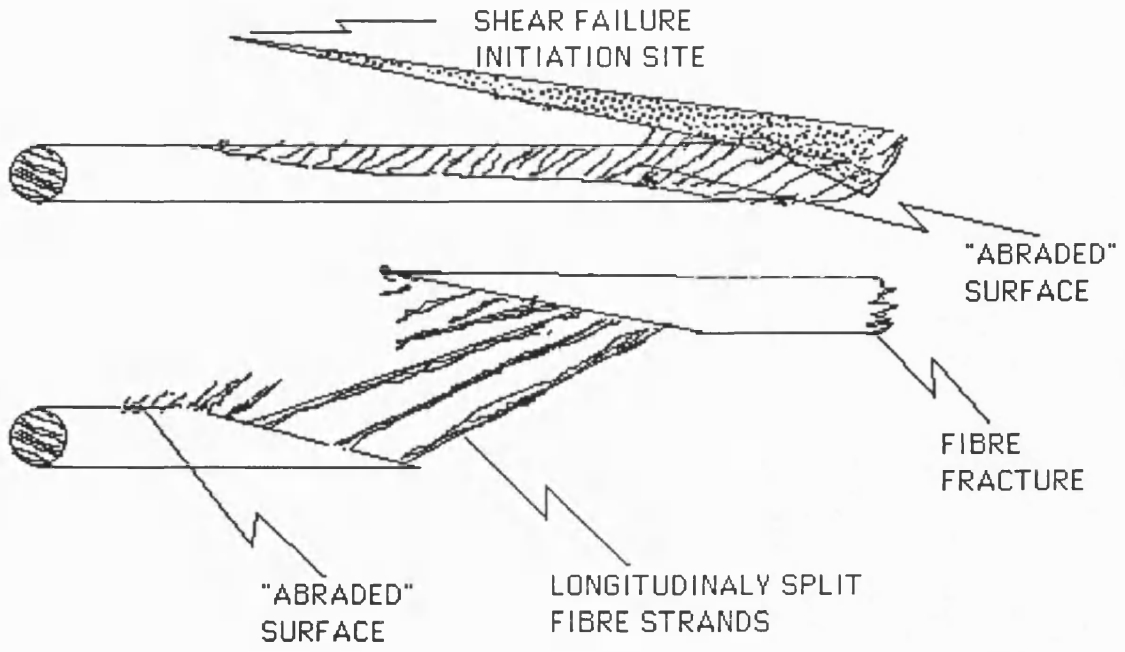

Figure 7.21 Illustration of speculated shear failure mechanism as the cause of the observed surface marking on T/C fatigue tested Kevlar.

Evidence from micrographic examinations for the shear mode of fibre failures are presented in Figure 7.22(a & b). Fibre-(ii) in Figure 7.22(b) illustrates a probable site where the failure initiated. Fibre-(i) in Figure 7.22(a) illustrates the type of damage depicted in the previous schematic illustration of a fibre that had undergone shear failure.

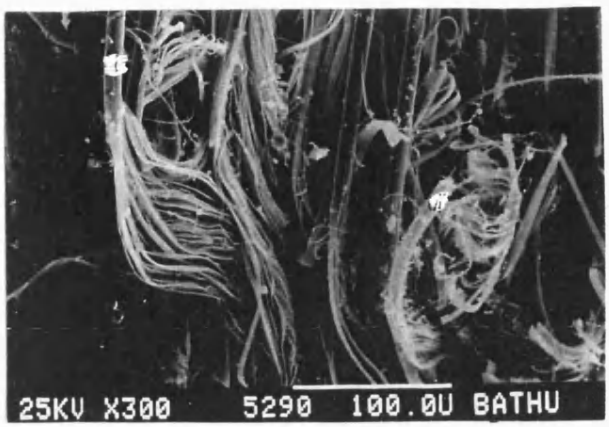

Figure 7.22(a) Evidence for failure modes depicted in Figures 7.20 and 7.21. Fibre-(i) exhibits extensive longitudinal splitting but the fibre has not fractured. Fibre-(ii) illustrates a transversely fractured fibre end with extensive longitudinal splitting away from the primary site.

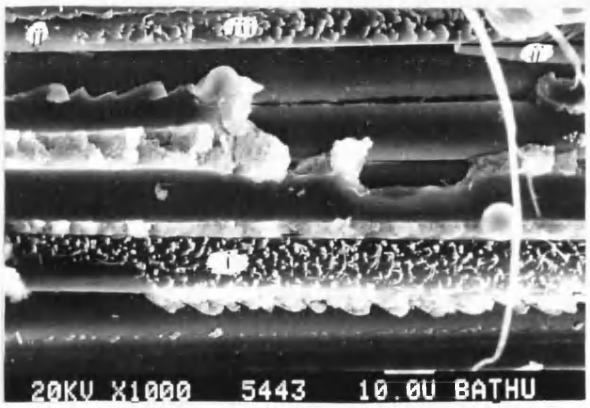

Figure 7.22(b) Fibre-(i) illustrates fibre surface damage due to T/C fatigue. Fibre-(ii) illustrates a probable initiation site for the type of damage mode shown in Figure 7.21. Fibre (iii) shows an advanced damage state.

Another form of Kevlar surface damage which was observed is illustrated in Figure 7.23(a), where the peeling seems to be across the circumference of the fibre and spaced at intervals of approximately 0.5-0.75 times the fibre diameter. Reference is made to a micrograph published by Konopasek and

Hearle[113], see Figure 7.23(b). They reported that slight bulges were also observed on untested aramid fibres and that these lines became more pronounced after fibre failure in a tensile test. They attributed the formation of the pronounced bulge lines to the fibre snapping back on failure. However, DeTeresa[120] also reported similar surface features on Kevlar fibres that had been subjected to controlled compressive loading. Drzal[162] suggested that these surface features were due to shear folding of the fibre skin in a helical manner. He provided micrographic evidence to show that these helical bands appear after unloading the specimen subsequent to a 5% compressive strain. However, he did not report the minimum compressive strain that was required to initiate these surface markings.

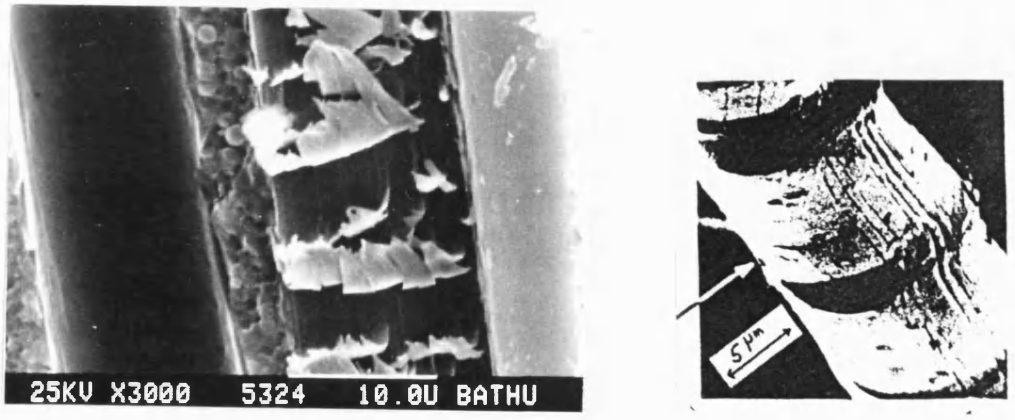

(a) (b)

Figure 7.23 (a) Surface peeling of the Kevlar fibre; Initiation sites seem to correspond to bulging on the fibre. (b) Bulging lines reported by Konopasek and Hearle. Copied from reference number 113.

The onion skin-like peeling effect seen in Figure 7.23(a) may be due to abrasion of the fibre surface originating at these bulge profiles. This may also account for the transverse

fibre markings observed in the optical micrographs, see Figures 7.18(a & b). SEM micrographs of polished Kevlar/914 composites (longitudinal sections) are presented in Figures 7.24(a & b). Polishing effects have been ruled out as a direct cause of these transverse fibre markings. Various polishes and polishing angles were attempted but they all gave the same final results. However, it is possible that these transverse markings observed in Figures 7.18 (a and b - mono-fibre Kevlar composite) and Figure 7.25 (hybrid composite) were highlights as a consequence of polishing the specimens. For example, if the bulges are assumed to extend into the whole circumference of the fibre at periodic intervals, see Figure 7.23(a), then polishing this fibre in its longitudinal plane would probably result in a profile illustrated in Figures 7.24 (a and b). Assuming that the surface kinking does not extend all the way to the core of the fibre, polishing to a depth greater than the region affected by the bulge should eliminate the ridges and depressions illustrated in Figure 7.25. This is indeed observed in Figure 7.25 fibre-(i), (edge view from a Kevlar/XAS hybrid composite).

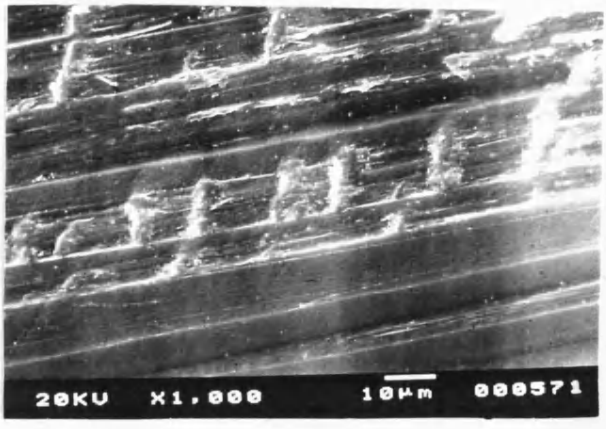

Figure 7.24(a) SEM of a polished longitudinal section of virgin Kevlar mono-fibre composite.

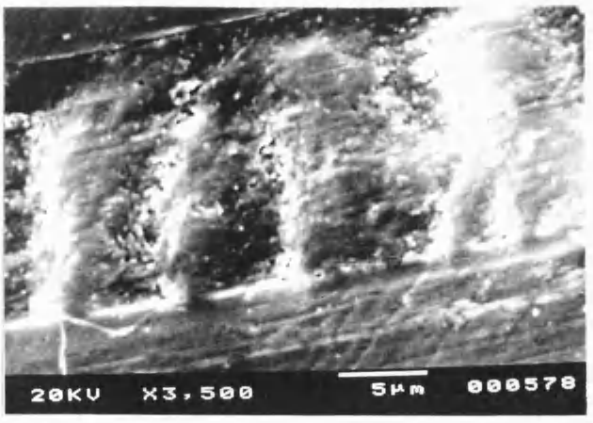

Figure 7.24(b) Magnified view of Figure 7.25(a) showing the transverse markings.

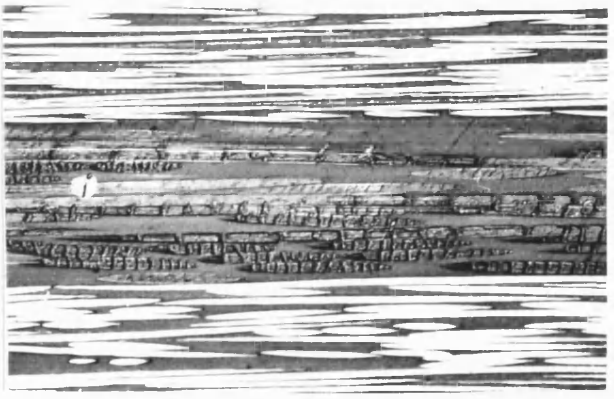

Figure 7.25 Optical micrograph of longitudinal section of a virgin hybrid composite showing areas on the Kevlar fibre free of the transverse markings; (fibre-(i)).

A schematic illustration of a possible cause for the formation of these surface marking on the Kevlar fibres subsequent to polishing in the longitudinal direction is described in Figures 7.26(a and b).

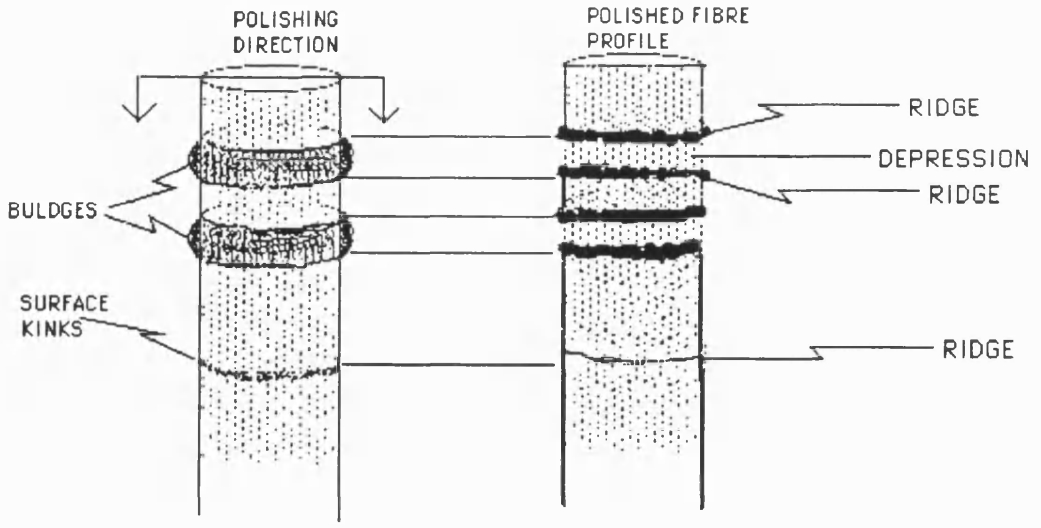

Figure 7.26 illustration of a possible mechanism for the formation of transverse markings on Kevlar fibres as observed in longitudinally polished sections.

(a) Assumes that the surface of the fibre has bulges spaced at regular intervals. The source origins of these bulges are not understood at present, but may be due to high temperature excursions during processing of the prepregs.

(b) On polishing, the bulges would be removed first compared to the areas away from the bulges on the fibre surface. However, because of the fibrillar nature of the Kevlar fibre, the base of these bulges, subsequent to polishing would tend to burr, thus appearing as ridges on the micrographs, see Figures 7.24(a and b). If these bulges are only present on the fibre surface, then further polishing would eliminate the fibre surface markings. This was indeed observed on successive polishing and an example of this is illustrated in Figure 7.25, fibre (i). Extensive waviness of the Kevlar

fibre are also apparent.

Other forms of Kevlar fibre damage observed in specimens that failed under T/C fatigue loading are briefly discussed. Figure 7.27 illustrates another compression induced failure mode that was observed for the Kevlar - failure via kinking.

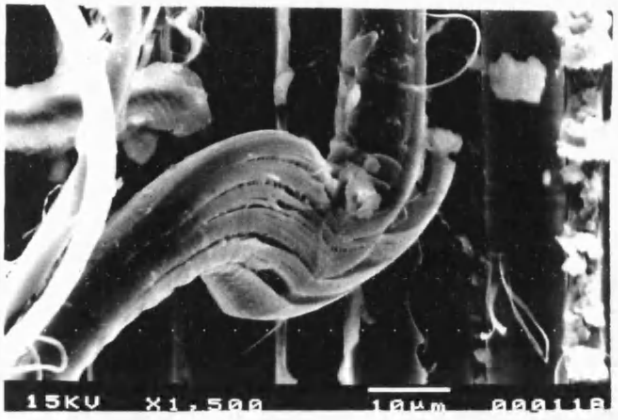

Figure 7.27 Failure of Kevlar fibre via kinking. The skin is seen to separate from the core.

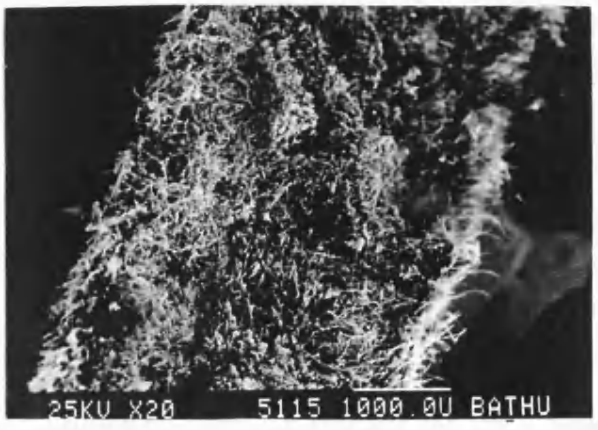

Figure 7.28 (a) Macroscopic failure mode observed for T/C ud Kevlar/914 mono-fibre composite, R=-0.6, σ+=0.32GPa.

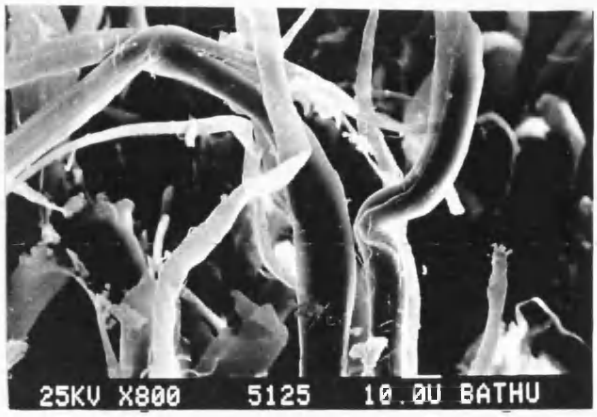

Figure 7.28(b) Gross fibre buckling of the Kevlar fibres in the vicinity of the main fracture site.

Figure 7.28(c) Magnified view of a T/C failure mode in a Kevlar fibre-transverse fibres fracture with limited longitudinal splitting. A per-cursor to this fracture mode may have been the features highlighted in Figures 7.28(b) and 7.27.

T/C specimens which experienced comparatively high compressive stresses exhibited a very planar fracture surface. Morgan et al found that kinked fibres which were fractured in tension exhibited planar fracture with the failure occurring in the region of the kink. They proposed that kinking resulted in polymer chain scission in the region

of the kink, thus facilitating an easy path for lateral crack propagation across the fibre when a subsequent tensile load was applied. Illustrations of these planar fracture modes are presented in Figures 7.29(a-c).

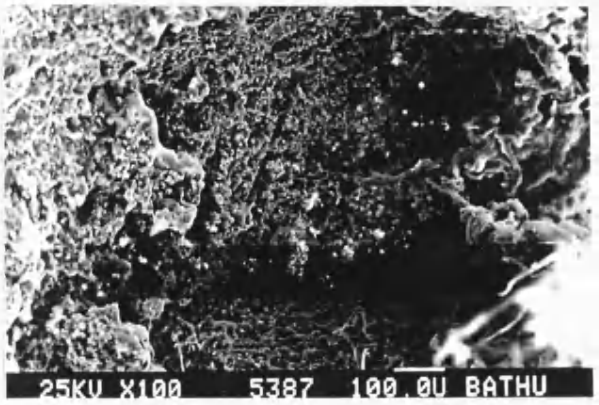

Figure 7.29(a) Macroscopic failure mode for a T/C ud mono-fibre Kevlar composite. The peak tensile stress was 0.4 GPa, R=-0.6. The fracture modes at high compressive stresses tended to be planar in nature.

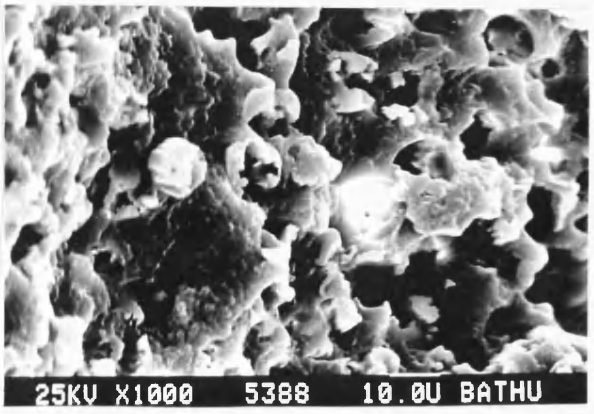

Figure 7.29(b) Illustration of planar transverse fracture of the Kevlar fibres, magnified view of previous Figure.

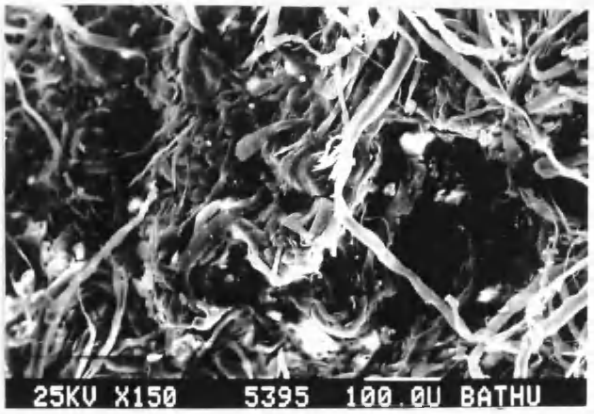

Figure 7.29(c) Illustration of areas where the Kevlar fibres had undergone crushing under T/C loading-vicinity of primary fracture site.

7.2.4 OBSERVED FAILURE MODES IN THE XAS/914 COMPOSITES

The macroscopic failure modes observed for the ud XAS composite was transverse fracture accompanied by longitudinal splitting, see Figure 30(a-b). In the majority of the specimens, the longitudinal splits were seen to originate from the vicinity of the end-tab and propagate longitudinally and through the thickness of the specimen.

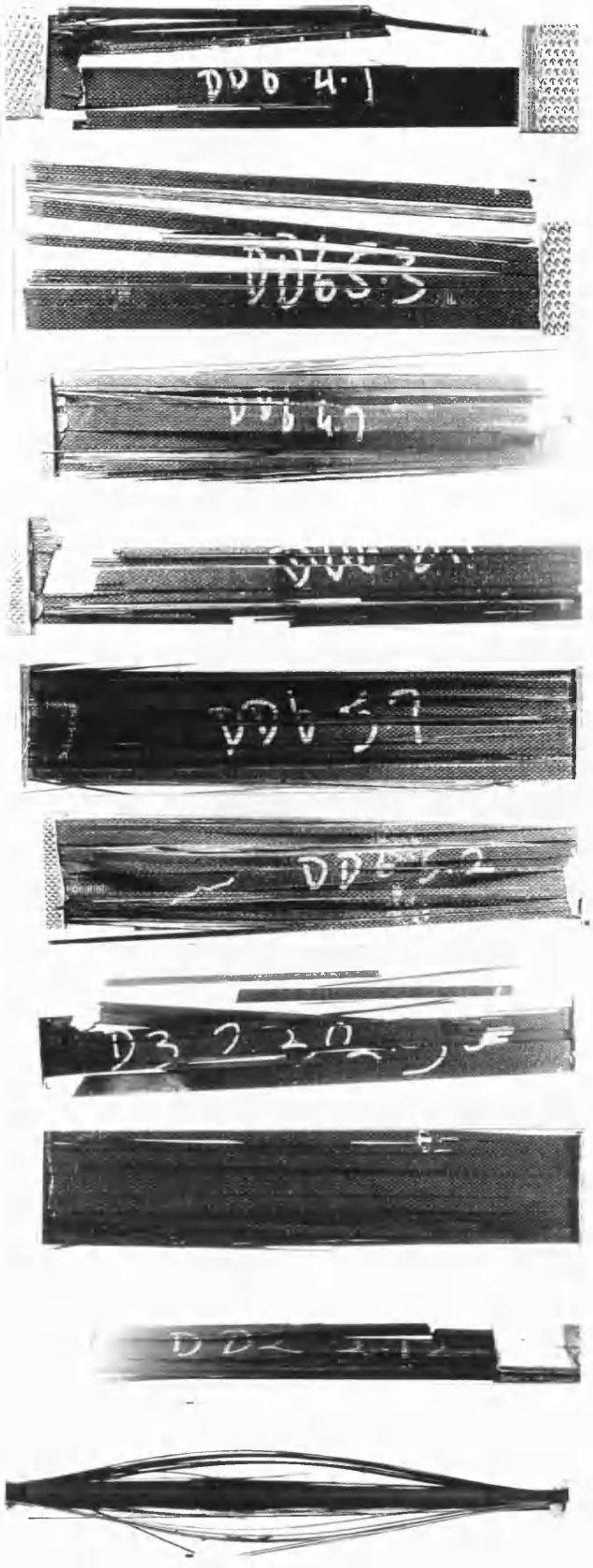

(a) Static Test

(b) Static Test

(c) σ=1.59GPa
R=0.1
CYF=170500

(d) σ=1.54GPa
R=0.1
CYF=loading failure

(e) σ=1.44GPa
R=0.1
CYF=277410

(f) σ=1.40GPa
R=0.1
CYF= $>10^6$

(g) σ+=1.40GPa
R=-0.6
CYF=1220

(h) σ+=1.20GPa
R=-0.6
CYF=56540

(i) σ+=1.0GPa
R=-0.6
CYF=55840

(j) σ+=0.87GPa
R=-0.6
CYF=850660

Figure 7.30 Macroscopic failure modes: (a-b) Static Tensile; (c-f) T/T; (g-j) T/C. See text for explanation.

The observed macroscopic failure modes for the XAS/914 composite as a function of the applied peak stress for T/T, R=0.1, fatigue test are illustrated in Figure 7.30(c-f). The T/C, R=-0.6 macroscopic failure modes are illustrated in Figure 7.30(g-j).

With reference to Figure 7.30; the longitudinal splitting was observed to develop more quickly at higher peak cyclic tensile stresses. However, the visual detection of these longitudinal cracks did not correspond nor indicate the onset of failure of the specimens.

In general under T/T fatigue testing it was observed that the effect of these longitudinal cracks was to initiate delamination of the surface plies into discreet strips. Sample (d) was a run-out, this specimen was mounted in resin polished for optical microscopy; the transverse sections showed no significant differences compared to the control specimens. The longitudinal sections showed a slight increased concentration of fibre breaks, especially along the 'new' edges of the delaminated specimen.

At peak stresses below approximately 70% of UTS, run-outs were obtained at 10^6 cycles. It is reasonable to speculate that Specimen (d) would have failed eventually if the test was not terminated at 10^6 cycles.

The effect of introducing a compressive stress component into the fatigue load cycle on the macroscopic failure modes are illustrated in Figure 30(g-j). No obvious differences were observed compared to the T/T specimens other than the rate of

delamination development was observed to be greater for the T/C fatigue tested specimens. Interply delaminations became more prominent for the T/C fatigue tested samples as the compressive stress component was increased.

With the Kevlar composite, fibre failure modes were unique to a particular loading regime and location in relation to the main fracture sites. However, in the case of the fatigue tested XAS composite, the predominant form of failure observed was transverse fibre fracture and longitudinal splitting in the matrix and delamination of the outer plies. However, some generalized observations on the failure modes of XAS/914 are presented below.

The matrix/fibre adhesion in the XAS composite was superior compared to that observed for the Kevlar/914 composite. A typical microscopic fracture surface for T/T fatigue tested XAS/914 composite are presented in Figure 7.31(a & b). The fracture surface was planar with extensive transverse fibre failures. Transverse fibre fractures were observed to occur in clusters in the vicinity of longitudinal matrix splits. Fibre fractures were also observed to occur in a transverse plane in between longitudinal matrix splits.

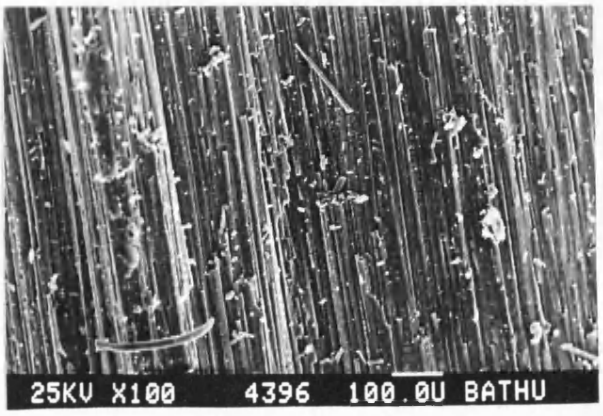

Figure 7.31(a) Edge view of (T/T) failed XAS/914 composite.

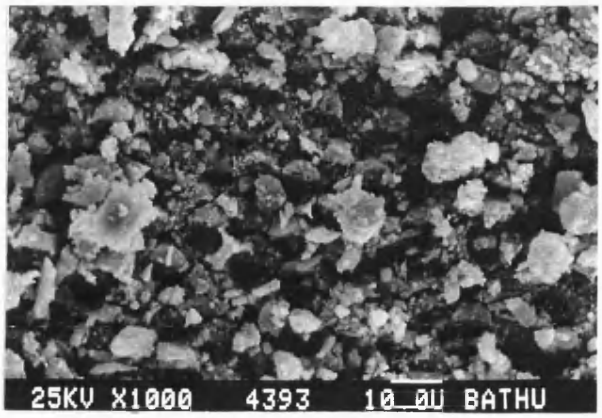

Figure 7.31(b) Vertical view of (T/T) failed XAS/914 composite.

The fractured surface was littered with resin particles and fractured fibres of varying lengths upto approximately 30 microns.

7.2.5 OBSERVED FAILURE MODES IN THE HYBRID COMPOSITES

No obvious differences were observed in the macroscopic failure modes for the ud 50%, 37.5% and 25% Kevlar/XAS hybrid composites. As in the mono-fibre composites, hybrid samples T/T fatigue tested at peak stresses greater than approximately 85% of the UTS, resembled static tested samples. Run-outs (at 10^6) for the R=0.1 tests carried out at stresses corresponding to less than 75% of UTS displayed a lower concentration of longitudinal splitting and inter and intra-ply delaminations. No micrographs of these samples have been presented in this report because these specimens were mounted in resin, sectioned and polished (edgewise longitudinally and transversely) to evaluate the extent of damage accumulation. No significant differences were observed in these samples compared to the control specimens.

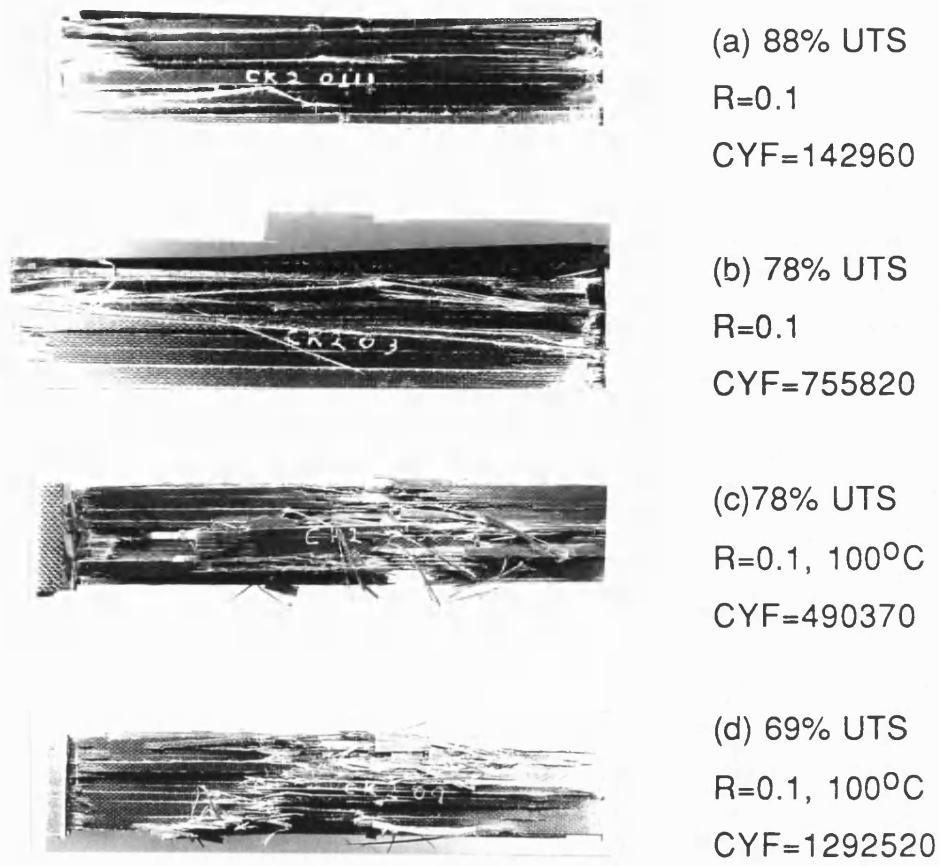

Figure 7.32(a-d) Macroscopic failure modes for the ud 50% Kevlar/XAS/914 hybrid, T/T fatigue tested, R= +0.1 and +0.01.

A change in failure mode was observed in going from R=0.1 to 0.01. The predominant failure mode for the R=0.1 specimens was extensive longitudinal splitting and inter and intra-ply delaminations. For the R=0.01 specimens, the extent of delaminations was considerably higher than that observed for the R=0.1 specimens. Furthermore, as shown previously, the fatigue performance for R=0.1 was greater than that obtained for R=0.01. A further discussion on the possible reasons for the observed differences in the fatigue lives of R=0.1 and 0.01 fatigue test is presented in the next section.

The 100°C T/T fatigue tested specimens also exhibited a different macroscopic failure mode to that observed for R=0.1 and 0.01 specimens. In the former case, there was a tendency for the specimens to exhibit a 'brush' like failure mode. The surface plies were seen to flake off into discreet rectangular pieces. A similar form of flaking was also observed for the T/C samples.

Microscopic examinations of the fracture surfaces of the 100°C specimens revealed the surface to be littered with polyethersulphone particles, see Figure 7.33(a & b). Extensive surface kinking was observed in the Kevlar plies, it was not possible to establish if these markings were caused by the fibre recoiling on fracture or if they were induced by the elevated temperature.

The microscopic tensile fracture modes observed for the hybrid composites in the Kevlar and XAS plies were similar to those observed for their respective mono-fibre composites; this was discussed previously.

Figures 7.34(a-c) illustrate surface views of a T/T, R=0.1 fatigue tested 50% hybrid away from the primary fracture site. Defibrillation of the fibre surfaces are apparent in Figure 7.34(a). A magnified view of some of the fibres in this region, see Figure 7.34(b &c), revealed the presence of ruptures/markings on the fibre surface. These took the form of bumps and regions of small swelling and transverse ruptures on the surface. Radiation damage was ruled out as a possible source as these features were not seen to develop on selected sites using a high beam current. It is possible

that these surface markings may have been caused by a fibre/fibre abrasion mechanism. The source origin of the depression on the fibre in Figure 7.34(c) and its significance was not established.

Figure 7.33(a) 50% hybrid, 100°C fatigue test at R=0.1: fracture surface of a Kevlar ply showing (i)-distribution of polyethersulphone particles, (ii)-compression damage due to recoil-subsequent tensile fracture or kink formation due to elevated temperature.

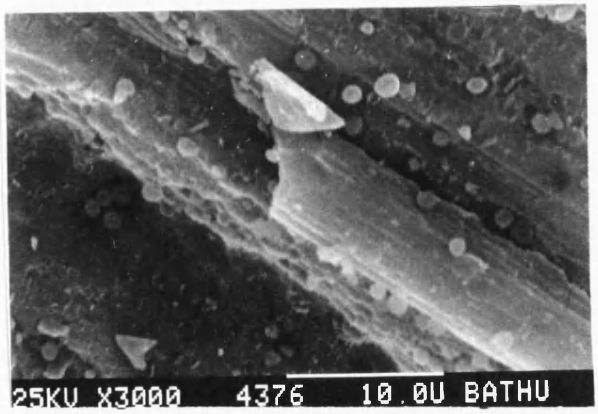

Figure 7.33(b) 50% hybrid, 100°C fatigue test at R=0.1: Fracture surface of the first XAS ply in above composite.

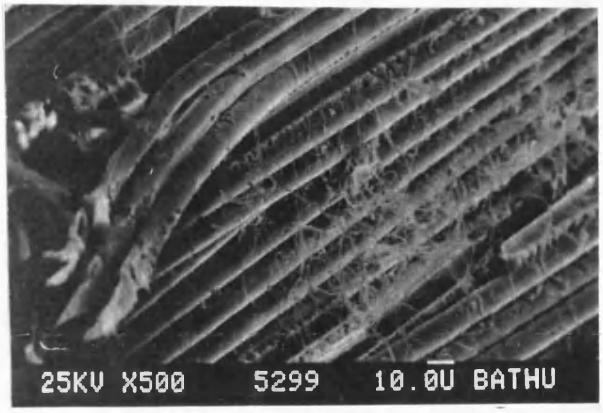

Figure 7.34(a) Surface view of T/T, R=0.1 50% hybrid. Illustrates a fracture site away from the main failure region, defibrillation is apparent.

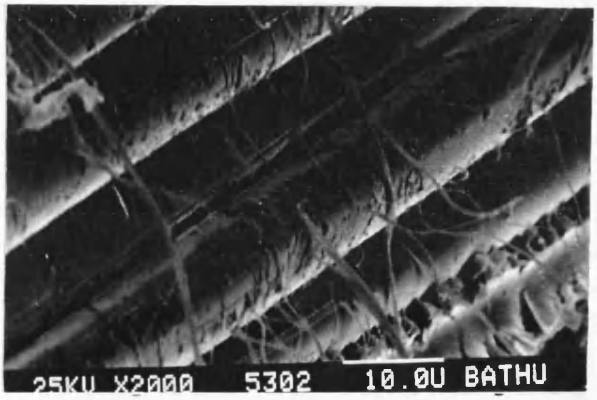

Figure 7.34(b) Surface view of T/T, R=0.1 50% hybrid. Magnified view of area illustrated in previous micrograph.

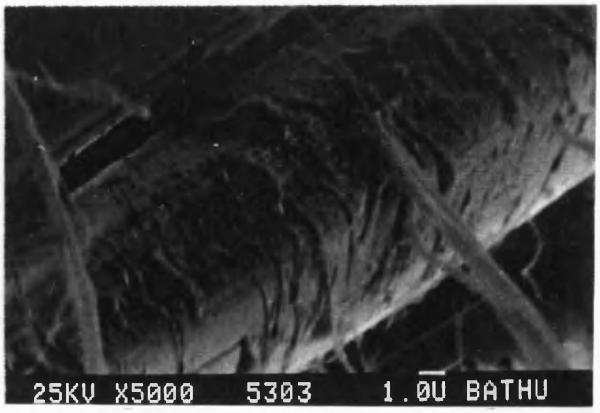

Figure 7.34(c) Magnified view of previous micrograph. The fibre profile is not circular. Note also the transverse marking on the fibre surface.

7.2.6 Observed Failure Modes In The Tension/Compression Fatigue Tested Hybrid Composites.

A change in the failure mode was observed for the three hybrid materials in going from a T/T to T/C loading regime. A selection of these macroscopic failure modes are illustrated in Figures 7.35-7.37. It is apparent from these micrographs that the introduction of a compressive load component into the fatigue load regime, alters the failure modes of the outer Kevlar plies. Direct observation of macroscopic damage development in the T/C tests was not possible because of the presence of the anti-buckling jig.

The following general conclusions are made with reference to Figures 7.35, 7.36 and 7.37 which correspond to the 50%, 37 .5% and 25% Kevlar/XAS/914 hybrids respectively.

(a) 50% Hybrid - The most prominent feature under T/C cycling was the development of delamination patches on the outer Kevlar plies accompanied by longitudinal splitting and extensive interply and intraply delaminations. The surface delaminations broke up into discrete rectangular pieces and flaked off with prolonged cycling. The extent of the delaminations in the inner ply were somewhat less extensive than the outer plies. In comparison with the other hybrids, the extent of delaminations for any (R) ratio was greatest for the 50% hybrid. The development of these surface delaminations was observed to be a function of the (R) ratio, peak stress value and the number of cycles.

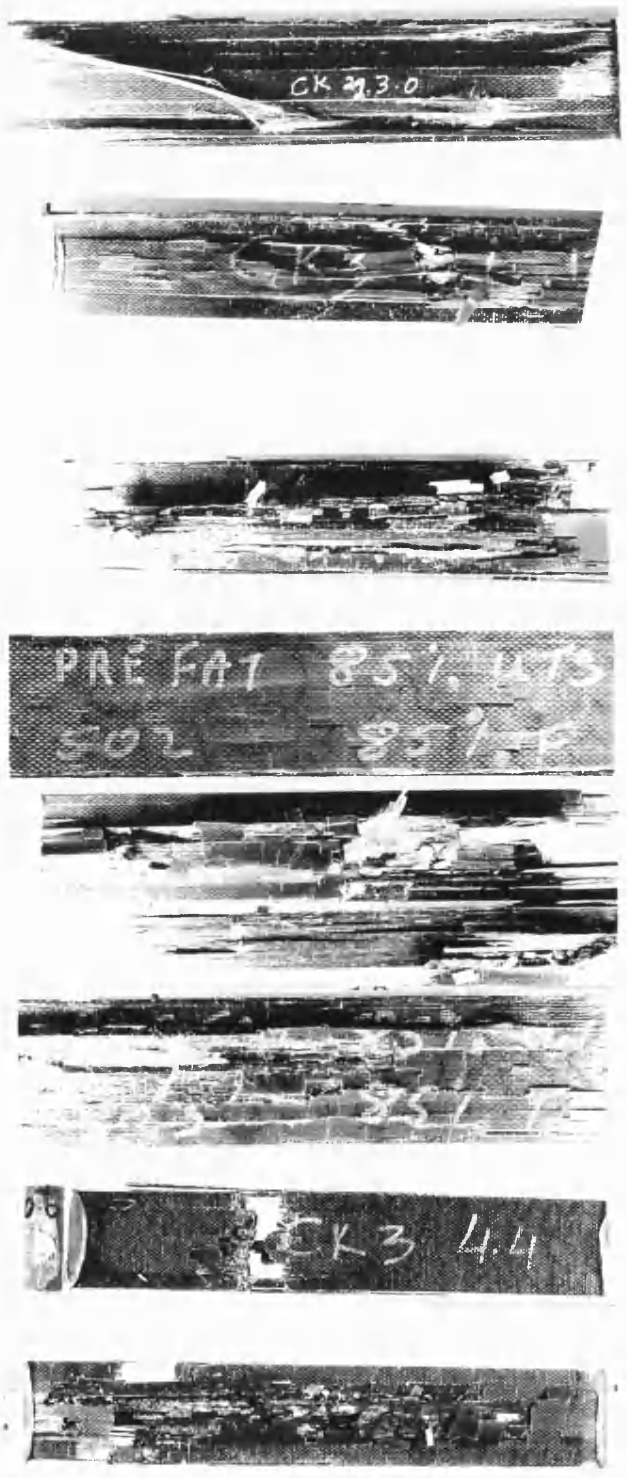

(a) σ+=1.06GPa
R=+0.1
CYF=45680

(b) σ+=0.91GPa
R=-0.1
CYF=238160

(c) σ+=1.06GPa
R=-0.3
CYF=175780

(d) σ+=0.8GPa
R=-0.3
CYF=182780

(e) σ+=0.78GPa
R=-0.3
CYF=445680

(f) σ+=0.68GPa
R=-0.3
CYF=278440

(g) σ+=0.9GPa
R=-0.6
CYF=17260

(h) σ=0.5GPa
R=-0.6
CYF=1292950

Figure 35 (a-h) Macroscopic failure modes exhibited by the 50% hybrid.

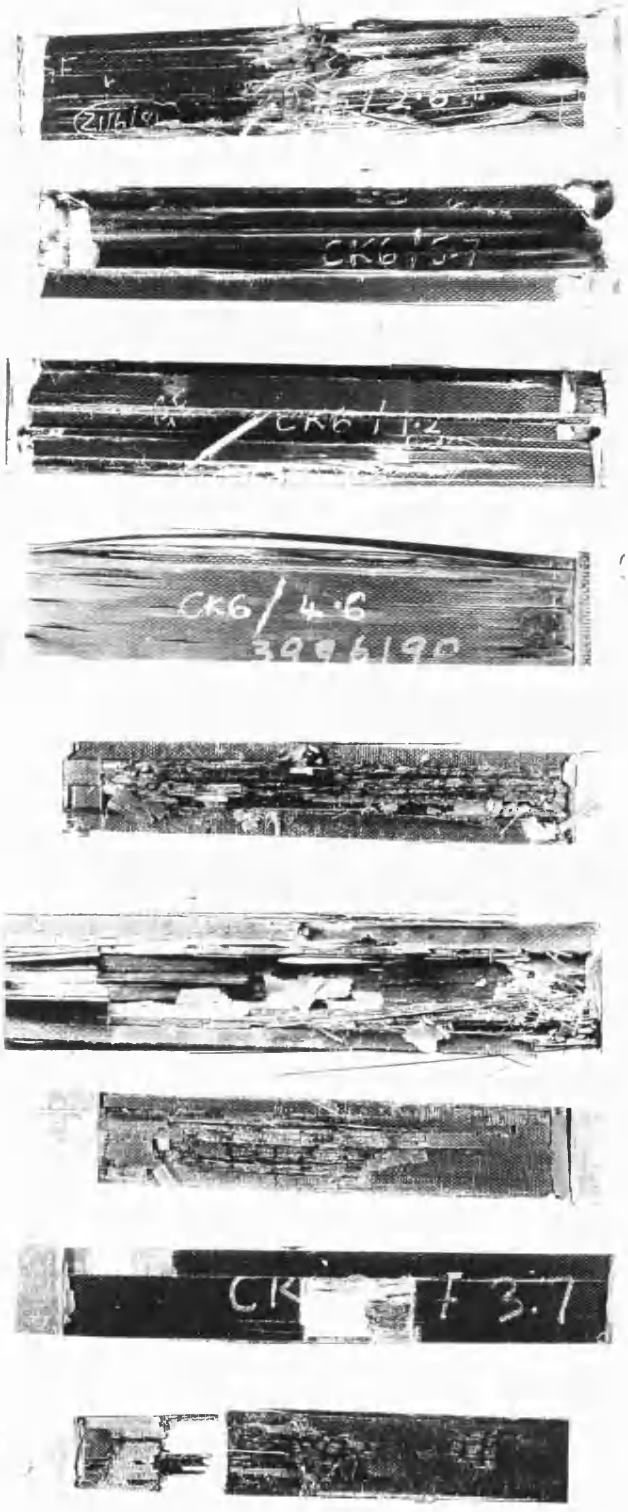

(a)Static Tensile

(b) σ+=1.25GPa
R=+0.1
CYF=34090

(c) σ=1.18GPa
R=+0.1
CYF=706760

(d) σ+=1.0GPa
R=+0.1
CYF=>10^6

(e) σ+=0.97GPa
R=-0.3
CYF=57440

(f) σ+=0.85GPa
R=-0.3
CYF=463710

(g) σ+=0.77GPa
R=-0.3
CYF=1628240

(h) σ+=0.87GPa
R=-0.6
CYF=24710

(i) σ+=0.77GPa
R=-0.6
CYF=78850

Figure 7.36 Selection of typical macroscopic failure modes exhibited by the 37.5% hybrid composite subjected to T/T and T/C fatigue loading.

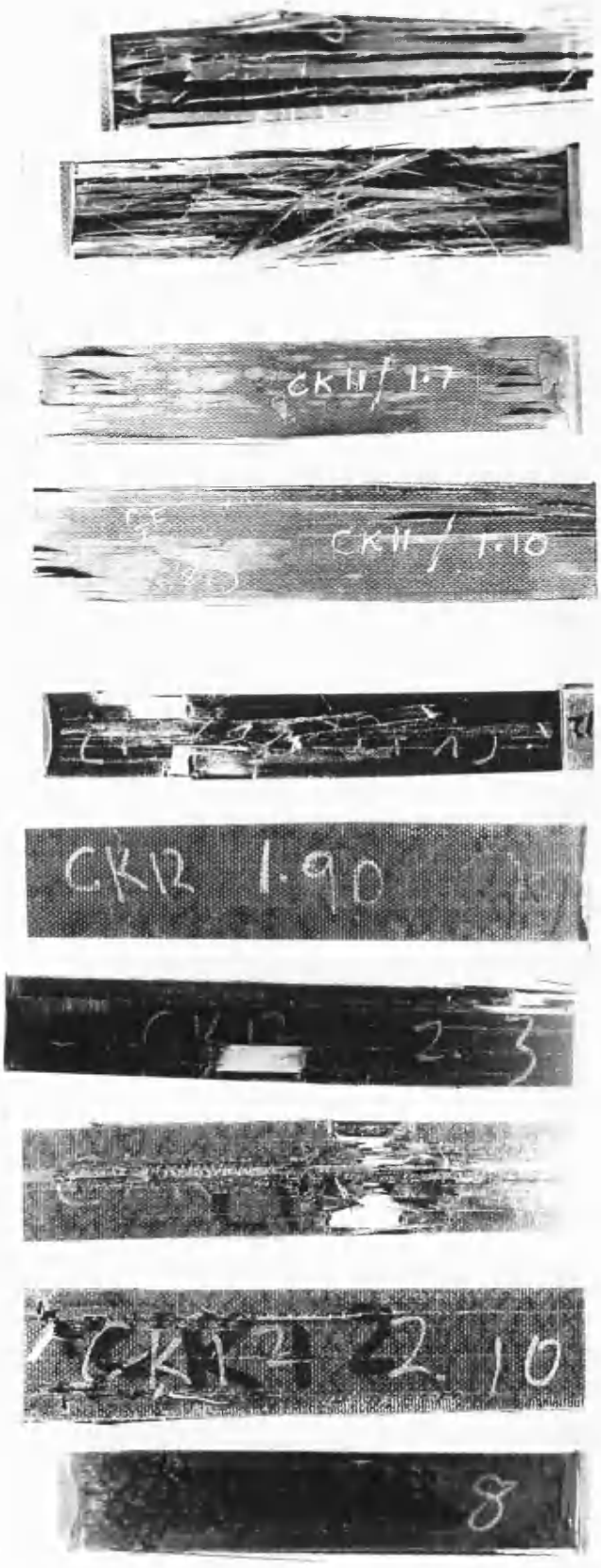

(a) Static Tensile

(b) σ+=1.29GPa
R=+0.1
CYF=1640900

(c) σ+=1.27GPa
R=+0.1
CYF=>10^5(terminated)

(d) σ=1.05GPa
R=+0.1
CYF=>10^6

(e) σ=1.0GPa
R=-0.3
CYF=6700

(f) σ=0.92GPa
R=-0.3
CYF=>10^6

(g) σ=0.95GPa
R=-0.6
CYF=12340

(h) σ=0.92GPa
R=-0.6
CYF=128940

(i) σ=0.83GPa
R=-0.6
CYF=136880

(j) σ+=0.78GPa
R=-0.6
CYF=499520

Figure 7.37 Selection of typical macroscopic failure modes for 25% hybrid.

37.5% Hybrid - The appearance of the failed T/T specimens were similar to that observed for the 50% hybrid. In general, the extent of delaminations for the T/C specimens were lower than those observed for the 50% hybrid composite.

25% Hybrid - As with the other hybrids, the macroscopic appearance of specimens T/T tested at relatively high peak stresses resemble the static tensile tested samples. Brush-like failure were observed, see Figure 7.37(b), for samples T/T tested at relatively low peak stresses. Delamination growth on the outer Kevlar plies was also observed during T/T fatigue testing (Figures 7.37(c & d)), however, no transverse cracking of the surface plies was observed. In the T/T samples, longitudinal splitting was the first visually detectable damage mode and these were located approximately at a distance corresponding to the thickness of the specimen. With cycling, delaminations were seen to originate from the end-tab region and these grew longitudinally, thus delaminating the outer plies into discreet strips. The extent of type of delaminations associated with T/C cycling was significantly less compared with the previous two hybrids.

A number of samples were fatigue tested to approximately 85% of the fatigue life and then mounted in resin and polished along the edge (edge view) and transverse to the fibre direction (vertical view); the end-tab regions were discarded. Figure 7.38 illustrates a transverse section through the fibre direction of a sample that was T/T fatigue tested to failure at R=0.1. Intra-ply cracking in the outer

plies is clearly evident along with a longitudinal crack that spanned the specimen thickness. Inspection of a number of transverse sections of samples fatigue tested at R=0.1 did not reveal any other form of damage.

Longitudinal edge sections of the R=0.1 samples exhibited a significant increase in the damage to the XAS fibres compared to the control specimens.

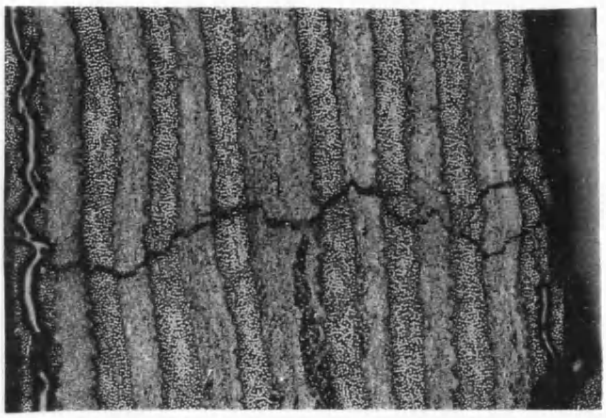

Figure 7.38 Transverse section through a failed T/T 50% hybrid composite.

Transverse sections of T/C tested specimens, see Figure 7.39(a and b), showed the presence of regularly spaced longitudinal cracks in the Kevlar plies. Extensive intra-ply fracture of the outer plies is also evident. Longitudinal edge sections of the T/C tested specimens showed the presence of regularly positioned transverse cracks in the Kevlar plies, see Figure 7.40(a & b).

It was previously seen that the outer Kevlar plies displayed delamination patches when subjected to T/C fatigue loading. These delaminations patches seemed to originate at intersections between longitudinal matrix cracks and

transverse cracks. A schematic illustration of a possible mechanism for the development of these surface features is illustrated in Figure 7.41.

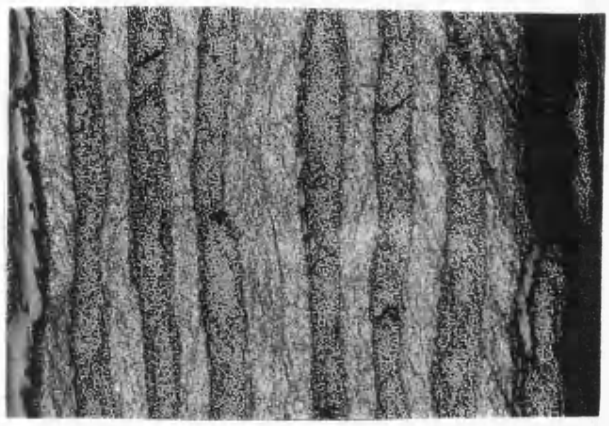

Figure 7.39(a) Transverse section of a 50% hybrid that had been subjected to T/C fatigue loading at R=-0.3. Note the regular crack spacing in the Kevlar plies.

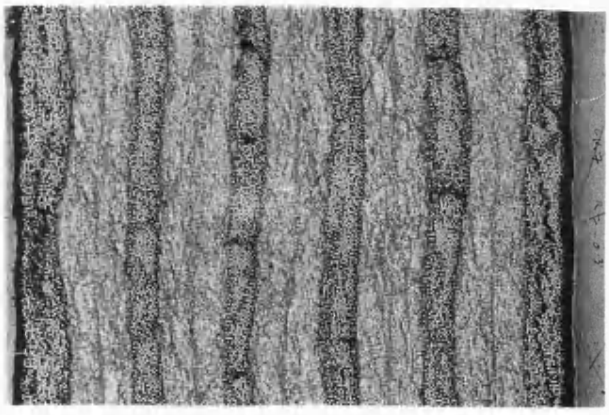

Figure 7.39(b) Transverse section of a 37.5% hybrid that had been subjected to T/C fatigue loading at R=-0.3. Note the regular crack spacing in the Kevlar plies. Ply waviness is also apparent.

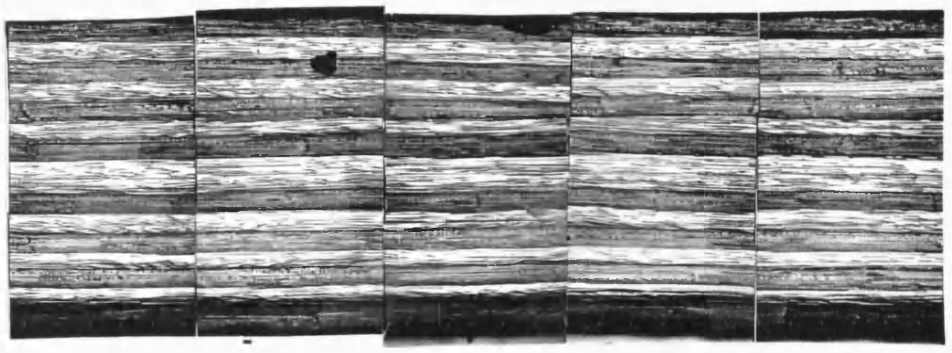

Figure 40 (a) Longitudinal edge section of a 50% hybrid T/C fatigue tested (run-out at 10^6); transverse cracking across the width of the Kevlar plies is evident. Longitudinal splitting originating at these transverse fracture sites were observed along the Kevlar/XAS ply interface.

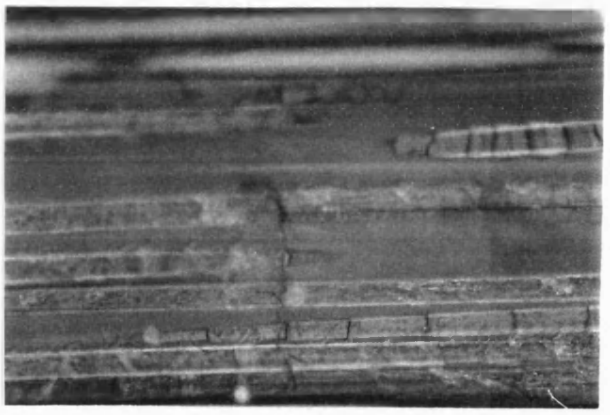

Figure 7.40 (b) Longitudinal edge section of a 37.5% hybrid T/C fatigue tested (stopped at 10^5); transverse cracking across the width of the Kevlar plies is evident.

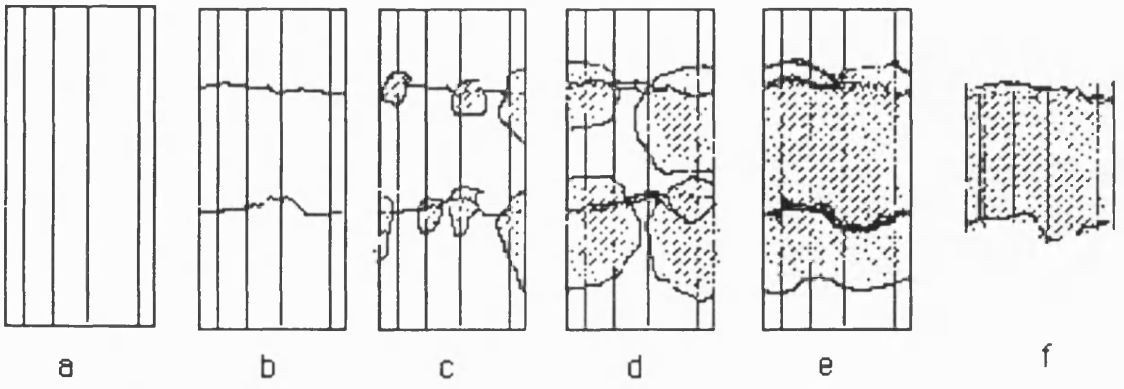

Figure 7.41 Schematic illustration of the formation of delamination patches on the surface of the Kevlar/XAS hybrid composites when subjected to T/C fatigue testing: see text for explanation.

With reference to Figure 7.41: (a) assumes the formation of longitudinal matrix cracks first; (b) this is then followed by the formation of transverse cracks. It is assumed that the formation of these transverse cracks in the Kevlar plies is a function of compressive stress component and number of cycles because it was previously discussed that Kevlar fibres which have been compressively damaged can exhibit transverse fracture of subsequent tensile loading. Furthermore, a regular array of transverse cracks were not detected in the static compression tested samples. (c) delaminations then grow at the intersections of the longitudinal and transverse cracks; (d) delaminations grow and merge with continued T/C cycling; (e) once the delamination has covered a region between two transverse cracks, it can then be dislodged from the surface of the composite (f).

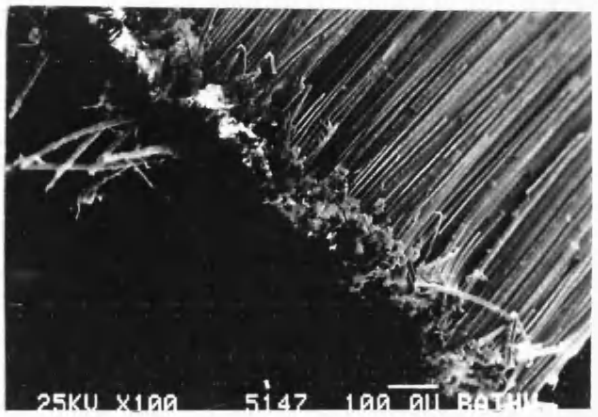

Figure 7.42(a) illustrates a surface view of a flaked-off outer Kevlar ply, a transverse fracture mode is apparent with little evidence of fibre splitting or fibrillation.

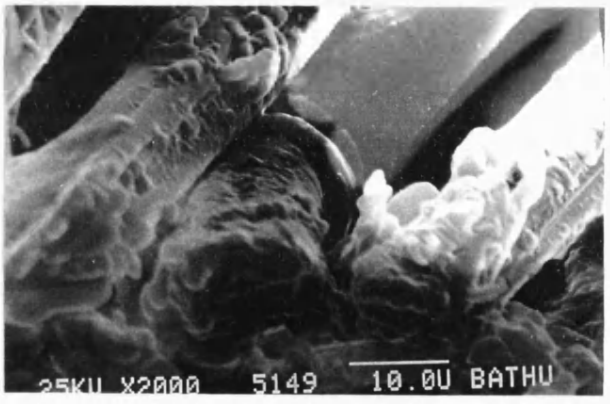

Figure 7.42(b) A magnified view of these fractured fibre-ends from the previous micrograph; fibre skin-core separation is evident.

The abrasion type features on the Kevlar fibre surface discussed previously for the T/C cycled mono-fibre Kevlar composite also manifested itself in the T/C fatigue tested hybrid composite, see Figures 7.43(a-c).

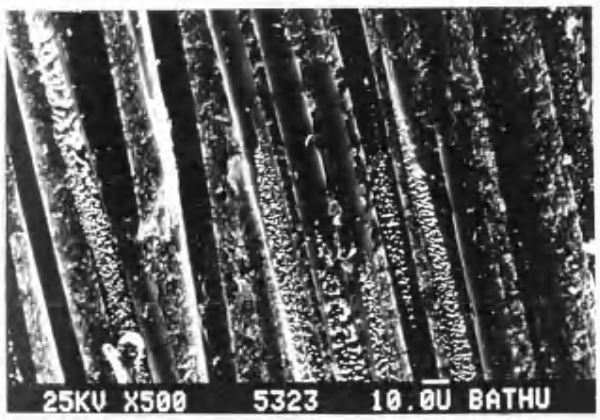

Figure 7.43(a) Surface view of exposed (under surface of delaminated area). Note the surface abrasion like markings on the Kevlar fibre surface.

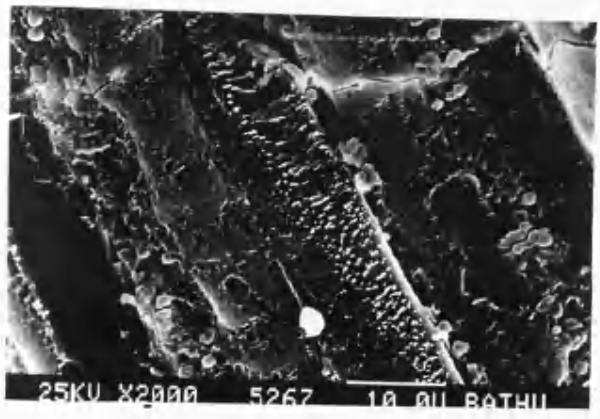

Figure 7.43(b) As above, the transverse crack is seen to run right through the Kevlar fibres.

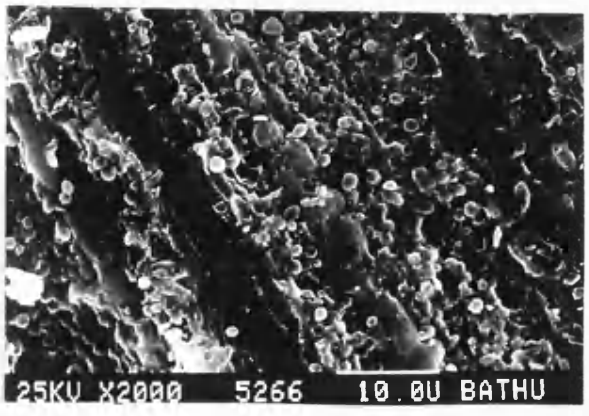

Figure 7.43(c) Visual appearance of exposed XAS ply surface due to delamination of the Kevlar ply.

8 RESULTS AND DISCUSSION - EFFECT OF ENVIRONMENT

8.1 Neat Resin - Diffusion of Moisture

The compression moulding technique used to produce neat resin plaques was consistent and yielded high quality samples with a very low void content. Samples produced using Silicone-moulds gave samples of inconsistent thickness and higher void content ~1-2%. Furthermore, the use of mould-release spray on the Si-moulds added a further complication as far as contaminating the resin was concerned. In the compression moulding technique, mould release cloth, similar to that used in the production of the composites was used. Furthermore, this meant that the surface profile and possibly the wetting characteristics were similar to those of the composite.

Three different aspects of sorption were initially investigated using a relative humidity of 100% at 25°C. Firstly, the initial desorption procedure was established. Secondly, the difference between polished and unpolished samples was investigated. The term `polished' in this context is taken to represent samples which were moulded in silicone rubber moulds and then abraded (polished) on 800 grit abrasive paper to yield the required thickness. Thirdly, compression moulded samples were compared with the silicone rubber moulded specimens.

Figures 8.1 and 8.2 illustrate the initial desorption of the Silicone rubber and compression moulded samples respectively. In the former case, an apparent equilibrium was reached after

about 120 hours; this corresponded to an equilibrium weight loss of approximately 0.9%. For the compression moulded samples, the time to achieve a constant mass was also approximately 120 hours with a equilibrium weight loss of approximately 0.8% at 60°C drying. Based on these findings, a minimum period of 160 hours of drying was chosen as the standard at a temperature of 60°C. The choice of drying temperature (60°C) was somewhat arbitrary and as shown in Figure 8.1, increasing the drying temperature to 120°C resulted in a further 0.1% weight loss[230]. Further work needs to be carried out to investigate if the chosen drying temperature can have any significant influence on the properties of the resin. For example, drying samples at elevated temperatures will result in thermal aging. The effects of thermal aging on sorption behaviour of epoxies has not received a great deal of attention in the literature.

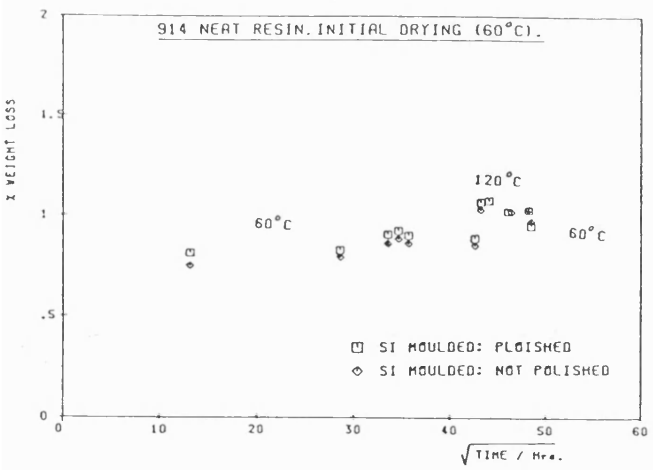

Figure 8.1 Initial desorption at 60°C for the neat 914 resin - Silicone rubber moulded.

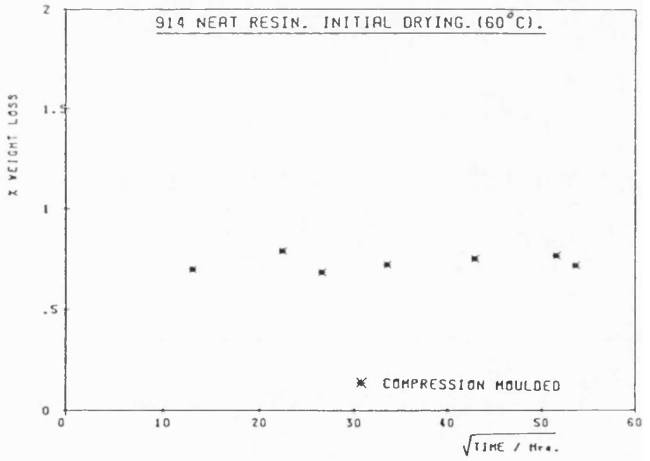

Figure 8.2 Initial desorption at 60°C for the neat resin - compression moulded.

With reference to Figure 8.3, it is evident that the

compression moulded samples (CMS) show a lower diffusion coefficient compared to the Si-moulded samples (SMS). The sorption behaviour was independent of initial drying temperatures. No significant differences were observed on comparing the polished and unpolished samples. However, it is clear that the production route of these neat epoxy specimens plays a significant role in determining their sorption behaviour.

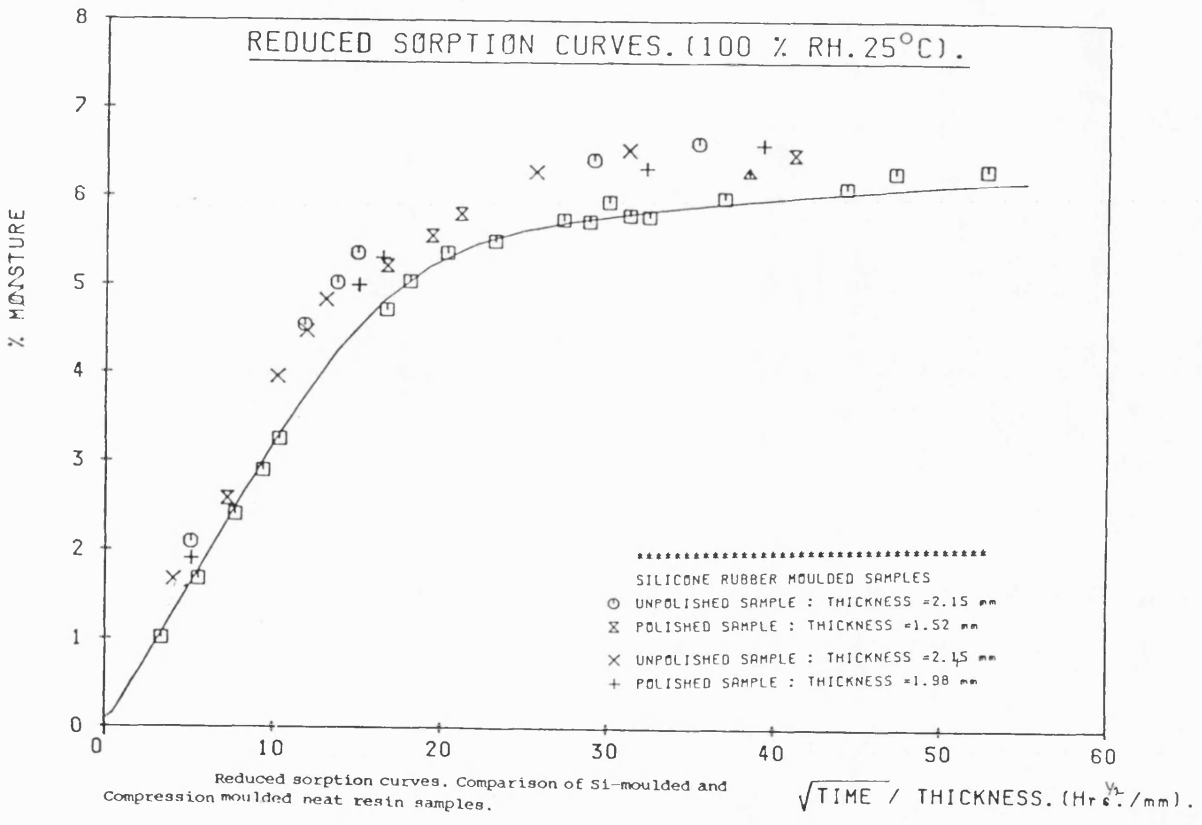

Reduced sorption curves. Comparison of Si-moulded and Compression moulded neat resin samples.

Figure 8.3 Reduced sorption curves illustrating the diffusion behaviour of the compression moulded and Silicone rubber moulded samples.

Modelling of the diffusion behaviour of the neat 914 resin system was carried out exclusively on the compression moulded samples and is illustrated in Figures 8.4 - 8.15.

The diffusion behaviour of the 914 resin system at 25°C and 65% relative humidity was adequately described by Fickian diffusion, see Figure 8.4. However, on subjecting the resin to 100% relative humidity, i.e. total immersion, the dual mode absorption model was found to give a more accurate description of the 914 resin system sorption behaviour, see Figure 8.5. The difference in the two models became more significant as the conditioning temperature was raised from 25°C to 50°, 75° and 100°C. The dual mode sorption model best described the sorption behaviour of the 914 resin system; this is discussed further in a later section.

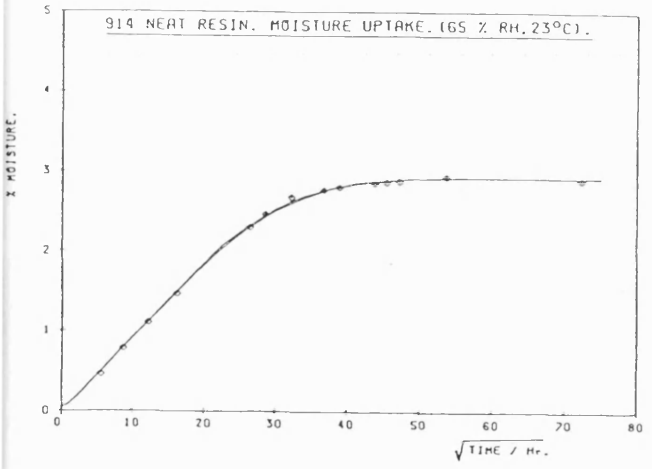

Figure 8.4 Sorption data for 914 neat resin, conditioned at 23°C, 65% RH. Both the Fickian and Dual mode sorption models were fitted to the data.

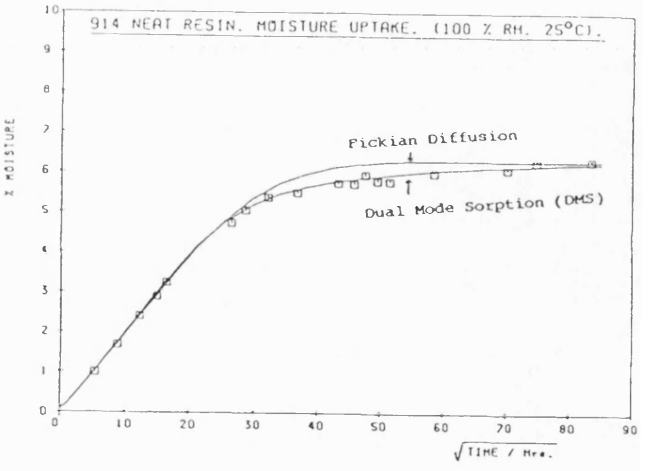

Figure 8.5 Sorption data for 914 neat resin conditioned at 23°C, 100%Rh.

Both the Fickian and Dual Mode Sorption models (discussed in the introduction) possess a summation term (n); Figure 8.6 illustrates the solution to the Fickian equation using three summation values, namely n=1, 10 and 100. With reference to

Figure 8.6, the only effect of (n) on the solution was when t=0. For the purposes of modelling the sorption behaviour of the 914 resin in this programme, a (n) value of 10 was chosen primarily due to the time that was required to generate a theoretical curve for large values of (n).

The equilibrium moisture content, (Mn), is a critical parameter in the solution of of the Fickian and Dual Mode Sorption (DMS) models. In experiments where the conditioning temperatures and relative humidities are high, the estimation of (Mn) is difficult. The findings of this study indicated that under total immersion conditioning, true equilibrium was not attained for the 914 resin system. This implies that the equilibrium moisture content for this resin system will be a function of the conditioning time. Furthermore, it will be shown later that the 914 resin system does react with moisture leading to changes in the resin properties.

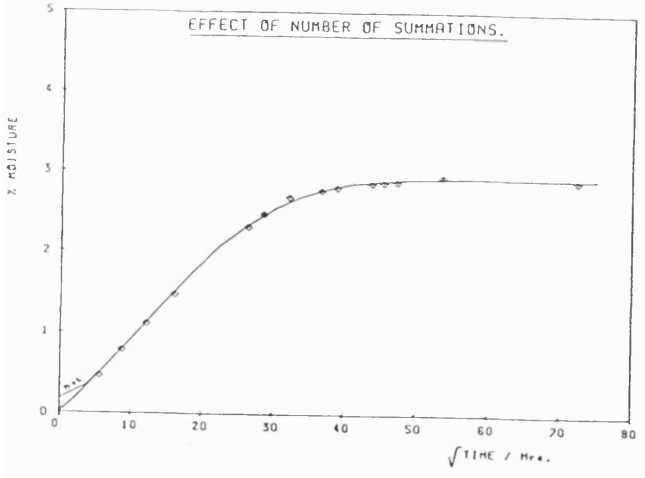

Figure 8.6 Data from Figure 8.4; illustrating the effect of summation (n) in the solution of the Fickian model for n=2,10 and 100.

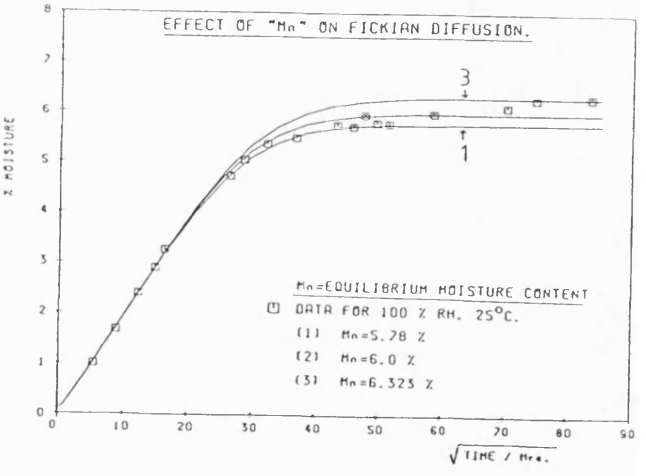

Figure 8.7 Illustration of effect of the equilibrium water content (Mn) on the Fickian diffusion model.

Figure 8.7 shows the effect of using three different (Mn) valued in the solution of the Fickian model. It is evident that the the Fickian diffusion model does not accurately describe the sorption behaviour of the 914 resin system even at 25°C.

The value of (Mn) assigned for generating the theoretical plots and in the calculation of diffusion coefficients for the various environmental conditioning used in this programme was obtained using the following criteria. (Mn) was defined as the highest percent moisture content attained during the duration of the sorption experiment.

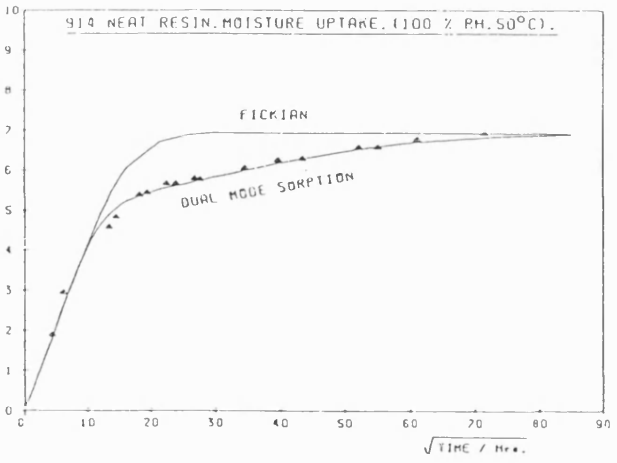

Figure 8.8 Sorption data for 100% RH 50°C. Illustration of the deviation from Fickian behaviour.

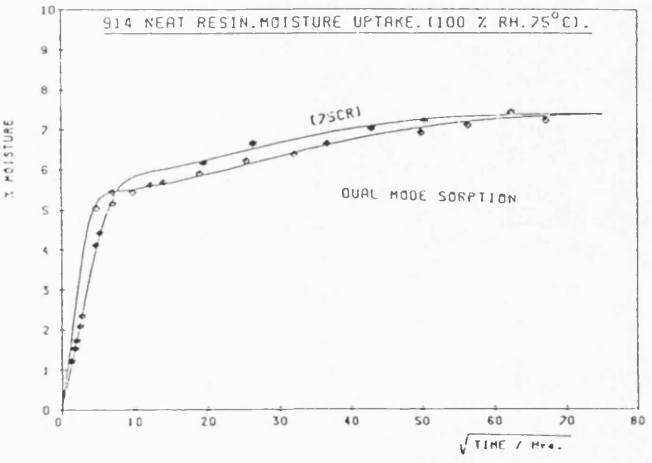

Figure 8.9 Sorption data for, 100% RH, 75°C. Illustration of the difference between the 75°C and 75°CR series.

Figures 8.8 and 8.9 illustrate the sorption data for the 50°C, 50°C(R) and 75°C, 75°C(R) samples respectively. As mentioned previously, the code (R) represents samples that were removed more frequently from their respective conditioning baths to

measure the increase in weight. With reference to Figures 8.5, 8.8 and 8.9, the deviation from Fickian behaviour becomes pronounced in going from 25°C to 75°C. Furthermore, it is apparent that an increase in the conditioning temperature resulted in a continued increase in moisture absorption with conditioning time, i.e., equilibrium moisture content (Mn) was not achieved.

The samples which were removed more frequently in the initial stages of the experiment for weight change measurements (50°CR and 75°CR) showed slightly higher plateau values, see Figures 8.9 and 8.10. The reasons for this observed differences are not understood at present. However, Shirrell[141] stated that the process of removing the specimens from an elevated conditioning bath to room temperature for weighing and then returning them back to the conditioning environment would expose the specimens to a mild thermal shock. He postulated that this mild thermal shock could induce surface cracking and sub-surface microvoids. This may be one of the reasons as to why the specimens which were removed more frequently for weight measurements showed a slightly higher moisture content, (50C(R), 75C(R), 100C(R)). The 50C(R) and the 100C(R) showed slightly higher diffusion coefficients. The only difference between these samples and the 50°, 75°, and the 100°C series was that the (R) series was dried for an extra month at 60°C before the sorption experiments were commenced. Surface cracking and subsurface microvoids may be partly responsible for the non-Fickian behaviour of these resins at these elevated temperatures. However, a more likely possibility for the creation of microvoids in the 914 resin system is hygrothermal degradation. Evidence for this

will be presented in a later section.

Figure 8.11 illustrates the sorption behaviour of the samples that were conditioned at 100°C. Once again, the sorption behavior of the 914 resin system at 100°C is seen to be accurately described by the Dual Mode Sorption Model. However, with prolonged conditioning, a decrease in the moisture content is apparent. With reference to Figure 8.11, the down-turn in the percent weight gain after about 2500 hours of conditioning at 100°C, suggests that resin had begun to undergo significant degradation. The colour of the specimens showed a progressive darkening with conditioning time. The observed differences in the sorption behaviour of the 100C and 100C(R) series were not obvious as those observed for the 50° and 75°C experiments.

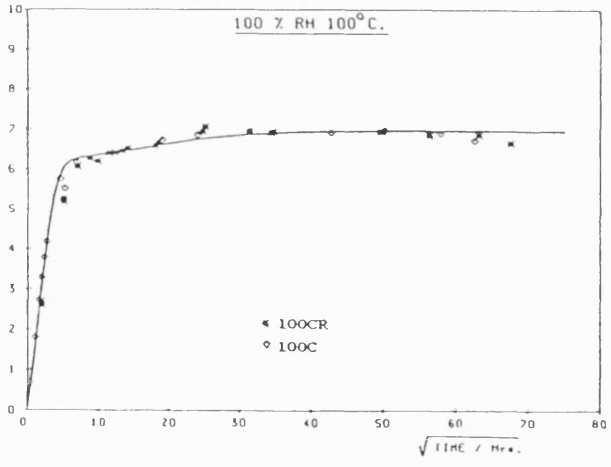

Figure 8.11 Sorption data for 100% Rh, 100°C conditioned neat 914 resin. Note the weight loss after approximately 2500. hours.

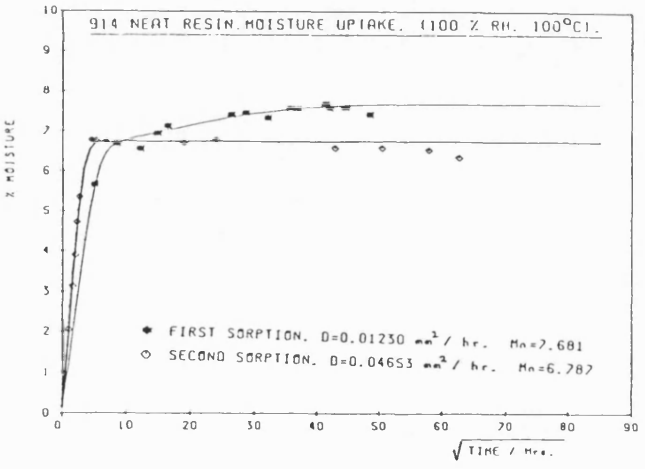

Figure 8.12 First and second sorption behaviour of the neat 914 resin, conditioned at 100% Rh, 100°C.

Figure 8.12 illustrates that the second sorption behaviour for the 100°C samples was much faster than the first sorption. However, surprisingly, the final equilibrium value for the second sorption was lower by approximately 1%. Furthermore, the second sorption behaviour did not show the typical two stage sorption observed in the first sorption experiments. The onset of weight loss for the second sorption experiments was after approximately 1600 hours of conditioning. The higher diffusion coefficient for the second sorption experiments may be due to the possibility that during the first sorption most of the microdamage/microcavilation was initiated. Therefore, during the second sorption, the diffusing penetrant has an easier route into the resin resulting in a higher diffusion coefficient.

The lower equilibrium moisture content for the second sorption experiments may possibly be due to the following reasons. During the first sorption experiments, any components in the resin capable of reacting, dissolving or forming hydrolyzed products with the absorbed moisture, will do so. During the second sorption experiment, the components capable of reacting with the absorbed moisture may not be present any longer, thus resulting in a reduced final equilibrium moisture content compared to the first sorption experiments.

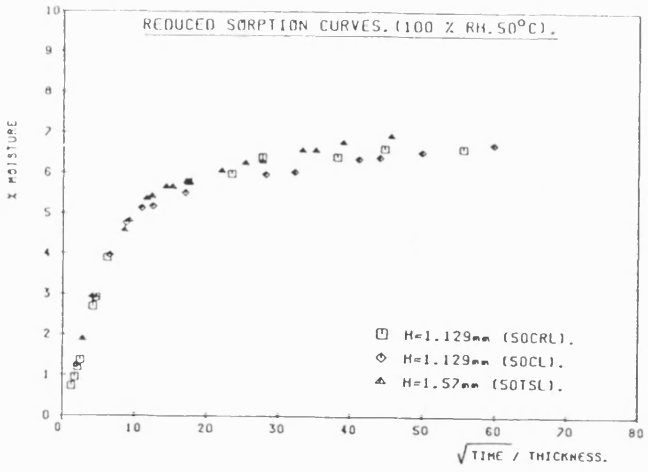

Figure 8.13 Reduced sorption curves for all the samples conditioned at 100% Rh, 50°C for the neat resin.

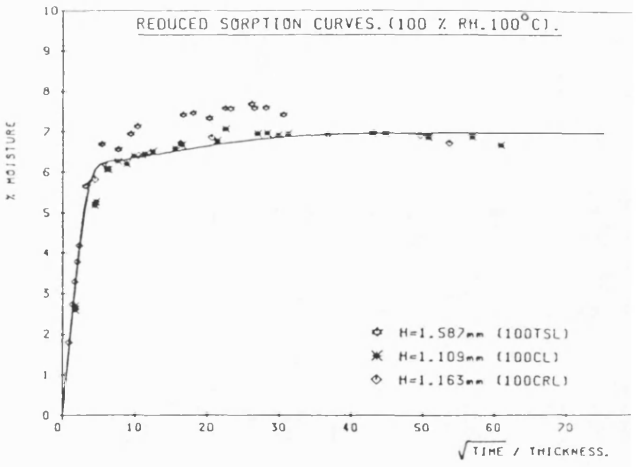

Figure 8.14 Reduced sorption curves for all the samples conditioned at 100% Rh, 100°C.

One of the requirements for Fickian diffusion is that when the initial concentration (M1) and the final concentration (Mn) are fixed, then a series of sorption curves for specimens of different thicknesses should render themselves superimposable on a single curve if each curve was plotted in the form of a reduced sorption curve (normalized to the respective specimen thicknesses). Reduced sorption curves for samples conditioned at 50°C and 100°C are presented in Figures 8.13 and 8.14. It is evident that the above mentioned criteria for Fickian diffusion is not satisfied. Reasons for deviations from Fickian behaviour were dealt with in the literature review.

Figure 8.15 represents a plot of sorption experiments carried out to investigate the 'reverse thermal effect' (RTE), a term coined by Adamson[142]. He found that on exposing a specimen

that had achieved an equilibrium moisture concentration at a specified temperature showed a further increase in the moisture concentration if the conditioning temperature was subsequently lowered. This is of significance as most fatigue work on pre-saturated samples conditioned at the higher temperatures are stored at ambient temperatures prior to testing. Furthermore, in practice, the reverse thermal effect can also have a significant effect on component life times. With reference to Figure 8.15, it is seen that on lowering the conditioning temperature from 100°C to 25°C resulted in 2% increase in the moisture content in the specimens. This is inspite of the fact that an apparent equilibrium moisture content had been reached at the higher temperature. A subsequent increase in the conditioning temperature from 25°C back to 100°C resulted in the loss of the moisture that was previously gained at 25°C.

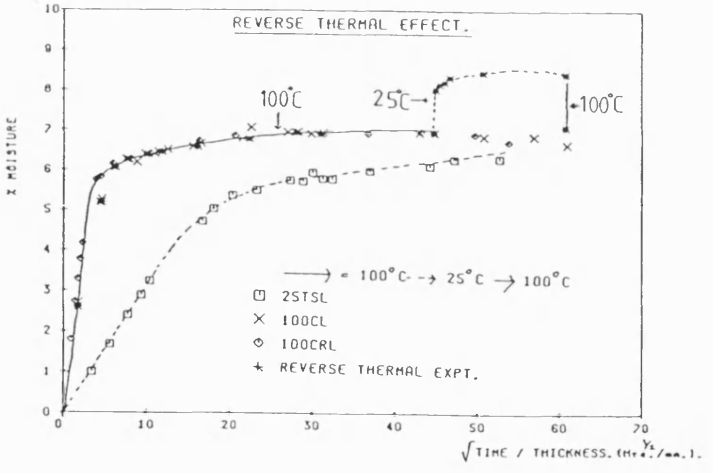

Figure 8.15 Illustration of the Reverse Thermal Effect (RTE) for the neat 914 resin system.

Adamson[142] proposed the following explanation to account for the (RTE). For a dry resin, the specific volume, (V) is the

sum of the occupied volume, (Vo) and the free volume, (Vf). The free volume (Vf) of a glassy polymer at the glass transition temperature, (Tg) was estimated to be 2.5% of the specific volume. On cooling the resin from a temperature (Tb) (below Tg) to a lower temperature, (Ta), the specified volume of the resin was said to decrease, see Figure 8.16. Adamson assumed that that the total volume contraction of the resin was less than that expected from a thermally induced contraction of the occupied volume. The remaining volume was said to be the nonequlibrium volume component of the free volume. Adamson proposed that this nonequlibrium volume component could be added to the equilibrium free volume, thus, making the total free volume greater at the lower temperature, see Figure 8.16.

It was previously seen that the initial diffusion of moisture into the neat resin samples was very rapid; Adamson suggested that the sorbed moisture, in the initial stages, filled the free volume of the resin. Other researchers too have found that the specific volume of the resin increased significantly less than the volume of water that was absorbed. Once the free volume within the resin was filled with water, the moisture sorption was said to slow down (as observed in this study) as equilibrium was reached accompanied by the swelling of the resin. Adamson suggested that the moisture could combine with the occupied volume to produce an equilibrium volume component as a result of swelling,(Vs), see Figure 8.16.

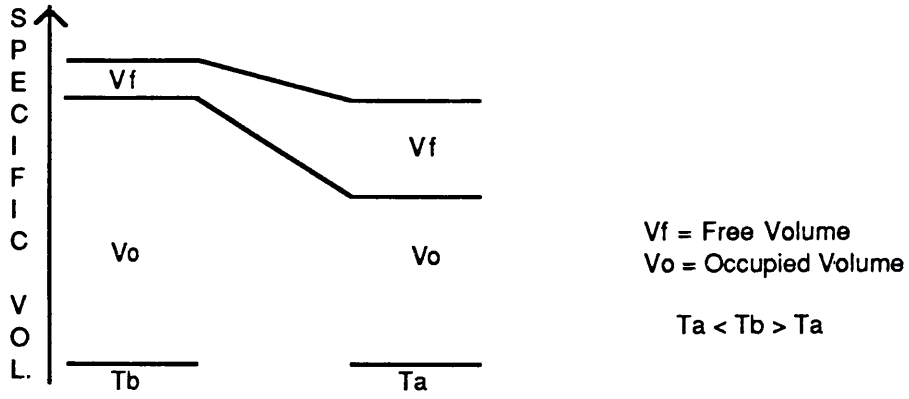

Figure 8.16 Illustration of the volume components at two temperatures (Ta and Tb) below the glass transition temperature. Copied from reference number 142.

Adamson's[142] explanation for the Reverse Thermal Effect is explained with reference to Figure 8.17. On reducing the conditioning temperature from 100°C to 25°C, the free volume in the resin increases. The moisture that previously (at 100°C) had occupied the swelling volume is now capable of filling the free volume created by the reduction in conditioning temperature. The right hand side of Figure 8.16 illustrates the case where the resin continues to absorb moisture at the lower temperature of 25°C until equilibrium is established. Increasing the conditioning temperature from 25°C back to 100°C would result in the contraction of the free volume and the swelling volume. As a consequence of this, the moisture (from the previous equilibrium value at 25°C) would be forced out of the free volume and swelling volume, and the moisture content is returned to its equilibrium value that was previously attained at 100°C.

The temperature dependence of the diffusion coefficient can be expressed by an Arrhenius type relationship, described as

equation [2.38]. Figures 8.18 and 8.19 represent the Arrhenius plots for Fickian and Dual Sorption (DMS) respectively. The linearity of these plots was taken as an indication that a single mechanism was responsible for the moisture diffusion over the range of temperatures investigated[208]. A summary of the diffusion parameters for the 914 neat resin system are presented in Table 8.1.

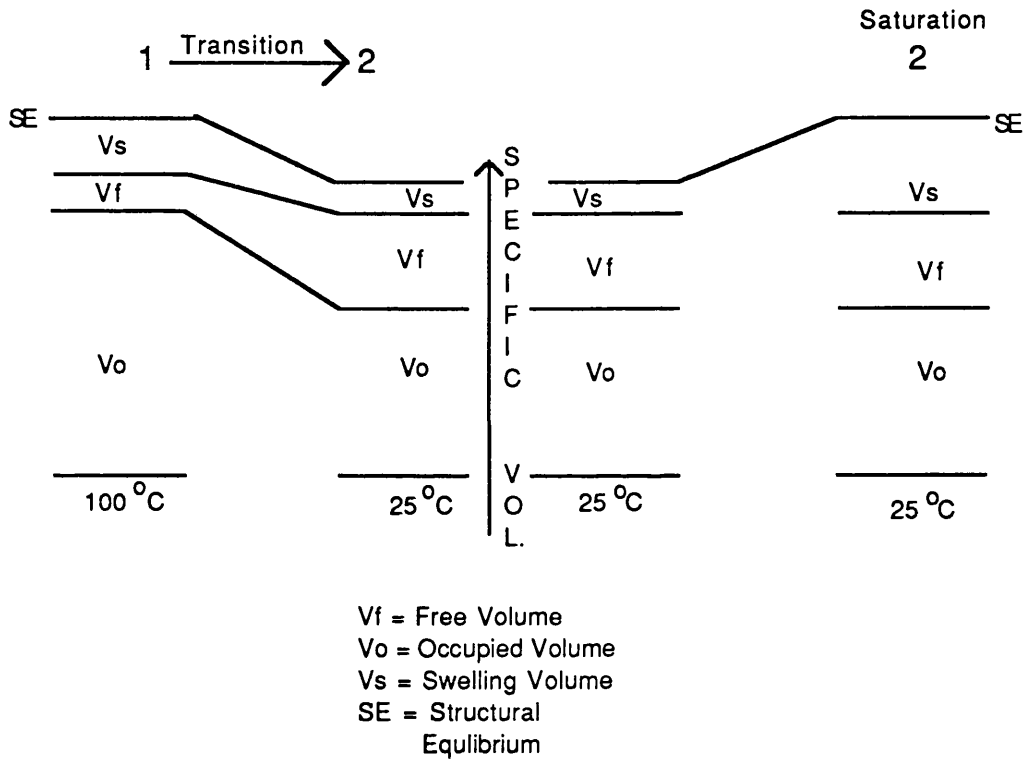

Figure 8.17 Adamson's[142] explanation from the Reverse Thermal Effect in polymer resin systems, see text form explanation.

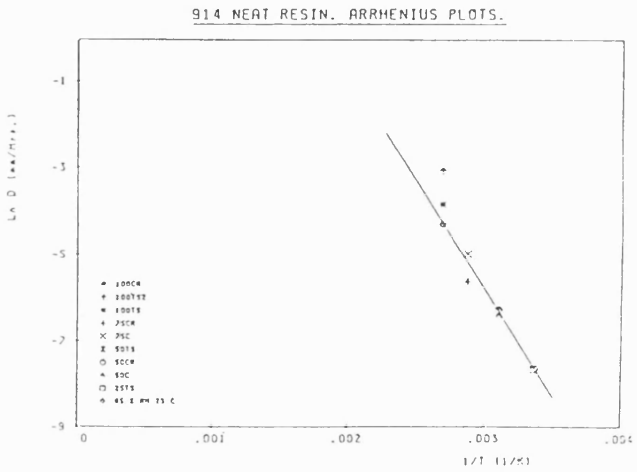

Figure 8.18 Arrhenius plot for the neat resin using the Fickian model diffusion coefficients.

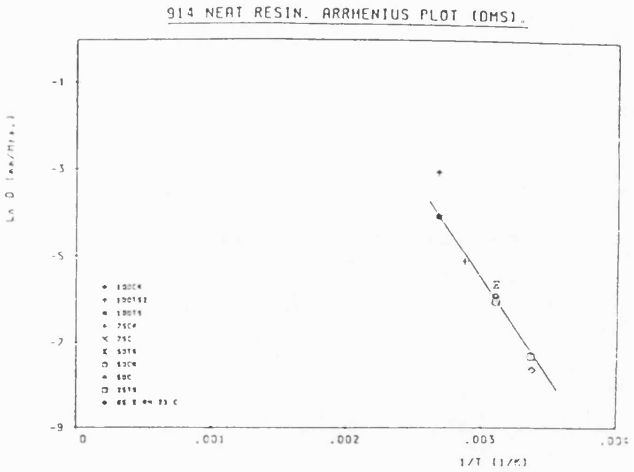

Figure 8.19 Arrhenius plot for the neat resin using DMS diffusion coefficients.

Conditioning Environment (code)	Average Thickness (mm)	Mn (%)	Diffusion Coeff. (mm^2/Hrs)	α (sec^{-1})	β (sec^{-1})
65% Rh 23°C	1.58	2.94	$4.85*10^{-4}$	$1.21*10^{-4}$	$1.89*10^{-3}$
100% Rh 25°C (25TS)	1.59	6.32	$4.76*10^{-4}$	$8.15*10^{-5}$	$0.05*10^{-4}$
100% Rh 50°C (50CR)	1.13	6.42	$1.88*10^{-3}$	$7.5*10^{-5}$	$6.2*10^{-4}$
100% Rh 50°C (50TS)	1.57	6.93	$1.78*10^{-3}$	$1.95*10^{-4}$	$5.6*10^{-4}$
100% Rh 50°C	1.13	6.72	$1.65*10^{-3}$	$2.5*10^{-4}$	$8.0*10^{-4}$
100% Rh 75°C (75CR)	1.16	7.43	$3.57*10^{-3}$	$2.6*10^{-4}$	$8.9*10^{-4}$
100% Rh 75°C	1.16	7.21	$6.79*10^{-3}$	$2.6*10^{-4}$	$6.9*10^{-4}$
100% Rh 100°C (100CR)	1.16	6.99	$1.35*10^{-2}$	$2.6*10^{-4}$	$2.1*10^{-3}$
100% Rh 100°C (100TS1)	1.59	7.68	$1.23*10^{-2}$	$2.6*10^{-4}$	$1.7*10^{-3}$
100% Rh 100°C (100TS2)	1.59	6.78	$4.65*10^{-2}$	-	-

Table 8.1 Moisture sorption data for the 914 neat resin system.

8.2 Effect of Absorbed Moisture on Neat Resin Properties

8.2.1 Glass Transition Temperature (Tg)

The glass transition (Tg) measurements were obtained on a Perkin Elmer DSC model-1B. All the tests were performed in a nitrogen atmosphere. The instrument was calibrated for temperature and enthalpy using tin and indium [92,143].

A number of trials on the neat resin were carried out to establish the optimum instrument settings to detect the glass transition temperature (Tg) of the 914 resin system. The following instrument settings proved to be satisfactory:

Range = 4-16 Mcal/sec;
Scan speed = 16^{o}C/min;
Chart speed = 20-40mm/min;
Slope setting = 6.8;
Gas flow = 25cc/min.

Figures 8.20(a) illustrates the first DSC scan for the neat (dry) Fiberdux 914 resin system. With reference to Figure 8.20(a), the glass transition temperature was defined as the mid-point of the change in the slope of the DSC trace[144]. In other words, the Tg was defined by the mid-point of the line (CD). The non-linearity of the line (AC) in the vicinity of point (B) may be due to the presence of a small concentration of absorbed moisture in the resin. However, the second and third DSC scans also indicated the presence of a change in the base line around 375K, thus implying that region (B) may

be indicative of a glass transition of one of the constituents of the resin system. All the first DSC scans of the neat (dry) resin exhibited a small plateau region (DE); however, on subsequent scans (using the same sample) this plateau region was extended, see Figure 8.21. This may have been due to further chemical reactions taking place at this temperature range. Therefore, the line (EF) may not represent the onset of thermal degradation in the resin. The second and third scans were carried out to investigate if the resin had undergone any significant degradation as a result of the previous thermal excursions, see Figures 8.21.

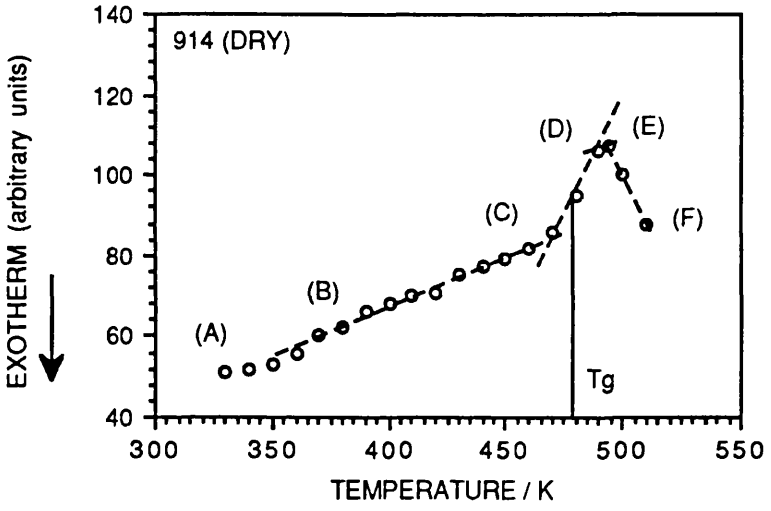

Figure 8.20(a) Illustration of a typical first DSC scan for the neat (dry) Fiberdux 914 resin system (Reproduced from original DSC trace). See text for explanation.

The measured Tg values for the first, second and third DSC scans for the neat (dry) 914 resin system were as follows;

First DSC scan, Tg = 478K.
Second DSC scan, Tg = 481K.
Third DSC scan, Tg = 482K.

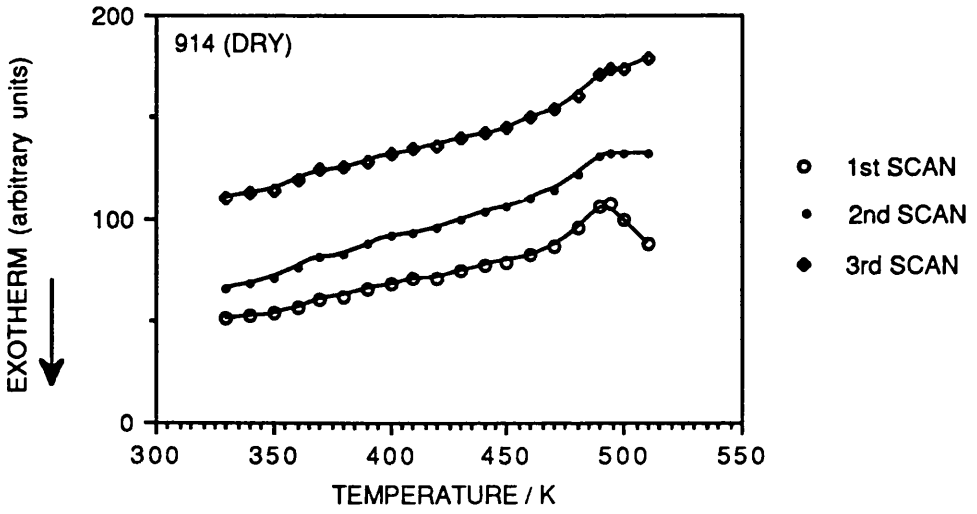

Figure 8.21 Illustration of typical DSC traces for the 914 resin system showing the first, second and third consecutive DSC scans.

The small difference in the Tg from the first, second and third DSC scans was assumed not to be significant and the first-scan Tg value of 478K was used as the reference standard for the dry 914 resin. It has to be pointed out that the Tg value quoted by the manufacturer[86] for the 914 resin system was 453K. It is difficult to account for the difference in the Tg quoted by the manufacturer and that obtained in this study. Over a dozen first-scans were performed on the neat (dry) resin in this study and a consistent Tg value of 478K was obtained. Furthermore, the calibration with tin and indium verified that the temperature scale was accurate to within a degree. The Tg value obtained in this study is consistent with those quoted by other researchers for aerospace epoxy resins, eg. Deiasi and McKague (see reference number 194).

The effect of absorbed moisture on the 914 resin system are illustrated in Figures 8.22-8.29. The Tg was lowered by approximately 10°K per percent of moisture uptake. The saturation moisture content in the samples was approximately 7%. Equation [2.46] was fitted to the experimental data and a good fit was obtained for the specimens conditioned at 50°C. The value, (K), in equation [2.46] was chosen to give the best fit curve.

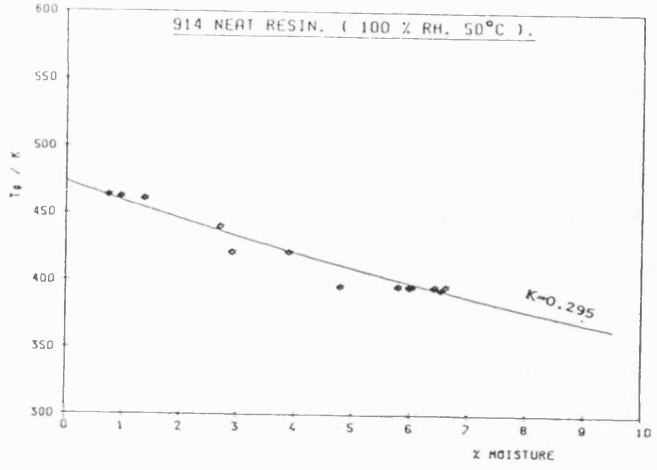

Figure 8.22 Effect of absorbed H_2O on Tg in the neat 914 resin. Samples conditioned at 50°C, 100% RH.

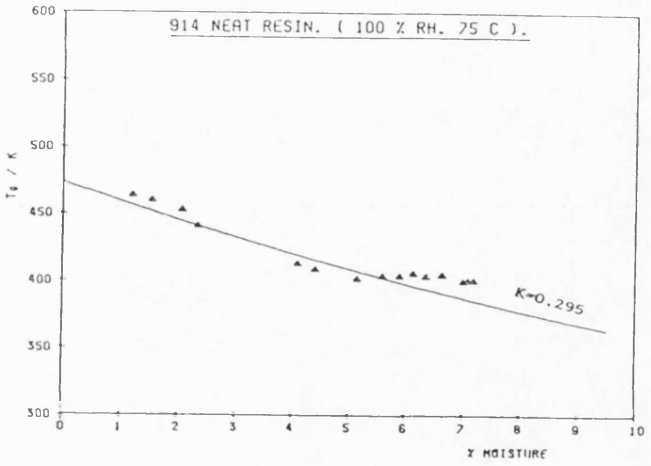

Figure 8.23 Effect of absorbed H_2O on Tg in the neat 914 resin. Samples conditioned at 75°C, 100% RH.

With reference to Figures 8.22 - 8.25 the following general comments can be made. The relationship between the Tg and the absorbed moisture exhibited a three stage behaviour. The first stage corresponded to a moisture concentration of approximately 1.5%. Here the Tg did not showed only a small reduction with absorbed moisture. The second stage corresponded to approximately 1.5% - 5.5% absorbed moisture and a steady decrease in the Tg was observed over this

moisture concentration. After approximately 5.5% of absorbed moisture, the Tg exhibited an apparent stablisation although a further increase in moisture concentration was recorded. Figure 8.25 suggest that specimens conditioned at higher temperatures resulted in the Tg being lowered to a greater extent for a given amount of moisture. However, this trend was reversed after prolonged conditioning. Further research is required to investigate this phenomenon further.

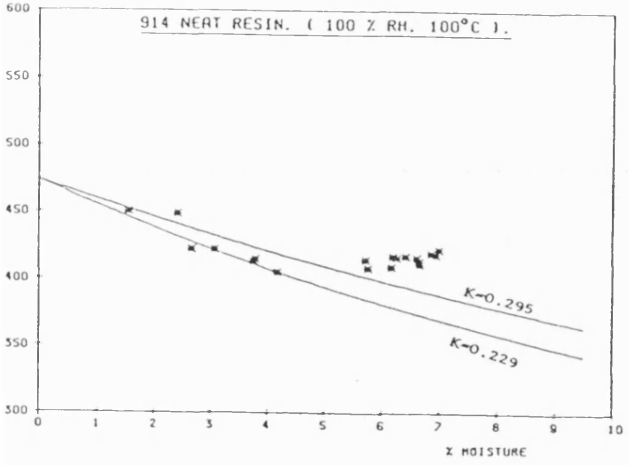

Figure 8.24 Effect of absorbed H_2O on Tg in the neat 914 resin. at 100°C, 100% RH.

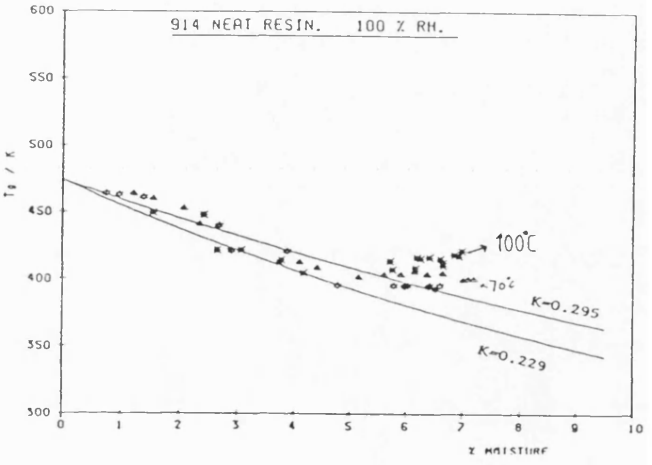

Figure 8.25 Effect of H_2O on Tg - combined plot for the three temperatures investigated.

Figure 8.24 shows that for the 100°C conditioned samples, the (K) value of 0.295 which was used to describe Tg lowering for the 50°C and the 75°C was inadequate. A lower value of 0.229 was found to describes the Tg lowering more closely upto about a moisture content of about 4%. The model used here does not directly take into account the mode of moisture introduction into the resin. The integrity for the resin

conditioned to saturation (around 7%) will depend on the conditioning temperature, the higher the temperature the greater was the degradation. Hence the mode of moisture introduction (conditioning temperature) may be reflected in the K value, ($K=Cp/p$), where Cp = heat capacity and p= density. Moy[233] showed that (K) decreased with increasing crosslink density. Some researchers invoke the idea of additional cure to take place as a result of the absorbed moisture. This is highly unlikely for the resin system under investigation because of the reactive nature of the hardener with the moisture. The possibility of low molecular weight products and unreacted resin components being leached out and the effect of this on Cp needs further investigation. It is reasonable to assume than regions of low crosslink density or areas of unreacted monomers in the resin will be degraded first under hygrothermal conditioning. If these regions/segments are preferentially attacked and leached out then the resultant polymer will possess a more uniform crosslink structure and this may result in a lower Cp value. Further detailed research is necessary to address this issue.

It must be remembered that the Tg data were obtained under non-equilibrium conditions. In other words, the concentration of penetrant decreases throughout the experiment as the sample is scanned from the ambient to about 200^{o}C. This is inevitable in an experiment of this nature. The obvious implication is that the measured Tg lowering by this method will underestimate the extent of plasticisation.

Another point to note is that the resin samples were not conditioned to saturation prior to testing. The Tg lowering

was measured as a function of moisture uptake. This means that the samples which were not conditioned to saturation would exhibit a moisture concentration gradient. This can be problem for specimens with a low percentage of moisture, resulting once again in an underestimation of the extent of plasticisation. The concentration gradient in the sample along with moisture evaporation may account for the higher than predicted values for Tg in the initial stages of the sorption experiments i.e. with low moisture contents.

It is also evident from Figures 8.22-8.25 that equation [2.46] does not predict the observed Tg lowered cut-off, i.e. after about a 4-5% moisture uptake the extent of plasicisation does not increase with the increase in the pentrant concentration. This phenomenon has been observed by other researchers[228,230] however no explanation was given. Moy's[233] explanation of the plasticicsation phenomenon of epoxies by sorbed moisture may hold the answer to the observed Tg cut-off. Moy suggest that H-bond formation is set-up between the water molecules and the polar functionalities in the cross-linked resin network. As water molecules are introduced into the network some degree of exchange was said to take place between the hydrogen bonded groups and the water molecules. On raising the temperature of the system, the relative difference in mobility between polymer segments and the water molecules becomes significant. The hydrogen bonds containing water bridges will be weaker and will therefore dissociate at lower temperatures. This in turn will initiates premature segmental flexing in the polymer chain introducing fluctuations in the free volume. This results in the lowering of the Tg.

Now, from the above discussion, the observed Tg cut-off may be accounted for as follows: if H-bond disruption is the major cause for the plasticisation effect, then a given volume of material will contain a specific number of hydrogen bondable sites. Once all these sites are consumed any further increase in moisture concentration will not have significant effect on the Tg. A somewhat similar observation was reported by Deiasi[208] with regards to the relationship between moisture concentration and the lowering of the Tg for a resin system which contained inorganic fillers. A relatively higher Tg than that predicted was experimentally measured. He proposed that a substantial portion of the total absorbed water was absorbed on the surface of the filler and therefore did not contribute to the mechanism by which the Tg was lowered. Deiasi also proposed that the formation of water clusters at the surface of the fillers or the phase boundaries could lead to a cut-off in the Tg with increasing moisture concentration. These water clusters were said to be highly organized, extending several molecular layers. These water clusters were said not to contribute to the lowering of the Tg. The 914 resin system used in this study contained particles of polyether sulphone particles. These particles were seen to be dislodged during fatigue testing and as a consequence of prolonged conditioning at 100^{o}C. This implies that the bonding between the polethersulphone particles and the base resin have been relatively weak, thus permitting water cluster formation at the interface. There may also be affinity of the absorbed moisture to the polyethersulphone (PES) particles as a result of the polarity of the PES particles. Microcracking in the resin was not detected in any of the contitioning

temperatures investigated.

The presence of unreacted hardener (DICY) particles in the 914 resin system has been observed and reported by a number of researchers[249-252]. Jones et al[249] found that the residual hardener concentrations correlated with the maximum water absorption for specimens conditioned at 50°C. They concluded that leaching of DICY from the composites in long term sorption experiments meant that true equlibrium and meaningful diffusion coefficients could not obtained.

Figures 8.26 - 8.28 illustrate the relationship between the measured Tg versus the conditioning temperatures at 50°C, 75°C and 100°C respectively.

The lowering of the Tg with increasing conditioning time (and moisture concentration) is readily apparent. With reference to Figure 8.29 the following conclusion can be made.

The lowering of the Tg for the 914 resin with conditioning time exhibited a three stage behaviour. Region (A) in Figure 8.29 represents a relatively slow drop in the Tg with conditioning time. Region (B) represents a rapid drop in the measured Tg with conditioning time. The relative decrease in the Tg was higher for the 100°C conditioned specimens followed by the 70°C and 50°C conditioned specimens. Region (C) illustrates the region where a slight increase in the Tg was observed with conditioning time. This increase in the Tg was greatest for the 100°C conditioned specimens followed by the 75°C and the 50°C conditioned specimens. The reasons for this apparent increase in the Tg with prolonged conditioning

time may be due to aging effects in the resin system. Further work is require to investigate and understand this increase in the Tg with conditioning time.

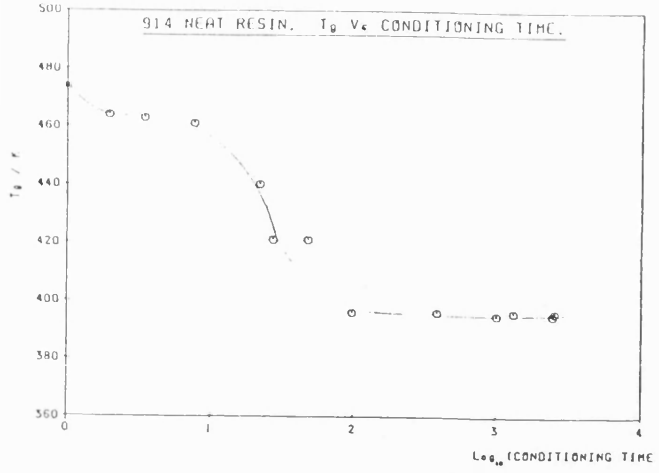

Figure 8.26 Effect of absorbed H_2O on Tg in the neat 914 resin. Plot of conditioning time vs. Tg. (50°C, 100% RH).

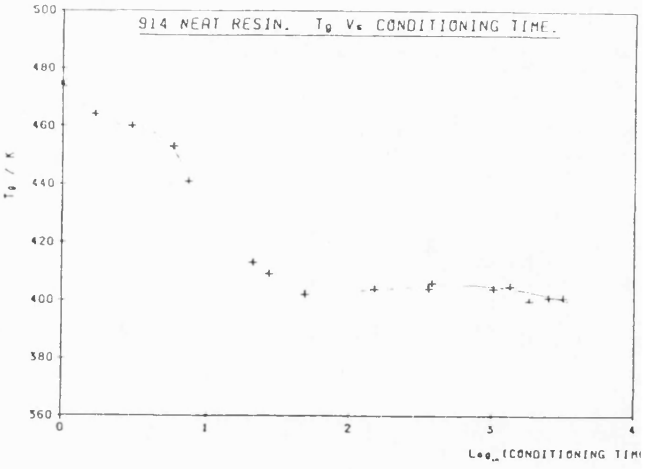

Figure 8.27 Plot of Tg versus conditioning time for the neat 914 resin. (75°C, 100% RH)

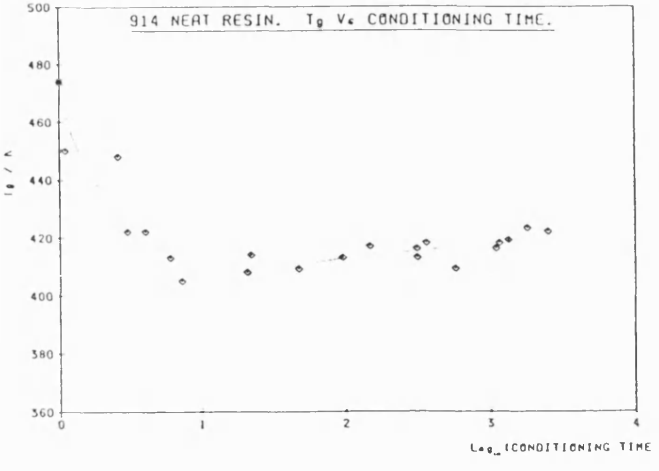

Figure 8.28 Plot of Tg versus conditioning time for the neat resin. (100°C, 100% RH).

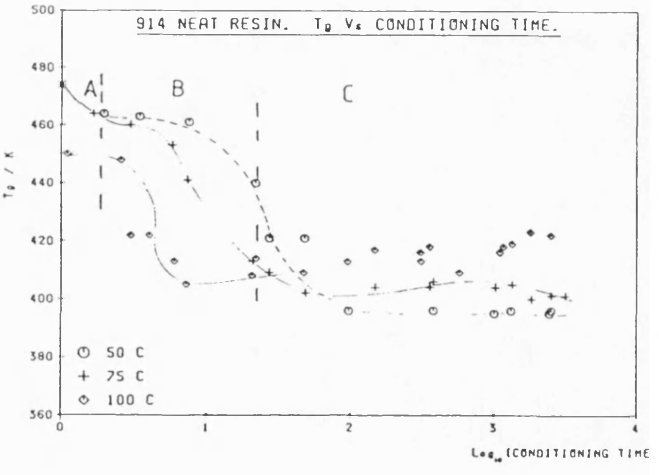

Figure 8.29 Combined plot of the data from the three previous figures.

8.3 MOISTURE ABSORPTION CHARACTERISTICS OF THE XAS AND KEVLAR MONO-FIBRE AND HYBRID COMPOSITES.

8.3.1 Diffusion Of Moisture In The Mono-Fibre Composites

The diffusion studies on the mono-fibre and hybrid composites were carried out under total immersion, i.e. 100% RH. The specimen edges were sealed with a moisture resistant lacquer. The 75°C and 100°C conditioning were carried out in reflux flask. These tests were terminated after 625 hours as a consequence of the water supply to the reflux condensers being turned off. Figure 8.30 illustrate the moisture absorption characteristics of the unidirectional, ± 45° and 90° Kevlar composites at 50°C, 75°C and 100°C. As expected, the lowering the conditioning temperature from 100°C to 50°C a reduction in the diffusion coefficient was observed, see Table 8.2. With reference to Figure 8.30, the dependence of the diffusion coefficient on the fibre angle is also apparent. During the initial sorption period the ± 45° Kevlar/914 composite exhibited the highest diffusion coefficient. However, with longer exposure, the maximum moisture content for the ± 45° Kevlar/914 composite was lower than the unidirectional composite at the three temperatures investigated in this programme. The 90° Kevlar/914 composite exhibited the lowest diffusion coefficient and the lowest maximum moisture concentration.

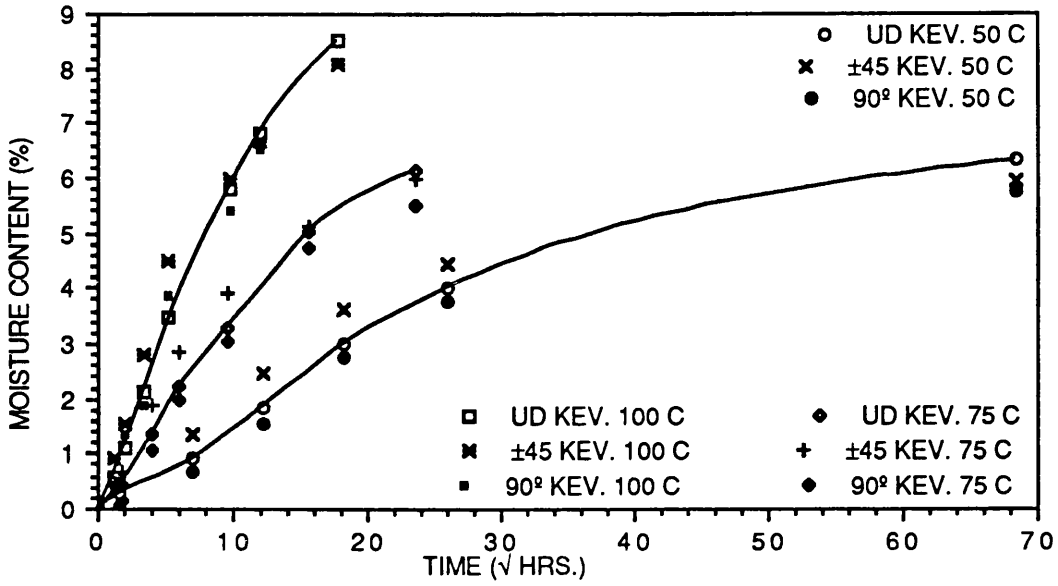

Figure 8.30 Moisture content as a function exposure time, conditioning temperature and fibre angle for Kevlar/914 composite - 100% RH. Lines were fitted through the data points for all the unidirectional composites at the three temperatures.

Kevlar/914	UD	±45°	90°	Pure Resin
	Diffusion Coefficient (mm^2/Hrs.)			
100°C	0.0069	0.013	0.006	0.0129
75°C	0.0049	0.0081	0.0047	0.00518
50°C	0.00070	0.00135	0.00064	0.00177

Table 8.2 Summary of diffusion coefficients for the Kevlar/914 composite.

The diffusion coefficients quoted in Table 8.2 were obtained

using equation [2.37], the diffusion coefficients for the neat resin at the relevant temperatures are also listed. The diffusion of moisture in the Kevlar/914 composite was not accurately predicted by Fickian diffusion. Even after 47600 hours of conditioning at 50°C, an equilibrium moisture content was not observed. The data points presented in figure 8.30 (and subsequent diffusion data) are an average of three or more individual data points. The average specimen thickness and maximum moisture concentrations were used in the calculation of the diffusion coefficients. As mentioned previously, the 100°C and 75°C tests were prematurely terminated; therefore, the 50°C results will be used for comparing the diffusion behaviour in the XAS and hybrid composites.

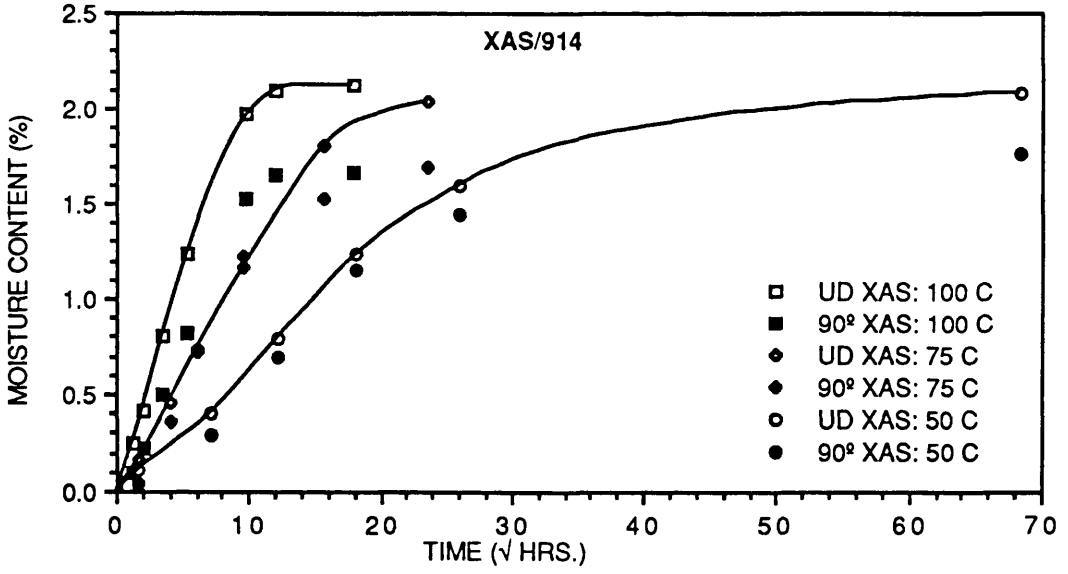

Figure 8.31 Measured changes in the weight for the initially dry unidirectional and 90º XAS/914 composite at the three conditioning temperatures.

Figure 8.31 illustrates the sorption behaviour for the XAS/914 unidirectional and 90º composites at 50°, 75° and 100°C. The

corresponding diffusion coefficients are listed in Table 8.3.

XAS/914	UD	90°	Pure Resin
	Diffusion Coefficient (mm^2/Hrs.)		
100°C	0.0099	0.006	0.0129
75°C	0.0029	0.0043	0.00518
50°C	0.00079	0.00083	0.00177

Table 8.3 Summary of diffusion coefficients for the XAS/914 composite.

Shen and Springer[196] proposed the following equation to describe the diffusivity (Dx) in the direction normal to the surface:

$$Dx = D_{11} \cos^2 a + D_{22} \sin^2 a \qquad [8.1]$$

where, (D11) and (D_{22}) are the diffusivities in the directions parallel and normal to the fibres (longitudinal and transverse) and (a) is the fibre angle relative to the surface.

Shen and Springer[196] proposed that the following equation could be used to calculate (Dx) from the diffusivity of the matrix (Dr) and the volume fraction of the fibres (Vf). It is assumed that the fibres do not absorb moisture.

$$Dx = Dr\ [(1-Vf) \cos^2 a + (1-2\sqrt{(Vf/\pi)}) \sin^2 a] \qquad [8.2]$$

Table 8.4 lists the calculated values for the diffusion

coefficients for the Kevlar/914 and XAS/914 using equation [8.2].

Temp.	Resin	ud XAS (EXPT.)	ud XAS (CALC.)	90$^{\emptyset}$ XAS (EXPT.)	90$^{\emptyset}$ XAS (CALC.) ($*10^{-3}$)	ud Kev (EXPT.)	ud Kev (CALC.)	90$^{\emptyset}$ Kev (EXPT)	90$^{\emptyset}$ Kev (CALC.)
50^{o}C	1.77	0.79	0.71	0.83	0.22	0.70	0.79	0.64	0.29
75^{o}C	5.18	2.9	2.1	4.3	0.65	4.9	2.3	4.7	0.85
100^{o}C	12.9	9.9	5.2	6.0	1.6	6.9	5.8	6.0	2.1

Table 8.4 Summary of experimental (EXPT) and calculated (CALC) diffusion coefficients for the unidirectional and 90$^{\emptyset}$ mono-fibre XAS and Kevlar/914 composites. The diffusion coefficients for the neat resin are also quoted.

A number of interesting features are readily apparent in Table 8.4. As expected, the diffusion coefficients increase with increasing temperature. The calculated diffusion coefficients using equation [8.2] gave a good agreement with the experimentally derived values for both the XAS and Kevlar composites at 50^{o}C. Surprisingly, the diffusion coefficients for the XAS and Kevlar/914 composites were similar. However, the major difference was in the moisture content at "equilibrium". The Kevlar/914 composite gave an equilibrium moisture content of 6.32% and the XAS/914 showed a moisture content of 2.09%.

8.3.2 Diffusion of Moisture in the Hybrid Composites

Figures 8.32, 8.33 and 8.34 illustrate the moisture absorption characteristics of the hybrid composites at 100°C, 75°C and 50°C respectively. The mono-fibre data is also represented to facilitate ease of comparison.

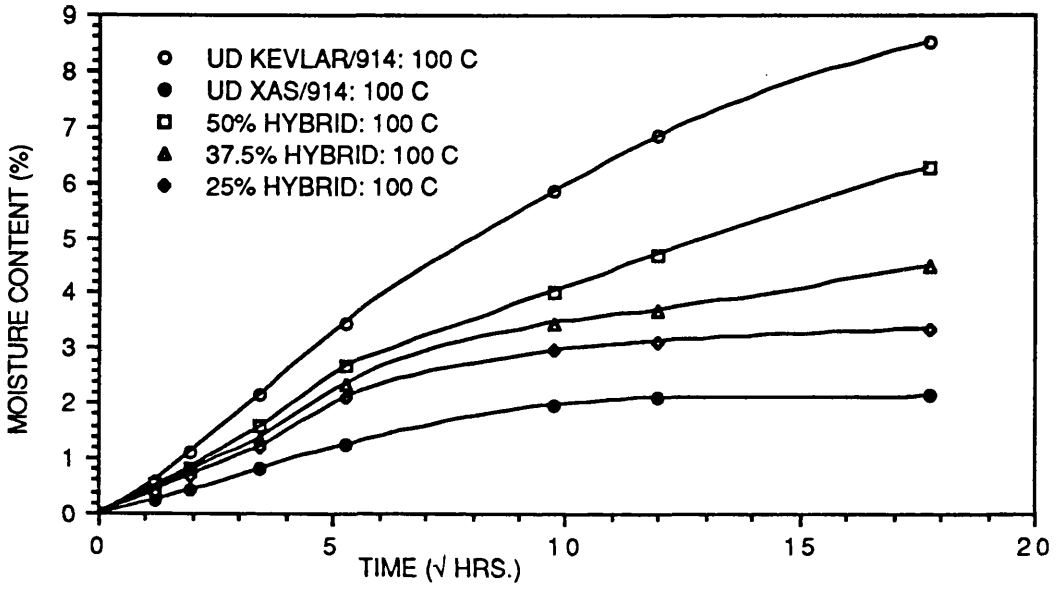

Figure 8.32 Percent weight gain versus exposure time at 100°C, 100% RH for the mono-fibre and hybrid composites.

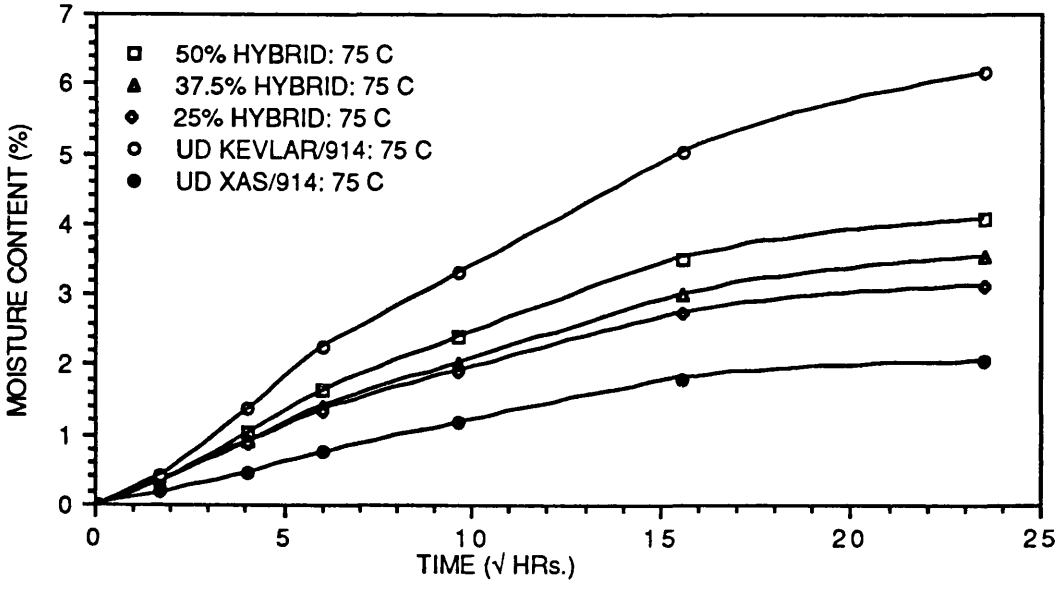

Figure 8.33 Percent weight gain versus exposure time at 75°C, 100% RH for the mono-fibre and hybrid composites.

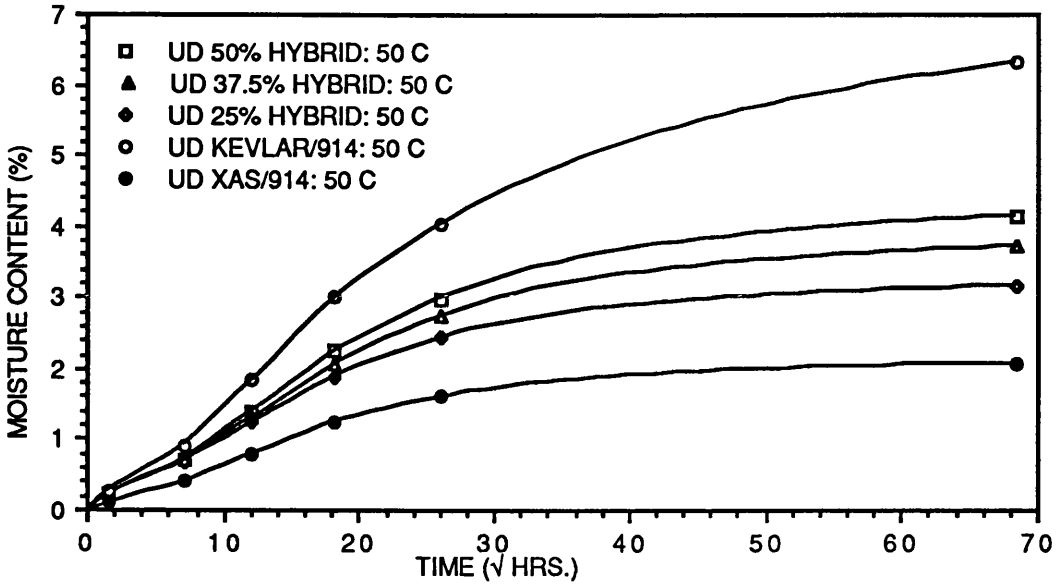

Figure 8.34 Percent weight gain versus exposure time at 50°C, 100% RH for the mono-fibre and hybrid composites.

Because of the non-Fickian diffusion behaviour of the mono-fibre Kevlar and hybrid composites, a comparison of the sorption behaviour of these materials was carried out in terms of the "equilibrium" moisture content subsequent to a specified conditioning time. The equilibrium moisture content presented in Figure 8.35 for the 50°C data-set was obtained after 4682 hours of conditioning and a total conditioning time of 315 hours for the 100°C data-set. It is apparent from Figure 8.35 that a simple rule of mixtures equation can be used to obtain the equilibrium moisture content of the hybrids from the mono-fibre data at 50°C.

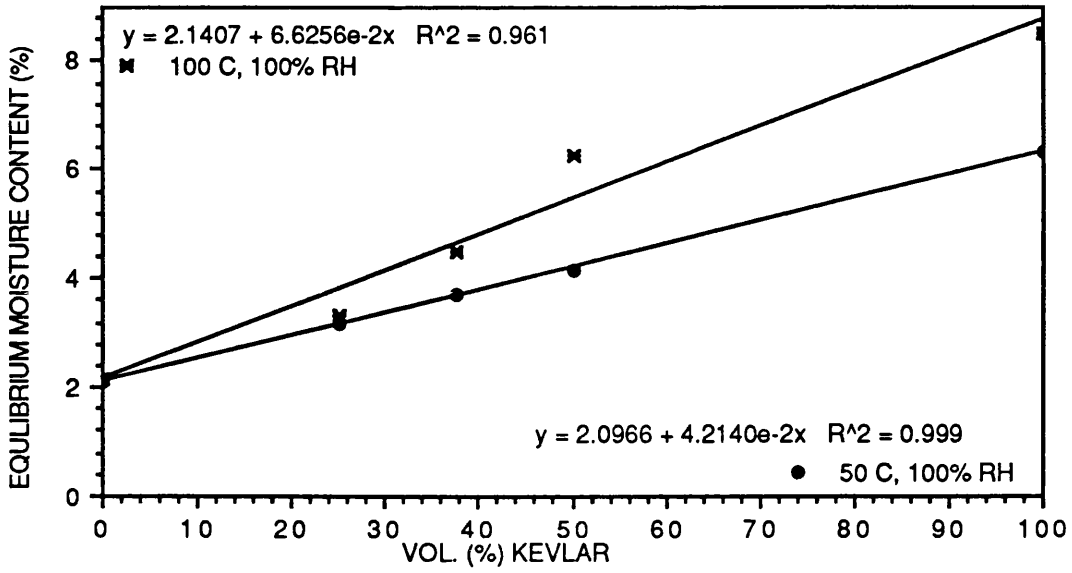

Figure 8.35 Equilibrium moisture content versus hybrid composition for samples conditioned at 50°C and 100°C.

Figure 8.36-8.38 illustrate the differences in the sorption behaviour of the 90° and unidirectional and hybrids at 50°, 75° and 100°C for the 50%, 37.5% and 25% hybrids respectively. The 50% and 37.5% 90° specimens exhibit a slightly higher diffusion coefficient compared to the unidirectional specimens; in the mono-fibre composites, the opposite was true.

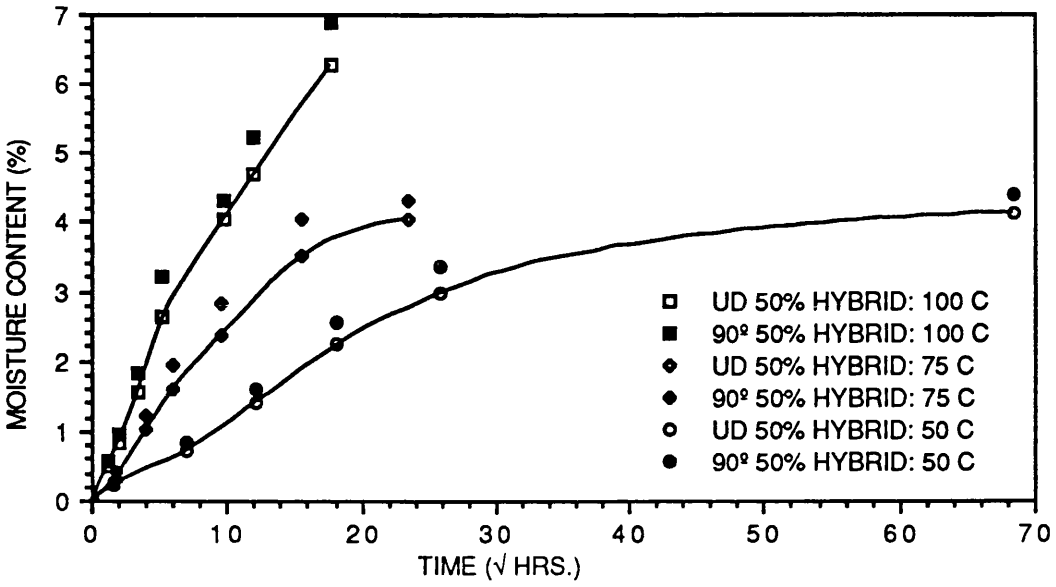

Figure 8.36 Illustration of the differences in the sorption behaviour of the unidirectional and 90$^{\emptyset}$ specimens for the 50% hybrid composite as function of conditioning time at 50^{o}, 70^{o}, 100^{o}C.

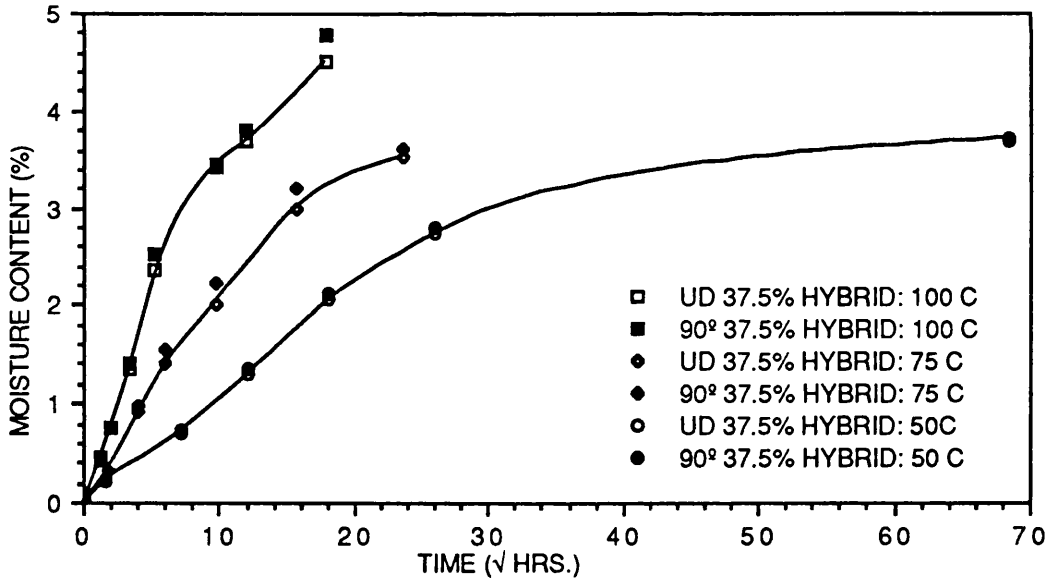

Figure 8.37 Illustration of the differences in the sorption behaviour of the unidirectional and 90$^{\emptyset}$ specimens for the 37.5% hybrid composite as function of conditioning time at 50^{o}, 70^{o}, 100^{o}C.

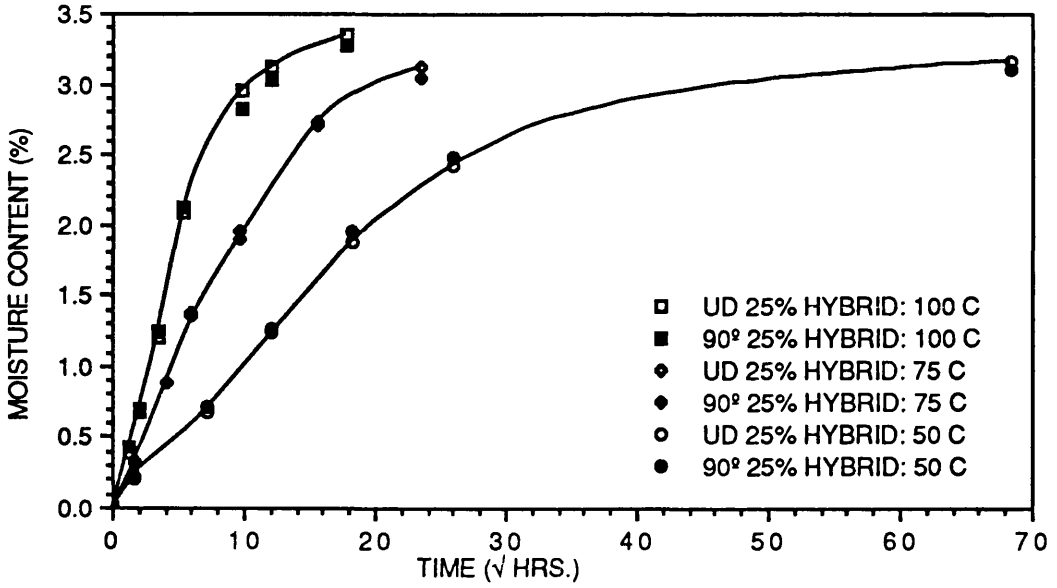

Figure 8.38 Illustration of the differences in the sorption behaviour of the unidirectional and 90$^{\emptyset}$ specimens for the 25% hybrid composite as function of conditioning time at 50^{o}, 70^{o}, 100^{o}C.

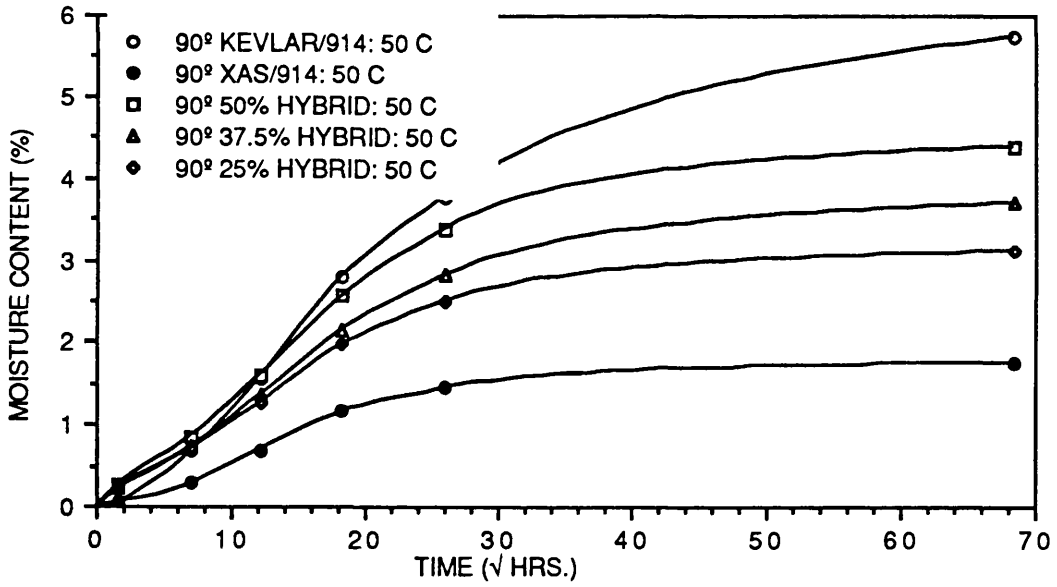

Figure 8.39 Combined representation of the sorption data for the 90$^{\emptyset}$ mono-fibre and hybrid composites at 50^{o}C.

8.4 Effect of Absorbed Moisture On Composite Properties.

8.4.1 Fatigue Behaviour

A very limited number of fatigue tests were carried out on specimens pre-conditioned at 100°C. The results of these tests are presented in Figures 8.40 and 8.41.

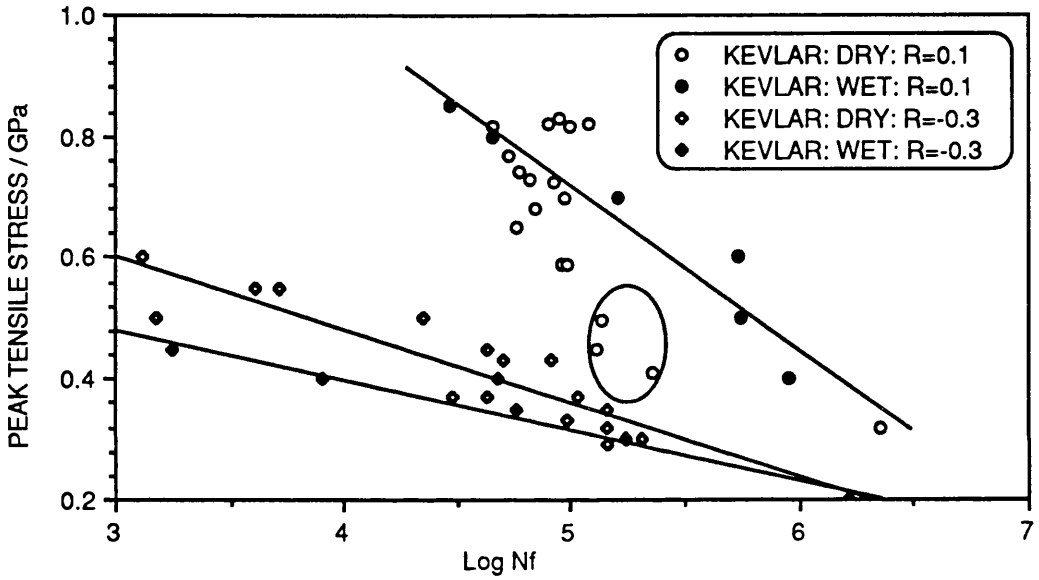

Figure 8.40 Effect of absorbed moisture on the fatigue response of the mono-fibre Kevlar composite. The wet samples were conditioned for two weeks at 100°C, 100% RH. See text for explanation.

With reference to Figure 8.40, the data for the fatigue response of the wet specimens at (R=0.1) seemed to be significantly better than that observed for the dry specimens. However, the uncertainties in the characterization of the fatigue curve for the ud Kevlar/914 mono-fibre composite were discussed in detail in a previous section. If a three stage fatigue response is assumed, (i.e., Regions I, II, and III,

including the three circled data points) then a significant improvement in the fatigue response at (R=0.1) is apparent for the wet specimens compared to dry specimens. On the other hand, if a two stage fatigue response is assumed for the dry mono-fibre kevlar/914 composite, the improvement in the fatigue response of the wet specimens is only marginal over those of the dry specimens. The wet specimens exhibited a two stage fatigue behaviour. This observation further strengthens the case for a two stage fatigue response for the dry mono-fibre Kevlar/914 composite.

Under tension/compression loading at (R=-0.3) a deterioration in the fatigue response of the wet specimens compared to the dry specimens was observed. This degradation of the T/C fatigue properties in the mono-fibre Kevlar and 50% hybrid composite properties is probably due to plasticisation of the matrix and the Kevlar fibres themselves. Plasticisation of the matrix would also lower matrix yield stress.

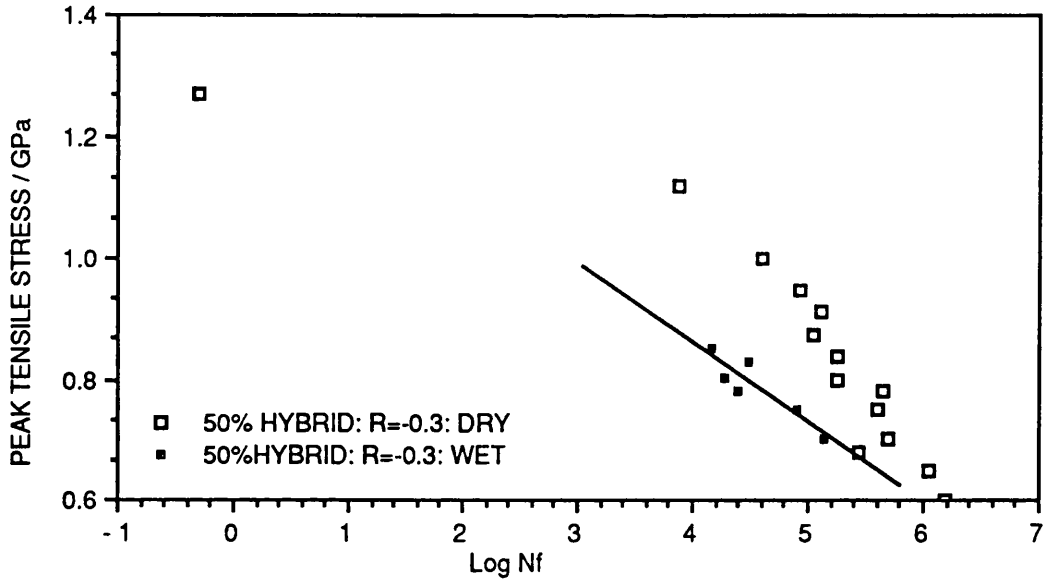

Figure 8.41 Effect of absorbed moisture on the tension/compression fatigue response of the 50% hybrid composite. The wet samples were conditioned for two weeks at 100°C, 100% RH.

The apparent increase in the fatigue behaviour of the "wet" Kevlar composite has also been reported by other researchers, for example, Roylance[112,149] and Jones[88]. Roylance proposed that the swelling of the matrix as a consequence of the absorbed moisture led to relieving the locked-in fabrication stresses. Roylance also suggested that the plasticization of the matrix by the absorbed moisture facilitated local flow for realignment of the fibres under load.

9 CONCLUSIONS

The static tensile, tension/tension and tension/compression fatigue response of mono-fibre and hybrid XAS/914 and Kevlar/914 fibre reinforced composites was investigated in this project.

The XAS/914 mono-fibre composite exhibited a non-linear stress-strain curve with the modulus increasing with applied strain and stress. Longitudinal modulus increases of between 6-21% were recorded. It was speculated that the observed stiffening effect may have been due to the initial waviness of the fibre crystallites and subsequent straightening out of these crystallites with applied stress. The Kevlar/914 mono-fibre composite exhibited longitudinal modulus increases of up to 5%.

The fibre volume fractions for the XAS and Kevlar mono-fibre composites was 60% and 55% respectively. A wider fibre volume fraction range was observed for the Kevlar composites along with some fibre waviness. The observed fibre waviness was in the plane of the composite panel and in the thickness directions. Polished longitudinal sections of the Kevlar mono-fibre composite exhibited the presence of regularly spaced transverse markings on the fibre surface. It was speculated that these markings may have originated as a consequence of compressive loading induced in the fibres resulting in the formation of bulges on the fibre surface.

The rule of mixtures equation was found to adequately

describe the tensile modulus for the hybrid composites investigated in this programme. However, the rule of mixtures approach over-predicted the tensile strength of the hybrid composites.

Linear regression lines were fitted to the experimental fatigue data points. The tension/tension fatigue response of the unidirectional XAS/914 mono-fibre composite composite was 'flat'. The slope of the S/Log (Nf) curve was -0.085; this corresponded to a fatigue strength reduction of 4.3% per decade of cycling. The fatigue life lines for the unidirectional mono-fibre Kevlar composite was initially represented by a 3 stages. However, further analysis indicated that the fatigue behaviour of the Kevlar composite was best represented by a two-stage fatigue life line. Stage 1 (Region I) was flat with a slope of -0.027; this extended to about 10^4 cycles after which a characteristic down-turn in the fatigue life or Stage 2 was observed.

Increasing the stress ratio from 0.1 to 0.5 was found to increase fatigue life times of the ud mono-fibre Kevlar composite. Reducing the stress ratio from 0.1 to 0.01 resulted in a worsening of the fatigue performance. Increasing the fatigue test temperature from ambient to 100^{o}C also resulted in a worsening of the fatigue performance for this composite.

The introduction of a compressive stress component into the fatigue load regime of the ud mono-fibre Kevlar composite resulted in a significant deterioration of the fatigue performance. Stress ratios of R=0.5,0.1,0.01,-0.3 and -0.6

were investigated for the Kevlar composite. A linear relationship was observed between the slopes of the fatigue life lines (Region II) and their corresponding stress ratios. An apparent convergence point was observed for the fatigue life line for this composite in the high cycle region.

The effect of lowering the fatigue stress ratio from 0.1 to -1.2 resulted in a worsening of the fatigue performance of the unidirectional XAS/914 mono-fibre composite. Once again a linear relationship was observed between the slopes of the fatigue life lines and their corresponding stress ratios. Superior linear regression line fits were obtained by including the ultimate tensile strength in the regression line calculations. Unlike the Kevlar composite, the XAS composite was best represented by a one-stage fatigue life line with the UTS acting as the reference point.

The fatigue response of the unidirectional 25% hybrid composite was found to resemble that of the XAS mono-fibre composite. In other words the fatigue behaviour was best described by a one stage fatigue life line and a superior linear regression line was obtained by including the ultimate tensile strength in the regression line calculations even for negative stress ratios. Once again, a linear relationship was observed between the slopes of the fatigue life lines and their respective stress ratios.

The fatigue response of the unidirectional 37.5% hybrid composite also resembled that of the XAS mono-fibre composite at the negative stress ratios investigated. However, at R=0.1, the fatigue data was best described by a two stage

fatigue life line; similar to the behaviour exhibited by the ud Kevlar mono-fibre composite.

The 50% hybrid composite exhibited a fatigue behaviour that was more akin to the response observed for the Kevlar composite than the XAS composite. The fatigue behaviour of this composite was best described by a two-stage fatigue life line. Increasing the stress ratio from R=0.1 to 0.5 was found to significantly improve the fatigue life times. Increasing the fatigue test temperature from ambient to 100^{o}C resulted in a deterioration of the fatigue performance.

Comparison of the fatigue behaviour of the hybrids against the mono-fibre composites by a simple rule of mixtures approach indicated that the fatigue performance of the hybrids at R=0.1 was superior than that of the rule of mixtures prediction at 10^5 and 10^6 cycles. The fatigue performance of the 25% and 37.5% hybrid was found to be marginally superior compared to the XAS mono-fibre composite at all the stress ratios investigated. The 50% hybrid composite exhibited a superior fatigue performance compared to the XAS composite at 10^5 cycles for all stress ratios investigated. However, a marginal decrease in the fatigue performance in the 50% hybrid compared to the XAS composite performance was observed for R=-0.3, -0.4 and -0.6 at 10^6 cycles.

The surface temperature rise in the specimens during fatigue testing was found to be a function of the peak stress, stress range and the cyclic frequency. A general trend observed in all the specimens was a very rapid rise in the surface

temperature at the commencement of the fatigue test. This was followed by a drop in the temperature and an equilibrium surface temperature being attained. A sharp rise in the surface temperature was observed just prior to failure. Surface temperature increases of up to 45^{o}C above ambient was recorded during fatigue testing of the unidirectional Kevlar composite.

The predominant failure mode observed for the ud Kevlar mono-fibre composite subjected to static tensile testing was longitudinal splitting, extensive intra-ply fibre defibrillation and inter-ply separation. Under T/T fatigue testing the extent of longitudinal splitting, fibre defibrillation and Guess was found to increase. The predominance of these failure modes under T/T fatigue loading was found to be a function of the applied peak stress.

The most predominant feature observed in the T/C fatigue tested ud Kevlar composites was the presence extensive surface abrasion damage on the Kevlar fibres. T/C specimens which experienced comparatively high compressive stresses exhibited a planar fracture surface.

The macroscopic failure modes observed for the XAS composite was transverse fracture followed by longitudinal splitting. Under T/T fatigue loading, longitudinal splitting was observed to develop early on in the fatigue life of the specimens. In general, the effect of these longitudinal cracks was to initiate delaminations of the surface plies into discreet strips. Under T/C loading, the rate of delamination development was observed to be greater compared

to T/T fatigue tested specimens.

No obvious differences were observed in the failure modes for the ud 50%, 37.5% and 25% hybrids compared to the mono-fibre composites. However, under T/C cycling, development of delamination patches on the outer Kevlar plies was observed. The development of these surface delaminations was observed to be a function of the stress ratio, peak stress and number of cycles. A mechanism to account for the formation of these delamination patches was proposed.

The diffusion of moisture into the neat 914 resin was modelled by using the Fickian and Dual Mode Sorption models. The Dual Mode Sorption model was found to accurately describe the diffusion of moisture in the neat 914 resin. The equilibrium moisture content in the hybrid composites was found to be a function of the volume fraction of Kevlar fibres.

No significant differences in the fatigue performance was observed between 'wet' and 'dry' ud Kevlar composite fatigue tested at R=0.1. However, a significant deterioration was observed in the 'wet' specimens when fatigue tested at R=-0.3. A similar trend was observed for the 'wet' and 'dry' 50% hybrid composite when subjected to fatigue testing at R=-0.3. A likely reason for deterioration of the T/C performance may have been due to the plasticisation of the matrix and the Kevlar fibres.

Infrared spectroscopy and Differential Scanning Calorimetry proved to be a very quick and effective way of monitoring the quality of prepregs prior to laying-up and processing.

REFERENCES

1 Belyea, M.O. and Deckman B.W.,
Materials and Design, Vol 9, No 2, p 78, (1988)

2 Steinberg, M.A.,
Scientific American, Vol 255, No 4, p 56, (1986).

3 Engineering Materials Handbook-Compsites, Vol 1, Section 12,Published by ASM International, (1987).

4 Zweben, C.,
Composites, Vol 12, p 235, (1981).

5 Short, D. and Summerscales, J.,
"Hybrids - a Review Part 1",
Composites, Vol. 10, No. 4, p 215, (1979).

6 Short, D. and Summerscales, J.
"Hybrids - a Review Part 2",
Composites,Vol. 11, No. 1, p 33, (1980).

7 Kulkarni, S.V., Rosen B.W. and Boehm, H.C.,
Evaluation of Hybrid CompOsite Material, AFML-TR-75-92, (1975).

8 Rose, P.G.,
Kungstoff Technic, Vdi-Verlaggmbh, Dussledorf, p 5, (1981).

9 Preston, J.,
Polymer Engineering and Science, Vol 15, No 3, p 199, (1975).

10 Dobb, M.G., Johnson D.J. and Saville B.P.,
Journal of Polymer Science, Vol 15, p 2201, (1977).

11 Dobbs M.G., Johnson D.J., Saville B.P.,
Journal of Polymer Science: Polymer Symposium, 58, p 237, (1977).

12 Dobbs M.G., Johnson D.J., Saville B.P.,
Phil. Trans. Royal Society London, A294, p 483, (1979).

13 Dobb M.G., Johnson, D.J. and Saville B.P.,
Polymer, Vol 20, p 1284, (1979).

14 Morgan R.J., Pruneda C.O. and Steele W.J.,
J. Polymer Sci., Polym Phys. Ed., Vol 21, p 1757, (1983).

15 Pruneda C.O., Steel W.J., Kershaw R.P. and Morgan R. J..
Composite Technology Reviews, 3(3), p 103, (1981).

16 Panar M., Aukian P., Blume R.C. and Gardner K.H.,
Journal of Polymer Science, Polymer Physics Edition, Vol 21,
p 1955, (1983).

17 Chamis C.C., Hanson M.P. and Serafini T.T.,
28th Annual Technology Conference - Reinforced Plastics/Composites Institute, The Society of the Plastics Industry Inc.

18 Agarwal B.D.and Broutman L.T.
"Analysis and Performance of Fibre Composites",
Wiley Interscience Publishers (1980).

19 Harris B.,
"Engineering Composite Materials", The Institute of Metals,
(1986).

20 Ishda H.L. and Roening J.L.(eds).,
Composite Interfaces, North-Hallord Publishers, p 333,
(1986).

21 Donnet J.B. and Ehrburger P.
Carbon, vol 15, p 143-152, (1977).

22 Jain M.K. and Abhiraman A.S.,
Journal of Material Science, Vol 22, p 278-300, (1987).

23 Penn L., Bystry F., Karp W., and Lee S.,
see reference No 20, p 93.

24 Hayashi, T.,
8th International Reinforced Plastics Conference, British Plastics Federation, Brighton, U.K., paper22, p 149, (1972).

25 Chou T.W. and Kelly A.
Annual Review Material Science, Vol 10, p 229, (1980).

26 Aveston J. and Kelly A.,
Phil. Trans. R. Soc. London, A 294, p 19, (1980).

27 Kalnin I.L.,
"Composite Materials: Testing and Design - 2nd Conference,
ASTM-STP 497, p 551, (1972).

28 Hancox N.L. and Wells H.
Composites, p 26, (1973).

29 Bunsell A.R. and Harris B.,
Composites, p 157, (1974).

30 Hancox N.L.(ed).,
Chapter 1, "Introduction to Fibre Composite Hybrids" in Fibre Composite Hybrid Materials, Applied Science Publishers Ltd., (1981).

31 "Fibre Reinforcements for Composite Material",Vol 2, Bunsell, A.R. editor, Elsevier Science Publications Co Inc.(1988).

32 Aveston J. and Sillwood J.M.,
Journal of Material Science, Vol 11, p 1877, (1976).

33 Rosen B.W.
AAIA Journal, Vol 2, p 1985, (1969).

34 Zweben C.,
Journal of Mechanics Physics Solids, Vol 18, p 189, (1970).

36 Zweben C.,
Journal of Material Science, Vol 12, p 1325, (1977).

Zweben, C and Rosen, B.W.,
J.,Mech., Phys., Solids, Vol 18, p 198, (1970).

37 Manders P.W. and Bader M.G.,
Material Science, Vol 16, p 2233, (1981).

38 Manders P.W. and Bader M.G.,
Journal of Materials Science, Vol 16, p 2246, (1981).

39 Manders P.W.,
PhD Thesis, University of Surrey, (1979).

40 Fernando G.F.,
"Environmental Fatigue of Hybrid Composites Part (A) Processing and Matrix Aspects", Bath University, Transfer Report, (1985).

41 Fakuda H.,
Journal of Material Science, Vol 19, p 974, (1983).

42 Xing J., Hsiao G.C. and Chou T.S.W.,
Journal of Compsite Materials, Vol 15, p 443, (1981).

43 Dharan C.K.H.,
Fatigue of Composite Materials ASTM STP 569, p 171, (1975).

44 Dharan C.K.H.,
Journal of Material Science, Vol 10, p 1665, (1975).

45 Weibull W.,
"Fatigue Testing and Analysis of Results", Published by Pergamon Press, (1961).

46 Hahn H.T. and Kim R.Y.,
Journal of Composite Materials, Vol 10, p 156, (1976).

47 Hahn H.T.,
"Fatigue Behaviour and Life Prediction of Composite Laminates",AFML-TR-78-43, (1978).

48 McGuire and Harris B.,
See p 84 reference No 19.

49 Stinchcomb W.W., Reifenider K.L., Yeung P. and Masters J.,
ASTM-STP 723- Fatigue of Fibres Composite Material, (1981).

50 Black N.F. and Stinchcomb W.W.,
ASTM-STP 813, p 95, (1983).

51 Ramkumar R.L.,
ASTM-STP 813, p 116, (1983).

52 Reifnider K.L., Schulte K. and Duke J.C.,
ASTM-STP 813, p 136, (1983).

53 Reifnider K.L.,
International Journal of Fracture, Vol 16, p 563, (1980).

54 Awerbuck J. and Hahn H.T.,
ASTM-STP 636, p 248, (1977).

55 Talreja R.,
Proceedings of the Royal Society London, Vol A 378, p 461, (1981).

56 Aveston and Kelly
Journal of Material Science, Vol 8, p 352, (1973).

57 Hull D.,
"An Introduction to Composite Materials", Cambridge University Press, (1981).

58 Stinchcomb W.W. and Reifsnider K.L.,
ASTM-STP 675, p 762, (1979).

59 Reifsnider K.L.,
International Journal of Fracture, Vol 16, p 563, (1980).

60 O'Brien T. K. and Reifsnider K.L.,
Journal of Composite Materials, Vol 15, p 55, (1981).

61 O'Brien T. K.,
ASTM-STP 775, p 140, (1982).

62 Wilkins D.J. and Eisenmann T.R.,
ASTM-STP 775, p 168, (1982).

63 Jamison R.D., Schulte, K., Reifsnider, K.L. and Stinchcomb, W.W.,
Presented at ASTM Symposium on "Effects of Defects in Composite Materials", San Francisco, California, (1982).

64 Valisetty R.R. and Rehfield L.W.,
ASTM-STP 876, p 82, (1985).

65 Wang A.S., Slomian M. and Bucinell R.,
ASTM-STP 876, p 135, (1985).

66 Rosen B.W.,
(As referenced in 57)

67 Greszczuk L.B.,
AIAA Journal , Vol 13 No 10, p 1311, (1975).

68 Hayashi T.,
Seventh International Reinforced Plastics Conference, p 11, (1975).

69 Greszczuk L.B.,
AIAA Journal, Vol 13 No 10, p 1311, (1975).

70 Ewins and Ham
Royal Aircraft Establishment Technical Paper 73057, (1973).

71 Kulkarni S.U., Rice, J.S. and Rosen B.W.,
Composites, p 217, (1975).

72 Weaver C.R. and Williams J.G.,
Journal of Material Science, Vol 10, p 1323, (1975).

73 Parry T.V. and Wronski A.S.,
Journal of Material Science, Vol 16, p 439, (1981).

74 Wronski A.S. and Parry T.V.,
Journal of Material Science, Vol 17, p 3657, (1982).

75 Chaplin C.R.,
Journal of Material Science, Vol 12, p 347, (1977).

76 Piggott M.R. and Harris B.,
Journal of Material Science, Vol 15, p 2523, (1980).

77 Martinez G.M. and Piggott M.R.,
Journal of Material Science, Vol 16, p 2831, (1981).

78 Piggott M.R. and Harris B.,
Journal of Material Science, Vol 16, p 687, (1981).

79 Piggott M.R.,
Journal of Material Science, Vol 16, p 2837, (1981).

80 Piggott M.R.,
Chapter 4 in "Developments in Reinforced Plastics", Vol 4, p 131, Elsevier Applied Science Publishers, London, (1984).

81 De Ferran E.M. and Harris B.,
Journal of Composite Materials, Vol 4, p 2881, (1980).

82 Wilde E.M. and Piggott M.R.,
Journal of Material Science, Vol 15, p 2881, (1980).

83 Swift D.G.,
Journal Phys. D., Vol 8, p 223, (1975).

84 Curtis P.T. and Moore B.B.,
Royal Aircraft Establishment Technical Report 82031, (1982).

85 Curtis P.T.,
Royal Aircraft Establishment Technical Report 85099, (1985).

86 CIBA-GEIGY Trade Literature, Fiberdux 91C, (1984).

87 Sturgeon J.B.,
Royal Aircraft Establishment Technical Report 75135, (1975).

88 Jones C.,
Phd Thesis, Bath University, (1985).

89 Dickson R.F.,
Phd Thesis, Bath University, (1985).

90 CIBA-GEIGY Trade Literature, Redux 403, (1982).

91 Barker A.T. and Balasundaram, V.,
"Compression Test for CFRP Laminates", University of Birmingham.

92 DSC 1-B Instruction Manual,
Perkin Elmer.

93 Chiao, T.T.,
Proceedings of the International Confernence on Fracture Mechanics in Engineering Applications, p 349, (1979).

94 Chiao, C.C. and Chiao, T.T.,
Handbook of Composite Materials, Ed. Lubin, G., Van Nosttrand Reinhold, ch 12, p 272, (1982).

95 Tashiro, K., Kobayshi M., and Tadokoro, H.,
Macromolecules, Vol 10, No 2, p 413, (1977).

96 Hagege R., Jarrin, M. and Sotton, M.,
Journal of Microscopy, Vol 115, Part 1, p 65, (1975).

97 Brydson
Plastics Materials, Published by Butterworth Scientific, (1982).

98 Delmonte, J.,
Technology of Carbon and Graphite Fibre Coumpounds, Litton Educational Publications Inc., (1981).

99 Waddams, A.C.,
Chemicals from Petroleum, Published by Buttler and Tonner Ltd., (1976).

100 McKague, E.L., Reynolds, J.D., and Halkias, J.E.,
Journal of Applied Ploymer Science, Vol 22, p 1643, (1978).

101 Bucknell, C.B. and Partridge, I.K.,
Polymer, Vol 24, p 639, (1983).

102 Johnson, J.W.,
Composites, Vol 14, No 2, p 107, (1983).

103 Kalble, D.H. and Dynes, P.J.,
Journal of Adhesion, Vol 8, p 195, (1977).

104 Lagace, P.A.,
AIAA Journal, Vol 23, No 10, p 1583, (1985).

105 Ishikawa T., Matsushima, M. and Hayashi, Y.,
Journal of Material Science, Vol 20, p 4075, (1985).

106 Hughes, j.D.H.,
Metals and Materials, p 365, (1986).

107 Van Dreumel, W.H.M. and Kamp, J.L.M.,
Journal of Compsite Materials, Vol 11, p 461, (1977).

108 Curtis, G.J., Milne, T.M., and Reynolds, W.N.,
Nature, Vol 220, p 1024, (1968).

109 Beetz, C.P.,
Proceeds of the 15th Binnial Conference on Carbon, American Carbon Society, p 302, (1981).

110 Jortner, J.,
ASTM-STP 836, p217, (1984).

111 Hysol-Grafil, Trade Literature.

112 Roylance, M.E. and Houghton, W.,
American Helicopter Society Journal, Vol 28, p 3, (1983).

113 Konopaser, L. and Hearle, J.W.S.,
Journal of Applied Polymer Science, Vol 21, p 2791, (1977).

114 Bunsell, A.R.,
Journal of Materials Science, Vol 10, p 1300, (1975).

115 Howard, A.,
Testing, Evaluation and Quality Control, Vol 183, p 264, (1983).

116 Zweben, C., Smith, W.S. and Wardee, M.W.,
Composite Materials: Testing and Design(Fifth Conference), ASTM STP 674, p 228, (1978).

117 Handbook of Resins.

118 Woolstencroft, D.H.,
Phd Thesis, Preston Polytechnic, (1981).

119 Lo, S.Y. andd Hahn, H.T.,
Hygrothermal Expansion of Kevlar 49/Epoxy and S2-Glass/Epoxy Composites, Report UCRL 15517, (1982).

120 DeTeresa, S.J., Farris, R.J. and Porter, R.S.,
37th Annual Conference of Reinforced Plastics/Composites Institute, The Society of the Plastics Industry Inc, Session 29-A, (1982).

121 DeTeresa, S.J., Farris, R.J., and Porter, R.S.,
Journal of Material Science, Vol 19, p 57, (1984).

122 DeTeresa, S.J., and Nicholais, L.,
Polymer Composites, Vol 9, p 192, (1988)

123 Sims, G.D. and Gladman, D.G.,
Plastics and Rubber: Materials and Applications, p 41, (1979).

124 Sims, G.D. and Gladman, D.G.,
Plastics and Rubber: Materials and Applications, p 122, (1980).

125 Roylance, M.E.,
Phd Thesis, Massachusetts Institute of Technology, (1980).

126 Jones, C.J., Dickson, R.F., and Adam, T., Reiter, H. and Harris B.,Proceedings of the Royal Society, London, A396, p 315, (1980).

127 Hahn, H.T. and Chin, W.K.,
37th Annual Conference of Reinforced Plastics/Composites Institute, The Society of the Plastics Industry Inc, Session 24-C, (1982).

128 DeTeresa, S.J. and Nicholais, L.,
Polymer Composites, Vol 10, No.3, p 202, (1989).

129 Hahn, H.T. and Chin, W.K.,
Composite Technolgy Review, Vol 3, No -, p 27, (1981).

130 Miner, L.H., Wolfe, R.A., and Zweben, C.H.,
Composite Reliablity, ASTM STP 580, p 549, (1975).

131 Dupont Kevlar Fibres-Trade Literature.

132 Hertzberg, R.W. and Manson, J.A.,
Fatigue of Engineering Plastics, Academic Press, (1980).

133 Cherry, B.W.,
Polymer Surfaces, Chapters 6 and 7, Cambridge University Press.

133 Chatfield, C.,
Statistics for Technology, Chapman and Mall, (1983).

134 Gerharz, J.J.,
Mechanism of Fatigue Damage and Fatigue Testing, AGARD Lecture Series, No 124, Section 7, (1982).

135 Schutz, D.,
Planning and Analyzing a Fatigue Test Programme, AGARD Lecture Series 118, Section 2, (1981).

136 Adam, T, Dickson, R.F., Fernando, G., Harris, B. and Reiter, H.
Fatigue Behaviour of Hybrid Composites, Final Progress Report, 2112/052 XR/MAT, The University of Bath, (1987).

137 Stugeon, J.B.,
Royal Aircraft Establishment Technical Report, TR 75135, (1975).

138 Owen, M.J.,
Fatigue of CFRP - Chapter 8, Composite Materials, Vol 5, "Fracture and Fatigue", Broutman, L.J.. Editor, Academic Press, (1974).

139 Gerharz, J.J. and Schutz, D.,
Royal Aircraft Establishment, Translation 2045, (1980).

140 Beaumont, P.W.R. and Harris, B.,
International Conference on Carbon Fibres: Their Composites and Applications, Paper 49, Plastics Institute, (1971).

141 Shirrell, C.D.,
ASTM STP 658, p 21, Vinson, J.R., Ed., (1978).

142 Adamson, M.J.,
ASTM STP 813, p 179, O'Brian, T.K.,Ed., (1983).

143 McNaughton, J.L., and Mortimer, C.T.,
Differential Scanning Calorimetry IRS,
Phy. Chem. Series, No.2, vol 10,
Publ., Butterworths, (1975).

144 Turi, A.,
"Thermal Analysis of Polymeric Materials",
Publ.,Academic Press Inc.,(1981).

145 Penn, L.S.,
ASTM STP 674, p 519, Tsai,S.W., Ed., (1979).

146 "Composite Materials: Quality Assurance And Processing",
ASTM STP 797, Browning, C.E., Ed., (1983).

147 Kemp, W.,
"Organic Spectroscopy",
Publ., The Macmillan Press Ltd., (1975).

148 Sesler, H.W. and Holland-Mortil, K.,
"IR and Raman Spectroscopy of Polymers",
Publ., Marcel Decker Inc., (1980).

149 Roylance, M.E.,
11th. SAMPE Tech. Conf., P 601, (1979).

150 Failure Analysis, Engineering Materials Handbook, ASM International, Section 11.

151 Johannesson, T. and Blikstad, M.,
Delaminations and Debonding of Materials, ASTM-STP 876, p 411, (1985).

152 Kline, R.A. and Chang, F.H.,
Journal of Composite Materials, Vol 14, p 315, (1980).

153 Theocras, P.S. and Stassinakis, C.A.,
Journal of Composite Materials, Vol 15, p 13, (1981).

154 Robertson, R.E., and Mindriou, V.E.,
Journal of Materials Science, Vol 20, p 2801, (1985).

155 Mittleman, A., Harel, H., Roman, I. and Maron, S.,
Journal of Materials Science, Vol 4, p 1361, (1985).

156 Clements, L.L.,
Journal of Materials Science, Vol 21, p 1853, (1985).

157 Purslow, D.,
Royal Aircraft Establishment Technical Report 8112T, (1981).

158 Purslow, D.,
Composites, Vol 17, No 4, p 289, (1986).

159 Purslow, D.,
Composites, Vol 19, No 5, p 358, (1988).

160 Erickson, A.H.,
Composites, p 189, (1976).

161 Evaluation of Filament-Wound Kevlar-49/Epoxy Fatigue Properties, Lawerence Livermore Laboratory, UCRL-15264, (1980).

162 Drzal, L.T.,
15th National SAMPE Technical Conference, p 190, (1983).

163 Mandell, J.F.,
Developments in Reinforced Plastics-2, Pritchard, G. editor, Applied Science Publications, London, p 67, (1982).

164 Lee, R.J.,
Composites, Vol 18 , No 1, p 35, (1987).

165 Barker, A.J. and Balasundaram, V.,
"A Compression Test for CFRP Laminates, Internal Report- Department of Chemical Engineering, University of Birmingham".

166 Curtis, P.T.,
Royal Aircraft Establishment Technical Report 86021, (1986).

167 Schultz D. and Gerharz, J.J.,
Composites, p 245, (1977).

168 Collins, J.A.,
Failure of Materials in Mechanical Design, Wiley International Science Publications, (1981).

169 Adam, T.,
School of Mechanical Engineering, University of Bath, Personal Communication.

170 Donnet, J.B. and Bansal, R.C.,
International Fibre Science and Technology/3 Carbon Fibres, Marcel Dekker Inc., (1984).

171 Li, L.S., Allard, L.F. and Bigelow, W.C.,
Journal of Macro Molecular Science- Physics, B22(2), p 269, (1983).

172 Pruneda, C.O., Morgan, R.J., Lim, R. and Gregory, L.J.,
30th National SAMPE Symposium, p 19, (1985).

173 Pruneda, C.O., Morgan, R.J. and Kong, F.M.,
29th National SAMPE Symposium, p 1213, (1984).

174 Saunders, J.,
Journal of Polymer Science, A-1, Vol 5, p 1609, (1967).

175 Hayes, B.,
Composites, Vol 14, No 2, p 107, (1983).

176 Johnson, J.W.,
Composites, Vol 14, No 2, p 107, (1983).

177 Bucknell, D.H. and Partridge, I.K.,
Polymer, Vol 24, p 639, (1983).

178 Kalble, D.H. and Dynes, P.J.,
Journal of Adhesion, Vol 8, p 195, (1977).

179 Whitney, J.M.,
SESA Monograph, Chapter 4, p 175, (1982).

180 Grimes, G.C.,
ASTM-STP 734, Chamis, C.C. editor, p 281, (1981).

181 Clark, R.K. and Lisagor, W.B.,
ASTM-STP 734, Chamis, C.C. editor, p 341, (1981).

182 Tarnopolskii, Y.M. and Kincis, T.,
Static Test Methods for Composites, Van Nostrand Reinhold Co. Inc., (1985).

183 Sinclair, J.H. and Chamis, C.C.,
ASTM-STP 808, Chait, R. and Papirno, R. editors, p 155, (1983).

184 Ryder, G.H.,
Strength of Materials, MacMillan Press Ltd., (1978).

185 Piggott, M.R.,
Failure of Parts, Brostow and Corneliussen editors, Hanser Publishers, Chapter 23, p 442, (1986).

186 Schulte, K.,
Proceedings of the European Symposium on Damage Development and Failure Processes in Composite Materials, p 39, (1987).

187 Jamison, R.D., Reifsnider, K.L., Schulte, K. and Stinchcomb, W.W.,
ASTM STP 836, p 36, (1984).

188 Bakis, E. C., Simonds, R.A. and Stinchcomb, W.W.,
ASTM-STP 1003, Chaims, C.C. editor, p 189, (1989).

189 Ramkumar, R.L.,
"Fatigue Degradation in Compressively Loaded Composite Laminates", Northrop Corporation, Hawthorne, NASA15956, (1981).

190 Saff, C.R.,
"Compression Fatigue Life Predictions for Composite Structures- Literature Survey", Report No NAC78203, (1980).

191 Phillips, L.N.,
Proceedings of Reinforced Plastics Conference, Brighton, British Plastics Federation, p 207, (1978).

192 Hofer, K.E. , Stander, M. and Vennett, L.C.,
Polymer Engineering and Science, Vol 18, p 120, (1978).

193 Barnard, P.M., and Young, J.B.,
"Cumulative Fatigue LIfe Predictions of Fibre Components, Part 1 and 2", Cranfield Institute of Technology, (1986).

194 "Advances in Composite Marterials Environmental effects",
ASTM-STP 658, Vinson, J.R. editor, (1978).

195 "Composites for Extreme Environments",
ASTM-STP 768, N.E. Adist editor, (1982).

196 Springer, G.S.,
"Environmental Effects on Composite Materials", Technology Publications Co. Inc., Vol 1, (1981).

197 Springer, G.S.,
"Environmental Effects on Composite Materials", Technology Publications Co. Inc., Springer, G.S. editor, (1984).

198 Dorey, G.,
AGARD Lecture Series, No 124, Vol 10-1, (1982).

199 Jones, C., Dickson, R.F., Adam, T., Reiter, H., and Harris, B.,
Proceedings of the Royal Society, London A396, p 315, (1984).

200 Eckstein, B.H.,
ACS Organic Coating Plastic Chemical Properties, Vol 38, p 503, (1978).

201 Enns, B.J., and Gillham, J.K.,
Journal of Applied Polymer Science, Vol 28, p 283, (1983).

202 Illinger, J.L. and Schneider, N.S.,
Polymer Engineering Science, , Vol 20, No 4, p 315, (1980).

203 Moy, P. and Karasz, F.E.,
Polymer Engineering Science, Vol 20, No 4, p 315, (1980).

204 Mikols, W.J., Jeferis, J.C., Apicella, A. and Nicolais, L.,Polymer Composites, Vol 3, p 118, (1982).

205 Carfaga C., Apicella, A. and Nicolais, L.,
Journal of Applied Polymer Science, Vol 27, p 105, (1982).

206 Goodrich, J. and Marom, G.,
Polymer Engineering Science, Vol 22, No 4, p 1052, (1982).

207 Charriere, B.,
Personal Communication.

208 Deiasi, R. and Whiteside, J.B.,
ASTM-STP 658, Vinson, J.R. editor, p 2, (1978).

209 Marom, G. and Broutman, L.J.,
Journal of Adhesion, Vol 12, p 153, (1986).

210 Gillato and Broutman, L.J.,
"Advanced Composite Materials- Environmental Effects", ASTM STP 658, Vinson, J.R. editor, p 6, (1978).

211 Marshall, J.M, Marshall, G.P. and Pinzelli, R.F.,
Polymer Composites, Vol 3, No 3, P 131, (1982).

212 Kasturiarchchi, K.A.,
Phd Thesis, Kingston Polytechnic, (1983).

213 Fahmy, A.A. and Hurt, J.C.,
Polymer Composites, Vol 1, No 2, p 77, (1980).

214 Hahn, H.T. and Kim, R.Y.,
"Advanced Composite Materials- Environmental Effects", ASTM-STP 658, Vinson, J.R. editor, p 98, (1978).

215 Lo, S.Y. and Hahn, H.T.,
"Hygrothermal Expansion of Kevlar 49/Epoxy and S2 Glass/Epoxy Composites", Lawerence Liverermore Laboratory, UCLR 15517, (1982).

216 Shen, C.H. and Springer, G.S.,
(Chapter 3, p 15, see reference No 196).

217 Crank, J.,
"The Mathmatics of Diffusion"' Oxford University Press, (1975).

218 Bragly and Long, (see reference No 217).

219 Newns,
(see reference No 217).

220 Vinson, J.R.,
(see reference No 217).

221 Brens, A.R. and Hoppenberg,
Polymer, Vol 19, p 489, (1978).

222 Smith, P.M. and Fisher, M.M.,
Polymer, Vol 25, p 84, (1984).

223 Diamant, Y., Marom, G. and Broutman, L.,
Journal of Applied Polymer Science, Vol 26, p 3015, (1981).

224 Frich, H.L.,
Polymer Engineering Science, Vol 20, p 2, (1980).

225 Carter, H.G. and Kibler, K.G.,
Journal of Composite Materials, Vol 12, p118, (1978).

226 Gurtin, M.E. and Yatomi, C.,
Journal of Composite Materials, Vol 13, p12, (1979).

227 Peyser, P. and Bascom, W.D.,
Journal of Material Science, Vol 16, p 75, (1981).

228 McKague, E.L., Reynolds, J.D., and Halkias, J.E.,
Journal of Applied Polymer Science, Vol 22, p 1643, (1978).

229 Augl, J.M.,
11 NWSG Technical Report, NSWC/WOL/TR 76-149, (1977).

230 Moy, P. and Karasz, F.E.
"Water in Polymers", Rowland, S.P. editor, ASC Symposium
Series 127, p 505, (1979).

231 Illinger, J.L. and Schneider, N.S.,
ibid, p 51.

232 Ellis, T.S. and Karasz, F.E.,
Polymer, Vol 25, p 664, (1984).

233 Moy, P.,
Phd Thesis, University of Massachusetts, (1981).

234 Gordon, J.M., Rouse, G.B., gibbs, J.M. and Risen, W.M.,
Journal of Chemical Physics, vol 66, p 4971, (1977).

235 Chouchman, P.R. and Karasz, F.E.,
Macromolecule, Vol 11, p 265, (1977).

236 Carter, H.G. and Kibler, K.G.,
Journal of Composite Materials, Vol 11, p 265, (1977).

237 Kretsis, G.,
Composites, Vol 8, No 1, p 13, (1987).

238 Davidson, R.G.,
ACS Division of Polymer Material Science. Eng Preprints, Vol 50, p 94,(1984)

239 Hagnayer, G.L. and Pearce, P.J.,
ACS Organic Coatings Plastics Chemical Properties, No 46, p 580, (1978).

240 Noll, T.E.,
Technical Paper IPC TP Institute of Printed Circuits, IPC-TP-140,(1977).

241 Santana, Z.N.,
Polymer Engineering Science, Vol 21, No 8, p 474, (1981).

242 Hagnaurer, G.L. and Dunn, D.A.,
Journal of Applied Polymer Science, Vol 26, p 1837, (1981).

243 Dynes, P.J. and Kallble, D.H.,
ASTM STP 674, p 566, (1979).

244 Brand, J.,
see refernece no 144

245 Sacher, E.,
Polymer, Vol 14, p 91, (1973).

246 Cole, K.C., Noel, D., and Hechler, T.J.,
Polymer Composites, Vol 10, No 3, p 150, (1989).

247 Jones, W.J. and Orville-Thomas, W.J.,
Trans Frad Society, p 193, (1959).

248 Hughes, E.W. and Stockwell, R.F.,
Jouranl of Chemical Education, Vol 46, p 391,(1969).

249 Jones, F.R., Shah, M.A. and Bader, M.G.,
(ICCM/ECCM), Beijing, p 87.

250 Johnson, J.W.,
Phil Trans. R. Society, London A 294, p 487, (1980).

251 Kasturiarachchi, K.A. and Pritchard, G.,
Composites, Vol 14, p 244, (1983).

252 Kasturiarachchi, K.A. and Pritchard, G.,
Journal of Material Science, Vol 3, p 283, (1984).

253 Barnet and Norr,
Proceeds of an International Conference on Carbon Fibres and Other Applications, Plastics Institute, p 32, (1974).

254 Perret, R. and Ruland, W.J.,
Journal of Applied Crystallography, Vol 3, p 525, (1970).

255 Diefendorf, R.J. and Tokarsky, E.,
Polymer Engineering Science, Vol 15, p 150, (1975).

256 Bennett and Johnson, D.J.,
Procedds of the Fifth London Carbon and Graphite Conference. Society of Chemical Industry, London, Vol 1, p 377, (1978).

APPENDIX 1 QUALITY CONTROL OF PREPREGS

A 1.1 INTRODUCTION

The work in this section was undertaken to establish the cause of the poor quality the prepreg material which was used in the preliminary stages of this research programme. The prepreg materials consisted of aligned XAS/914 and HMS/914 intra-ply, mono-fibre and hybrid composites. Details of the research and results were published previously in reference numbers 40 and 136.

The quality and reliability of any composite system will depend on the quality of the starting materials. Therefore, it is absolutely essential to fully characterize the raw material and to have a carefully controlled manufacturing process.

Penn[145] reviewed several methods that are currently used to determine the physiochemical properties of prepregs and also emphasized the need for a standard procedure. A further review of quality assurance and processing of composite materials may be obtained from reference number 146.

Information on resin composition are difficult to obtain from the manufacturers. Hence, in most cases only comparisons can be carried out to check the quality of incoming resins. Composite users generally rely on the manufacturers release specifications as a criteria for the quality of the material. Release specifications must not and cannot be treated as the

sole criteria for the quality of the materials. On the other hand, the resin film and the prepreg used for this study were not released to any specification. The importance of recommended storage temperature and handling of prepregs must be understood and practised[175].

Details of the quality control procedures used to evaluate the prepregs used in this program were were presented in a previous publication[40] where infrared spectroscopy along with differential scanning calorimetry proved to be a simple and quick method to assess the integrity of the prepregs. For the purposes of this thesis, only aspects relating to the effect of absorbed moisture and cure chemistry are reported.

A 1.2 Infrared Analysis

Infrared spectroscopy (IR) is used to investigate quantified molecular resonance that absorb electromagnetic energy selectively from a broad band infrared source[147,148]. A molecule will absorb infrared radiation if it vibrates in such a way that its electric dipole moment changes during vibrations. The absorbance of a particular frequency by a molecule will depend on the permitted vibrational states available for that molecule. The spectrum of a compound is a plot of the amount of radiation absorbed at each frequency.

Vibrational frequencies, so called group frequencies are that mode of vibrations associated with a particular bond or sets of bonds. The vibrational frequency of a bond is determined by the bond strength and mass of the atoms involved and this frequency is often unchanged or nearly unchanged by other

atoms connected to the original group. Hence, this near constant absorption frequency of a particular group can be used to investigate the presence of absence of certain bonds in a sample or to follow the progress of a reaction. Infrared spectroscopy is most sensitive up to 70% cure in resin systems and then loses its sensitivity as the cure process slows because of gelation and network formation[145]. Furthermore, frequency assignment becomes difficult because of overlapping peaks. A particular part of the IR spectrum is referred to either by its wavelength or by its frequency. Wavelength is expressed in microns and the frequency in reciprocal centimeters.

Spectrum 1, 2 and 3 were from 914 long fibre (prepreg) resin, 914 solid resin (supplied by the manufacturer) and 914 film resin (used in the production of aligned short fibre composites) respectively. The frequency assignments to the peaks are given in Tables A.1 and A.2. Spectrum 1. 2 and 3 were used as reference standards.

Samples for spectra 4, 5 and 6 were obtained from the suspect prepreg (see reference number 40 for details). There are two major differences in these spectra 4, 5 and 6 compared to the reference standards. Firstly, there was a greatly reduced intensity of the nitrile peaks of solid DICY at 2203cm^{-1}. From the known formulation of the 914 resin system and the frequency assignments in Tables A.1 and A.2, it is clear that the nitrile absorption region is free of overlapping absorption frequencies. Therefore, peaks in this region give clear indication of the chemical state of the hardener. Secondly, samples which showed no absorption in the nitrile

region showed a broadening of the N-H and O-H absorption regions. The effect of temperature and moisture with exposure time on the 914 resin system was investigated to elucidated the reasons for the disappearance of the nitrile peak in the IR spectrum of the suspected batch of prepreg materials.

Wave Number (cm^{-1})	Functional Group
3389	OH
3049	C-H, aromatic and epoxy rings.
2956, 2857	CH_2 (as)
1605, 1574, 1515	C=C
1449	CH_2
1034, 914, 863, 841, 971, 775	(EPOXY RING)
1110	C-O
829	=CH (AROMATIC)
1340, 1290, 1165, 1120	O=S=O
1700-1725	C=O

Wave No. cm^{-1}	Group
3365 3323	$\upsilon_a (NH_2)$
3170 3147	$\upsilon_s (NH_2)$
2203 2163	$\upsilon_a (N^3CN^4)$
1657 1639	$d (NH_2)$
1587	$\upsilon_a (N^5CN^6)$
1570 1502	$\upsilon_a (N^4CN^5)$
1252	$\upsilon_s (N^3CN^4)$
1081	$r (NH_2)$
982	$\upsilon_s (N^4CN^5)$
718	$W (N^5CN^6)$

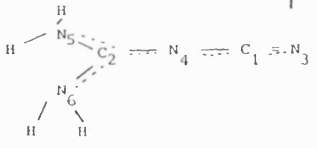

Table A.1 Infrared absorption frequency assignments for TGMDA based resins and DICY. Compiled from reference numbers 145-148 and 247-248.

NO.1

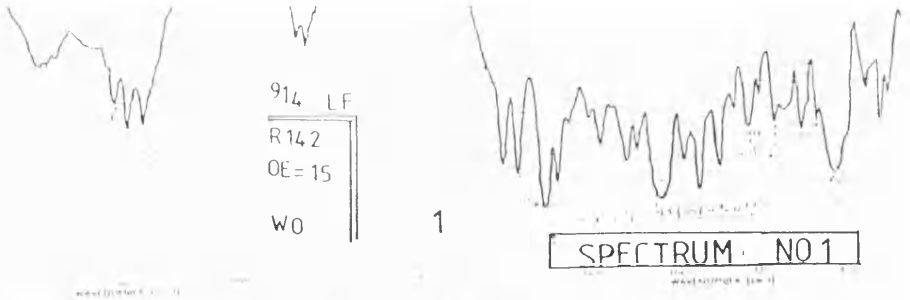

NO.2

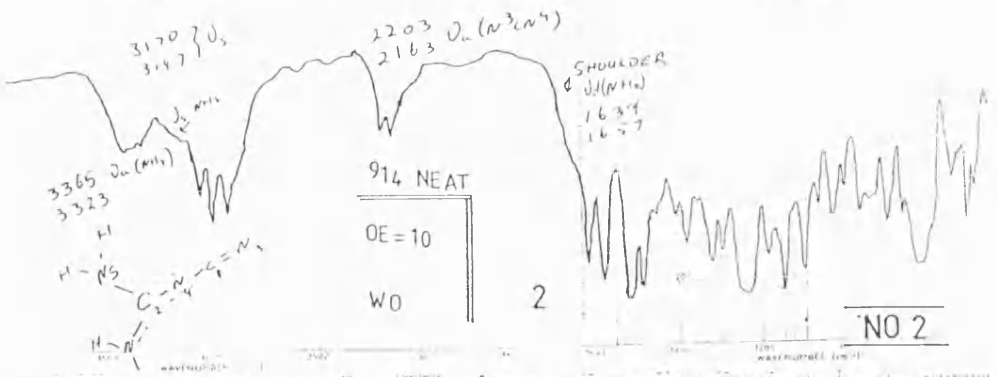

NO.3

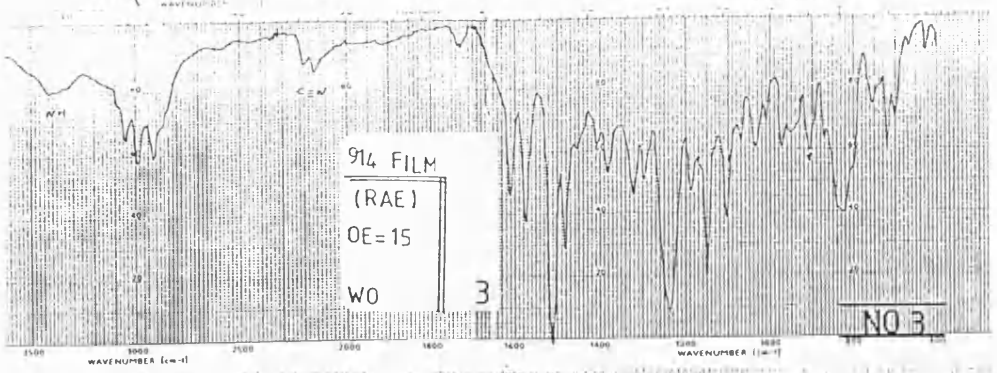

NO.4

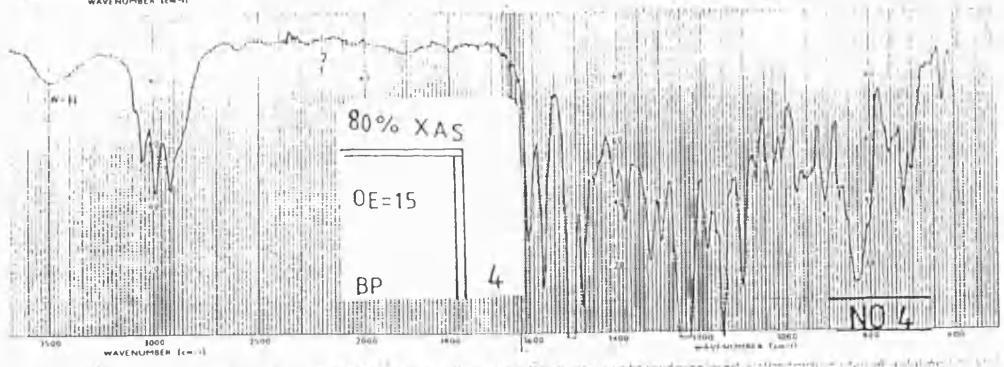

NO.5

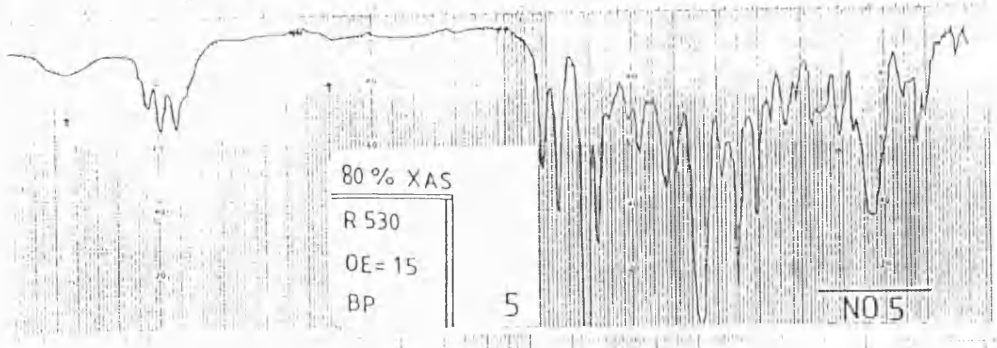

NO.6

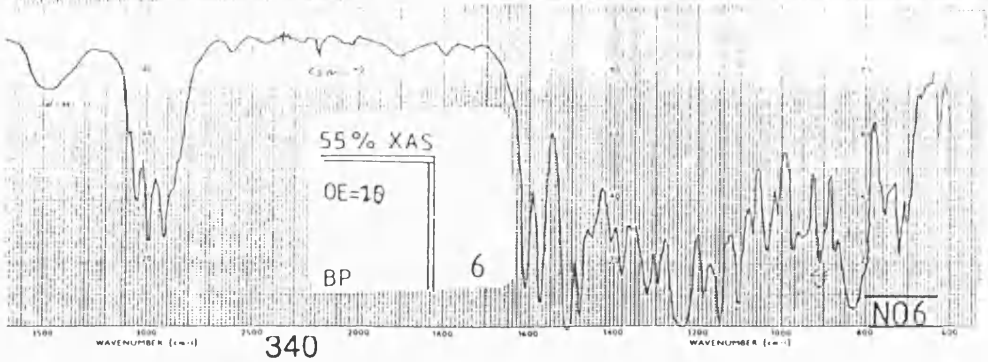

A 1.2.1 Effect of Temperature/Time on the 914 Resin System

The effect of temperature on the resins was investigated by heating the resin on KBr discs at 110°C for varying lengths of time, see spectra 7-10. On heating the resin for 5 minutes at 110°C, the occurrence of a small new peak centered at 2801 cm^{-1} was observed with the solid DICY peaks at 2203 and 2160 cm^{-1} diminishing in intensity, see spectrum number 7. After 10 minutes heating, the peak at 2203 cm^{-1} has almost disappeared with the peak at 2181 cm^{-1} showing a gain in intensity, see spectrum no. 8. Davidson[238] attributed this peak at 2181 cm^{-1} to a new species or extensive hydrogen bonding in dissolved DICY. The effect of having dissolved DICY instead of solid DICY on the shelf-life and processability of the prepregs needs further investigation. Hagnauer[239] found that heating a DICY/accelerator/epoxy system to 100°C followed by room temperature storage promoted ambient temperature epoxy reactions. After two months storage, less than 0.01wt% of DICY remained with 88wt% of the epoxy reacted.

NO.7

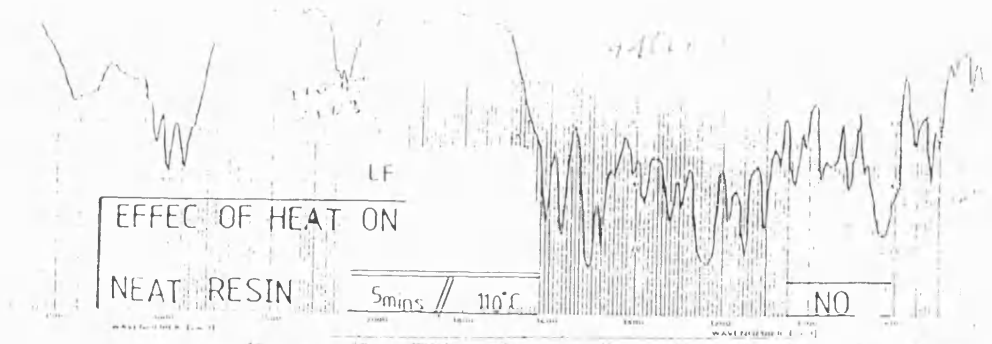

NO.8

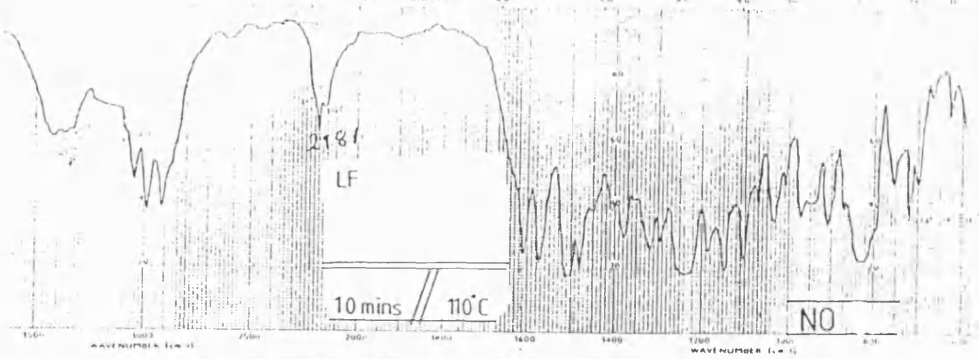

NO.9

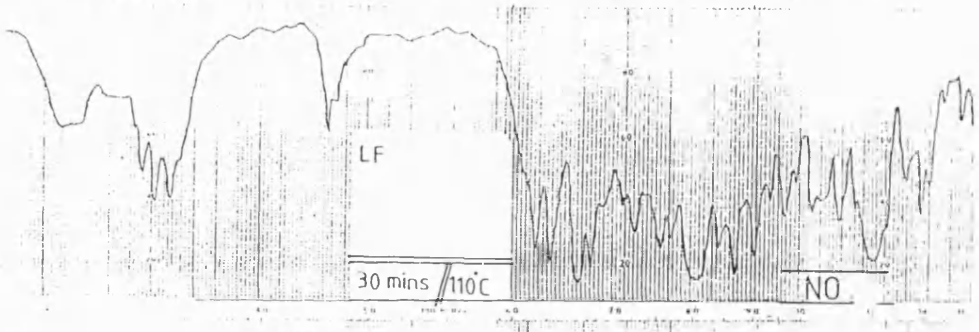

NO.10

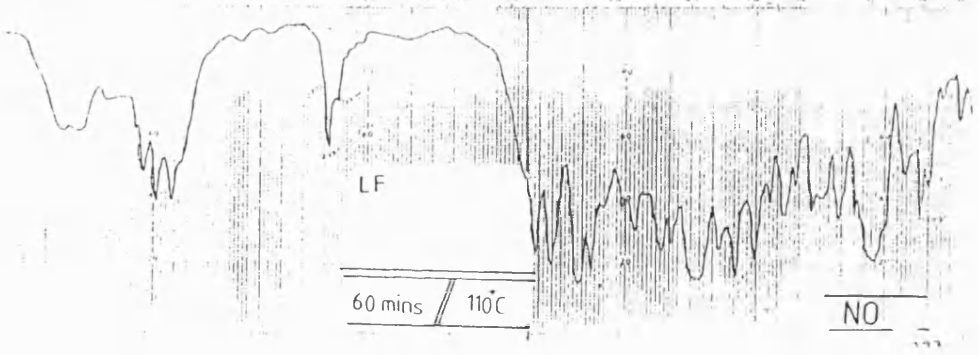

A 1.2.2 Effect of Moisture on 914 Resin Based Prepregs

Spectra 11, 12 and 13 illustrate the effect of exposing neat 914 resin to 65% Rh at 23°C for varying lengths of time. After five days of conditioning the emergence of the dissolved DICY peak at 2180 cm^{-1} is observed. At this stage there was no detectable change in the epoxy content. A pronounced modification of the resin is seen after 17 days of exposure to 65%Rh, spectrum number 12. The broad peak around 3300-3500 cm^{-1} is an overlap of the N-H and O-H-O bonds. The diffused peak at 1650 cm^{-1} is due to H-O-H deformation. Also noticeable is the reduced intensities of the epoxy ring absorption frequencies, see Table A.1. The loss of the epoxy peak is more pronounced after 4 months of exposure at 65%Rh, see spectra number 13.

Also seen in spectra 12 and 13 are the presence of peaks at 1710 and 1720 cm^{-1}. This is most probably due to carbonyl groups produced by the interaction of DICY and water[212,240].

Illinger et al[202] showed that moisture reacted irreversibly with epoxies, i.e. the epoxy ring is not regenerated upon drying out. Santana[241] carried out a detailed study on the effect of aging and moisture on the reactivity of Hercules 3501-6/AS prepregs. Santana found that the samples which were aged in high humidities showed increased conversion of monomer to polymer as compared to the dry aged samples. Furthermore, prepregs which had prolonged humidity exposure showed a much faster reactivity particularly at temperatures below the recommended final cure temperature.

Hagnauer et al[239,242] investigated the hydrolytic stability of TGMDA. Purified samples were found to be considerably more hydrolyticlaly stable than the commercial resin. In the early stage of hydrolysis the major product was identified as partially hydrolysed TGMDA with two epoxy groups unreacted and two epoxy groups ring-opened to form a-glycols. In samples aged at 60^{o}C and 96% Rh over a period of 1 week, the percentage TGMDA dropped from 69% to 47%. The hydrolytic stability of old MY 720 samples was found to be significantly less stable than new resin batches even though the percentage TGMDA was nearly identical.

It is quite evident from the above discussion that epoxy resins are extremely sensitive to moisture. It was shown that moisture can react with DICY and also result in the consumption of the epoxy groups thereby rendering the prepregs useless. The findings of this study has shown that transmission IR can be used to establish the integrity of prepregs[246].

NO.11

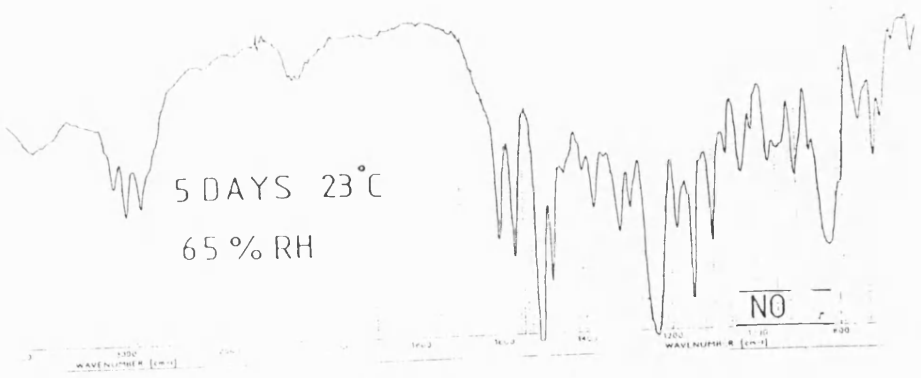

NO.12

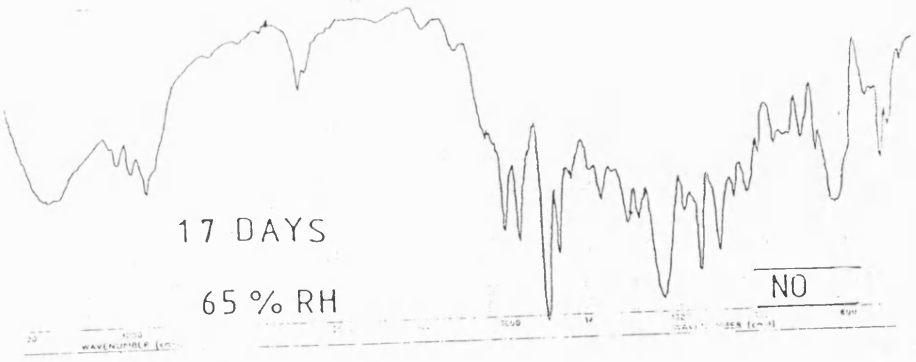

NO.13

A 1.3 Differential Scanning Calorimetry (DSC)[144]

The DSC instrument can be divided into two main control loops, namely the average and differential temperature controls. In the average temperature loop, the programmer provides an electrical signal which is proportional to the required temperature of the sample and reference. This program temperature information is relayed to the recorder pen and appears as the abscissa scale marking. The programme signal is compared with the average signal from platinum resistance thermometers permanently embedded in the sample and reference holders. The resultant difference signal is amplified in the average temperature amplifier. If the temperature called for by the programmer is greater than the average temperature of the sample and reference holders, more power will be fed to the heaters of both sample holders, which like the resistance thermometers, are embedded in the holders. If the average temperature is higher than that demanded by the programmer, the power to both heaters will be decreased. In this way, the average temperature of the holders is made to track the command from the programmer.

In the differential temperature control loop signals representing the sample and reference temperature, measured by the platinum thermometers, are fed to a circuit which determines whether the reference or sample temperature is greater. The differential temperature amplifier output will then proportion a small increment of power between the reference and sample heaters in such a way as to correct any temperature difference between them. This is done by

increasing the power to one while decreasing the power to the other. A signal proportional to the differential power is also transmitted to the main recorder pen. The integral of the resulting peak is the internal energy change. The direction of the pen movement will depend on whether more power is required in the sample or reference heaters.

A 1.3.1 DSC Analysis of 914 Resin Prepregs

The DSc analysis was carried out on a Perkin Elmer model 1B. The instrument was calibrated for temperature and enthalpy using tin and indium. The tests were performed in a nitrogen atmosphere with the following conditions:

Range = 16 Mcal/sec
Scan speed = 8^{o}C/min
Chart speed = 10mm/min
Nitrogen flow = 25cc/min

Prepreg resin samples were obtained from the backing paper and prepreg sheets were also tested. Approximately 6-8mg of the resin was transferred to the aluminium test pans and put under vacuum for 30 minutes prior to testing.

Figures A1 (A and B) illustrates DSC scans for the reference standard materials. They show a major exotherm with a maximum at 468K. The reaction initiation temperature is around 423K. A second minor exothermic peak is present between 500-552K. The major exotherm is due to the reaction of the hardener with epoxy groups. The magnitude of this peak is proportional to the enthalpy of the reaction and

hence the concentrations of hardener and epoxy. The decrease in the peak areas or degree of cure can be followed by measuring peak areas of samples which have been cured for varying lengths of time at any specified temperatures. The minor exotherm present between 500-552K disappears only if the sample is heated to 190^{o}C, the postcure temperature. The origins of this peak are not clear, however it is most probably due to homopolymerisation of residual epoxies.

When one compares the scans for the (standard) prepreg resin with the suspect prepreg resin, a totally different cure behaviour is seen, Figures A1 (D, E and F). The most prominent feature of these scans is the absence or near absence of the primary exothermic peak centered at 469K. However a major exotherm is present centered around 572-580K. Dynes et al[243] showed that pure TGMDA without any hardener required a high temperature for homopolymerisation to occur with a T_{max} value of 575K. This is close to the T_{max} value observed for the suspect prepreg resins.

Brand[244] showed that curing B-staged samples in a saturated water environment at 150^{o}C caused an irreversible lowering of the T_g by approximately 10^{o}C relative to the dry samples cured in ambient air. Sacher[245] investigated the effects of the DICY particle size on the curing behaviour of an epoxy resin. He found that fine particles (<125um) gave a longer shelf life and higher activation energy of curing than coarse DICY particles.

This study has shown that DSC can be used to verify the integrity and quality of prepregs. The experimental

procedures are simple and quick to perform. The main findings of this study indicated that heating the 914 resin at 110°C resulted in the hardener dissolving in the resin. Other researchers have shown that this facilitates room temperature reactions. The effect of 65% Rh, 23°C also resulted in the dissolution of the hardener and in consumption of epoxy groups.

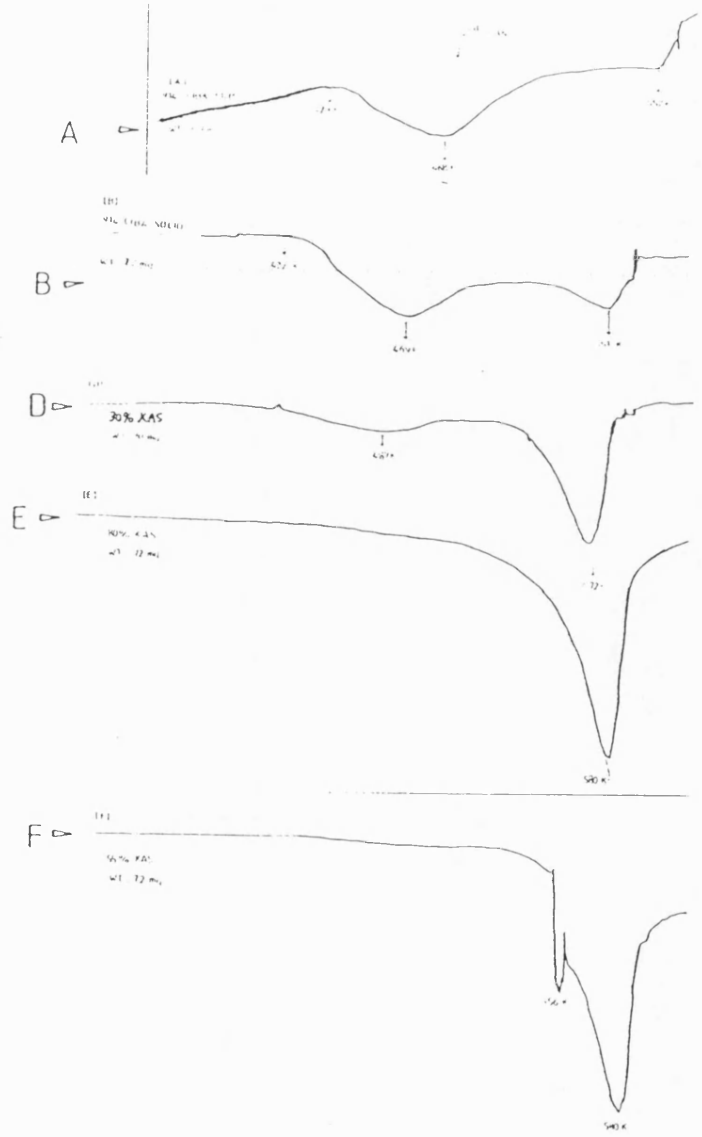

Figure A1 DSC scans for the neat 914 resin and the "suspect" resin.